PROTEIN RESISTANT BIOMATERIAL ARCHETYPES FOR OCULAR APPLICATION

ONYINYE JENNIFER UWAEZUOKE

A thesis submitted to the Department of Pharmacy and Pharmacology, Faculty of Health Sciences, University of the Witwatersrand in fulfilment of the requirements for the award of the degree, Doctor of Philosophy



WITS
UNIVERSITY

Supervisors

Professor Yahya Essop Choonara

Department of Pharmacy and Pharmacology, University of the Witwatersrand, Johannesburg, South Africa.

and

Professor Pradeep Kumar

Department of Pharmacy and Pharmacology, University of the Witwatersrand, Johannesburg, South Africa.

October 2022

DECLARATION

I, Onyinye Jennifer Uwaezuoke, hereby declare that the work presented in this thesis was conceptualized, designed, and done by me and submitted to the Faculty of Health Sciences of the University of the Witwatersrand for the award of the degree of Doctor of Philosophy. I hereby declare that it has not been submitted anywhere else for the award of any other degree.

Signature 

Date: 16/10/2022

ANIMAL ETHICS DECLARATION

I hereby declare that all animal work carried out in this study titled ‘‘Protein resistant biomaterial archetypes for ocular application’’ was approved by the Animal Research Ethics Committee of The University of the Witwatersrand with ethics clearance certificate no 2021-07-03C (**Appendix A**)

DEDICATION

To all those who through doggedness, determination, diligence, and faith obtain that which is promised……

PRESENTATIONS ARISING FROM THIS WORK

1. Onyinye J. Uwaezuoke, Pradeep Kumar, Yahya. E. Choonara. Zwitterionization and in vitro characterization of a UV cross linkable polyvinyl alcohol hydrogel for the ocular delivery of Cyclosporine A. An oral presentation at the BRICS summit hosted at the University of the Witwatersrand, on the 4th of November 2021. (**Appendix B**)
2. Onyinye. J. Uwaezuoke, Pradeep Kumar, Viness Pillay, and Yahya. E. Choonara. A neoteric biomaterial design for limiting mucous interaction with pandemic causing viral proteins-An abstract and oral presentation at the first PhD Seminar competition organized for all PhD students at The University of the Witwatersrand between the 29th and 30th of September 2020. (**Appendix C**)
3. Onyinye J Uwaezuoke, Pradeep Kumar, and Yahya Choonara. A Novel Ocular Hydrogel For Limiting Biofilm Adhesion.: An oral presentation at the 13th cross faculty postgraduate symposium of the University of the Witwatersrand held between the 12th and 13th of July 2022. **(Appendix I)**

PUBLICATIONS ARISING FROM THIS WORK

1. Uwaezuoke OJ, Kumar P, Pillay V, Choonara YE. Fouling in ocular devices: implications for drug delivery, bioactive surface immobilization, and biomaterial design. Drug Deliv Transl Res [Internet]. 2021 Jan 16 [cited 2021 Mar 2]; Available from: https://doi.org/10.1007/s13346-020-00879-1. (***Appendix D***)
2. Uwaezuoke Onyinye, Lisa C. Du Toit, Pradeep Kumar, Naseer Ally, and Yahya E. Choonara. 2022. "Linoleic Acid-Based Transferosomes for Topical Ocular Delivery of Cyclosporine A" Pharmaceutics 14, no. 8: 1695. https://doi.org/10.3390/pharmaceutics14081695 (***Appendix E***)
3. Onyinye J. Uwaezuoke, Naseer Ally, Pradeep Kumar, and Yahya. E. Choonara. Synthesis And Characterization of A Mechanically-Robust Zwitterionic Polyvinyl Alcohol Ocular Hydrogels With Anti- Fouling Potential.
4. Onyinye J. Uwaezuoke, Naseer Ally, Pradeep Kumar, and Yahya. E. Choonara. Low-biofouling potential of PVA -sulfobetaine methacrylate crosslinks: *In vitro-in vivo* correlation.
5. Onyinye J. Uwaezuoke, Naseer Ally, Pradeep Kumar, and Yahya. E. Choonara. Zwitterionization and impact on *in vitro* drug release of a poorly soluble drug from a superhydrophilic hydrogel.

ABSTRACT

The challenging nature of the ocular drug delivery terrain continues to drive the search for innovative platforms that will counter the challenges of delivering effective patient-friendly therapeutic solutions. For many ocular therapeutics, the challenge has been finding a means to deliver high molecular weight, poorly soluble bioactives, across the formidable barriers presented by the physio-anatomical ocular structures. This challenge is more for bioactives used to treat chronic ailments in predominantly vulnerable populations such as the elderly and the children. In addition, many ocular conditions co-exist in an individual, necessitating the need for multiple treatment plans. For such individuals, using safer delivery options with higher bioactive loading capacity is a *sine qua non.* This thesis details the design, development, characterization, and evaluation of a novel ocuterial to overcome the challenge of cytocompatibility for implantable ocular devices. Modification by bulk zwitterionization was adopted as opposed to surface modification given that surface modification is short-lived in the dynamic ocular space.

Polyvinyl alcohol (PVA) was selected as the ideal polymer framework given its ocular application history together with the bioinspired sulfobetaine methacrylate. Facile photo-initiated crosslinking polymerization (a process amenable to both moulding and 3D printing) was used to synthesize and optimize the novel hydrogel properties. *In vitro* characterization was undertaken to assess the physicochemical parameters such as water contact angle, that underscore the hydrophilicity and consequently protein resistance potential of the novel hydrogel. The mechanical strength of the novel hydrogel that delineates its ability to withstand stress that could arise from handling (with forceps during implantation or by patients for contact lens application) was also evaluated. The optimized hydrogels' crushing strength was above 21 Mpa % at 70 % strain and translates to a superior mechanical robustness for a super-hydrophilic hydrogel. Zwitterionization increased the transparency (shown by over 99 % transmittance, a perquisite for lens applications); improved equilibrium water content (directly correlates with oxygen transmissibility and permeability that is specifically important for corneal health in extended wear contact lenses); contributed to superhydrophilicity (shown by a water contact angle < 10º) and translates to a high protein resistance/antifouling potential; improved *in vitro* protein adhesion resistance (< 0.1 µg/mm^2); facilitated drug loading and *in vitro* drug release of a model hydrophobic drug molecule, cyclosporine A; and decreased biofouling potential (>87%) to *S. aureus* and *E. coli*. *In vivo* sub conjunctival implantation of the optimized hydrogel in New Zealand albino rabbits

demonstrated its low capacity to trigger pro-inflammatory responses, an absolute requirement for implantable ocular devices given the risks inflammation presents in the ocular space. These results underscore the potential for application of the novel ocular biomaterial as an intraocular sub-conjunctival implantable device that could double as a drug delivery device.

ACKNOWLEDGEMENT

My gratitude goes to the Almighty God who has deemed me fit for this work. I thank Him for His protection. Provision, and grace.

I acknowledge with deep gratitude, the immense contributions of my academic mentors to this success story. At the top of this pack is Professor Viness Pillay of the blessed memory. Today, I am proudly Witsie because he looked beyond the surface, saw the deep desire for sound research, and offered me a place in his world class lab despite my financial inadequacy at the time. I hope that somehow, Prof, you can look down from your now elevated status in the spirit world and see that your faith in me was not misplaced. To the chairman of the Department of Pharmacy and Pharmacology, and my chief mentor, Prof Yahya Choonara, thank you for going the extra mile with the CTG funds, thank you for not settling for mediocrity in science and thank you for throwing me up, turning me around and presenting the scientist that now emerges. To Prof Pradeep Kumar, thank you for being passionate about science, for inculcating confidence in me as a researcher, for the numerous, invaluable tricks I learnt on how to get things done. Thank you, Prof Lisa DuToit for standing with me in silent understanding when things really got rough and all your behind the scenes moves to get me through particularly with my animal work. Thank you, Dr. Nasser Ally for bringing your expertise to the animal studies and for all the sacrifices you made as regards timing. I will not forget Prof Ndidi Ngwuluka, proudly witsie and a true product of WADDP, on whose back I rode to Wits. To Prof Helen Myzewa, the current Head Of the School of Therapeutic Sciences, thank you for all you do for your students across board. Thank you for putting us first and thank you for being The Head Of School with a heart.

Thank you, to the technical crew of WADDP, Mr. Sello Ramarumo, Mr. KB who always went the extra mile to ensure we were okay with all we needed, Bafana, Tshidi Moshete for those encouraging smiles, Dr Hillary Ndlovu who came in and revolutionized the way things worked in the Lab and to Busi, thank you for everything.

To my WADDP family amongst whom I met the good, the bad, and the ugly-a perfect mix that consolidates its products, thank you. Thank you, Gillian Mahume; for those hugs that utters peace in silence. Thank you, Dr Tayo Adekiya for motivating and encouraging me by your work ethics and style. Thank you, Dr. Phil Ubaneko, for your dedication to teaching me cell lab routine. Thank you, Ayesha Suleman for those wonderful chocolates when tiredness had crept in. Thank you, my friend, Yosra Abdallah. In you, I finally found a friend in WADDP. Thank you, Petra Dinham of

the Engineering department, for working until our SEM was publishable. Thank you to the staff and crew of the Wits Research Animal Facility: Amelia, Mduduzi, Dr. Kim Jardine, Nicole. You guys are simply awesome.

To my sisters, Mrs. Pearl Ibeanusi, Hope Duruewuru, and Faith Ezezue, Thank you for all the support both financial and otherwise. Thank you, Brother Uba Akanno, for everything. Thank you Mr. Ibechedo Akanno, My wonderful Father, for your wise counsel and moral support always.

Finally, thank you to my wonderful kids Emanuel, Adaugo, Shalom, Glory, and Kingsley. You sacrificed those 4 years I should have been part of your lives. It paid off. Thank you Mr. Emmanuel Uwaezuoke, for taking upon yourself the job of mother and father to our kids in the last 4 years and for your support both financial and otherwise.

TABLE OF CONTENTS

PROTEIN RESISTANT BIOMATERIAL ARCHETYPES FOR OCULAR APPLICATION i

DECLARATION i

ANIMAL ETHICS DECLARATION ii

DEDICATION iii

PRESENTATIONS ARISING FROM THIS WORK iv

PUBLICATIONS ARISING FROM THIS WORK v

ABSTRACT vi

ACKNOWLEDGEMENT viii

TABLE OF CONTENTS x

LIST OF FIGURES xvi

LIST OF TABLES xxiii

LIST OF APPENDICES xxv

Chapter One 26

Introduction And Thesis Overview 26

1.1 Introduction 26

1.2 Rational and motivation for the study 28

1.3 Aim and objectives of this study 29

1.4 Overview of the thesis 30

1.4.1 Chapter One 30

1.4.2 Chapter Two 31

1.4.3 Chapter Three 31

1.4.4 Chapter Four 31

1.4.5 Chapter Five 32

1.4.6 Chapter Six 32

1.5 References 32

Chapter Two 34

Fouling in Ocular Devices: Implications for Drug Delivery, Bioactive Surface Immobilization, and Biomaterial Design 34

2.1 Introduction 35

2.2 The impact of fouling in the ocular environment.....39

2.3 The extent and implications of fouling in implanted ocular devices 41

2.3.1 Contact lens (CL) devices 42

2.3.2 Intraocular lens (IOL) devices 48

2.3.3. Glaucoma drainage (GD) devices 51

2.3.4 Intravitreal devices 55

2.3.5 Miscellaneous ocular devices 58

2.4 Modification of biomaterials as an anti-fouling approach.....60

2.5 The design of immunological responsive anti-fouling biomaterials for ocular devices…….. 61

2.6 Future perspectives and conclusions.....63

2.7 References.....64

Chapter Three.....86

Synthesis And Characterization Of A Mechanically Robust Zwitterionic Poly (Vinyl Alcohol) Ocular Hydrogel With Anti-Fouling Potential 86

3.1 Introduction 86

3.2. Materials and methods 88

3.2.1. Materials 88

3.2.2 Synthesis of the sulfobetaine methacrylate 88

3.2.3. Synthesis of the GMA modified PVA (PVA-GMA) 88

3.2.4. Zwitterionization and photoinitiated crosslinking copolymerization of PVAGMA and SBMA ……89

3.2.5. Characterization of the PVAGMA base material and ocular hydrogel.....89

3.2.5.1. Determination of the molecular transitions in the pristine and modified starting materials … … …

Linoleic Acid Based Transferosomes For Topical Ocular Delivery Of Cyclosporine A 136

4.1. Introduction 136

4.2 Materials and Methods 138

4.2.1 Materials 138

4.2.2 Preparation of the cyclosporine-A loaded transferosomes 138

4.2.3 Characterization of the transferosomes.....138

4.2.4 Encapsulation efficiency (EE%) and in vitro release of cyclosporine A from the transferosomes 139

4.2.5 *Ex vivo* corneal permeability of the transferosomes 140

4.2.6 Cytotoxicity studies of the transferosomes in human retinal epithelial primary cell line 140

4.2.7 Statistical analysis 141

4.3 Results and Discussion 141

4.3.1 Formulation and characterization of transferosomes.....141

Table 4.1. Composition of the transferosomes.....142

Table 4.2. Size distribution and polydispersity of blank and loaded transferosomes 143

4.3.2 Physicochemical characterization of the transferosomes 144

Table 4.3. Effect of incorporation of linoleic acid on the stability of transferosomes 144

4.3.3. Transferosomes deformability and flexibility studies.....149

4.3.4 Cytocompatibility of transferosomes 151

4.3.5 Encapsulation efficiency and *in vitro* release profile of CysA from loaded transferosomes prepared with Tween 80.....152

4.3.6 *Ex-vivo* permeability and flux across the rabbit's cornea 155

4.4 Conclusions.....157

4.5 References.....157

Chapter Five 162

In Vitro And *In Vivo* Assessment Of Anti-Fouling, And *In Vitro* Drug Release From Zwitterionized Photo-Crosslinked Hydrogels.....162

5.1. Introduction 162
5.2. Materials and Methods 164
5.2.1. Materials 164
5.2.1. Hydrogel preparation by photoinitiated crosslinking polymerisation 164
5.2.2. *In vitro* quantitative determination of protein adsorption 164
5.2.3. *Ex vivo* qualitative determination of protein adsorption on hydrogel discs 165
5.2.4. Determination of cell adhesion using HREP 165
5.2.5. Assessment of biofouling potential of hydrogels 166
5.2.6. In vivo assessment of cytocompatibility of the hydrogel discs 166
5.2.7. Cyclosporine A loading into hydrogel discs 167
5.2.8. Characterisation of Cyclosporine A loaded hydrogels 167
5.2.9. *In vitro* drug release from Cyclosporine A loaded hydrogels 167
5.3. Results and discussion 168
5.3.1. Preparation and CysA loading in hydrogels 168
5.3.2. *In vitro* and *ex vivo* protein adsorption studies result 169
5.3.3. Qualitative determination of adsorbed protein by SDS-PAGE 171
5.3.4. Cell adhesion studies on the hydrogel 173
5.3.5. Biofouling resistance assessment for hydrogels 178
5.3.6. *In vivo* evaluation of hydrogel discs in New Zealand albino rabbits 180
5.3.7. Characterization of CysA loaded gels 192
5.3.8. *In vitro* cyclosporine A release from hydrogels 192
5.4. Conclusions 198
5.5. References 198
Chapter Six 205
Conclusion And Recommendations 205
6.1 Concluding remarks 205
6.2 Future perspectives 206

Appendix A. Animal Ethics Certificate.....207

Appendix B. Oral presentation at the BRICS Conference hosted by South Africa November 2021. 208

Appendix C. Certificate of participation for the PhD seminar competition, 2020.....209

Appendix D. Screenshot of the first page of publication 1……210

Appendix E. Screenshot of the first page of publication 2……211

Appendix F. Certificate of biofilm analysis 212

Appendix G. Certificate for histopathological analysis 215

Appendix H. Turnitin Report 216

Appendix I. Oral presentation at the 13th cross faculty postgraduate symposium……217

LIST OF FIGURES

Figure 1.1 Pathway for zwitterionization of a typical natural polymer, Hyaluronan 29

Figure 2.1 Protein adhesion, coagulation cascade and complement activation with consequent release of PMN and macrophages. B. Damaged tissue releases which lead to further immune response. C) Continued inflammatory response leads to release of proteolytic enzymes and reactive oxygen species (ROS) which may damage the biomaterial surface. Adapted from Biomaterials, vol.32, no. 28, S. Franz, S. Rammelt, D. Scharnweber, and J. C. Simon, “Immune responses to implants - A review of implications for the design of immunodulatory biomaterials,” Copyright (2011) with permission from Elsevier (Franz et al. 2011) 41

Figure 2.2 Possible sites of ocular implant placement. Adapted from Adv. Drug Deliv. Rev., vol. 128, pp. 148–157, H. Kaji, N. Nagai, M. Nishizawa, and T. Abe, “Drug delivery devices for retinal diseases,” Copyright (2018) with permission from Elsevier ((Kaji et al. 2018))……..42

Figure 2.3 Contact lens with hyaluronan ring prepared by cast moulding. Reprinted from Acta Biomater., vol. 53, no. 15, F. A. Maulvi, A. A. Shaikh, D. H. Lakdawala, A. R. Desai, M. M. Pandya, S. S. Singhania, R. J. Vaidya, K. M. Ranch, B. A. Vyas, D. O. Shah “Design and optimization of a novel implantation technology in contact lenses for the treatment of dry eye syndrome: In vitro and in vivo evaluation”. Copyright (2017) with permission from Elsevier. (Maulvi et al. 2017).....43

Figure 2.4 2018 (A) and 2019 (B) prescription of CL by material in the US courtesy of Jason J. Nichols, OD, MPH, PhD. Adapted and Reused with permission from the January 2019 and January 2020 issues of Contact Lens Spectrum.....46

Figure 2.5 Schematic illustration of trends in lipid and protein deposits on different contact lens materials Adapted from (68). Mann A and Tighe B. Contact lens interactions with the tear film. Experimental Eye Research, 2013;117:88-98) with permission from Elsevier.....48

Figure 2.6 Quantity of protein adsorbed on modified silicone; (MPC-ipn-PSiMA), Poly (MPC-co-SiMA), and marketed ACUVUE OASYS. Reprinted from Biomaterials, vol. 31, no. 12, T. Shimizu, T. Goda, N. Minoura, M. Takai, and K. Ishihara, “Super-hydrophilic silicone hydrophilic silicone hydrogels with interpenetrating poly (2-methacryloyloxyethyl phosphorylcholine) networks,” Copyright (2010) with permission from Elsevier (Shimizu et al. 2010).....48

Figure 2.7 Light Photomicrograph of the a) Pristine b) pegylated IOL. The arrow shows the magnitude of posterior capsule hyperplasia. Reproduces with permission from (104) 49

Figure 2.8 The effect of syndecan-4 in the development of ASC. Reprinted from (Qin et al. 2017) 50

Figure 2.9 Schematic representation of the capsule drug ring. Reprinted from Vision Res., vol. 50, no. 7, pp. 680–685, Sarah A. Molokhia, Himanshu Sant, Jacquelyn Simonis, C.J. Bishop, R.M. Burr, Bruce K. Gale, Balamurali K. Ambati “The capsule.....51

Figure 2.10 An illustration of the microfluidic meshwork that replaced the plate of a traditional GDD. Reproduced from. (Behzad Amoozgar et al. 2017).....55

Figure 2.11 Possible architectures/configurations for surface modified materials. Reproduced from B. K.D. Ngo and M. A. Grunlan, Protein Resistant Polymeric Biomaterials, ACS Macro Lett. Vol. 6, no 9, pp. 992-1000, (2017) with permission from American Chemical Soc 62

Figure 3.1 FTIR spectra of SBMA monomer, PVA, and PVAGMA.....94

Figure 3.2 Comparative FTIR spectra of PVAGMA hydrogel with varying content of SBMA 96

Figure 3.3 1HNMR of pristine PVA and methacrylated PVA.....98

Figure 3.4 1HNMR Double methacrylation (A) and single methacrylation (B).....99

Figure 3.5 A DSC thermograms of A pristine PVA.....100

Figure 3.6 TGA of the starting materials and hydrogels.....104

Figure 3.7 TGA weight derivative of PVA, PVAGMA and the hydrogels.....105

Figure 3.8 Comparative XRD spectra of PVA, PVAGMA, SBMA and a hydrogel sample.....106

Figure 3.9 Comparative XRD of PVA AND PVAGMA.....107

Figure 3.10 FWHM for PVA.....108

Figure 3.11 FWHM for PVAGMA.....109

Figure 3.12 Compression stress-strain curves for cyclic (A) at 40% strain and compression to failure (B) at 70% strain for hydrogels.....112

Figure 3.13 Graph displaying the inter-relationship between the G', G'', G*, and tan d of hydrogel PM 100-SM0.....114

Figure 3.14 Graph displaying the inter-relationship between the G', G'', G*, and tan d of hydrogel PM 67-SM33.....115

Figure 3.15 Graph displaying the inter-relationship between the G', G'', G*, and tan d of hydrogel PM 88-SM12.....116

Figure 3.16 Graph displaying the inter-relationship between the G', G'', G*, and tan d of hydrogel PM 80-SM20.....117

Figure 3.17 Damping potential of the hydrogels.....118

Figure 3.18 SEM digital images of the planar and cross-sectional surface of dried hydrogels with SBMA: A (1-4) and without SBMA: B (1 -4) 119

Figure 3.19 Digital images of a sessile drop of water on some hydrogel samples 123

Figure 3.20 Chart of percent swelling as a function of degree of methacrylation. 124

Figure 3.21 Digital images of some hydrogels displaying their transparency.....126

Figure 3.22 Calibration curve (A) and a chart of total adsorbed protein on the hydrogels (B). 127

Figure 3.23 MTT assay against 3T3, HEK 293, and HREP cells at 24 and 48 hours.....129

Figure 3.24 Morphology of HREP cells before and after treatment with hydrogel extract.....130

Figure 4.1 FTIR analysis of empty and drug loaded transferosomes.....145

Figure 4.2 Differential scanning calorimetry of pure CysA, blank transferosomes, and Cyclosporine loaded transferosomes.....146

Figure 4.3 Digital images from SEM of transferosomes reflecting the impact of drug loading on the polydispersity and size of transferosomes 147

Figure 4.4 TEM images of lyophilized and un-lyophilized samples of CysA loaded transferosomes based on Span 80 and Tween 80. 148

Figure 4.5 Viability of HREP cells against CysA loaded transferosomes and blank transferosomes 151

Figure 4.6 Morphology of HREP cells treated with (A)CysA loaded Span transferosome; (B) blank span transferosomes, (C) blank tween transferosomes, (D) CysA loaded tween transferosomes, (E) ATF, and (F) before treatment.....152

Figure 4.7 Release profile from transferosomes: (a) In vitro release of CysA from transferosomes; (b) The predicted release profile based on the Korsmeyer–Peppas model. ..153

Figure 4.8 The predicted release profile versus actual release based on the Korsmeyer-Peppas model.....155

Figure 4.9 Corneal permeability of span 80 (A) and tween 80 (B) transferosomes.....156

Figure 5.1 Protein adsorption on hydrogel discs with differing SBMA content 169

Figure 5.2 *Ex vivo* protein adsorption using aqueous and vitreous humour.....170

Figure 5.3 SDS -PAGE of proteins adsorbed on hydrogels from *in vitro* studies.....172

Figure 5.4 SDS-PAGE of protein from *ex vivo* studies 173

Figure 5.5 Images showing the pattern of cell adhesion on the PM100-SM0 hydrogels (3 replicates). The first row represents the border between the well plate and the hydrogels; the middle row represents focus on the centre of the hydrogels; and the last row represents hydrogels after they were transferred to a fresh medium for the 3 hydrogel replicates…...175

Figure 5.6 Images showing the pattern of cell adhesion on the PM80-SM20 hydrogels (3 replicates). The first row represents the border between the well plate and the hydrogels; the middle row represents focus on the centre of the hydrogels; and the last row represents hydrogels after they were transferred to a fresh medium for the 3 hydrogel replicates…...176

Figure 5.7 Images showing the pattern of cell adhesion on the PM67-SM33 hydrogels (3 replicates). The first row represents the border between the well plate and the hydrogels; the middle row represents focus on the centre of the hydrogels; and the last row represents hydrogels after they were transferred to a fresh medium for the 3 hydrogel replicate…..177

Figure 5.8 Slit hydrogel showing that cells were attached on the well plate and not on the hydrogel 178

Figure 5.9 Graph showing the no of bacterial cells adhered to each hydrogel at different time points for *S. aureus*, (A) and *E. coli*, (B) 180

Figure 5.10 Time modulated variation in acute, chronic and granulation tissue inflammation and the effect of cellular immune factors on intensity. Reprinted from Monitoring and Evaluation of Biomaterials and their Performance In Vivo, S. Maity, A. Sarkar, Monitoring fibrous capsule formation: pg 69-80. Copyright (2017) with permission from Elsevier 182

Figure 5.11 Representative image of a rabbit eye just after implantation.....183

Figure 5.12 Digital image of PM67-SM33 hydrogel disc 8 weeks post implantation.....184

Figure 5. 13 Digital image of a hydrogel disc explanted after 8 week 185

Figure 5.14 The histopathological images reflecting the effect of implanted hydrogel discs on conjunctival tissues after 1 week. The blue arrows show the implant embedded in the tissue. 186

Figure 5.15 The histopathological images reflecting the effect of implanted hydrogel discs on conjunctival tissues after 4 weeks 187

Figure 5.16 The histopathological images reflecting the effect of implanted hydrogel discs on conjunctival tissues after 8 weeks. The blue slide is the explanted hydrogel implant 188

Figure 5.17 Size of collagen capsule formed around the implant after 1-, 4-, and 8-weeks implantation measured with Fiji (Image J).....189

Figure 5.18 Sample of collagen capsule measurement using ImageJ yellow measuring tool. .190

Figure 5. 19 SEM image of hydrogel disc explanted after 4 weeks. (A3 and A4). A1 and A2 are blanks of the same hydrogel at equivalent magnifications 190

Figure 5.20 SEM images of cells captured from two representative hydrogels explanted after 8 weeks.....191

Figure 5.21 Comparative FTIR of loaded and unloaded PM80-SM20.....193

Figure 5.22 FTIR of unloaded and preloaded PM80-SM20 194

Figure 5.23 DSC of transferosome preloaded, pure drug preloaded, and xerogel loaded by soaking.....195

Figure 5.24 Calibration curve of CysA at wavelength of 213 (A) and trend of release over time (B). 195

Figure 5.25 *In vitro* release profile for hydrogels in which CysA was loaded after (A) and before (B) crosslinking.....196

LIST OF TABLES

Table 2.1 Ocular implants in the horizon 34

Table 2.2 Marketed GDDs and materials of construction. Reproduced from (Br. J. Ophthalmol. "Glaucoma drainage devices; past, present, and future. Lim, B. Allan, A. Lloyd, A. Muir, and P. Khaw., Vol. 82, no.9, pp. 1083-1089, Sept. 1988.) with permission from BM.....53

Table 2.3 FDA approved drug delivery implants.....56

Table 2.4 Categories of surface modifications applied to ocular biomaterials 61

Table 3.1 FTIR Wave number assignments in PVA and PVAGMA.....95

Table 3.2 The FWHM for the component peaks in SBMA monomer, SBMA polymer, PVAGMA and PM89-SM11 110

Table 3.3 Mechanical parameters of the hydrogel samples compressed to failure at 70% strain. 113

Table 3.4 Porosity analysis for selected hydrogels.....121

Table 3.5 Water contact angle measurements 123

Table 3.6 Percent transmittance of hydrogels 125

Table 4.1 Composition of transferosomes.....142

Table 4.2 Size distribution and polydispersity of blank and loaded transferosomes.....143

Table 4.3 Effect of incorporation of linoleic acid on the stability of transferosomes.....144

Table 4.4 Stability profile of the transferosomes.....149

Table 4.5 Flexibility of the transferosomes.....150

Table 5.1 Composition of the hydrogels for *in vitro* CysA release.....168

Table 5.2 Cell types appearing in each subsection of the tissue……180

Table 5.3 Parameters from modeling release from hydrogels.....197

LIST OF APPENDICES

Appendix A Animal Ethics Certificate 207

Appendix B Oral presentation at the BRICS Conference hosted by South Africa November 2021. 208

Appendix C Certificate of participation for the PhD seminar competition, 2020 209

Appendix D Screenshot of the first page of publication 1……210

Appendix E Screenshot of the first page of publication 2……211

Appendix F Certificate of biofilm analysis..... 212

Appendix G Certificate for histopathological analysis 215

Appendix H Turnitin Report..... 216

Appendix I Oral presentation at the 13th cross faculty postgraduate symposium……217

CHAPTER ONE

INTRODUCTION AND THESIS OVERVIEW

1.1 Introduction

The eye is the second most complex organ in the body after the brain and contributes to about 85% to an individual's total knowledge. Ocular biomaterials (hereafter referred to as ocuterials) are increasingly playing major innovative roles in advancing ocular treatments for many functional deficiencies brought about by age, disease, and trauma. Demographics has also shown that most prevailing ocular pathologies will require one or more forms of ocuterial as drug delivery platforms, vitreous substitutes, intraocular and contact lens devices, corneal implants, keratoprosthetics and scleral buckles. The search for ocuterials is a continuum driven by the need to satisfy the conflicting material properties requirement often in similar or different applications. (Tummala et al. 2016) Biocompatibility, biodegradability, optical clarity, oxygen permeability, mechanical strength, low-cost, and non-fouling interfaces are some requirements for ocuterials with variations depending on specific applications. (Chen et al. 2018)

Fouling of biomaterials that involves adhesion of biofilms of microorganisms, proteins, and lipids has remained a challenge, amid efforts to design bio-interfaces, leading to inflammation, fibrosis, thrombosis, multidrug resistant infections, blockage (for filtration and sensor devices such as glaucoma drainage devices and diagnostic devices dependent on sensing signals from the body), and device rejection/failure in ocular implants such as glaucoma shunts, punctal plugs, intraocular lens, and soft contact lens. In contact lens, lipid and protein adsorption has also been implicated to reduce wettability leading to high attrition rates in contact lens wearers (Asbell 2017). Deposition of tear film lipids and protein starts within minutes of insertion into the eye resulting in tear film instability and malfunction of the ocular surface, sight threatening infections and clouding of the device. Posterior capsule opacification likewise is a severe complication which results from proliferation of lens epithelial cells across the path of vision on intraocular lenses after cataract surgery (Simon et al. 2015). It is only natural that as new inroads into ocular drug delivery are tending towards extended-release devices, there is an ever-increasing need to design new biomaterials amenable to extended application in the ocular space.

An ideal antifouling biomaterial should be electrically neutral, accept hydrogen bonding and incapable of donating hydrogen. (Ngo and Grunlan 2017) Many approaches have been explored and others commercialized for keeping the limits on fouling with various degrees of success. These include the use of cation grafted chemistries that act as biocides (though the use of antimicrobials usually leading to selection of resistant species over time), micro-patterned self-cleaning Lotus leaf bio-inspired surfaces (Xu et al. 2016), and the use of hydrophilic polymers to create a tight hydration layer that cannot be displaced by the protein. In the latter case, polymers like polyvinyl alcohol (PVA), polyvinyl pyrrolidine (PVP), polyethylene glycol (PEG) and more recently superhydrophilic zwitterionic polymers with unique capability for ligand immobilization have been used as surface or bulk coating materials to prevent fouling. Phosphoryl choline coupled polymers (2-methacryloyloxyethyl phosphoryl choline (MPC) are zwitterionics inspired from nature and were among the first to be used. Others that have been used include phosphobetaine, sulfobetaine and carboxybetaine. In addition, self-assemblies of nanomaterials acting as zwitterionics has also been explored. (Kopeček 2009)

A recent study explored MPC as an antifouling copolymer to produce a glaucoma filtration device (GDD) (Al-shohani, 2016) In addition, other polymers like polysaccharides and carbohydrates (dextran) inspired by the glycocalyx membrane that protects biological interfaces has been shown to have antifouling activity. (Seymour, Tucker, and Leach 2004) Their antifouling activity depends on prevailing conditions like the presence of cations. Synthetic polymer hydrogels such as polyurethane, 2-hydroxyethylmethacrylate (HEMA), polydimethylsiloxane (PDMS), and polymethylmethacrylate (PMMA) have traditionally been used in implantable ocular devices. In addition, natural polymers, such as collagen have found application as corneal shield and regeneration material, but its use is limited due to instability to collagenases. Others like silk are used as suture materials and rarely for corneal regeneration. (Palchesko, Carrasquilla, and Feinberg 2018) Antifouling materials should be able to maintain all the desirable properties of the implant material in addition to its antifouling activity. Unfortunately, currently synthesized antifouling polymers lack the inherent mechanical strength requirement for these devices when used alone due to their hydrophilic nature. Tectonic advancements have been made in biomaterials research particularly for tissue engineering utilizing a hybrid of natural and synthetic polymers, but these have rarely been applied to the ocular field.

This research therefore proposes to explore the potential of a novel ocuterial that will be developed from exploiting the inherent capabilities of a natural or semi-synthetic polymer

functionalized with antifouling groups amenable for use in the ocular environment. The challenge was to use a simple and economical fabrication method.

1.2 Rational and motivation for the study

A wide range of opportunities for designing new biomaterials lie in the field of ocular applications. These become more apparent as the underlying causes of treatment failure in ocular pathologies involving devices are exposed. A growing number of the world population is burdened with chronic and sight threatening pathologies that could benefit from ocuterials with biorelevant interfaces. The problem of dry eye has continued to plague a great number of people especially contact lens wearers despite efforts geared towards improving the material properties of the predominantly 'synthetic only' contact lens materials. A major cause is lipid and protein adsorption that mars the other excellent characteristics of these innovations. Incidentally, many of the bioinspired antifouling surfaces developed has scarcely been applied to the ocular field. In addition, the synthesis of many of the effective antifouling materials are extremely expensive and may account for the snail speed in reaching the market. Also, the challenging nature of delivering drugs to the eye is garnering concerted efforts by formulation scientists to try out hydrogels in the form of contact lens and implantable devices to reach the "unreachable posterior segment'' (Humayun et al. 2014). Likewise, many ocular diseases like cataract and glaucoma and dry eye at certain point may require surgery with implantation of devices that hitherto have been prone to failure because of protein adhesion in the long run (Peng et al. 2012).

The possibility of developing effective antifouling ocuterials is bioinspired from the naturally occurring glycocalyx that effectively keeps proteins and other adhesives at bay. Many natural polymers such as alginic acid, hyaluronic acid, dextran and dipalmitoyl phosphatidyl choline have been shown to have antifouling activity though with shortcomings bordering on stability for long term use. Others such as collagen and silk have excellent properties such as transparency, mechanical strength, viscoelastic properties that can be harnessed for ocular application. Silk and Hyaluronan have been shown also to have relieving effect on eye conditions like dry eye and hence may play an active role in alleviating it when used as a material of construction. (Colter, Wirostko, and Coats 2017) There is hope of improving compliance and patient outcomes through the use fabrication materials that minimize discomfort and frequent hospital visits.

An ocuterial, for instance, developed from conjugates of a natural polymer such as Hyaluronan, a synthetic polymer such as silicone, poly vinyl alcohol or polyurethane and, modified with or coupled with zwitterionic groups such as sulfobetaine, phosphobetaine, carboxybetaine will

produce an antifouling material with improved viscoelastic properties. **Figure 1.1** show a hypothetical reaction for such coupling.

The novelty of this study lies in the synergistic use of two polymers with limited mechanical robustness to achieve super hydrophilicity and superior strength reinforcement that enabled the anti-fouling potential and handing ability for ocular applications. For the first time, the possible influence of zwitterionics on enhancing and sustaining drug release from biomaterials was additionally explored.

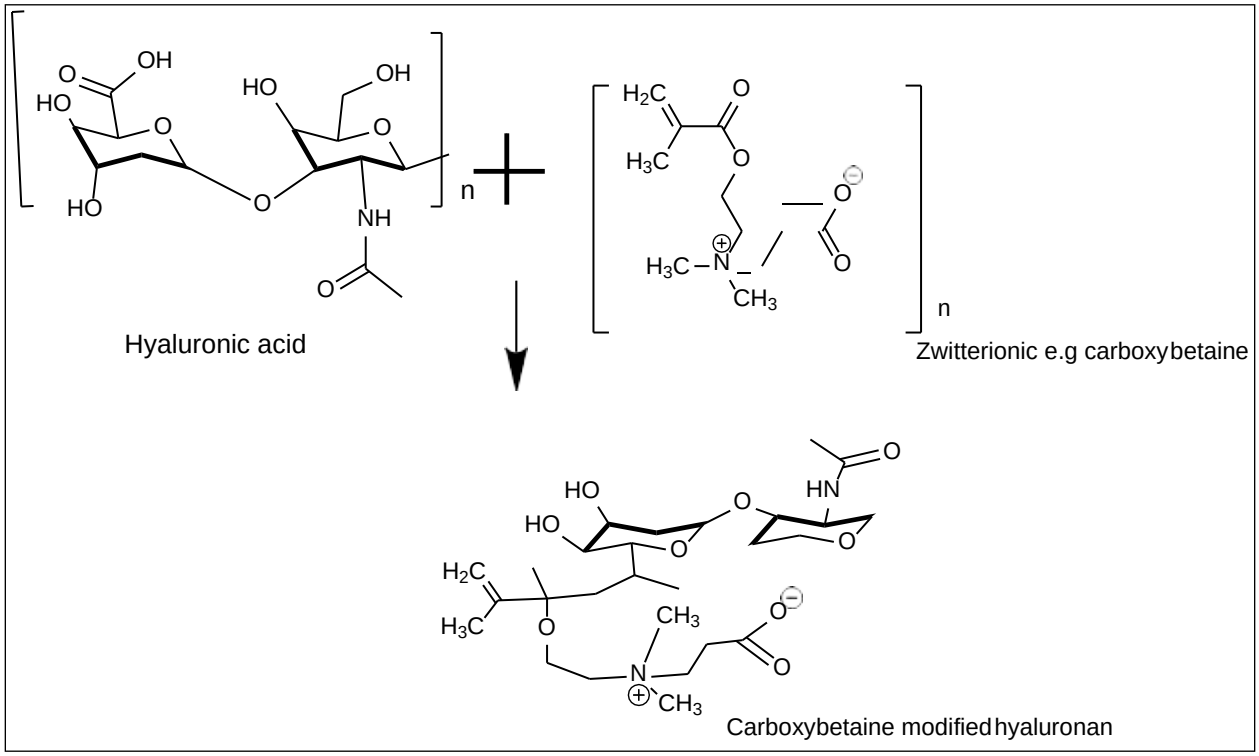


Figure 1.1 Pathway for zwitterionization of a typical natural polymer, Hyaluronan.

1.3 Aim and objectives of this study

The aim of this research was to develop a Bioinspired Protein Resistant Ocuterial (BioPROT) that by limiting protein adhesion may enable anti-fouling potential in implantable ocular applications (such as contact lenses, punctal plugs, intraocular lenses, etc.) that can double as drug delivery devices. Inclusion of protein drugs in the BioPROT will additionally solve the challenge of adsorption of protein drugs from primary packaging materials that leads to issue with dosage

uniformity. The success of such devices especially, as extended-release devices will depend on their ability to remain patent in the face of attack from the body's inflammatory response arsenal (a challenge additionally addressed by the protein resistance potential). Inspiration to modify the chosen base polymer with zwitterionics was drawn from its similarity to key membrane proteins such as taurine. To achieve this aim, the following specific objectives were employed:

1. Synthesis of the base polymer based on graft polymerization of a composite polymer such as Hyaluronan-g-methacrylate or PVA-g-methacrylate, through any suitable polymerization technique such as ring opening radical polymerization, and microwave assisted polymerization.
2. Functionalization of the ocuterial with antifouling zwitterionic groups through photo-initiated crosslinking polymerization, to yield the BioPROT.
3. Characterization of the developed BioPROT in terms of physicochemical properties such as micro and nano level mechanical strength and protein adsorption properties of the developed BioPROT in *vitro*.
4. Development of an applicable nano-based drug formulation (nano transferosomes) to be loaded into the BioPROT and evaluation of its *in vitro* release properties
5. Investigation of the ocular antifouling activity of, and the inflammatory response to the BioPROT in New Zealand albino rabbits through sub-conjunctival implantation in ocular tissue.
6. Evaluation of the *in vitro* release of a typical hydrophobic drug, cyclosporine A from the BioPROT.

1.4 Overview of the thesis

1.4.1 Chapter One

Chapter 1 of this thesis summarizes the background and rationale for the development of the BioPROT in the introduction. It further highlights the aim and objectives of the study and suggests possible applications. Protein adhesion is usually the first of many steps that will eventually culminate in fouling or biofouling, fibrous encapsulation, and potent inflammatory responses that may ultimately lead to device failure and sight threatening maladies. For ocular devices such as contact lenses, punctal plugs, and intraocular lens currently being positioned to additionally act as drug delivery platforms, it becomes very important that their material of fabrication will limit as

much as possible the protein adhesion step to which many ocuterials in current use are prone. (Uwaezuoke et al. 2021). The proposed ocuterial will by default eliminate or greatly reduce the unwanted effects in the applicable ocular device that occurs as a result of protein adhesion.

1.4.2 Chapter Two

In chapter 2, an in-depth review of literature is presented that explored the possible applications of protein resistant ocuterial as compared to what is currently available. The role of protein adhesion and by extension fouling in currently applied ocular devices are x-rayed. Additionally, different approaches to engineering protein resistance into ocuterials were examined through the lens of different studies that have ventured into this area. The importance of bulk modification, as against the current practice of surface modification, to the dynamic nature of the ocular environment was highlighted. Through this review, possible biomaterials to be used were identified based on the history of ocular use.

1.4.3 Chapter Three

Chapter 3 describes the synthesis, characterization, and optimization of the protein resistant ocuterial. Ease of manufacture and amenability to modification was considered in choosing a fabrication method. Photo-initiated crosslinking polymerization of a methacrylated polyvinyl alcohol with a zwitterionic monomer was used to achieve bulk zwitterionization of the base polymer. Optimization was necessary to achieve robustness in the mechanical properties of the developed ocuterial since it is known that zwitterionics and polymers with very high-water content were usually weak mechanically.

1.4.4 Chapter Four

Chapter 4 discusses the development and characterization of a nano transferosomal system as a potential system for inclusion of a hydrophobic drug into the hydrogel fabricated in chapter 3. Loading hydrophobic drugs into hydrogels has always proved challenging due to the wide differences in polarity, ultimately resulting in poor loading. Hydrophilic drugs on the other hand are relatively easier to load unto hydrogels but challenged by the ease and promptness of diffusion from such hydrogels resulting in immediate or very short release times. In addition, should a contact lens application be considered, a nano system becomes important so that transparency and light transmittance is not compromised.

1.4.5 Chapter Five

Chapter 5 details the evaluation of the various characteristics of the hydrogel that resulted from the protein resistance ability. Such features include cell adhesion, ex vivo protein resistance using aqueous and vitreous humour, and resistance to biofilm formation, In addition, cell adhesion and inflammatory response was evaluated *in vivo* in New Zealand albino rabbits.

Characterization of *in vitro* drug release was also undertaken and derives from the current positioning of implantable ocular devices as additional drug delivery platforms. Building on the understanding of the challenges that could arise from loading a hydrophobic drug into a hydrophilic hydrogel, different approaches were explored. Both the transferosomes prepared in chapter 4 and drug solutions were incorporated into both the formed hydrogel and the hydrogel precursor before crosslinking and the *in vitro* release evaluated.

1.4.6 Chapter Six

The limitations and challenges encountered in the course of this study were highlighted in this chapter. The chapter also presented the concluding remarks summarising what was done. Additionally, recommendations for future work were also presented in chapter 6.

1.5 References

Al-shohani, Athmar Dhahir Habeeb. n.d. “Hydrogel Formulations For Ophthalmic Delivery,” 244.

Asbell, Penny A. 2017. “Contact Lens Discomfort: Can We Prevent Dropout?” *Eye & Contact Lens* 43 (1): 1. https://doi.org/10.1097/ICL.0000000000000358.

Chen, Zhi, Jingjing You, Xiao Liu, Simon Cooper, Christopher Hodge, Gerard Sutton, Jeremy M. Crook, and Gordon G. Wallace. 2018. “Biomaterials for Corneal Bioengineering.” *Biomedical Materials* 13 (3): 032002. https://doi.org/10.1088/1748-605X/aa92d2.

Colter, Jourdan, Barbara Wirostko, and Brittany Coats. 2017. “Coefficient of Friction Between Carboxymethylated Hyaluronic Acid-Based Polymer Films and the Ocular Surface.” *Investigative Ophthalmology & Visual Science* 58 (14): 6166–74. https://doi.org/10.1167/iovs.17-22414.

Humayun, Mark, Arturo Santos, Juan Carlos Altamirano, Ramiro Ribeiro, Roberto Gonzalez, Alejandro de la Rosa, Jason Shih, et al. 2014. “Implantable MicroPump for Drug Delivery in Patients with Diabetic Macular Edema.” *Translational Vision Science & Technology* 3 (6): 5. https://doi.org/10.1167/tvst.3.6.5

.

Kopeček, Jindřich. 2009. “Hydrogels From Soft Contact Lenses And Implants To Self-Assembled Nanomaterials.” *Journal of Polymer Science. Part A, Polymer Chemistry* 47 (22): 5929–46. https://doi.org/10.1002/pola.23607

Ngo, Bryan Khai D., and Melissa A. Grunlan. 2017. “Protein Resistant Polymeric Biomaterials.” *ACS Macro Letters* 6 (9): 992–1000. https://doi.org/10.1021/acsmacrolett.7b00448.

Palchesko, Rachelle N., Santiago D. Carrasquilla, and Adam W. Feinberg. 2018. “Natural Biomaterials for Corneal Tissue Engineering, Repair, and Regeneration.” *Advanced Healthcare Materials*, May, e1701434. https://doi.org/10.1002/adhm.201701434.

Peng, Cheng-Chun, Michael T. Burke, Blanca E. Carbia, Caryn Plummer, and Anuj Chauhan. 2012. “Extended Drug Delivery by Contact Lenses for Glaucoma Therapy.” *Journal of Controlled Release: Official Journal of the Controlled Release Society* 162 (1): 152–58. https://doi.org/10.1016/j.jconrel.2012.06.017

Seymour, Graham B., Gregory Tucker, and Lop A. Leach. 2004. “Cell Adhesion Molecules in Plants and Animals.” *Biotechnology and Genetic Engineering Reviews* 21 (1): 123–32. https://doi.org/10.1080/02648725.2004.10648051.

Simon, V., T. Radu, A. Vulpoi, C. Rosca, and D. Eniu. 2015. “Microscopic and Spectroscopic Investigation of an Explanted Opacified Intraocular Lens.” *Applied Surface Science* 325 (January): 124–31. https://doi.org/10.1016/j.apsusc.2014.10.178.

Tummala, Gopi Krishna, Thomas Joffre, Viviana R. Lopes, Aneta Liszka, Oleksiy Buznyk, Natalia Ferraz, Cecilia Persson, May Griffith, and Albert Mihranyan. 2016. “Hyperelastic Nanocellulose-Reinforced Hydrogel of High Water Content for Ophthalmic Applications.” *ACS Biomaterials Science & Engineering* 2 (11): 2072–79. https://doi.org/10.1021/acsbiomaterials.6b00484.

Uwaezuoke, Onyinye J., Pradeep Kumar, Viness Pillay, and Yahya E. Choonara. 2021. “Fouling in Ocular Devices: Implications for Drug Delivery, Bioactive Surface Immobilization, and Biomaterial Design.” *Drug Delivery and Translational Research*, January. https://doi.org/10.1007/s13346-020-00879-1.

Xu, Quan, Wenwen Zhang, Chenbo Dong, Theruvakkattil Sreenivasan Sreeprasad, and Zhenhai Xia. 2016. “Biomimetic Self-Cleaning Surfaces: Synthesis, Mechanism and Applications.” *Journal of the Royal Society Interface* 13 (122). https://doi.org/10.1098/rsif.2016.0300

CHAPTER TWO

FOULING IN OCULAR DEVICES: IMPLICATIONS FOR DRUG DELIVERY, BIOACTIVE SURFACE IMMOBILIZATION, AND BIOMATERIAL DESIGN

Drug Delivery and Translational Research (2021) 11:1903–1923
https://doi.org/10.1007/s13346-020-00879-1

REVIEW ARTICLE

Fouling in ocular devices: implications for drug delivery, bioactive surface immobilization, and biomaterial design

Onyinye J. Uwaezuoke[1] · Pradeep Kumar[1] · Viness Pillay[1] · Yahya E. Choonara[1]

Accepted: 24 November 2020 / Published online: 16 January 2021
© Controlled Release Society 2021

Abstract
The last 30 years has seen a proliferation of research on protein-resistant biomaterials targeted at designing bio-inert surfaces, which are prerequisite for optimal performance of implantable devices that contact biological fluids and tissues. These efforts have only been able to yield minimal results, and hence, the ideal anti-fouling biomaterial has remained elusive. Some studies have yielded biomaterials with a reduced fouling index among which high molecular weight polyethylene glycols have remained dominant. Interestingly, the field of implantable ocular devices has not experienced an outflow of research in this area, possibly due to the assumption that biomaterials tested in other body fluids can be translated for application in the ocular space. Unfortunately, progression in the molecular understanding of many ocular conditions has brought to the fore the need for treatment options that necessitates the use of anti-fouling biomaterials. From the earliest implanted horsehair and silk seton for glaucoma drainage to the recent mini telescopes for sight recovery, this review provides a concise incursion into the gradual evolution of biomaterials for the design of implantable ocular devices as well as approaches used to overcome the challenges with fouling. The implication of fouling for drug delivery, the design of immune-responsive biomaterials, as well as advanced surface immobilization approaches to support the overall performance of implantable ocular devices are also reviewed.

Keywords Biomaterials · Ocular · Fouling · Protein adsorption · Implantable device · Drug delivery · Immune responsive

Abbreviations

MEMS	Microelectromechanical systems
DME	Diabetic macular edema
AMD	Age-related macular degeneration
FBR	Foreign body response
GDD	Glaucoma drainage device
TF	Tissue factor
PMN	Polymorphonuclear leucocytes
ACAID	Anterior chamber-associated immune deviation
ROS	Reactive oxygen species
TLR	Toll-like receptors
PRR	Pattern recognition receptor
HMGB 1	High mobility group box 1
MCP	Monocyte chemotactic protein
MIP 1β	Macrophage inflammatory protein 1β
DC	Dendritic cells
CLs	Contact lens
IPN or ipn	Interpenetrating polymer networks
MPC	2-Methacryloyloxyethyl phosphorylcholine
PMPC	Poly(2-methacryloyloxyethyl) phosphorylcholine
PSiMA	Poly(bis(trimethylsilyloxy)methylsilylpropyl glycerol methacrylate)
IOL	Intraocular lens
ACO	Anterior capsular opacification
PCO	Posterior capsule opacification
FGF	Fibroblast growth factor
LBL	Layer by layer
ASC	Anterior subcapsular cataract
MIGS	Minimally invasive glaucoma surgery
TBO	Trabeculectomy
TBE	Trabeculectomy
GFS	Glaucoma filtration surgery
MMPC	2-(Methacryloyloxy)ethyl-[N-(methacryloyloxy)ethyl phosphorylcholine
BSA	Bovine serum albumin
FIH	First in humans

✉ Yahya E. Choonara
yahya.choonara@wits.ac.za

[1] Wits Advanced Drug Delivery Platform Research Unit, Department of Pharmacy and Pharmacology, School of Therapeutic Sciences, Faculty of Health Sciences, University of the Witwatersrand, Johannesburg 2193, South Africa

2.1 Introduction

Ocular implants have been promoted as being able to overcome patient compliance issues and other limitations with chronic topical ocular drug administration (Neves 2013). The physiological and anatomical structures of the eye maintain a formidable barrier to prolonged contact and drug release from topical eye drops and hence have become a trade-off for invasive implantable devices (Du Toit et al. 2013), (Subrizi et al. 2019). It is therefore not surprising that the current landscape for ocular drug delivery comprises a host of implantable devices (**Table 2.1**) that ranges from simple contact lenses to advanced electroscope/cameras that can aid the blind eye. Such devices also include platforms for ocular fluid drainage in glaucoma, punctal plugs, polymeric drug reservoirs, microfluidic devices, microelectromechanical systems, scleral buckles, and diagnostic devices. These devices are becoming increasing common for treating a variety of difficult-to-treat (due to anatomical and physiological barriers) anterior and posterior segment eye diseases and disorders (Choonara et al. 2006). Incidentally, the demand for such devices will continue to increase with the steady increase in the life expectancy of patients since most chronic eye diseases such as age-related macular degeneration (AMD), cataract, diabetic macular edema (DME) and retinopathy are age related (Humar et al. 2016). Consequently, the demand for newer biomaterials that are ocular compatible has also increased.

The advanced ocular implantable technologies available today began a journey over 100 years ago, with the first device consisting of horsehair implanted in 1906 by Rollet (Cullen 2007) and an intraocular lens in 1949 by Ridley (Lim et al. 1998). Continuous innovation has led to the development of a wide range of synthetic, semi-synthetic and natural biomaterials and bioadhesives (including nano-enabled systems) for use as ocular implants (Toit et al. 2011). Hence, ocular devices have become routine as part of treatment modalities provided by ophthalmologists (Humar et al. 2016). Nevertheless, the available ocular biomaterials are not without application constraints in terms of mechanical appropriateness, ocular toxicity, biodegradability profile and desirable surface properties such as their bio-inertness or anti-fouling features. Several researchers have produced disruptive innovations to overcome these challenges particularly for implantable ocular devices.

Table 2.1 Ocular implants in the horizon

Implant	API	Company	Development stage	Ocular site	Reference
BIM ring	Bimatoprost	ForSight VISION5	ii	Fornix	(Brandt et al. 2017)
iDose™	Travoprost	Glaukos Corp.	iii	Intracameral	(Glaukos Corporation, 2018)
OTX-TP	Travoprost	Ocular Therapeutix	iib	Intracanalicular	(Walters et al, 2020)
Dextensa	Dexameth asone	Ocular Therapeutix	iii	Intracanalicular	(Ocular Therapeutix, 2019)
Implant	Dexameth asone		Preclinical Development	Suprachoroidal	(Barbosa Saliba et al. 2016)
Magnetic micropump	Ranibizumab	Replenish Inc.	i	subconjuctival	(Humayun et al. 2014)
Triggerfish®	sensor	SENSIMED	iv	Corneal	(Dunbar et al. 2017)
Port delivery system	Ranibizum ab	Genetech	ii	Vitreous	(Campochiaro et al. 2019), (C. Wang et al. 2018)

Fouling is the accumulation of cellular matter or bio-organisms on non-biological surfaces (biomaterials) when such biomaterials are found in contact with fluids or tissues in an environment. The ocular space as a biological environment is discussed in this review. Fouling is initiated within seconds of implanting a device in the body. The first step in fouling is the non-specific protein adsorption onto the surface of the device closely followed by the cascade of scarring, blockage, and possible failure of the devices to function as expected (Vassileva 2018). When microorganisms are the foulants, this is termed biofouling (Bixler Gregory D. and Bhushan Bharat 2012). Fouling is an integral part of the self-preservation, foreign body response cascade by which a surface (perceived by the body as intruding) is cordoned off in a collagenous capsule (Onuki et al. 2008). Fouling presents a significant challenge in terms of device and treatment failure as well as the potential for life threatening complications to the patient (Chen et al. 2010). With certain devices such as the contact lens, proteins are the only foulants and the effect of fouling may be limited to diminishing lens performance whereas with other ocular devices it can progress to a full foreign body response (FBR) resulting in device failure. Therefore, the development of biomaterial surfaces that are resistant to protein adhesion, being the first and limiting step to fouling, is critical to ensure optimum device performance (Chen et al. 2010) and often presents a clue to device bio-inertness and biocompatibility (Zhang, Zhang, and Deng 2018).

Prior to the prolific use of polymers for designing implantable devices, metals, and their alloys such as gold, silver, stainless steel, platinum, and cobalt, were used for the bio-fabrication of such devices. Others that followed include ceramics, pyrolytic carbon, and composites (Chirila and Harkin 2016). However, polymeric biomaterials are now predominantly used due to their bio-mimetism, relative light weight and flexibility, processability, versatility, tunable physical properties, and amenability to functionalization for advanced ocular drug delivery. In addition, continuous innovation has yielded biomaterials that can elicit a stimuli-responsive function in the ocular space (Bawa et al. 2009) (du Toit et al. 2014).

Biopolymers used for intraocular drug delivery can be broadly classified as either biodegradable or non-biodegradable. The process of fouling has more significance for non-biodegradable devices than biodegradable systems. Whereas biodegradable polymers are inherently biodegraded in concert with the mechanisms of drug release, non-biodegradable polymers remain intact representing a continuous “threat” and therefore, a focus of attack by the body’s defence mechanism. Paradoxically, bio-fabricated scaffolds and implants used in tissue engineering applications such as those for corneal transplantation must support protein adhesion, cell

proliferation and integration for efficacy. In keratoplasty, a biodegradable biomaterial is used to replace, repair, or regenerate a diseased of destroyed cornea. The biomaterial must support the attachment, migration, and proliferation of corneal cells to enable the integration of the newly placed biomaterial into the ocular surface (Isaacson, Swioklo, and Connon 2018).

Ocular implantable devices vary with respect to their application i.e., either for diagnostics, drug delivery or tissue replacement. Some have overlapping function such as theragnostic devices (Xie, Lee, and Chen 2010). Contemporary drug delivery devices may be made up of various components depending on the application. The components of such devices that make direct contact with the ocular environment needs to be rendered biocompatible. Hence, polymers such as polyvinyl alcohol (PVA), poly (1-2-vinyl pyrrolidinone) (PVP), polymethyl methacrylate (PMMA), poly (hydroxy ethyl methacrylate) (PHEMA), ethylene-vinyl acetate (EVA), poly(propylene) and silicone have been used extensively in the production of many commercially available ocular devices. Also, studies have shown that these polymers can be made anti-fouling in laboratory experiments (Pop-Georgievski et al. 2013). However, multiplicity of issues that have hindered the translation of biomaterials developed at lab scale to clinical use have been compounded by the relative lack of harmonized experiments and disease models. For instance, Ronbeck and colleagues (2014) compared the posterior opacification outcomes in different intraocular lenses namely, round edge heparin surface modified PMMA, round edge silicon and sharp edge hydrophobic acrylic (Rønbeck and Kugelberg 2014). Despite having three different biomaterials all also had three different modifications effectively making objective comparison difficult. This means that it may not be clear whether the best performing intraocular lens is as a result of specific modification or material properties. In addition, many biomaterials that have been developed to inhibit the protein adhesion step of fouling have performed well under *in vitro* test conditions (i.e., in the presence of one or two-proteins) but perform poorly under more complex in *vivo* test conditions. This reflects the relative lack of optimal models for *in vitro* experimentation (Jiang and Cao 2010).

The ocular space is uniquely different from other confined areas of the body in many aspects. It is an immune privileged environment and therefore, the inflammatory response differs. This requires modifications to intraocular devices that are customizable to either the anterior or posterior segment of the eye (Onuki et al. 2008) as there are reported instances of failed performance of biomaterials or devices within the ocular environment that performed well in other areas of the body as an implant. Ayyala and co-workers (1999) evaluated a biomaterial, Vivathane, developed and tested for heart valve function (McKeown et al. 1993) and developed

the biomaterial as a glaucoma drainage device (Ayyala et al. 1999). Its performance in the eye was abysmal relative to results obtained in the heart. It may be possible that fouling played a significant role in failure of the biomaterial or device for intraocular application. Therefore, this review provides a concise incursion into the phenomenon of fouling applied to ocular implantable devices to achieve bio-inertness and biocompatibility. It examines different devices such as topical vision correcting contact lenses as well as intraocular lenses, telescopes/camera devices, glaucoma drainage systems, punctal plugs for treating dry eyes, scleral buckles for correcting retinal detachments and ocular inserts for advanced drug delivery to the posterior and anterior segments of the eye. In each of these areas, emphasis is placed on the influence of fouling on device performance and its implications for drug delivery and the future development of ocular biomaterials.

2.2 The impact of fouling in the ocular environment

The response of the eye to an implanted device generally comprises two phases. The first phase is an inflammatory response involving acute and chronic stages and aimed at repairing the surgical wound from implant insertion. The second phase is an immune response to ‘’eliminate’’ the implant. Each phase is preceded by the adsorption of proteins from the injured blood vessels, ocular fluids, and tissues to form a film, that constitutes the foulant, on the implanted device (Gullapalli et al. 2013). Usually, the device surface is enclosed within a complex fusion of adsorbed proteins based on affinity for the biomaterial. According to the Vromans effect (Hoffman 1999), even though the types of adsorbed proteins may transition over time, the quantity remain stable due to the inability of proteins to absorb non-specifically to the monolayer. The properties of the device such as surface charge, matrix stiffness, rugosity, physiochemical characteristics, and topography play a significant role in determining the quantity and composition of the protein biofilm during fouling (Ferrari, Cirisano, and Morán 2019). **Figure 2.1** depicts the activation of the coagulation cascade, compliment, and platelet adhesion through different but interconnected pathways in response to an implanted device. Factor XII, XIIa and Tissue Factor (TF) work concurrently in the coagulation cascade to release thrombin followed by platelet activation to form a transient blood cloth matrix from fibrin deposition. Complement proteins such as polymorphonuclear leucocytes (PMN) and monocytes activated through pathways C1 to C5 can sense fibrinogen adsorbed onto the surface of devices (biomaterials) and induces platelet activation as well as cell adhesion that leads to a coagulation cascade. The extracellular matrix (ECM) releases fibronectin and vitronectin that regulate the inflammatory process and facilitate the fusion of macrophages to foreign body giant cells on the device. This either increases

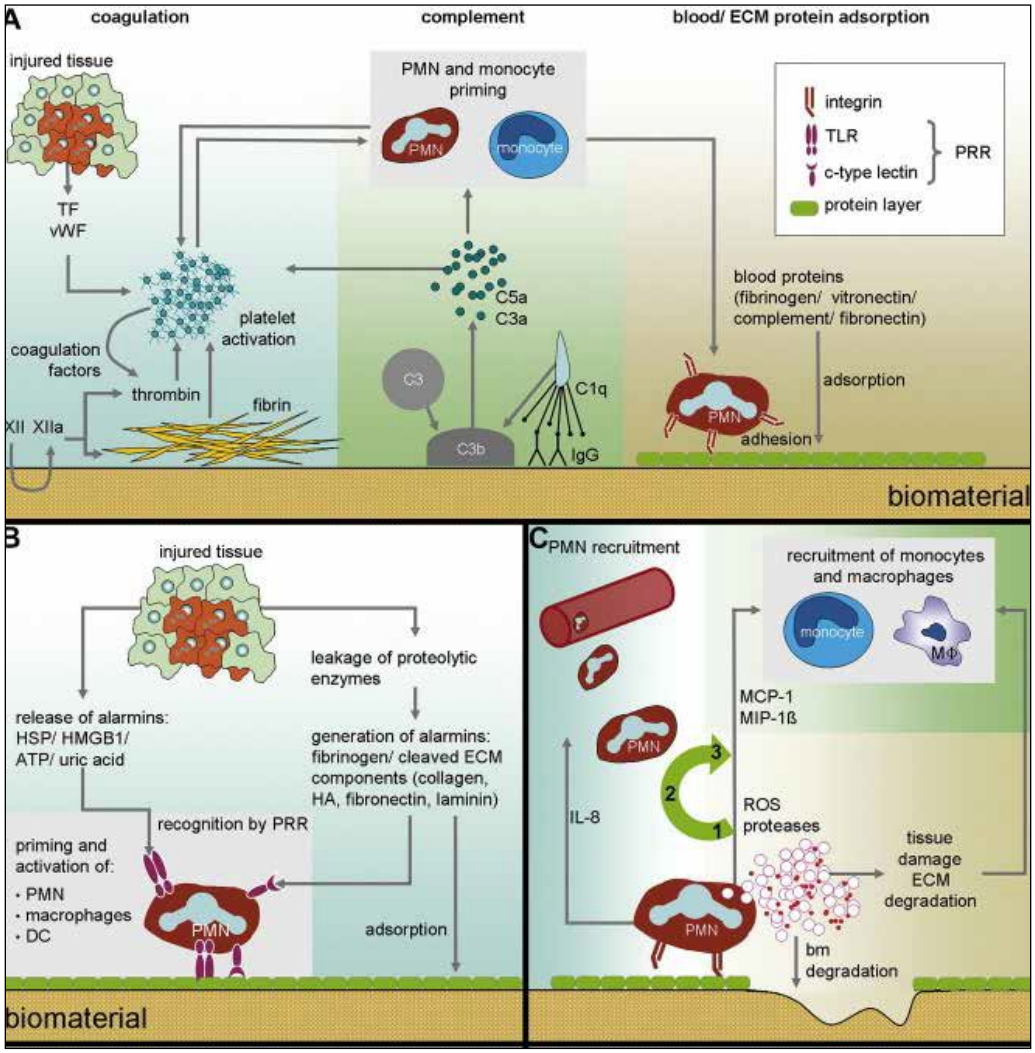


Figure 2.1 Protein adhesion, coagulation cascade and complement activation with consequent release of PMN and macrophages. B. Damaged tissue releases which lead to further immune response. C) Continued inflammatory response leads to release of proteolytic enzymes and reactive oxygen species (ROS) which may damage the biomaterial surface. Adapted from Biomaterials, vol.32, no. 28, S. Franz, S. Rammelt, D. Scharnweber, and J. C. Simon, "Immune responses to implants - A review of implications for the design of immunodulatory biomaterials," Copyright (2011) with permission from Elsevier (Franz et al. 2011).

inflammation or assists in wound healing. Persistent stimuli will lead to the chronic inflammatory stage with the release of T lymphocytes and Natural Killer Cells (NKC). The implanted device becomes engulfed in a collagenous sheet which stimulates angiogenesis or neovascularization

(Kohn et al. 2010) (Puleo and Bizios 2009). The foreign body response to implanted devices (or biomaterials) varies in different regions of the eye. A more detailed description of the processes is provided in other reviews of the literature (Mariani et al. 2019) (Franz et al. 2011). The eye is a regionally immune privilege organ and when the blood-ocular barriers are intact, the inflammatory immune response is limited to the anterior chamber, vitreous, and subretinal space, while the cornea, iris, ciliary body, retina, and subconjunctival space are prone to regulated immune functions (Masli and Vega 2011). T regulatory cells secreted by the Anterior Chamber-Associated Immune Deviation (ACAID), corneal endothelial cells and retinal pigment epithelial cells are together responsible for maintaining the immune privilege status of the ocular micro-environment (Keino, Horie, and Sugita 2018). In any case, the degree of immune privilege of any part of the eye can be compromised by factors such as the disease state and surgical invasiveness.

2.3 The extent and implications of fouling in implanted ocular devices

Several anatomical sites in the eye are amenable to the implantation of ocular devices ranging from contact lens devices for vision correction and drug delivery, intraocular lenses, glaucoma drainage devices and predominantly intravitreal devices for sustained and site-specific drug delivery (Davis, Gilger, and Robinson 2004) (**Figure 2.2**). The extent of fouling associated with these devices is critical in order to evaluate device performance and varies with implantation site and in severity of adverse outcomes. Excessive fibrosis in the formation of a bleb for certain glaucoma drainage devices has been shown to be responsible for up to 50 % of resulting complications ("US Patent Application for Compositions, Systems, And Methods For Scar Tissue Modification Patent Application (Application #20190117746 Issued April 25, 2019) - Justia Patents Search" n.d.). Outcomes of protein adsorption on contact lenses has been shown to depend not only on the quantity of adsorbed protein but also on the quality, speed of adsorption and the location (Veys, Meyler, and Davies 2020). Protein denatured by interaction with contact lens biomaterial can lead to discomfort, may trigger immune reactions such as contact lens papillary conjunctivitis, and may lead to dry eyes as an inflammatory outfall (Mann and Tighe 2013). Likewise, biofilm formation with consequent bacterial adhesion also results in inflammatory response such as contact lens induced red eye and peripheral ulcers (Willcox 2019). These adverse events lead to approximately 50 % drop out in contact lens wearers (Fonn 2007).

2.3.1 Contact lens (CL) devices

Contact Lens (CL) devices are designed to be inserted onto the tear fluid layer covering the cornea and were originally intended for vision enhancement but has morphed to include cosmetic applications and for therapeutic drug delivery. CLs are not considered as implantable devices

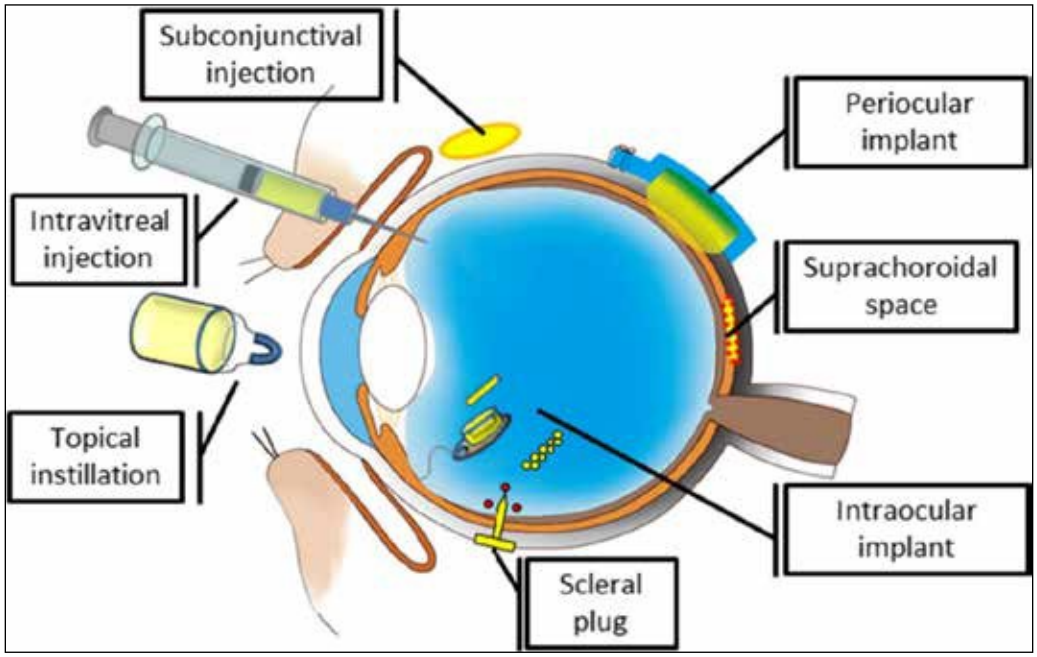


Figure 2.2 Possible sites of ocular implant placement. Adapted from Adv. Drug Deliv. Rev., vol. 128, pp. 148–157, H. Kaji, N. Nagai, M. Nishizawa, and T. Abe, "Drug delivery devices for retinal diseases," Copyright (2018) with permission from Elsevier ((Kaji et al. 2018))

(Chirila and Harkin 2016) but its intimate contact with the eye surface and increasing propensity to be used as a drug delivery device has necessitated its inclusion in this review. Although fouling does not proceed further than the initial protein adhesion step in CL devices, changes in the secondary structure of proteins adsorbed on the CL device leads to changes in the tear fluid, causes possible dehydration of the cornea, and may reduce visual acuity. Incidentally the tear fluid is very rich, (though in varying proportions) in simple and complex proteins such as lysozyme, lactoferrin, albumin, fibronectin and vitronectin (Willcox 2019). Once in contact with the tear fluid, these proteins are adsorbed to the CL device surface and this interaction causes changes in the adsorbed protein's secondary structure (Jacob 2013). These denatured proteins can trigger inflammatory immune response which contributes to the 12-15 % adverse events in

properly fitted CLs (Jacob 2013). On the other hand, adsorption of certain proteins such as lysozyme and lactoferrin can lead to a reduction in viable bacterial count and an improvement on the antimicrobial properties of the adsorbed proteins (Willcox 2019). This effect, however, depends on the co-adsorption or otherwise of other competing proteins. In the case of lactoferrin and lysozyme, the effect of adsorbed lysozyme on *P. aeruginosa* depends on the amount of lactoferrin co-adsorbed (Willcox 2019). It is worthy of note that the nature of the interaction with the biomaterial surface (Veys, Meyler, and Davies 2020) greatly determines the outcome of such Interaction. CL devices were introduced over 50 years ago by Wichterle and Lim (Hui 2017). Since then, there has been a continuous improvement on the biomaterial properties to optimize functionalities that limit the perceived drawbacks over time. The early approaches to incorporating drugs into CLs involved immersion into drug solutions that resulted in bursts of drug release (Choi and Kim 2018). As nanotechnology emerged, so did CLs containing drugs dispersed as nanoparticles (Nasr et al. 2016) (Lu et al. 2013), nanomicelles (Mandal et al. 2017), nanoliposomes (Danion, Arsenault, and Vermette 2007) and nano-emulsions (Katzer et al. 2014). However, these nano-colloidal systems affected the transparency of CLs and modified the properties of the pre- and post-lens tear fluid (Lattimore, Harding, and Williams 2018). In order to overcome this challenge different archetypes of CL inserts such as rings (Lorenz et al. 2014) and sandwiches (Choi and Kim 2018) emerged. Goda and colleagues (2009) also improved the surface properties of PDMS with 2- (methacryloyl)ethyl-[N-(2- methacryloyl) ethyl]phosphorylcholine (MMPC) crosslinked 2 methacryloyloxyethylphosphorylcholline (MPC) and showed that it minimized protein adhesion in the ocular environment (Goda et al. 2009). Maulvi and coworkers (2016) developed a CL loaded with hyaluronan formed as a ring outward from the centre to prevent vision obstruction (**Figure 2.3**) (Maulvi et al. 2017). Other researchers designed CLs in the form of nanowafers containing an array of nano-enabled drug-reservoirs for sustained drug delivery (Yuan et al. 2015). Ciolino and colleagues (2014) demonstrated that careful choice of components can minimize the effect of drug loading on the transparency of drug loaded CLs (Ciolino et al. 2014). The continuous improvement of biomaterials has seen a comparative exponential progression in the number of CL users and serves as a catalyst for the design of newer biomaterials with properties that can improve CL platforms for drug delivery (Maulvi, Soni, and Shah 2016). **Figure 2.4** depicts the progressive market shift of various types of CL biomaterials in the US for 2018 and 2019 (Jason and Nichol 2018) In addition, the limitations of topical eye drops and the invasiveness of intravitreal implants for treating posterior segment eye diseases have positioned CLs as the ocular drug delivery device of the future. This limitation, for topical instillation, arises because the

bioavailability of topically administered drops rarely exceeds 5 % due to the short residence time and rapid tear turnover (Peng, Burke, et al. 2012). On the other hand, this limitation for intravitreal implants arises due to the corneal enforced, limited accessibility of topically administered drugs to the posterior segment. Peng and co-workers (2012) demonstrated that the CLs device can be

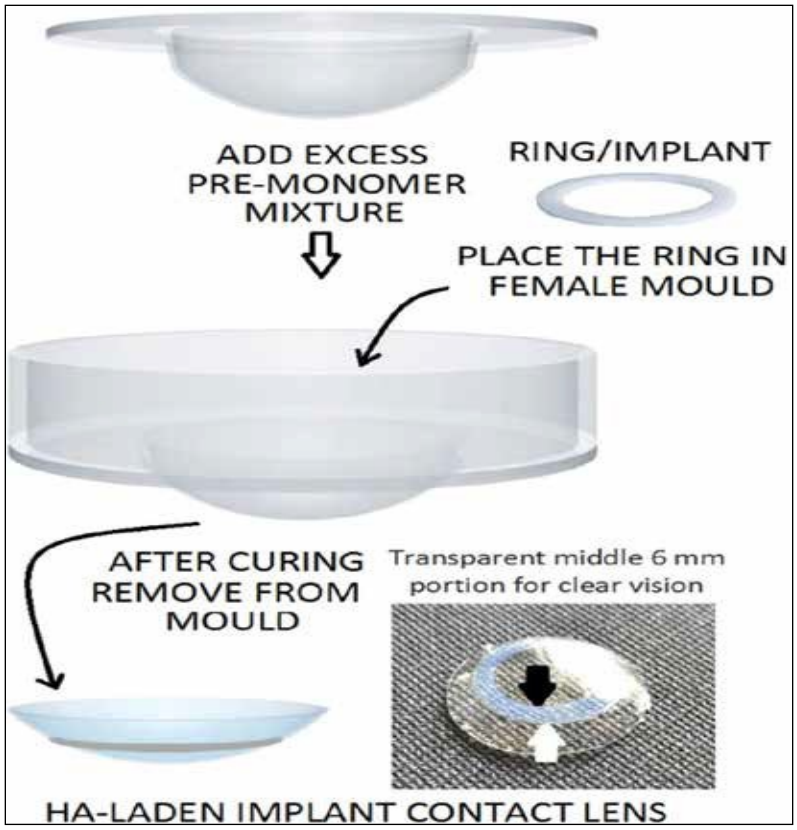


Figure 2.3 Contact lens with hyaluronan ring prepared by cast molding. Reprinted from Acta Biomater., vol. 53, no. 15, F. A. Maulvi, A. A. Shaikh, D. H. Lakdawala, A. R. Desai, M.M. Pandya, S. S. Singhania, R. J. Vaidya, K. M. Ranch, B. A. Vyas, D. O. Shah "Design and optimization of a novel implantation technology in contact lenses for the treatment of dry eye syndrome: In vitro and in vivo evaluation". Copyright (2017) with permission from Elsevier. (Maulvi et al. 2017)

used as a platform to extend the release and by extension, bioavailability of a topically administered timolol in beagle dogs (Peng et al. 2012). Studies by Ross and colleagues (2019) showed that the contact lens device can be used to overcome the formidable corneal barrier and deliver dexamethasone, over several Weeks to the retina in a non-invasive application

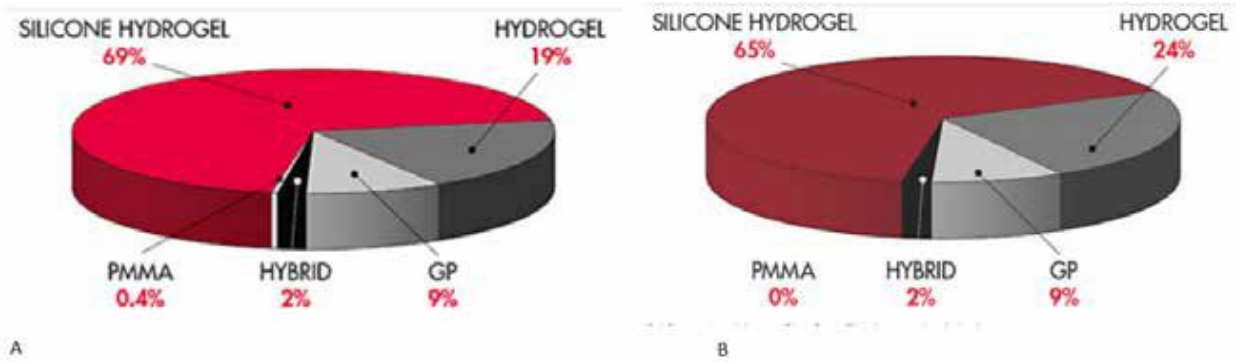


Figure 2.4 2018 (A) and 2019 (B) prescription of CL by material in the US courtesy of Jason J. Nichols, OD, MPH, PhD. Adapted and Reused with permission from the January 2019 and January 2020 issues of Contact Lens Spectrum.

(Ross et al. 2019). DiPasquale and co-workers (2018) developed a CL device based on a silicon hydrogel in which receptor sites are embedded for commonly used ocular drugs, particularly antibiotics and anti- inflammatory agents via molecular imprints. These sites create strong affinity between the drug and the CL thereby achieving sustained drug release (DiPasquale and Byrne 2016).

The prediction that CLs can do more than correct vision is also witnessed in the design of the Triggerfish® device (Dunbar et al. 2017). Triggerfish® is a CL device made up of a sensor designed to detect changes in the cornea that arises from the constantly changing aqueous humor volume in glaucomatous eyes over a 24-hour period. This platform could also be used as a micro-electromechanical system (MEMS) as proposed by Lee and coworkers (Lee et al. 2012) for drug delivery. Similarly, in pursuit of more non-invasive ocular technologies, Badugu and co-workers (2018) developed a CL device comprising a silicon hydrogel inter-penetrating network (IPN) that was conjugated with glucose sensitive fluorophores (Quin C18) that fluoresced in inverse proportion to the concentration of glucose absorbed (Badugu, Reece, and Lakowicz 2018). With an appropriate UV detection device, the concentration of glucose in tear fluid was accurately measured from the CL under conditions of minimal disturbance of the tear fluid to enhance the reliability of measurements. It should be noted that the insertion and prolonged wearing of CL devices has not always been comfortable for patients and had led to instances of poor compliance. Approximately 50 % of contact lens wearers experience some form of discomfort till date (Omali et al. 2015). Proteins and lipids are the main foulants in CLs and this fouling constitutes the major source of discomfort experienced with the wearing of CL devices.

These foulants are adsorbed from tear fluid and results in conformational changes in cationic lysozymes and lactoferrin that are predominantly present (Peng et al. 2015). In addition, certain forms of keratitis, dry eye syndrome (Krysztofiak and Szyczewski 2014) and even blurring of the lens (Zhang et al. 2017) (Choi and Kim 2018) can result. The surface modification of biomaterials has been a predominant method of limiting fouling in silicon hydrogels used in the design of CL devices. The surface modification has been shown to reduce the protein adhesion step (Chirila and Harkin 2016) due only temporarily to the fluid dynamics involved. The major categories of soft contact lens biomaterial currently in use were classified by the International Organization for Standards, ISO. These are predominantly silicone hydrogels and hydrogels and their susceptibility to protein or lipids adsorption is illustrated in **Figure 2.5**. According to ISO, group II materials conventionally contain silicone and represented by non-ionic hydrogels with medium to high content water. Group IV materials are ionic and contains fluorine rather than silicone. It can be seen from **Figure 2.5** that both group ii and iv materials attract a high level of proteins. Shimizu and colleagues (2010) developed a CL polymeric biomaterial based on random block copolymers, Poly (MPC-co-SiMA) and an IPN, (MPC-ipn-PSiMA), of silicone base material, (bis(trimethylsilyloxy)methylsilylpropyl glycerol methacrylate) (SiMA) and poly (2-methacryloyloxyethyl phosphorylcholine) (MPC). **Figure 2.6** shows the result of protein adsorption studies of the IPN, (MPC-ipn-PSiMA), the block copolymers, Poly (MPC-co-SiMA), and a commercially available CL device. MPC-ipn-PSiMA and Poly (MPC-co-SiMA) containing 30 % and 39 % of MPC respectively had the least protein adsorbed indicating a reduction in fouling (Shimizu et al. 2010).

2.3.2 Intraocular lens (IOL) devices

Intraocular lens replacement following phacoemulsification has been the standard of cataract treatment as the most common lens disorder. (Nanu et al. 2018) Cataract is the leading cause of reversible blindness. With over 20 million surgeries annually, cataract surgery is the most commonly performed procedure not requiring hospitalization (Humar et al. 2016) (Thrimawithana et al. 2018). Before the introduction of phacoemulsification (that reduced the time spent in surgery and utilizes minimal 2.8 mm incisions) by Kelman and coworkers (1979), cataract extraction involved creating large incisions that resulted, in addition to other complication, astigmatism (Callahan 1979) (Nanu et al. 2018). Despite advanced micro-incisive.

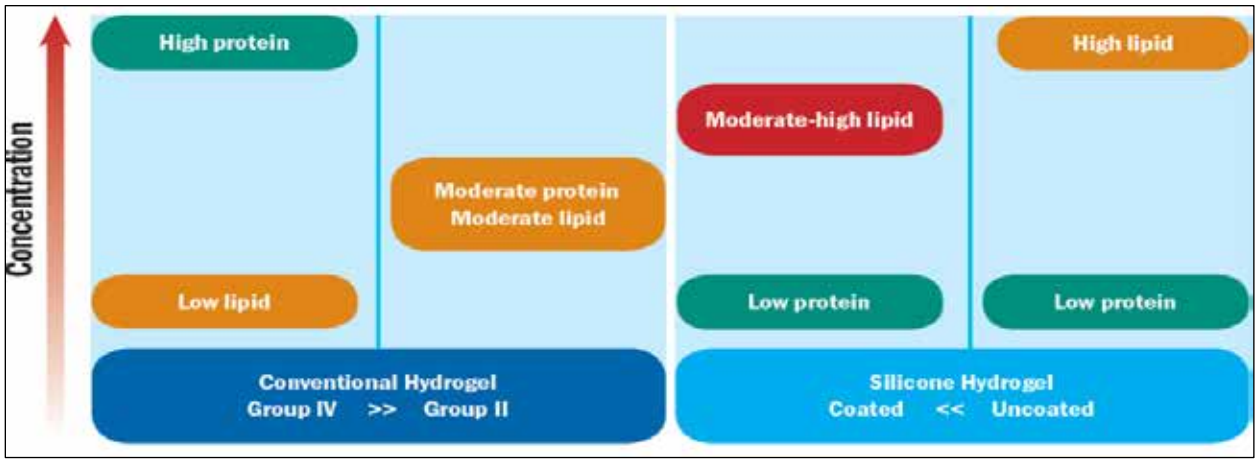


Figure 2.1 Schematic illustration of trends in lipid and protein deposits on different contact lens materials Adapted from (68). Mann A and Tighe B. Contact lens interactions with the tear film. Experimental Eye Research, 2013;117:88-98) with permission from Elsevier.

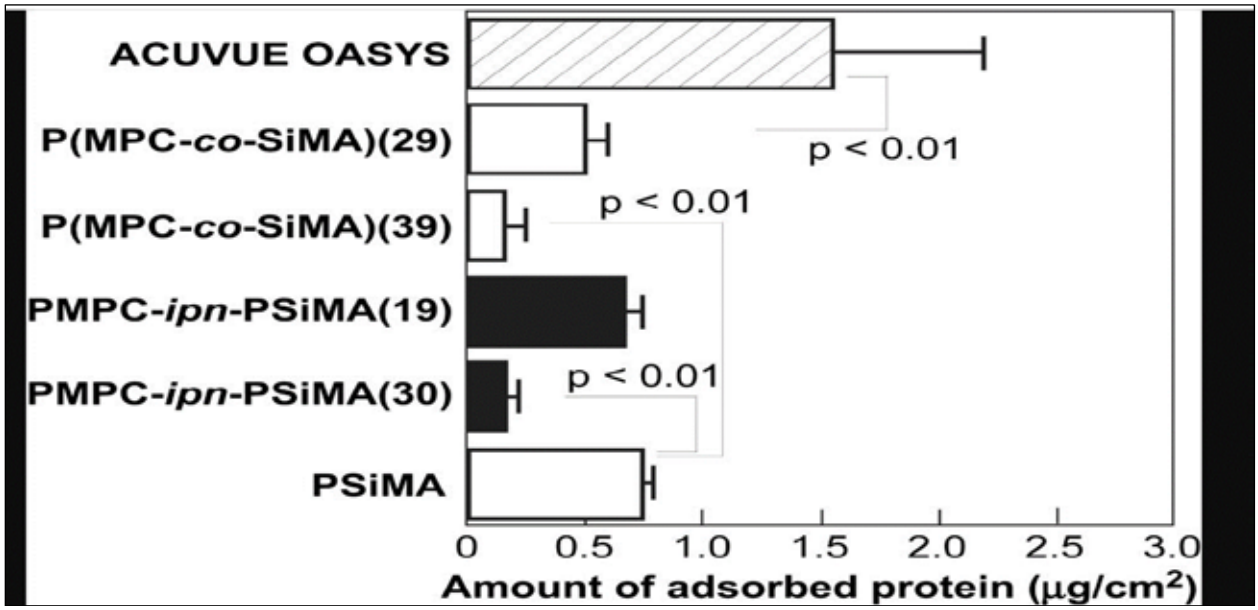


Figure 2.2 Quantity of protein adsorbed on modified silicone; (MPC-ipn-PSiMA), Poly (MPC-co-SiMA), and marketed ACUVUE OASYS. Reprinted from Biomaterials, vol. 31, no. 12, T. Shimizu, T. Goda, N. Minoura, M. Takai, and K. Ishihara, "Super-hydrophilic silicone hydrophilic silicone hydrogels with interpenetrating poly (2-methacryloyloxyethyl phosphorylcholine) networks," Copyright (2010) with permission from Elsevier (Shimizu et al. 2010).

phacoemulsification, the prospects of complete success in cataract surgery remains limited by posterior and anterior capsule opacification (PCO and ACO). These usually necessitates a second procedure (Nd-YAG laser capsulectomy) causing further complicated and serious adverse events (Hucknall, Rangarajan, and Chilkoti 2009). Although the anterior chamber of the eye is an immune privilege site, the injury caused by the surgical incision (however minimal) leads to the disruption of the blood-aqueous barrier and influx of inflammatory cells that will eventually lead to PCO and ACO. ACO is often, initiated by protein and lens epithelial cell adhesion (mediated by integrin) while migration and proliferation (mediated by fibroblast growth factor, FGB) leads to PCO. Simultaneously, the presence of inflammatory cytokines in the aqueous humor with the surgical incision promotes opacification of the newly implanted lens (Xu et al. 2016). Fibronectin and fibrin have been identified as the major proteinaceous adsorbing components on Rabbit eyes implanted with IOL devices (Kochounian et al. 1994) and may contribute to the formation of fibrinous uveitis after phacoemulsification (Han et al. 2018). While ongoing efforts such as the use of antioxidants are targeted at the prophylaxis of cataract, there is an immediate need to improve the outcomes of surgical treatment for approximately 40% of adults and 100% of children patients affected by cataract surgery complications annually (Qin et al. 2017) (Chirila and Harkin 2016).

It has been established that the most important factors predisposing to PCO and ACO are the surface properties of the biomaterial used and the design of the IOL device (Chen et al. 2019) (Pérez-Vives 2018). These remain a recurring challenge in determining the outcome of cataract surgery. In order to reduce PCO, cataract surgery is always followed by the administration of topical drops containing proliferation inhibitors and antibiotics (Han et al. 2018). From topical drops, ophthalmologists began immersing IOL devices into drug solution of proliferation inhibitors before insertion. However, drug loaded IOL devices afforded drug release as a bolus over a short period of time (Liu, Wong, and Mehta 2013) and efforts geared towards the use of drug loaded IOL devices for site-specific drug delivery to minimize post-surgical inflammation have continued.

Adjunctive therapy with anti-inflammatory agents (and antioxidants) has also effectively brought to the fore the possibility of using IOL devices for vitreo-retinal drug delivery (Han et al. 2018). Han and co-workers (2018) developed a drug eluting IOL device by condensing doxorubicin (DOX) into chitosan nanoparticles prepared by polyelectrolyte condensation between cationic chitosan and tripolyphosphate (Han et al. 2018). The DOX-loaded chitosan nanoparticles were loaded into the IOL device using Layer-by-Layer (L-b-L) assembly to achieve a multi-layered IOL device. The DOX concentration increased as the layering increased. Previously high dose

dexamethasone-loaded devices (such as Ozurdex®) were implanted into the posterior chamber in an additional surgery that led to cataract development in pristine lenses due to the multiplicity of surgical invasions in the ocular space particularly in patients with co-existing morbidities such as glaucoma (du Toit et al. 2014). Rugose device surfaces (comparatively sharp and rounded device edges) have also been shown by several researchers to retard protein adhesion as the first step to limit fouling (Kao, McCanna, and Jones 2011). Auffarth and coworkers (2003) evaluated the effect of edge design of IOL devices on PCO development (Auffarth et al. 2003) and found a close correlation between the edge type and development of PCO. Findl and co-workers (2005) also confirmed that rounded edges preferentially predisposed to PCO than sharper edge designs (Findl et al. 2005). Consequently, there has been a concerted effort to improve the design of IOL devices through the development of biomaterials that limit the protein adhesion step in fouling. Early attempts at improving the properties of IOL devices involved the use of coating materials such as Teflon (Werner et al. 1999), F+ ion (Li, Cui, and Gu 1999) and titanium (Wang et al. 2013). Current modifications focus on using super hydrophilic polymers and heparin (Haldar et al. 2014) as coating materials. Xu and coworkers (2016) examined the effect of pegylation on the biocompatibility of a silicon hydrogel-based IOL device in rabbits (Xu et al. 2016). In their study a commercially available silicon hydrogel-based IOL device was compared against a polydimethylsiloxane (PDMS)-based device designed in their lab. Although statistically weak, there was claimed difference in posterior capsule hyperplasia from histology studies between the pristine and pegylated IOL device as shown in **Figure 2.7**.

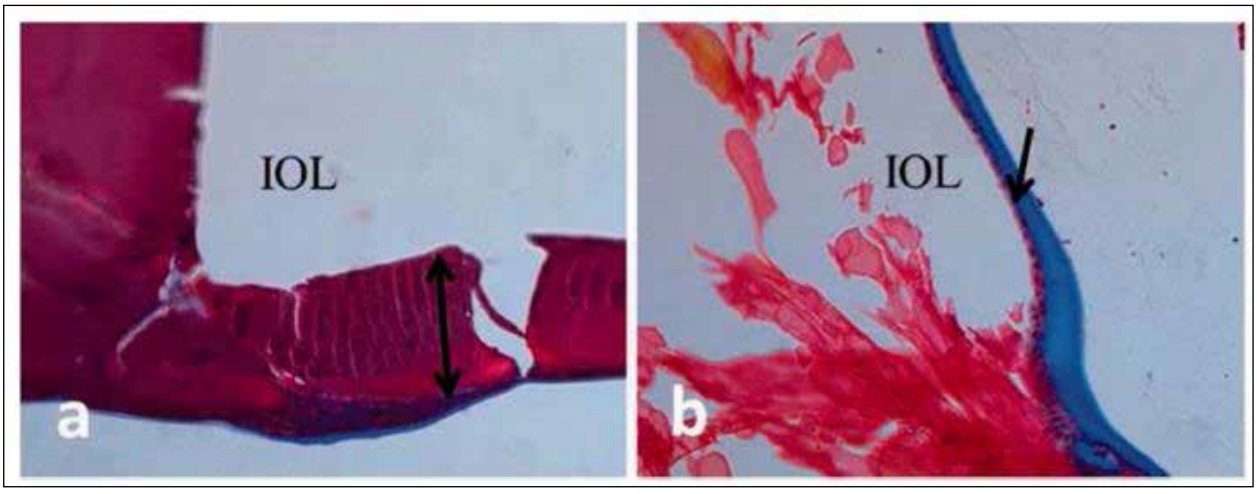


Figure 2.7 Light Photomicrograph of the a) Pristine b) pegylated IOL. The arrow shows the magnitude of posterior capsule hyperplasia. Reproduces with permission from (104).

Similarly, Tan and colleagues (2017) demonstrated the uveal and capsular biocompatibility of surface modified hydrophobic IOL devices. They modified the surface by plasma grafting of copolymers of MPC and methacrylic acid with the aim of utilizing the expected synergistic action between the negatively charged hydrophilic polymers to minimize the interaction between adhering protein and the IOL devices thereby reducing inflammatory response (Tan et al. 2017). Qin and co-workers (2017) elucidated the role played by syndecan-4 in the signalling pathway of integrin and fibroblast and hence a possible therapeutic target for limiting capsular opacification (Qin et al. 2017). They induced injury in the lens capsule and monitored anterior subcapsular cataract (ASC) formation in both wild type rats (WT) and syndecan-4 (SDC-4) deficient rats. The wild type rats developed ASC within 3 days while syndecan-4 deficient group barely exhibited ASC as shown **Figure 2.8**. This could be charting a course for ocular biomaterials conjugated or ligated with Syndecan-4 inhibitors as immunomodulatory materials for effective non fouling applications. Molokhia and coworkers also proposed the capsule drug ring - a possible refillable drug reservoir (**Figure 2.9**) that was intended to take advantage of the unfilled space left in the lens capsule after surgery. The group demonstrated the proof of concept using a protein drug Avastin® to achieve the release of the drug *in vitro* (Molokhia et al. 2010).

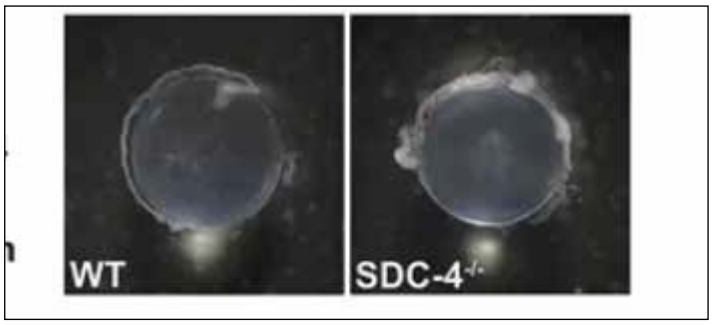


Figure 2.8 The effect of syndecan-4 in the development of ASC. Reprinted from (Qin et al. 2017).

2.3.3 Glaucoma drainage (GD) devices

Glaucoma is the leading cause of irreversible blindness, and the aetiology is based on optic nerve damage resulting from the proliferation of inflammatory cytokines in the presence or absence of chronically elevated intraocular pressure (IOP) (Pan, Brown, and Ziaie 2006) (Natarajan et al. 2012). It has been shown that elevated IOP leads to the multiplication of inflammatory cytokines *ab initio* (Kent 2015).

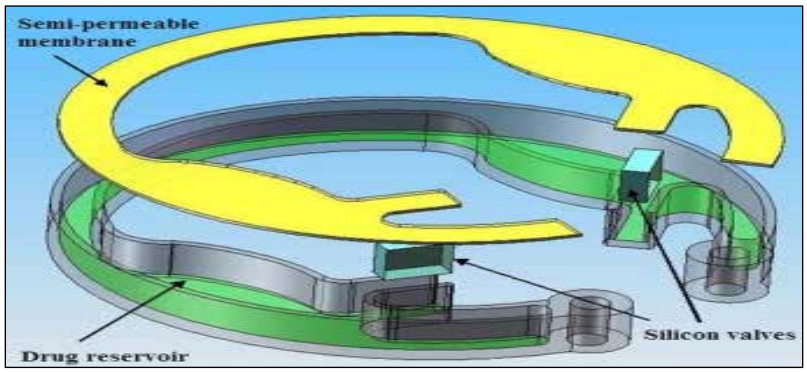


Figure 2.9 Schematic representation of the capsule drug ring. Reprinted from Vision Res., vol. 50, no. 7, pp. 680–685, Sarah A. Molokhia, Himanshu Sant, Jacquelyn Simonis, C.J. Bishop, R.M. Burr, Bruce K. Gale, Balamurali K. Ambati "The capsule''.

The therapeutic management of glaucoma is aimed at lowering IOP either by reducing aqueous humor production or by increasing its outflow through various procedures such as trabeculoctomy (TBO), trabeculectomy (TBE), minimally invasive glaucoma surgery (MIGS) and the use of GD devices. While β-blockers, carbonic anhydrase inhibitors, α2 adrenergic agonists and prostaglandin analogues are the first line drugs for primary open angle glaucoma (which is the most common type) (Li et al. 2016), glaucoma filtration surgery (GFS) is reserved for patients in whom the maximum tolerated drug therapy fails to lower IOP (Salim et al. 2019). TBO involves the removal of some components of the trabecular mesh in a bid to improve aqueous humor flow. It is the glaucoma filtration surgical procedure of choice (Lim et al. 1998). TBE is the creation of an ostium into the interior chamber from under a scleral flap that leads to the formation of a filtering bleb (Sali et al. 2019). GD device surgery (also called tube shunts) presents an alternative to TBO as an initial procedure or in the event of failure (Ko, Papadopoulos, and Khaw 2015). GD devices have traditionally been used to physically drain aqueous humor in conditions of high IOP and has the capacity to maintain flow consistency and reduce hypotony (Kent 2015). Fouling of GD devices. resulting from foreign body response to the device ultimately causes fibrosis and closure of blebs in GFS and around GD device plates. Currently, antimetabolites such as mitomycin C, 5- fluorouracil (Mercieca et al. 2018) and pirfenidone [86] are often used to manage inflammatory response that leads to the fouling of GD devices.

Unfortunately, the life span of the most innovative GD device does not exceed 5 years (Lim et al. 1998) due to fibrosis, scarring and blockage leading to device failure (Behzad Amoozgar et al. 2017). An attempt to undo scar-induced blockages of GD devices involved the use of an enzyme injection that dissolved the fibrocystic tissue. However, the sustainability of this approach remains to be tested ("Enzyme Injection to Reopen Blocked Ocular Drainage Devices in Glaucoma Patients - 15872 - University of Florida Office of Technology Licensing" n.d.). The most important factors in the fouling of a GD device are the nature and design of the biomaterial used for the fabrication of the device. Elevated IOP always results in the build-up of proinflammatory cytokines in the aqueous chamber. GD devices by design must be able to withstand the surge of pro- inflammatory cytokines in the aqueous chamber post-insertion of the device. The FBR process can be impeded if there is a way of reducing the level of Transforming Growth Factor β-2 (TGFβ-2) that is induced by the high IOP and elevating the level of pro-apoptotic FAS-ligand that promote fibrosis resolution. Various attempts have also been made to modify the biomaterials for constructing GD devices in order to minimize fibrosis. Ayyala and coworkers (1999) explored Ahmed GD devices (propylene), Baerveldt GD devices (silicone) and a third material Vivathane® developed by the university of southern Florida and used in a magnetically actuated left ventricular assist device (Ayyala et al. 1999). Their findings supported an earlier study by the same authors (Ayyala et al. 1998) on the comparative inertness of silicone over the other biomaterials. Acosta and coworkers (2006) also evaluated the biocompatibility of a novel polymer hybrid polystyrene–polyisobutylene triblock polymers (Quartromer™) as a possible GD device biomaterial. The properties were compared to that of PDMS and found to be superior (Acosta et al. 2004). Likewise, Choritz and colleagues (2010) demonstrated the influence of surface topography on the long-term performance of GD devices (Choritz et al. 2010). The surface evenness of four commercially available GD devices were studied using scanning electron microscopy (SEM) and cell proliferation studies. Results obtained indicated that the smoother surfaces (through a combination of mechanical stimulation and early cell attachment) were less prone to fibrosis and may be why anti-inflammatory agents are less effective in minimizing GD device's fibrosis. **Table 2.2** provides a list of selected commercially available GD devices and their biomaterial of construction.

Table 2.2 Marketed GDDs and materials of construction. Reproduced from (Br. J. Ophthalmol. "Glaucoma drainage devices; past, present, and future. Lim, B. Allan, A. Lloyd, A. Muir, and P. Khaw., Vol. 82, no.9, pp. 1083-1089, Sept. 1988.) with permission from BM

GDDs	Year introduced	Tube diameter/Material	Plate size/Material	Resistance mechanism
Molteno	1979	0.63 mm OD 0.30 mm ID Silicone	135 mm^2 Polypropylene	None
Baerveldt	1990	0.63 mm OD 0.30 mm ID Silicone	200, 250, 350, 500 mm^2 Silicone	None
Krupin with disc	1990	0.58 mm OD 0.38 mm ID Silicone	180 mm^2 Silicone	Slit valve
Ahmed	1993	0.63 mm OD 0.30 mm ID Silicone	185 mm^2 Polypropylene with silicone	Venturi valve
Optimed model 1014	1995	0.56 mm OD 0.30 mm ID	140 mm^2 Silicone with PMMA matrix	Microtubules

Note: OD = outside diameter, ID = inside diameter

Historically, the efficiency of most GD devices was measured at 70% with an annual failure rate of 10 % predominantly caused by device scarring (Patel and Pasquale 2010). With improvement in the design of biomaterials with anti-fouling properties, minimally invasive devices and procedures are now preferred. In 2006, Pan and co-worker designed an artificial nano drainage implant that exploited MEMS miniaturization technology to produce a nanoporous mesh mounted at one end of a polymeric shaft (Pan, Brown, and Ziaie 2006) to drain aqueous humor via the uveo-scleral pathway. The nanopores also prevented bacterial invasion while PEGylation of its silanol grafted surface provided anti-fouling properties (improved bio-inertness). Similarly, Amoozgar and colleagues (2017) used the concept of a micro-fluidics meshwork to replace the plate in traditional GD devices (Behzad Amoozgar et al. 2017) (**Figure 2.10).** In 2018, Ahmed and coworkers started first in human trials of a minimally invasive glaucoma surgery (MIGS) device known as MINIjet® and developed by iSTAR medical SA ("Investigational MIGS Device Could Minimize Fibrotic Response" 2017). The injectable device comprises medical grade soft and flexible porous silicone that utilizes the uveo-scleral pathway for draining aqueous humor. The device pores are coated with a loose collagen capsule after bio-integration such that each drainage pore remains viable for a long time. Another MIGS-based stent, Xen45® gel (a gelatin-based stent) was developed by Allergan has also been evaluated (Chaudhary et al. 2018), (Buffault, Baudouin, and Labbé 2019). This injectable implant is made from collagen derived gelatin and crosslinked with glutaraldehyde. Studies shows that there was no fibrosis for the duration of the study (Lewis 2014).

2.3.4 Intravitreal devices

Intravitreal devices are a group of implants designed from biodegradable and non-biodegradable biomaterials used to target posterior segment eye diseases that often require chronic management (Choonara et al. 2010). Posterior segment eye diseases/disorders being predominantly age related and chronic are on the increase as a result of prolonged life expectancy. Unfortunately, because of the inaccessibility of drug molecules to the posterior segment from current topically administered eye drops or therapeutic inserts, intravitreal injections of drug have become the mainstay of intraocular therapy. To further complicate matters, most bio actives used to treat retinal diseases are macromolecules that are easily degraded and necessitate frequent intravitreal injection and specialized molecular carriers. A selection of FDA-approved retinal inserts is shown in **Table 2.3**.

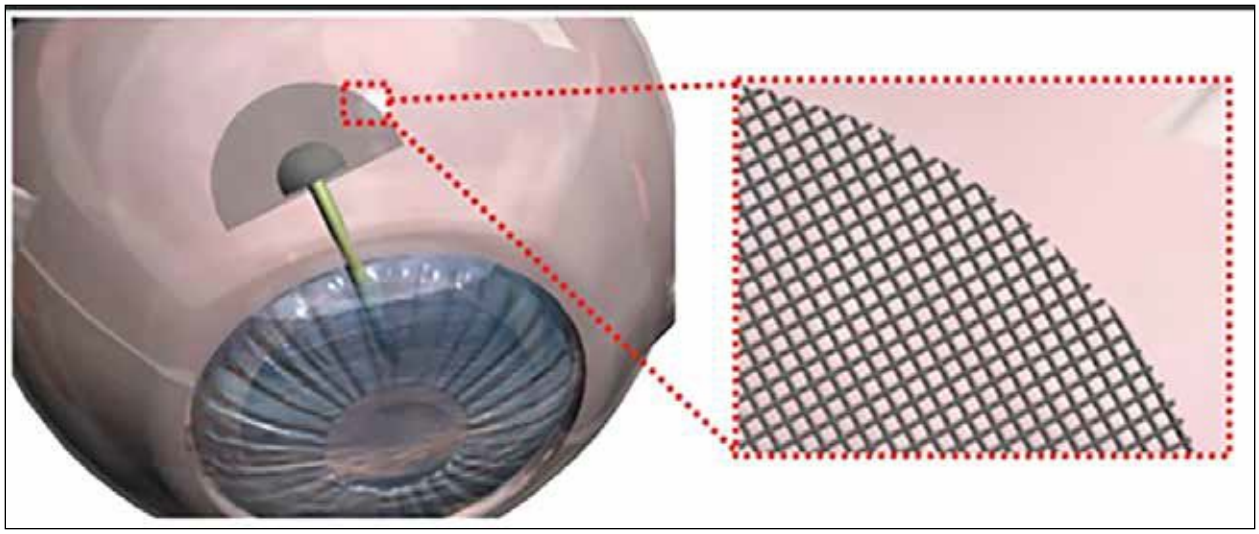


Figure 2.10 An illustration of the microfluidic meshwork that replaced the plate of a traditional GDD. Reproduced from. (Behzad Amoozgar et al. 2017)

Biodegradable intraocular devices are designed from biomaterials (polymers) that are easily degraded by enzymes in the body. The rate at which drug is released depends on the rate of biodegradation. The predominantly used biodegradable polymers in commercially available intravitreal devices comprise polylactide (PLA), poly (lactic-co-glycolic acid) (PLGA) and hydroxypropylmethyl cellulose (HPMC). For non-biodegradable polymeric devices, polyvinyl alcohol (PVA), ethylene vinyl acetate (EVA), and silicone have been mostly used. PVA is highly hydrophilic and if used alone will result in rapid drug release. It is therefore frequently used in combination with hydrophobic EVA to control drug release over a prolonged period. For certain devices the biomaterial contributes significantly to an FBR as shown in a study with the intravitreal device Retisert®. The increased incidences of PCO in all phakic patients compared with those treated with drug alone (Wang et al. 2013) was seen as a confirmation of this contribution. Another major complication is the dislocation of the drug reservoir posing serious sight threatening danger (Chang et al. 2015). Du Toit and colleagues (2014) developed an intelligent intraocular implant as a stimuli-responsive system to deliver ciprofloxacin and indomethacin to the posterior segment (du Toit et al. 2014). The bio-responsive polymer matrix developed was targeted to be switched on and off in response to inflammation. Even though fouling was not important for the biodegradable implant, the smart response to inflammation elicited could be the basis of engineering non-biodegradable devices that minimize fouling through inflammation prevention.

Table 2.3 FDA approved drug delivery implants.

Implant	API	company	Material	Size (diameter.length) /implant style	Approximate Duration of release /strength	Approval Year	Reference
Ozurde®	Dexamethasone	Allergan Inc	PLGA	0.46mm x 6mm /0.7 mg	6months/0.7 mg	2009	(Frère et al. 2017) (Lowder et al. 2011
Retisert®	Flucinolone acetonide	Bausch &Lomb	PVA/Silion	1.5mm x 6mm x (2 mm wide)/surgical insertion	30 months/0.5 9 mg	2005	(Pearson et al.2011)
Illuvein®	Flucinolone acetonide	Alimera Sciences	PVA matrix in Polyimide tube	3.5 mm x 0.37mm/ Intravitreal injection with 25G needle	36 months/0.7 mg	2014	(Campochiaro et al. 2012)
Vitasert®	Ganciclovir	Bausch & Lomb	PVA/EVA	(Pellets)4.5mg/	8months/4.4 mg	1996	(Martin et al.1994)
Surodex®	Dexamethasone	Oculex Pharmaceuticals Inc.	PLGA/HPMC	1 mm x 0.4 mm/ Intracameral insertion with 25G needle	10 days/0.06 mg		(Liu, Wong, and Mehta 2013)
DEXYCU™	Dexamethasone	Eyepoint Pharmaceutical Inc.	Durasert™ Technology	Intraocular suspension/Intracameral injection	21 days/0.52 mg	2018	(Donnenfeld et al. 2018)
YUTIQ™	Flucinolone acetonide	Eyepoint Inc.	Durasert™ Technology	Microinsert/intravitreal in a preloaded applicator	36 months/ 18 mg	2018	(Jabs et al. 2013)

Several researchers are working on micro pump (MP) refillable devices for intravitreal implantation with many granted patents in this regard although none have been approved by the FDA for commercial availability. First in Human trials on MP devices that reported promising results was undertaken in 2014 by Humayun and co-workers. They aimed at establishing device safety and surgical practicality (Humayun et al. 2014). MPs are designed to deliver predetermined doses of drug to the retina (posterior segment) or to the anterior segment with each comprising wireless charging (with bidirectional communication with the device) and drug refilling capability (reservoir-based).

2.3.5 Miscellaneous ocular devices

Other devices (or biomaterials) implanted (or used) in the ocular space include scleral buckles, punctal plugs, corneal bandages, and orbital prosthetics. These are considered separately in that their frequency of use is relatively low, and their site of implantation (or insertion) is not confined to a single area within the ocular environment. However, these devices may also present with fouling and ultimately lead to device or therapy failure.

Scleral buckles are (drug-free) devices used to reconnect detached retina to sub-retinal tissues (Lloyd 2001). Retinal detachment can result from many ocular procedures such as chronic intravitreal injections or implantation of devices. Scleral buckles are currently made from silicone elastomers and earlier systems comprised hydrogels but were discontinued due to late-stage swelling. Scleral buckles also present an approach that can be used for site-specific drug delivery although this has rarely been explored. Reabsorbable pigskin gelatin-soaked with antibiotics was used at one point but development of low grade inflammatory response that can escalate limited its use (Williams et al. 2019). In addition, hydrophilic hydrogel materials such as MIRAgel that had great potential for drug delivery was introduced about forty years ago but late complications arising from swelling of the matrix also stopped its use (Thompson and Chambers 2016).

Punctal plugs (similar to canalicular plugs) are small, elongated pellets used to block the lacrimal duct to limit tear drainage (Song et al. 2018). It is used to treat dry eye syndrome and useful for contact lens wearers. Two categories exist based on their biodegradability profile i.e., resorbable (collagen-based) or non-resorbable (silicone-based) plugs (Haddril 2019). A significant challenge with punctal plugs is related to fouling elicited as a result of the constituent biomaterial. This fouling is presented as granular tissue formation (Kim et al. 2005)

and may result to plug migration (with consequent dacryocystitis), excessive tearing and eye infection (Song et al. 2018). Researchers have also explored the use of punctal plugs as drug delivery device for three concentrations of latanoprost and has passed Phase 2 clinical trial (Butchofsky 2008). Another intra canalicular plug from Ocular Therapeutix Inc, Dextenza® containing 0.4 mg dexamethasone and delivers the drug for up to 30 days is the first to receive FDA approval ("Ocular Therapeutix 2019). Another punctual plug from the same company, OTX-TP®, containing travoprost is currently in phase 3 clinical trial ("Ocular Therapeutix Announces DEXTENZA® (Dexamethasone Ophthalmic Insert) Recommended for Unique J-Code by CMS" n.d.).

Corneal lens bandages are frequently used during keratoplasties and for keratoprosthesis to treat possible vision loss that can result from corneal injury, lacerations, or infection (Palchesko, Carrasquilla, and Feinberg 2018). Usually, cadaveric corneas are used though the process is fraught with challenges such as graft rejection and availability. The paucity of cadaveric grafts has catalyzed research in this direction. However, the biomaterial specifications required complicates the process of developing such grafts. Essentially the biomaterial should have specific anti-fouling properties by supporting cell adhesion at the periphery while resisting protein adsorption at the centre (Isaacson, Swioklo, and Connon 2018). This is a unique requirement since the cornea provides two thirds of the eye's refractive power while doubling as a barrier to environmental assault. The most commonly used artificial corneal replacement is made from PMMA and a titanium lock (the PMMA base plate has been replaced with titanium to eliminate the need for the lock) and a device comprising poly-2-hydroxyethyl methacrylate (PHEMA) (Akpek et al. 2014). Recent advances include the development of a 3D bio-printable device consisting of collagen and alginate polymers for the production of patient specific corneas (Isaacson, Swioklo, and Connon 2018). Currently, there is no mention of such corneal bandages to be used as drug delivery devices though this may be feasible for conditions requiring corneal repair.

Orbital implants are moulded biomaterials (mainly silicone, polyethylene, and PMMA) that can be inserted into the eye socket after eye enucleation for volume replacement and aesthetics. These implants have evolved from simple brittle, non-porous spheres to complex multifunctional devices that are available in specific shapes (Baino and Potestio 2016). Fouling and FBR are some of the challenges faced with orbital implants since the underlying tissues remain active after enucleation (Baino and Potestio 2016).

2.4 Modification of biomaterials as an anti-fouling approach

Ideal ocular biomaterial properties include optical clarity, structural integrity, stability, durability (for non-biodegradable materials), non-toxicity, biocompatibility, and tear film stability for contact lens applications (Pillay, Choonara, and Kumar 2016). Modification methods are aimed at maintaining these properties while imparting anti-fouling behaviour (resistance to protein adsorption and surface biofilm formation). There is no consensus on the limit of protein adhesion for optimal biomaterial performance and differs for various types of proteins and applications. For instance, the adsorption maximum for fibrinogen has been reported at approximately 5 ng/cm^2 (Jiang and Cao 2010) (Vermette 2001). Various approaches have been explored to solve the challenge of fouling. Preference has been given to device surface modifications and involves the use of poly(ethylene glycol) (PEG), poly(2-oxazolines) (poly(2-methyly-2-oxazoline) and poly(2-ethyl-2-oxazoline); polyglycerols (poly glycidol); carbohydrate derivatives (dextran), methylated sorbitol, heparin and poly zwitterionics (polysulfobetaines and polycarboxybetaines) (Tsay and Imae 2016) in the form of coatings, grafts, conjugates that can be physically adsorbed or covalently grafted on or from the surface in a wide range of architectures (**Figure 2.11**) such as polymer brushes (Feng et al. 2005), self-assembling monolayers (SAM) (Senaratne, Andruzzi, and Ober 2005), layer by layer assembly (LBL) (Kujawa et al. 2007) and interpenetrating polymer networks (IPN) (Gong et al. 2012). **Table 2.4** provides a summary of the various categories that exist for surface modification of biomaterials intended for ocular device fabrication. In addition to surface modification, researchers also sought to understand the role of biomaterial surface packing and homogeneity (topography) in controlling the conformation and orientation of adsorbed proteins and their interactions during the process of fouling (Hoffman 1999). Roach and coworkers (2006) studied the effect of surface topography and hydrophobicity on the binding characteristics of biomaterials such as bovine serum albumin (BSA) and bovine fibrinogen (BF) to silica nanospheres (Roach, Farrar, and Perry 2006). The study concluded that BF lost its secondary structure in binding to particles whereas the structure of BSA became disordered. These hydrophilic molecules (BSA and BF) were bound strongly to surface water such that proteins could not adhere and affording an anti-fouling behaviour.

Current attempts to improve the bio-inertness of ocular biomaterials are gradually moving beyond surface modification. Alternative modification method involves bulk processes in which same properties are achieved both externally on the surface and internally in the bulk of the material. For instance, for biomaterials such as polyurethanes that are made up of hard and soft segments (i.e., the degree of crystallinity determines their surface properties by microphase separation), the

Table 2.4 Categories of surface modifications applied to ocular biomaterials.

Category	Biomaterial	Modifier	Archetype	Reference
Surface methods				
Grafting to	Silicone, glass.	Poly (glycidyl methacrylate-*co*-sulfobetaine methacrylate)	Self-assembled monolayers (SAM)	(Chou et al. 2016)
Grafting	Acrylic IOL	Poly (MPC-MAA)	Covalent grafting with Ammonia plasma	(Tan et al. 2017a)
Functionalization	PCL	Helium-Oxygen plasma	Electro spun fibers	(Sharma et al. 2014)
Grafting	Silicone hydrogels	UV activated surface		(Wang and Liu 2011)
Grafting from	IOL	PEG	Polymer brushes	(Lin et al. 2017)
Photochemical and plasma modification	IOL	UV/Ozone or Argon	Hydroxyl and carboxyl groups	(Matsushima et al. 2006)
Surface tethering	PDMS	Sulfadiazine	TIMP	(Bahram et al.2013)
Surface coating	PDMS CL	Alginate/chitosan	LBL assembly	(Silva et al. 2016)
Bulk methods				
Introduction of functional groups	PHEMA	Carboxylic acid, quaternary ammonium.	-	(Ashtiani et al. 2018)
Free radical polymerization	Silicone based diacrylate lens	Polyethylene glycol diacrylate	-	(Askari et al. 2019)
Crosslinking	Silicone hydrogel lens	MMPC	IPN	(Shimizu et al. 2010)
Crosslinking	MPC	MMPC	Hydrogels	(Goda et al. 2009b)
Copolymerization	HEMA- NVP	Sulfobetaine methacrylate	Hydrogel	(Zhang et al. 2017)

bulk properties are more significant to ensure anti-fouling behaviour. Nanu and coworkers (2018) recognized the importance of the bulk properties of biomaterials and their influence on bio-inertness. They attempted to modify the properties of an aromatic methacrylate copolymer using bulk incorporation of heparin (Nanu et al. 2018) instead of regular surface coating with heparin. Ruiz and colleagues (2014) also studied the effect of this approach on hyaluronic acid incorporation into polyurethane and its influence on stability and biocompatibility. Their study found that even though there were no statistically significant difference in protein adsorption (fouling) between the surface and bulk modified polyurethane, the difference became significant when the samples were subjected to dynamic fluid flow in favour of bulk modified samples (Ruiz, Rathnam, and Masters 2014). This may be particularly important for ocular devices that are used for aqueous humor drainage in glaucoma.

2.4 The design of immunological responsive anti-fouling biomaterials for ocular devices

Contemporary biomaterial design has geared towards the development of smart materials that respond intelligently to stimuli that either turn on or turn off specific application. Protein adhesion and the resultant fouling of implanted devices is an integral part of the body's immune response to the device targeted at tissue repair or regeneration or foreign body response to encapsulate the device. The idea of designing immunologically responsive materials is hinged on manipulating the immune response to an implanted device as a strategy for improving drug delivery of biomaterials. Successful methods will initially identify the immunological targets that can serve as a stimulus for drug release. Some potential targets may include temperature change, pH change, reactive oxygen species release, and release of cytokines, interleukins, and other markers of inflammation. A critical look at the biomarkers of ocular immune response shows the release of different proteins, lipids, ions, cells, through the three stages of response that comprises the acute innate inflammatory response that lasts from 0 – 4 hours, subacute induced innate inflammatory response that lasts from 4 hours - 4 days and the chronic adaptive immune response that lasts from 4 days till resolution or healing occurs (Vishwakarma et al. 2016). Determining the role played by these proteins in the inflammatory process may underscore their potential use as stimuli for immunologic responsive smart biomaterial. It is known, for instance, that the abnormalities with glucose metabolism in diabetic patients result in systemic inflammation that ultimately remodels their physiology through upregulation of immune responses, excessive generation of reactive oxygen species leading ultimately to diabetic retinopathy (Homme et al. 2018). One enzyme that has been implicated in the pathogenesis of ocular diseases with

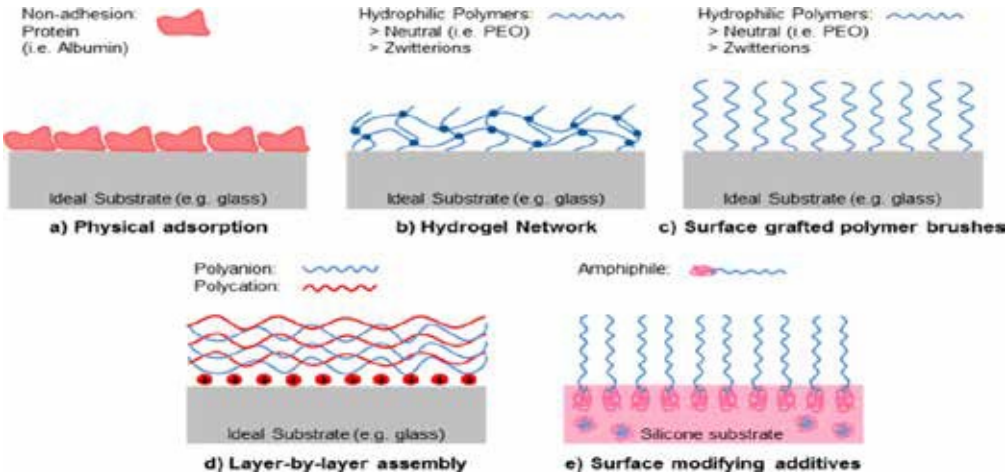


Figure 2.11 Possible architectures/configurations for surface modified materials. Reproduced from B. K.D. Ngo and M. A. Grunlan, Protein Resistant Polymeric Biomaterials, ACS Macro Lett. Vol. 6, no 9, pp. 992-1000, (2017) with permission from American Chemical Society.

Inflammatory undertone is the matrix metalloproteinases (MMPs) and their regulators, tissue inhibitors of metalloproteinases (TIMP) (Sivak and Fini 2002). MMPs are a family of neutral zinc dependent proteolytic enzymes secreted by the ocular surface alongside the inflammatory cells that proliferate in the tissues (Zaleska-Żmijewska et al. 2019) and are regulated by TIMPs. Their major substrate is the extracellular cell matrix (ECM) components, secreted cytokines, and ocular surface molecules (Sivak and Fini 2002). The balance between MMPs and TIMPs is strictly maintained for normal physiology. Dysregulation or imbalance in the ratio of MMPs: TIMPs can induce cellular changes in the ECM that can lead to the liberation of inflammatory mediators and oxidative stress biomarkers (Singh and Tyagi 2017) and hence many ocular diseases. Proposed treatment modalities target strict control or inhibition of MMPs in diseases including cancer metastasis, diabetic foot ulcer and periodontal diseases (Weinreb et al. 2020).

Purcell and co-workers (2014) developed an in-situ forming MMP responsive hydrogel based on polysaccharides. The aim was to overcome the dose limiting side effects of systemically injected recombinant TIMPs (rTIMPs) and develop a biomaterial that releases the rTIMPs in response to presence of MMP (Purcell et al. 2014). The hyaluronan based gel remains stable when incubated in the absence of collagenase type MMP but degraded proportionally in the presence of the enzyme. Though their study was targeted at cardiovascular tissues, the same principle can be harnessed to develop hydrogels that can only release their medicament at the presence of excess

MMP activity in ocular tissues in diseases such as glaucoma. The closest to an immunologic responsive biomaterial was designed by du Toit and colleagues (2014). They designed an intelligent intraocular implant that could release an anti-inflammatory agent in response to hydroxyl radical as biochemical implicated in inflammatory processes. The developed implant released increasing quantity of both an antibiotic, ciprofloxacin and an anti-inflammatory agent, indomethacin.

It is obvious that not much has been done in this area with respect to ocular biomaterials although a huge majority of debilitating and chronic ocular illnesses are tied up to immunological undertones. Inflammation and oxidative stress are major markers of immune response. It is possible to utilize immune response to implanted biomaterial to the advantage of drug delivery by designing materials that interact with the inflammatory markers that were designed by the body to attack the material.

2.5 Future perspectives and conclusions

Zwitterionic polymers are emerging as biomaterials of the future and are being repositioned as anti-fouling polymers with superior bio-inertness (Vassileva 2018). This is attributed to their striking similarity to membrane phospholipids such as glycine betaine and phosphorylcholine that renders them non-toxic while promoting tissue integration (Zhang et al. 2013).

Past research efforts have concentrated on developing surface coatings for ocular biomaterials, but emerging clinical outcomes have shown that in certain dynamic environments, the effect of surface coatings wear off and their stability is dependent on the coating process and application. The density and packing of polymer brushes as well as their configuration determines their anti-fouling properties and efficiency in resisting protein adsorption. An important question is why these zwitterionic biomaterials (that have proven efficient as anti-fouling surface coatings) have not been explored as bulk polymeric biomaterials. A literature search revealed that due to their hydrophilicity, such polymers does not facilitate physicomechanical robustness (Goda et al. 2009b). Jansen and co- workers (2018) developed hydrogels from co-monomers of PEG and phosphorylcholine with the intention of leveraging on their synergistic action. Surprisingly, hydrogels with the higher monomer content elicited the highest FBR. They showed that inhibition of the FBR was closely related to the mechanical modulus of the hydrogel (Jansen et al. 2018). Goda and co-workers (2009) hypothesized that mechanical deficits of zwitterionic polymers could be as a result of the structural dissimilarities between the monomers and the crosslinkers. They were the first to synthesize a zwitterionic crosslinker, 2-(methacryloyloxy) ethyl-N-(2-methacryloyloxy)ethyl]phosphorylcholine that differed from the monomer in having an extra

methacrylate group and was used for the crosslinking of 2-methacryloyloxyethylphosphorylcholline (Goda et al. 2009a). Later on, Carr and colleagues (2011) synthesized a zwitterionic crosslinker for carboxybetaine methacrylate (Carr, Xue, and Jiang 2011). The new crosslinkers (instead of the commonly used N, N' -methylene bis(acrylamide)) yielded hydrogels that were mechanically robust while maintaining protein resistance. Therefore, current research should be geared towards bulk grafting methods utilizing zwitterionic polymers that have shown promise in laboratory settings. With persistent research in this direction the status quo could be disrupted for implantable ocular devices to yield biomaterials with contradicting properties of desirable tissue integration and anti-fouling behaviour.

2.6 References

Acosta, A. C., V. Fernandez, P. D. Lamar, M. Orozco, S. Dubovy, J. Stoiber, L. Pinchuk, F. Fantes, and J.-M. Parel. 2004. "Ocular Biocompatibility of QuatromerTM (Polystyrene–Polyisobutylene Triblock Polymers) for Glaucoma Implants." *Investigative Ophthalmology & Visual Science* 45 (13): 2929–2929.

Akpek, Esen K, Majed Alkharashi, Frank S Hwang, Sueko M Ng, and Kristina Lindsley. 2014. "Artificial Corneas versus Donor Corneas for Repeat Corneal Transplants." *The Cochrane Database of Systematic Reviews* 11 (November): CD009561. https://doi.org/10.1002/14651858.CD009561.pub2.

"Alimera Sciences Receives FDA Approval For ILUVIEN®, The First Long-Term Treatment For Diabetic Macular Edema." n.d. Alimera Sciences. Accessed March 26, 2019. /news-releases/news-release-details/alimera-sciences-receives-fda-approval-iluvienr-first-long-term.

Amoozgar, Bahram, Diana Morarescu, and Heather Sheardown. 2013. "Sulfadiazine Modified PDMS as a Model Material with the Potential for the Mitigation of Posterior Capsule Opacification (PCO)." *Colloids and Surfaces B: Biointerfaces* 111 (November): 15–23. https://doi.org/10.1016/j.colsurfb.2013.05.002.

Amoozgar, Behzad, Xiaoling Wei, Jun Hui Lee, Michele Bloomer, Zhengtuo Zhao, Paul Coh, Fei He, Lan Luan, Chong Xie, and Ying Han. 2017. "A Novel Flexible Microfluidic Meshwork to Reduce Fibrosis in Glaucoma Surgery." *PloS One* 12 (3): e0172556. https://doi.org/10.1371/journal.pone.0172556.

Askari, Fahimeh, Mojgan Zandi, Parvin Shokrolahi, Mitra Hashemi Tabatabaei, and Elnaz Hajirasoliha. 2019. “Reduction in Protein Absorption on Ophthalmic Lenses by PEGDA Bulk Modification of Silicone Acrylate-Based Formulation.” *Progress in Biomaterials* 8 (3): 169–83. https://doi.org/10.1007/s40204-019-00119-x.

Auffarth, Gerd U., Ariadne Golescu, Klio A. Becker, and Hans E. Völcker. 2003. “Quantification of Posterior Capsule Opacification with Round and Sharp Edge Intraocular Lenses.” *Ophthalmology* 110 (4): 772–80. https://doi.org/10.1016/S0161-6420(02)01980-2.

Ayyala, R. S., D. Zurakowski, J. A. Smith, R. Monshizadeh, P. A. Netland, D. W. Richards, and W. E. Layden. 1998. “A Clinical Study of the Ahmed Glaucoma Valve Implant in Advanced Glaucoma.” *Ophthalmology* 105 (10): 1968–76. https://doi.org/10.1016/S0161-6420(98)91049-1

Ayyala, Ramesh S., Lynn E. Harman, B. Michelini-Norris, Leo E. Ondrovic, Edward Haller, Curtis E. Margo, and Scott X. Stevens. 1999. “Comparison of Different Biomaterials for Glaucoma Drainage Devices.” *Archives of Ophthalmology* 117 (2): 233–36. https://doi.org/10.1001/archopht.117.2.233.

Badugu, Ramachandram, Edward Albert Reece, and Joseph R. Lakowicz. 2018. “Glucose-Sensitive Silicone Hydrogel Contact Lens toward Tear Glucose Monitoring.” *Journal of Biomedical Optics* 23 (5): 1–9. https://doi.org/10.1117/1.JBO.23.5.057005.

Baino, Francesco, and Isabel Potestio. 2016. “Orbital Implants: State-of-the-Art Review with Emphasis on Biomaterials and Recent Advances.” *Materials Science and Engineering: C* 69 (December): 1410–28. https://doi.org/10.1016/j.msec.2016.08.003.

Barbosa Saliba, Juliana, Lorena Vieira, Gabriella Maria Fernandes-Cunha, Gisele Rodrigues Da Silva, Sílvia Ligório Fialho, Armando Silva-Cunha, Elodie Bousquet, et al. 2016. “Anti-Inflammatory Effect of Dexamethasone Controlled Released From Anterior Suprachoroidal Polyurethane Implants on Endotoxin-Induced Uveitis in Rats.” *Investigative Ophthalmology & Visual Science* 57 (4): 1671–79. https://doi.org/10.1167/iovs.15-18127.

Bawa, Priya, Viness Pillay, Yahya E. Choonara, and Lisa C. du Toit. 2009. “Stimuli-Responsive Polymers and Their Applications in Drug Delivery.” *Biomedical Materials (Bristol, England)* 4 (2): 022001. https://doi.org/10.1088/1748-6041/4/2/022001.

Bixler Gregory D. and Bhushan Bharat. 2012. “Biofouling: Lessons from Nature.” *Philosophical Transactions of the Royal Society A: Mathematical, Physical and Engineering Sciences* 370 (1967): 2381–2417. https://doi.org/10.1098/rsta.2011.0502.

Brandt, James D., Harvey B. DuBiner, Robert Benza, Kenneth N. Sall, Gary A. Walker, Charles P. Semba, and Collaborators. 2017. “Long-Term Safety and Efficacy of a Sustained-Release Bimatoprost Ocular Ring.” *Ophthalmology* 124 (10): 1565–66. https://doi.org/10.1016/j.ophtha.2017.04.022.

Butchofsky Bob. 2008. “QLT Begins Phase 2 Trial of Punctal Plug Drug Delivery System for Treating Glaucoma, Ocular Hypertension.” *Ophthamlology Web* Accessed March 27, 2019. https://www.healio.com/ophthalmology/glaucoma/news/online/%7ba3de4c13-da9a-4508-948e-7333145a0f8e%7d/qlt-begins-phase-2-trial-of-punctal-plug-drug-delivery-system-for-treating-glaucoma-ocular-hypertension.

Buffault, J., C. Baudouin, and A. Labbé. 2019. “XEN® Gel Stent for Management of Chronic Open Angle Glaucoma: A Review of the Literature.” *Journal Francais D’ophtalmologie* 42 (2): e37–46. https://doi.org/10.1016/j.jfo.2018.12.002.

Callahan, Michael A. 1979. “Technique of Congenital Cataract Surgery with the Kelman Cavitron Phacoemulsifier.” *Ophthalmology* 86 (11): 1994–98. https://doi.org/10.1016/S0161-6420(79)35319-2.

Campochiaro, Peter A., David M. Brown, Andrew Pearson, Sanford Chen, David Boyer, Jose Ruiz-Moreno, Bruce Garretson, et al. 2012. “Sustained Delivery Fluocinolone Acetonide Vitreous Inserts Provide Benefit for at Least 3 Years in Patients with Diabetic Macular Edema.” *Ophthalmology* 119 (10): 2125–32. https://doi.org/10.1016/j.ophtha.2012.04.030.

Campochiaro, Peter A., Dennis M. Marcus, Carl C. Awh, Carl Regillo, Anthony P. Adamis, Vladimir Bantseev, Yawen Chiang, et al. 2019. “The Port Delivery System with Ranibizumab for Neovascular Age-Related Macular Degeneration: Results from the Randomized Phase 2 Ladder Clinical Trial.” *Ophthalmology* 126 (8): 1141–54. https://doi.org/10.1016/j.ophtha.2019.03.036.

Carr, Louisa R., Hong Xue, and Shaoyi Jiang. 2011. “Functionalizable and Nonfouling Zwitterionic Carboxybetaine Hydrogels with a Carboxybetaine Dimethacrylate Crosslinker.” *Biomaterials* 32 (4): 961–68. https://doi.org/10.1016/j.biomaterials.2010.09.067.

Chang, Peter Y., Zvi Kresch, C. Michael Samson, and Ronald C. Gentile. 2015. “Spontaneous Dissociation of Fluocinolone Acetonide Sustained Release Implant (Retisert) with Dislocation into the Anterior Chamber.” *Ocular Immunology and Inflammation* 23 (6): 454–57. https://doi.org/10.3109/09273948.2014.902074.

Chaudhary, Ankita, Lauriane Salinas, Jacopo Guidotti, André Mermoud, and Kaweh Mansouri. 2018. “XEN Gel Implant: A New Surgical Approach in Glaucoma.” *Expert Review of Medical Devices* 15 (1): 47–59. https://doi.org/10.1080/17434440.2018.1419060.

Chen, Hung-Chi, Chia-Yi Lee, Chi-Chin Sun, Jing-Yang Huang, Hung-Yu Lin, and Shun-Fa Yang. 2019. “Risk Factors for the Occurrence of Visual-Threatening Posterior Capsule Opacification.” *Journal of Translational Medicine* 17 (1): 209. https://doi.org/10.1186/s12967-019-1956-6.

Chen, Shenfu, Lingyan Li, Chao Zhao, and Jie Zheng. 2010. “Surface Hydration: Principles and Applications toward Low-Fouling/Nonfouling Biomaterials.” *Polymer* 51 (23): 5283–93. https://doi.org/10.1016/j.polymer.2010.08.022.

Chirila, Traian, and Damien Harkin. 2016. *Biomaterials and Regenerative Medicine in Ophthalmology*. Woodhead Publishing.

Choi, Seung Woo, and Jaeyun Kim. 2018a. “Therapeutic Contact Lenses with Polymeric Vehicles for Ocular Drug Delivery: A Review.” *Materials* 11 (7). https://doi.org/10.3390/ma11071125.

Choonara, Yahya E., Viness Pillay, Trevor Carmichael, and Michael P. Danckwerts. 2006. “An in Vitro Study of the Design and Development of a Novel Doughnut-Shaped Minitablet for Intraocular Implantation.” *International Journal of Pharmaceutics* 310 (1–2): 15–24. https://doi.org/10.1016/j.ijpharm.2005.10.019.

Choonara, Yahya E., Viness Pillay, Michael P. Danckwerts, Trevor R. Carmichael, and Lisa C. du Toit. 2010. “A Review of Implantable Intravitreal Drug Delivery Technologies for the Treatment of Posterior Segment Eye Diseases.” *Journal of Pharmaceutical Sciences* 99 (5): 2219–39. https://doi.org/10.1002/jps.21987.

Choritz, Lars, Kaloian Koynov, Giulia Renieri, Keith Barton, Norbert Pfeiffer, and Hagen Thieme. 2010. “Surface Topographies of Glaucoma Drainage Devices and Their Influence on Human Tenon Fibroblast Adhesion.” *Investigative Ophthalmology & Visual Science* 51 (8): 4047–53. https://doi.org/10.1167/iovs.09-4759.

Chou, Ying-Nien, Ten-Chin Wen, and Yung Chang. 2016. “Zwitterionic Surface Grafting of Epoxylated Sulfobetaine Copolymers for the Development of Stealth Biomaterial Interfaces.” *Acta Biomaterialia* 40: 78–91. https://doi.org/10.1016/j.actbio.2016.03.046.

Ciolino, Joseph B., Cristina F. Stefanescu, Amy E. Ross, Borja Salvador-Culla, Priscila Cortez,

Eden M. Ford, Kate A. Wymbs, et al. 2014. “In Vivo Performance of a Drug-Eluting Contact Lens to Treat Glaucoma for a Month.” *Biomaterials* 35 (1): 432–39. https://doi.org/10.1016/j.biomaterials.2013.09.032.

Cullen, Cheryl L. 2007. “Glaucoma Drainage Devices.” In *Visual Prosthesis and Ophthalmic Devices: New Hope in Sight*, edited by Joyce Tombran-Tink, Colin J. Barnstable, and Joseph F.

Rizzo, 173–90. Ophthalmology Research. Totowa, NJ: Humana Press. https://doi.org/10.1007/978-1-59745-449-0_12.

Danion, Anne, Isabelle Arsenault, and Patrick Vermette. 2007. “Antibacterial Activity of Contact Lenses Bearing Surface-Immobilized Layers of Intact Liposomes Loaded with Levofloxacin.” *Journal of Pharmaceutical Sciences* 96 (9): 2350–63. https://doi.org/10.1002/jps.20871.

Davis, Jennifer L., Brian C. Gilger, and Michael R. Robinson. 2004. “Novel Approaches to Ocular Drug Delivery.” *Current Opinion in Molecular Therapeutics* 6 (2): 195–205

DiPasquale SA, Byrne ME. 2016. Controlled architecture for improved macromolecular memory within polymer networks. *Current Opinion in Biotechnology*. 40: 170-176. PMID 27322505 DOI: 10.1016/j.copbio.2016.06.001

Donnenfeld, Eric, and Edward Holland. 2018. “Dexamethasone Intracameral Drug-Delivery Suspension for Inflammation Associated with Cataract Surgery: A Randomized, Placebo-Controlled, Phase III Trial.” *Ophthalmology* 125 (6): 799–806. https://doi.org/10.1016/j.ophtha.2017.12.029.

Du Toit, Lisa C., Thirumala Govender, Trevor Carmichael, Pradeep Kumar, Yahya E. Choonara, and Viness Pillay. 2013. “Design of an Anti-Inflammatory Composite Nanosystem and Evaluation of Its Potential for Ocular Drug Delivery.” *Journal of Pharmaceutical Sciences* 102 (8): 2780–2805. https://doi.org/10.1002/jps.23650.

Dunbar, G.E., Shen, B.Y., Aref, A.A., 2017. The Sensimed Triggerfish contact lens sensor: efficacy, safety, and patient perspectives. Clin. Ophthalmol. Auckl. NZ 11, 875–882. https://doi.org/10.2147/OPTH.S109708

“Enzyme Injection to Reopen Blocked Ocular Drainage Devices in Glaucoma Patients - 15872 - University of Florida Office of Technology Licensing.” n.d. Accessed March 4, 2019. http://technologylicensing.research.ufl.edu/technologies/15872_enzyme-injection-to-reopen-blocked-ocular-drainage-devices-in-glaucoma-patients.

“FDA Accepts Second Application for Ocular Therapeutix’s Drug-Delivering Implant.” 2019. Drug

Delivery Business. April 3, 2019. https://www.drugdeliverybusiness.com/fda-accepts-second-application-for-ocular-therapeutixs-drug-delivering-implant/.

Feng, Wei, Shiping Zhu, Kazuhiko Ishihara, and John L. Brash. 2005. “Adsorption of Fibrinogen and Lysozyme on Silicon Grafted with Poly(2-Methacryloyloxyethyl Phosphorylcholine) via Surface-Initiated Atom Transfer Radical Polymerization.” *Langmuir: The ACS Journal of Surfaces and Colloids* 21 (13): 5980–87. https://doi.org/10.1021/la050277i.

Ferrari, Michele, Francesca Cirisano, and M. Carmen Morán. 2019. “Mammalian Cell Behavior on Hydrophobic Substrates: Influence of Surface Properties.” *Colloids and Interfaces* 3 (2): 48. https://doi.org/10.3390/colloids3020048.

Findl, Oliver, Wolf Buehl, Rupert Menapace, Stefan Sacu, Michael Georgopoulos, and Georg Rainer. 2005. “Long-Term Effect of Sharp Optic Edges of a Polymethyl Methacrylate Intraocular Lens on Posterior Capsule Opacification: A Randomized Trial.” *Ophthalmology* 112 (11): 2004–8. https://doi.org/10.1016/j.ophtha.2005.06.021.

Fonn, Desmond. 2007. “Targeting Contact Lens Induced Dryness and Discomfort: What Properties Will Make Lenses More Comfortable.” *Optometry and Vision Science* 84 (4): 279–85. https://doi.org/10.1097/OPX.0b013e31804636af.

Franz, Sandra, Stefan Rammelt, Dieter Scharnweber, and Jan C. Simon. 2011. “Immune Responses to Implants – A Review of the Implications for the Design of Immunomodulatory Biomaterials.” *Biomaterials* 32 (28): 6692–6709. https://doi.org/10.1016/j.biomaterials.2011.05.078.

Frère, Ariane, Laure Caspers, Dorine Makhoul, Lia Judice, Laurence Postelmans, Xavier Janssens, Pierre Lefebvre, Christian Mélot, and François Willermain. 2017. “Single Dexamethasone Intravitreal Implant in the Treatment of Noninfectious Uveitis.” *Journal of Ocular Pharmacology and Therapeutics: The Official Journal of the Association for Ocular Pharmacology and Therapeutics* 33 (4): 290–97. https://doi.org/10.1089/jop.2016.0139.

“Glaukos’ IDose Travoprost Achieves Sustained IOP Reduction and Favorable Safety Profile in 12-Month Interim Cohort.” n.d. Eyewire News. Accessed February 26, 2020. https://eyewire.news/articles/glaukos-corporations-idose-travoprost-achieves-sustained-iop-reduction-and-favorable-safety-profile-in-12-month-interim-cohort/.

Goda, Tatsuro, Ryosuke Matsuno, Tomohiro Konno, Madoka Takai, and Kazuhiko Ishihara. 2009a. “Protein Adsorption Resistance and Oxygen Permeability of Chemically Crosslinked

Phospholipid Polymer Hydrogel for Ophthalmologic Biomaterials." *Journal of Biomedical Materials Research Part B: Applied Biomaterials* 89B (1): 184–90. https://doi.org/10.1002/jbm.b.31204.

Gong, Mei, Li Zhang, Yi Zuo, Qin Zou, Yanying Wang, Li Wang, and Yubao Li. 2012. "Investigation on the Interpenetrating Polymer Networks (Ipns) of Polyvinyl Alcohol and Poly(N-Vinyl Pyrrolidone) Hydrogel and Its in Vitro Bioassessment." *Journal of Applied Polymer Science* 125 (4): 2799–2806. https://doi.org/10.1002/app.36247.

Gullapalli, Vamsi K., Mohamad A. Khodair, Hao Wang, Ilene K. Sugino, Steven Madreperla, and Marco A. Zarbin. 2013. "Chapter 125 - Transplantation Frontiers." In *Retina (Fifth Edition)*, edited by Stephen J. Ryan, SriniVas R. Sadda, David R. Hinton, Andrew P. Schachat, SriniVas R. Sadda, C. P. Wilkinson, Peter Wiedemann, and Andrew P. Schachat, 2058–77. London: W.B. Saunders. https://doi.org/10.1016/B978-1-4557-0737-9.00125-9.

Haddril Marilyn, 2019. Punctal Plugs for Dry Eyes." All About Vision. Accessed March 27, 2019. https://www.allaboutvision.com/conditions/punctal-plugs.htm.

Haldar, R. S., R. Chauhan, K. Kapoor, and U. K. Niyogi. 2014. "Development of a Hydrophobic Polymer Composition with Improved Biocompatibility for Making Foldable Intraocular Lenses." *Optical Materials* 36 (7): 1165–76. https://doi.org/10.1016/j.optmat.2014.02.022.

Han, Yuemei, Xu Xu, Yuqin Wang, Sihao Liu, Xia Zhao, Hao Chen, and Quankui Lin. 2018. "Drug Eluting Intraocular Lens Surface Modification for PCO Prevention." *Colloid and Interface Science Communications* 24 (May): 40–44. https://doi.org/10.1016/j.colcom.2018.03.007.

Hoffman, Allan S. 1999. "Non-Fouling Surface Technologies." *Journal of Biomaterials Science, Polymer Edition* 10 (10): 1011–14. https://doi.org/10.1163/156856299X00658.

Homme, Rubens P., Mahavir Singh, Avisek Majumder, Akash K. George, Kavya Nair, Harpal S. Sandhu, Neetu Tyagi, David Lominadze, and Suresh C Tyagi. 2018. "Remodeling of Retinal Architecture in Diabetic Retinopathy: Disruption of Ocular Physiology and Visual Functions by Inflammatory Gene Products and Pyroptosis." *Frontiers in Physiology* 9 (September). https://doi.org/10.3389/fphys.2018.01268.

Hucknall, Angus, Srinath Rangarajan, and Ashutosh Chilkoti. 2009. "In Pursuit of Zero: Polymer Brushes That Resist the Adsorption of Proteins." *Advanced Materials* 21 (23): 2441–46. https://doi.org/10.1002/adma.200900383.

Hui, Alex. 2017. "Contact Lenses for Ophthalmic Drug Delivery." *Clinical and Experimental*

Optometry 100 (5): 494–512. https://doi.org/10.1111/cxo.12592.

Humar, Matjaž, Sheldon J. J. Kwok, Myunghwan Choi, Ali K. Yetisen, Sangyeon Cho, and Seok-Hyun Yun. 2016. “Toward Biomaterial-Based Implantable Photonic Devices.” *Nanophotonics* 6 (2): 414–34. https://doi.org/10.1515/nanoph-2016-0003.

Humayun, Mark, Arturo Santos, Juan Carlos Altamirano, Ramiro Ribeiro, Roberto Gonzalez, Alejandro de la Rosa, Jason Shih, et al. 2014. “Implantable MicroPump for Drug Delivery in Patients with Diabetic Macular Edema.” *Translational Vision Science & Technology* 3 (6): 5. https://doi.org/10.1167/tvst.3.6.5.

“Investigational MIGS Device Could Minimize Fibrotic Response.” 2017. American Academy of Ophthalmology. October 19, 2017. https://www.aao.org/headline/investigational-migs-device-could-minimize-fibroti.

Isaacson, Abigail, Stephen Swioklo, and Che J. Connon. 2018a. “3D Bioprinting of a Corneal Stroma Equivalent.” *Experimental Eye Research* 173: 188–93. https://doi.org/10.1016/j.exer.2018.05.010.

Jabs, Douglas A., Alka Ahuja, Mark Van Natta, JP Dunn, and Steven Yeh. 2013. “Comparison of Treatment Regimens for Cytomegalovirus Retinitis in Patients with AIDS in the Era of Highly Active Antiretroviral Therapy.” *Ophthalmology* 120 (6): 1262–70. https://doi.org/10.1016/j.ophtha.2012.11.023.

Jacob, Jean T. 2013. “Biocompatibility in the Development of Silicone-Hydrogel Lenses.” *Eye & Contact Lens* 39 (1): 13–19. https://doi.org/10.1097/ICL.0b013e31827dbb00.

Jansen, Lauren E., Luke D. Amer, Esther Y.-T. Chen, Thuy V. Nguyen, Leila S. Saleh, Todd Emrick, Wendy F. Liu, Stephanie J. Bryant, and Shelly R. Peyton. 2018. “Zwitterionic PEG-PC Hydrogels Modulate the Foreign Body Response in a Modulus-Dependent Manner.” *Biomacromolecules* 19 (7): 2880–88. https://doi.org/10.1021/acs.biomac.8b00444.

Jason, J. and Nichol, S. 2018. ‘’Continuing Upward Trends in Daily Disposable Prescribing and Other Key Segments Maintained a Healthy Contact Lens Spectrum.’’ *Contact Lens Spectrum* 33 (1): 20-25,42. Accessed March 2019. https://www.clspectrum.com/issues/2018/january-2018/contact-lenses-2017.

Jiang, Shaoyi, and Zhiqiang Cao. 2010a. “Ultralow-Fouling, Functionalizable, and Hydrolyzable Zwitterionic Materials and Their Derivatives for Biological Applications.” *Advanced Materials*. https://doi.org/10.1002/adma.200901407.

Kaji, Hirokazu, Nobuhiro Nagai, Matsuhiko Nishizawa, and Toshiaki Abe. 2018. “Drug Delivery Devices for Retinal Diseases.” *Advanced Drug Delivery Reviews* 128 (March): 148–57. https://doi.org/10.1016/j.addr.2017.07.002.

Kao, Elizabeth C. Y., David J. McCanna, and Lyndon W. Jones. 2011. “Utilization of in Vitro Methods to Determine the Biocompatibility of Intraocular Lens Materials.” *Toxicology in Vitro* 25 (8): 1906–11. https://doi.org/10.1016/j.tiv.2011.06.005.

Katzer, Tatiele, Paula Chaves, Andressa Bernardi, Adriana R. Pohlmann, Silvia S. Guterres, and Ruy C. R. Beck. 2014. “Castor Oil and Mineral Oil Nanoemulsion: Development and Compatibility with a Soft Contact Lens.” *Pharmaceutical Development and Technology* 19 (2): 232–37. https://doi.org/10.3109/10837450.2013.769569.

Keino, Hiroshi, Shintaro Horie, and Sunao Sugita. 2018. “Immune Privilege and Eye-Derived T-Regulatory Cells.” Review Article. Journal of Immunology Research. 2018. https://doi.org/10.1155/2018/1679197.

Kent Christopher, 2015. Managing & Preventing Tube Shunt Problems. *Review of Ophthalmology* June 2015. Accessed July 11, 2018. https://www.reviewofophthalmology.com/article/managing--preventing-tube-shunt- problems.

Kim, Bryan M., Smajo S. Osmanovic, and Deepak P. Edward. 2005. “Pyogenic Granulomas after Silicone Punctal Plugs: A Clinical and Histopathologic Study.” *American Journal of Ophthalmology* 139 (4): 678–84. https://doi.org/10.1016/j.ajo.2004.11.059.

Ko, Fang, Maria Papadopoulos, and Peng T. Khaw. 2015. “Chapter 9 - Primary Congenital Glaucoma.” In *Progress in Brain Research*, edited by Giacinto Bagetta and Carlo Nucci, 221:177–89. New Trends in Basic and Clinical Research of Glaucoma: A Neurodegenerative Disease of the Visual System, Part B. Elsevier. https://doi.org/10.1016/bs.pbr.2015.06.005.

Kochounian, Harold H., Shirley A. Kovacs, Jose Sy, David E. Grubbs, and W. Andrew Maxwell. 1994. “Identification of Intraocular Lens-Adsorbed Proteins in Mammalian In Vitro and In Vivo Systems.” *Archives of Ophthalmology* 112 (3): 395–401. https://doi.org/10.1001/archopht.1994.01090150125034.

Kohn, J., I. J. Khan, C. Iovine, P. Velagaleti, E. Anglade, and B. Gilger. 2010. “Ocular Biocompatibility, Toxicity, and Distribution From Erodible Polycarbonate Polymer Episcleral Implants (LX212) in Rabbits.” *Investigative Ophthalmology & Visual Science* 51 (13): 5326–5326.

Krysztofiak, K., and A. Szyczewski. 2014. “Study of Dehydration and Water States in New and

Worn Soft Contact Lens Materials." *Optica Applicata* Vol. 44 (nr 2). https://doi.org/10.5277/oa140206.

Kujawa, Piotr, Gregory Schmauch, Tapani Viitala, Antonella Badia, and Françoise M. Winnik. 2007. "Construction of Viscoelastic Biocompatible Films via the Layer-by-Layer Assembly of Hyaluronan and Phosphorylcholine-Modified Chitosan." *Biomacromolecules* 8 (10): 3169–76. https://doi.org/10.1021/bm7006339.

Lattimore, Morris R., Thomas H. Harding, and Steven T. Williams. 2018. "Hydrogel Contact Lens Water Content Is Dependent on Tearfilm PH." *Military Medicine* 183 (suppl_1): 224–30. https://doi.org/10.1093/milmed/usx233.

Lee, Jae-Hwan, Ramana M. Pidaparti, Gary M. Atkinson, and Ramana S. Moorthy. 2012. "Design of an Implantable Device for Ocular Drug Delivery." Research article. Journal of Drug Delivery. 2012. https://doi.org/10.1155/2012/527516.

Lewis, Richard A. 2014. "Ab Interno Approach to the Subconjunctival Space Using a Collagen Glaucoma Stent." *Journal of Cataract & Refractive Surgery* 40 (8): 1301–6. https://doi.org/10.1016/j.jcrs.2014.01.032.

Li, D. J, F. Z Cui, and H. Q Gu. 1999. "F+ Ion Implantation Induced Cell Attachment on Intraocular Lens." *Biomaterials* 20 (20): 1889–96. https://doi.org/10.1016/S0142-9612(99)00084-8.

Li, Tianjing, Kristina Lindsley, Benjamin Rouse, Hwanhee Hong, Qiyuan Shi, David S. Friedman, Richard Wormald, and Kay Dickersin. 2016. "Comparative Effectiveness of First-Line Medications for Primary Open Angle Glaucoma – A Systematic Review and Network Meta-Analysis." *Ophthalmology* 123 (1): 129–40. https://doi.org/10.1016/j.ophtha.2015.09.005.

Lim, K, B Allan, A Lloyd, A Muir, P Khaw, K LIM, B ALLAN, A LLOYD, A MUIR, and P KHAW. 1998. "Glaucoma Drainage Devices; Past, Present, and Future." *The British Journal of Ophthalmology* 82 (9): 1083–89.

Lin, Quankui, Junmei Tang, Yuemei Han, Xu Xu, Xiaojuan Hao, and Hao Chen. 2017. "Hydrophilic Modification of Intraocular Lens via Surface Initiated Reversible Addition-Fragmentation Chain Transfer Polymerization for Reduced Posterior Capsular Opacification." *Colloids and Surfaces. B, Biointerfaces* 151 (March): 271–79. https://doi.org/10.1016/j.colsurfb.2016.12.028.

Liu, Yu-Chi, Tina Wong, and Jodhbir Mehta. 2013. "Intraocular Lens as a Drug Delivery Reservoir." *Current Opinion in Ophthalmology* 24 (1): 53–59. https://doi.org/10.1097/ICU.0b013e32835a93fc.

Lloyd, A. W. 2001. “Ophthalmology: Biomaterials.” In *Encyclopedia of Materials: Science and Technology*, edited by K. H. Jürgen Buschow, Robert W. Cahn, Merton C. Flemings, Bernhard

Ilschner, Edward J. Kramer, Subhash Mahajan, and Patrick Veyssière, 6411–15. Oxford: Elsevier. https://doi.org/10.1016/B0-08-043152-6/01134-7.

Lorenz, Kathrine Osborn, Joseph Kakkassery, Danielle Boree, and David Pinto. 2014. “Atomic Force Microscopy and Scanning Electron Microscopy Analysis of Daily Disposable Limbal Ring Contact Lenses.” *Clinical & Experimental Optometry* 97 (5): 411–17. https://doi.org/10.1111/cxo.12148.

Lowder, Careen, Rubens Belfort, Sue Lightman, C. Stephen Foster, Michael R. Robinson, Rhett M. Schiffman, Xiao-Yan Li, Harry Cui, and Scott M. Whitcup. 2011. “Dexamethasone Intravitreal Implant for Noninfectious Intermediate or Posterior Uveitis.” *Archives of Ophthalmology* 129 (5): 545–53. https://doi.org/10.1001/archophthalmol.2010.339.

Lu, Changhai, Roshan B. Yoganathan, Michael Kociolek, and Christine Allen. 2013. “Hydrogel Containing Silica Shell Cross-Linked Micelles for Ocular Drug Delivery.” *Journal of Pharmaceutical Sciences* 102 (2): 627–37. https://doi.org/10.1002/jps.23390.

Mandal, Abhirup, Rohit Bisht, Ilva D. Rupenthal, and Ashim K. Mitra. 2017. “Polymeric Micelles for Ocular Drug Delivery: From Structural Frameworks to Recent Preclinical Studies.” *Journal of Controlled Release* 248 (February): 96–116. https://doi.org/10.1016/j.jconrel.2017.01.012.

Mann, Aisling, and Brian Tighe. 2013. “Contact Lens Interactions with the Tear Film.” *Experimental Eye Research*, Tears: A Unique Mucosal Surface Secretion, 117 (December): 88–98. https://doi.org/10.1016/j.exer.2013.07.013.

Mariani, Erminia, Gina Lisignoli, Rosa Maria Borzì, and Lia Pulsatelli. 2019. “Biomaterials: Foreign Bodies or Tuners for the Immune Response?” *International Journal of Molecular Sciences* 20 (3): 636. https://doi.org/10.3390/ijms20030636.

Martin, Daniel F., David J. Parks, Susan D. Mellow, Frederick L. Ferris, R. Christopher Walton, Nancy A. Remaley, Emily Y. Chew, Paul Ashton, Matthew D. Davis, and Robert B. Nussenblatt. 1994. “Treatment of Cytomegalovirus Retinitis With an Intraocular Sustained-Release Ganciclovir Implant: A Randomized Controlled Clinical Trial.” *Archives of Ophthalmology* 112 (12): 1531–39. https://doi.org/10.1001/archopht.1994.01090240037023.

Masli, Sharmila, and Jose L. Vega. 2011. “Ocular Immune Privilege Sites.” *Methods in Molecular Biology (Clifton, N.J.)* 677: 449–58. https://doi.org/10.1007/978-1-60761-869-0_28.

Matsushima, Hiroyuki, Hidetoshi Iwamoto, Kouichiro Mukai, and Yoshitaka Obara. 2006. “Active Oxygen Processing for Acrylic Intraocular Lenses to Prevent Posterior Capsule Opacification.” *Journal of Cataract & Refractive Surgery* 32 (6): 1035–40. https://doi.org/10.1016/j.jcrs.2006.02.042.

Maulvi, Furqan A., Anjum A. Shaikh, Dhara H. Lakdawala, Ankita R. Desai, Mihir M. Pandya, Sulabh S. Singhania, Rutvi J. Vaidya, Ketan M. Ranch, Bhavin A. Vyas, and Dinesh O. Shah. 2017. “Design and Optimization of a Novel Implantation Technology in Contact Lenses for the Treatment of Dry Eye Syndrome: In Vitro and in Vivo Evaluation.” *Acta Biomaterialia* 53: 211–21. https://doi.org/10.1016/j.actbio.2017.01.063.

Maulvi, Furqan A., Tejal G. Soni, and Dinesh O. Shah. 2016. “A Review on Therapeutic Contact Lenses for Ocular Drug Delivery.” *Drug Delivery* 23 (8): 3017–26. https://doi.org/10.3109/10717544.2016.1138342.

McKeown, Peter P., Stephen G. Kovacs, Masahiro Aiba, Leo E. Ondrovic, George Koroknai, Yukifusa Yokoyama, and Dimitri Novitzky. 1993. “Magnetically Actuated Left Ventricular Assist Device (LVAD): Acute Animal Test Results.” In *Heart Replacement: Artificial Heart 4*, edited by Tetsuzo Akutsu and Hitoshi Koyanagi, 295–99. Tokyo: Springer Japan. https://doi.org/10.1007/978-4-431-67023-0_40.

Mercieca, Karl, Brett Drury, Archana Bhargava, and Cecilia Fenerty. 2018. “Trabeculectomy Bleb Needling and Antimetabolite Administration Practices in the UK: A Glaucoma Specialist National Survey.” *The British Journal of Ophthalmology* 102 (9): 1244–47. https://doi.org/10.1136/bjophthalmol-2017-310812.

Molokhia, Sarah A., Himanshu Sant, Jacquelyn Simonis, C. J. Bishop, R. M. Burr, Bruce K. Gale, and Balamurali K. Ambati. 2010. “The Capsule Drug Device: Novel Approach for Drug Delivery to the Eye.” *Vision Research*, Mechanisms in Macular Degeneration, 50 (7): 680–85. https://doi.org/10.1016/j.visres.2009.10.013.

Nanu, Razvan Vladimir, Emil Ungureanu, Sinziana Luminita Instrate, Alexandra Vrapciu, Roxana Cozubas, Laura Carstocea, Liliana Mary Voinea, and Radu Ciuluvica. 2018. “An Overview ofthe

Influence and Design of Biomaterial of the Intraocular Implant of the Posterior Capsule Opacification." *Romanian Journal of Ophthalmology* 62 (3): 188–93.

Nasr, Farzaneh Hashemi, Sepideh Khoee, Mohammad Mehdi Dehghan, Sirous Sadeghian Chaleshtori, and Abbas Shafiee. 2016. "Preparation and Evaluation of Contact Lenses Embedded with Polycaprolactone-Based Nanoparticles for Ocular Drug Delivery." *Biomacromolecules* 17 (2): 485–95. https://doi.org/10.1021/acs.biomac.5b01387.

Natarajan, Jayaganesh V, Marcus Ang, Anastasia Darwitan, Sujay Chattopadhyay, Tina T Wong, and Subbu S Venkatraman. 2012. "Nanomedicine for Glaucoma: Liposomes Provide Sustained Release of Latanoprost in the Eye." *International Journal of Nanomedicine* 7: 123–31. https://doi.org/10.2147/IJN.S25468.

Neves, H. P. 2013. "1 - Materials for Implantable Systems." In *Implantable Sensor Systems for Medical Applications*, edited by Andreas Inmann and Diana Hodgins, 3–38. Woodhead Publishing Series in Biomaterials. Woodhead Publishing. https://doi.org/10.1533/9780857096289.1.3.

"Ocular Therapeutix Announces DEXTENZA® (Dexamethasone Ophthalmic Insert) Recommended for Unique J-Code by CMS." n.d. BioSpace. Accessed April 27, 2020. https://www.biospace.com/article/ocular-therapeutix-announces-dextenza-dexamethasone-ophthalmic-insert-recommended-for-unique-j-code-by-cms/.

"Ocular Therapeutix. 2019. OTX-TP Can't Match Timolol in Phase IIb Glaucoma Study." *BioSpace*. Accessed March 22, 2019. https://www.biospace.com/article/ocular-therapeutix-s-otx-tp-can-t- match-timolol-in-phase-iib-glaucoma-study-/.

Omali, Negar, Lakshman Subbaraman, Chantal Coles-Brennan, Zohra Fadli, and Lyndon Jones. 2015. "Biological and Clinical Implications of Lysozyme Deposition on Soft Contact Lenses." *Optometry and Vision Science* 92 (7): 750–57. https://doi.org/10.1097/OPX.0000000000000615.

Onuki, Yoshinori, Upkar Bhardwaj, Fotios Papadimitrakopoulos, and Diane J. Burgess. 2008. "A Review of the Biocompatibility of Implantable Devices: Current Challenges to Overcome Foreign Body Response." *Journal of Diabetes Science and Technology* 2 (6): 1003–15. https://doi.org/10.1177/193229680800200610.

Palchesko, Rachelle N., Santiago D. Carrasquilla, and Adam W. Feinberg. 2018. "Natural Biomaterials for Corneal Tissue Engineering, Repair, and Regeneration." *Advanced Healthcare Materials*, May, e1701434. https://doi.org/10.1002/adhm.201701434.

Pan, T., J. D. Brown, and B. Ziaie. 2006. “An Artificial Nano-Drainage Implant (ANDI) for Glaucoma Treatment.” In *2006 International Conference of the IEEE Engineering in Medicine and Biology Society*, 3174–77. https://doi.org/10.1109/IEMBS.2006.260147.

Patel, Shuchi, and Louis R. Pasquale. 2010. “Glaucoma Drainage Devices: A Review of the Past, Present, and Future.” *Seminars in Ophthalmology* 25 (5–6): 265–70. https://doi.org/10.3109/08820538.2010.518840.

Pearson, P. Andrew, Timothy L. Comstock, Michael Ip, David Callanan, Lawrence S. Morse, Paul Ashton, Brian Levy, Eric S. Mann, and Dean Eliott. 2011. “Fluocinolone Acetonide Intravitreal Implant for Diabetic Macular Edema: A 3-Year Multicenter, Randomized, Controlled Clinical Trial.” *Ophthalmology* 118 (8): 1580–87. https://doi.org/10.1016/j.ophtha.2011.02.048.

Peng, Cheng-Chun, Anna Ben-Shlomo, Edward O. Mackay, Caryn E. Plummer, and Anuj Chauhan. 2012. “Drug Delivery by Contact Lens in Spontaneously Glaucomatous Dogs.” *Current Eye Research* 37 (3): 204–11. https://doi.org/10.3109/02713683.2011.630154.

Peng, Cheng-Chun, Michael T. Burke, Blanca E. Carbia, Caryn Plummer, and Anuj Chauhan. 2012. “Extended Drug Delivery by Contact Lenses for Glaucoma Therapy.” *Journal of Controlled Release: Official Journal of the Controlled Release Society* 162 (1): 152–58. https://doi.org/10.1016/j.jconrel.2012.06.017.

Peng, Cheng-Chun, Neil P. Fajardo, Trust Razunguzwa, and Clayton J. Radke. 2015. “In Vitro Spoilation of Silicone-Hydrogel Soft Contact Lenses in a Model-Blink Cell.” *Optometry and Vision Science: Official Publication of the American Academy of Optometry* 92 (7): 768–80. https://doi.org/10.1097/OPX.0000000000000625.

Pérez-Vives, Cari. 2018. “Biomaterial Influence on Intraocular Lens Performance: An Overview.” Review Article. Journal of Ophthalmology. 2018. https://doi.org/10.1155/2018/2687385.

Pillay, Viness, Yahya E. Choonara, and Pradeep Kumar. 2016. *Frontiers in Biomaterials: Unfolding the Biopolymer Landscape*. Bentham Science Publishers.

Pop-Georgievski, Ognen, Cesar Rodriguez-Emmenegger, Andres de los Santos Pereira, Vladimír Proks, Eduard Brynda, and František Rypáček. 2013. “Biomimetic Non-Fouling Surfaces: Extending the Concepts.” *Journal of Materials Chemistry B* 1 (22): 2859–67. https://doi.org/10.1039/C3TB20346H.

Puleo, David A., and Rena Bizios. 2009. *Biological Interactions on Materials Surfaces: Understanding and Controlling Protein, Cell, and Tissue Responses*. Springer Science & Business Media.

Purcell, Brendan P., David Lobb, Manoj B. Charati, Shauna M. Dorsey, Ryan J. Wade, Kia N. Zellars, Heather Doviak, et al. 2014. "Injectable and Bioresponsive Hydrogels for On-Demand Matrix Metalloproteinase Inhibition." *Nature Materials* 13 (6): 653–61. https://doi.org/10.1038/nmat3922.

Qin, Yingyan, Yi Zhu, Furong Luo, Chuan Chen, Xiaoyun Chen, and Mingxing Wu. 2017. "Killing Two Birds with One Stone: Dual Blockade of Integrin and FGF Signaling through Targeting Syndecan-4 in Postoperative Capsular Opacification." *Cell Death & Disease* 8 (7): e2920. https://doi.org/10.1038/cddis.2017.315.

Roach, Paul, David Farrar, and Carole C. Perry. 2006. "Surface Tailoring for Controlled Protein Adsorption: Effect of Topography at the Nanometer Scale and Chemistry." *Journal of the American Chemical Society* 128 (12): 3939–45. https://doi.org/10.1021/ja056278e.

Rønbeck, Margrethe, and Maria Kugelberg. 2014. "Posterior Capsule Opacification with 3 Intraocular Lenses: 12-Year Prospective Study." *Journal of Cataract & Refractive Surgery* 40 (1): 70–76. https://doi.org/10.1016/j.jcrs.2013.07.039.

Ross, Amy E., Lokendrakumar C. Bengani, Rehka Tulsan, Daniel E. Maidana, Borja Salvador-Culla, Hidenaga Kobashi, Paraskevi E. Kolovou, et al. 2019. "Topical Sustained Drug Delivery to the Retina with a Drug-Eluting Contact Lens." *Biomaterials* 217 (October): 119285. https://doi.org/10.1016/j.biomaterials.2019.119285.

Ruiz, Amaliris, Kashmila R. Rathnam, and Kristyn S. Masters. 2014. "Effect of Hyaluronic Acid Incorporation Method on the Stability and Biological Properties of Polyurethane–Hyaluronic Acid Biomaterials." *Journal of Materials Science: Materials in Medicine* 25 (2): 487–98. https://doi.org/10.1007/s10856-013-5092-1.

Salim, Sarwat, Piltz-Seymour Jody, Siegfried Carla, and Sheybani Arsham. 2019. Trabeculotomy. EyeWiki.

Senaratne, Wageesha, Luisa Andruzzi, and Christopher K. Ober. 2005. "Self-Assembled Monolayers and Polymer Brushes in Biotechnology: Current Applications and Future Perspectives." *Biomacromolecules* 6 (5): 2427–48. https://doi.org/10.1021/bm050180a.

Sharma, Shweta, Deepika Gupta, Sujata Mohanty, Manjeet Jassal, Ashwini K. Agrawal, and Radhika Tandon. 2014. “Surface-Modified Electrospun Poly(ε-Caprolactone) Scaffold With Improved Optical Transparency and Bioactivity for Damaged Ocular Surface Reconstruction.” *Investigative Ophthalmology & Visual Science* 55 (2): 899–907. https://doi.org/10.1167/iovs.13-12727.

Shimizu, Takanori, Tatsuro Goda, Norihiko Minoura, Madoka Takai, and Kazuhiko Ishihara. 2010. “Super-Hydrophilic Silicone Hydrogels with Interpenetrating Poly(2-Methacryloyloxyethyl Phosphorylcholine) Networks.” *Biomaterials* 31 (12): 3274–80. https://doi.org/10.1016/j.biomaterials.2010.01.026.

Silva, Diana, Luís F. V. Pinto, Dimitriya Bozukova, Luís F. Santos, Ana Paula Serro, and Benilde Saramago. 2016. “Chitosan/Alginate Based Multilayers to Control Drug Release from Ophthalmic Lens.” *Colloids and Surfaces B: Biointerfaces* 147 (November): 81–89. https://doi.org/10.1016/j.colsurfb.2016.07.047.

Singh, Mahavir, and Suresh C Tyagi. 2017. “Metalloproteinases as Mediators of Inflammation and the Eyes: Molecular Genetic Underpinnings Governing Ocular Pathophysiology.” *International Journal of Ophthalmology* 10 (8): 1308–18. https://doi.org/10.18240/ijo.2017.08.20.

Sivak, Jeremy M., and M. Elizabeth Fini. 2002a. “MMPs in the Eye: Emerging Roles for Matrix Metalloproteinases in Ocular Physiology.” *Progress in Retinal and Eye Research* 21 (1): 1–14. https://doi.org/10.1016/s1350-9462(01)00015-5.

Song, Jong, In Woo, Youngsub Eom, and Hyo Kim. 2018. “Five Misconceptions Related to Punctal Plugs in Dry Eye Management.” *Cornea* 37 (November). https://doi.org/10.1097/ICO.0000000000001734.

Subrizi, Astrid, Eva M. del Amo, Viktor Korzhikov-Vlakh, Tatiana Tennikova, Marika Ruponen, and Arto Urtti. 2019. “Design Principles of Ocular Drug Delivery Systems: Importance of Drug Payload, Release Rate, and Material Properties.” *Drug Discovery Today*, February. https://doi.org/10.1016/j.drudis.2019.02.001.

Tan, Xuhua, Jiezhao Zhan, Yi Zhu, Ji Cao, Lin Wang, Sa Liu, Yingjun Wang, et al. 2017a. “Improvement of Uveal and Capsular Biocompatibility of Hydrophobic Acrylic Intraocular Lens by Surface Grafting with 2-Methacryloyloxyethyl Phosphorylcholine-Methacrylic Acid Copolymer.” *Scientific Reports* 7: 40462. https://doi.org/10.1038/srep40462.

Thompson, J.T., Chambers, W.A., 2016. Good Ideas Gone Bad: The MIRAgel Saga. Ophthalmology 123, 5–6. https://doi.org/10.1016/j.ophtha.2015.09.038

Thrimawithana, Thilini R., Ilva D. Rupenthal, Simon S. Räsch, Julie C. Lim, James D. Morton, and Craig R. Bunt. 2018. “Drug Delivery to the Lens for the Management of Cataracts.” *Advanced Drug Delivery Reviews*, Drug Delivery Approaches for Improved Ocular Therapeutics, 126 (February): 185–94. https://doi.org/10.1016/j.addr.2018.03.009.

Toit, Lisa C. du, Trevor Carmichael, Thirumala Govender, Pradeep Kumar, Yahya E. Choonara, and Viness Pillay. 2014. “In Vitro, in Vivo, and in Silico Evaluation of the Bioresponsive Behavior of an Intelligent Intraocular Implant.” *Pharmaceutical Research* 31 (3): 607–34. https://doi.org/10.1007/s11095-013-1184-3.

Toit, Lisa C. du, Viness Pillay, Yahya E. Choonara, Thirumala Govender, and Trevor Carmichael. 2011. “Ocular Drug Delivery – a Look towards Nanobioadhesives.” *Expert Opinion on Drug Delivery* 8 (1): 71–94. https://doi.org/10.1517/17425247.2011.542142.

Tsay, Ruey-Yug, and Toyoko Imae. 2016. “Development of Nonfouling Biomaterials.” In *Encyclopedia of Biocolloid and Biointerface Science 2V Set*, 145–60. John Wiley & Sons, Ltd. https://doi.org/10.1002/9781119075691.ch11.

“US Patent Application for COMPOSITIONS, SYSTEMS, AND METHODS FOR SCAR TISSUE MODIFICATION Patent Application (Application #20190117746 Issued April 25, 2019) - Justia Patents Search.” n.d. Accessed April 27, 2020. https://patents.justia.com/patent/20190117746.

Vassileva, Elena. 2018. “The Challenge of Non Fouling Surfaces: Polymers Could Be the Answer.” *Journal of Polymer Science & Applications* 2017 (January). https://www.scitechnol.com/abstract/the-challenge-of-non-fouling-surfaces-polymers-could-be- the-answer-6004.html.

Vermette, Patrick. 2001. *Biomedical Applications of Polyurethanes*. Landes Bioscience.

Vishwakarma, Ajaykumar, Nupura S. Bhise, Marta B. Evangelista, Jeroen Rouwkema, Mehmet R. Dokmeci, Amir M. Ghaemmaghami, Nihal Engin Vrana, and Ali Khademhosseini. 2016. “Engineering Immunomodulatory Biomaterials To Tune the Inflammatory Response.” *Trends in Biotechnology* 34 (6): 470–82. https://doi.org/10.1016/j.tibtech.2016.03.009.

Wang, Cong, Seung-Jun Seo, Jin-Seong Kim, Se-Hee Lee, Jae-Kun Jeon, Jae-Woo Kim, Ki-Hong Kim, Jong-Ki Kim, and Jungyul Park. 2018. “Intravitreal Implantable Magnetic Micropump for On-Demand VEGFR-Targeted Drug Delivery.” *Journal of Controlled Release* 283 (August):

105–12. https://doi.org/10.1016/j.jconrel.2018.05.030.

Wang, Jillian, Angela Jiang, Malav Joshi, and John Christoforidis. 2013. “Drug Delivery Implants in the Treatment of Vitreous Inflammation.” Research article. Mediators of Inflammation. 2013. https://doi.org/10.1155/2013/780634.

Wang, Jing Jing, and Fang Liu. 2011. “Photoinduced Graft Polymerization of 2-Methacryloyloxyethyl Phosphorylcholine on Silicone Hydrogels for Reducing Protein Adsorption.” *Journal of Materials Science. Materials in Medicine* 22 (12): 2651–57. https://doi.org/10.1007/s10856-011-4452-y.

Weinreb, Robert N., Michael R. Robinson, Mohammed Dibas, and W. Daniel Stamer. 2020. “Matrix Metalloproteinases and Glaucoma Treatment.” *Journal of Ocular Pharmacology and Therapeutics*, April. https://doi.org/10.1089/jop.2019.0146.

Werner, L., J. M. Legeais, M. D. Nagel, and G. Renard. 1999. “Neutral Red Assay of the Cytotoxicity of Fluorocarbon-Coated Polymethylmethacrylate Intraocular Lenses in Vitro.” *Journal of Biomedical Materials Research* 48 (6): 814–19.

Willcox, Mark DP. 2019. “Tear Film, Contact Lenses and Tear Biomarkers.” *Clinical and Experimental Optometry* 102 (4): 350–63. https://doi.org/10.1111/cxo.12918.

Williams, Rachel L., Hannah J. Levis, Rebecca Lace, Kyle G. Doherty, Stephnie M. Kennedy, and Victoria R. Kearns. 2019. “Biomaterials in Ophthalmology.” In *Encyclopedia of Biomedical Engineering*, edited by Roger Narayan, 289–300. Oxford: Elsevier. https://doi.org/10.1016/B978-0-12-801238-3.11034-7.

Xie, Jin, Seulki Lee, and Xiaoyuan Chen. 2010. “Nanoparticle-Based Theranostic Agents.” *Advanced Drug Delivery Reviews* 62 (11): 1064–79. https://doi.org/10.1016/j.addr.2010.07.009.

Xu, Xu, Jun-Mei Tang, Yue-Mei Han, Wei Wang, Hao Chen, and Quan-Kui Lin. 2016. “Surface PEGylation of Intraocular Lens for PCO Prevention: An in Vivo Evaluation.” *Journal of Biomaterials Applications* 31 (1): 68–76. https://doi.org/10.1177/0885328216638547.

Yuan, Xiaoyong, Daniela C. Marcano, Crystal S. Shin, Xia Hua, Lucas C. Isenhart, Stephen C. Pflugfelder, and Ghanashyam Acharya. 2015. “Ocular Drug Delivery Nanowafer with Enhanced Therapeutic Efficacy.” *ACS Nano* 9 (2): 1749–58. https://doi.org/10.1021/nn506599f.

Zaleska-Żmijewska, Anna, Ewa Strzemecka, Zbigniew M. Wawrzyniak, and Jacek P. Szaflik. 2019. “Extracellular MMP-9-Based Assessment of Ocular Surface Inflammation in Patients with Primary Open-Angle Glaucoma.” Research Article. Journal of Ophthalmology. Hindawi. 2019.

https://doi.org/10.1155/2019/1240537.

Zhang, Lei, Zhiqiang Cao, Tao Bai, Louisa Carr, Jean-Rene Ella-Menye, Colleen Irvin, Buddy D. Ratner, and Shaoyi Jiang. 2013. “Zwitterionic Hydrogels Implanted in Mice Resist the Foreign-Body Reaction.” *Nature Biotechnology* 31 (6): 553–56. https://doi.org/10.1038/nbt.2580.

Zhang, Tuo-Di, Xi Zhang, and Xudong Deng. 2018. “Applications of Protein-Resistant Polymer and Hydrogel Coatings on Biosensors and Biomaterials.” In. https://doi.org/10.33582/2637-4927/1006.

Zhang, Wanlu, Guangji Li, Yinlei Lin, Liying Wang, and Shuqing Wu. 2017. “Preparation and Characterization of Protein-Resistant Hydrogels for Soft Contact Lens Applications via Radical Copolymerization Involving a Zwitterionic Sulfobetaine Comonomer.” *Journal of Biomaterials Science, Polymer Edition* 28 (16): 1935–49. https://doi.org/10.1080/09205063.2017.1363127

CHAPTER THREE

SYNTHESIS AND CHARACTERIZATION OF A MECHANICALLY ROBUST ZWITTERIONIC POLY (VINYL ALCOHOL) OCULAR HYDROGEL WITH ANTI-FOULING POTENTIAL

3.1 Introduction

Delivery of therapeutics to the eye continues to be challenging due to the ocular tissue barriers and the physicochemical nature of new chemical entities used to treat ocular conditions. (Uwaezuoke et al., 2021) Compounding these challenges is the skewing of the patient population requiring chronic therapeutic management of ocular conditions towards the aged due to improved life expectancy. Biomaterials are therefore increasingly being positioned to tackle this challenge in terms of maintaining the stability, presence, and deliverability of bioactives over an extended period of time from a single implant application. Deriving from these needs, contemporary ocular drug delivery is moving towards the use of devices such as the punctal plugs, contact/intraocular lenses as drug delivery systems. (Uwaezuoke et al., 2021) Such implants must, in addition, be able to limit the adsorption of proteins from body fluid that occurs ubiquitously with most biomaterials when placed in proximity with ocular fluids as this may lead to fouling, biofilm formation and ultimate implant failure.

Zwitterionic polymers possessing both cations and anions in their molecular backbone structure are an alternative to the use of polyethylene glycols (PEGs) as agents that limit protein adhesion in biomaterials. This followed from the connection of the protein resistant activity of phosphorylcholine to its zwitterionic structure. (Chen et al., 2005) The close structural resemblance of zwitterionics to naturally occurring molecules (sulfobetaine methacrylate to 2-aminoethane sulfonic acid (taurine) (a naturally occurring amino acid component of human muscular tissues)), the super-hydrophilicity of zwitterionics, their biocompatibility and the additional potential to serve as ligands for conjugating drug molecules through the free carboxylic acid group as is in the case of carboxybetaine methacrylate makes them appealing. Since then, several studies employing zwitterionic polymers such as sulfobetaine methacrylate (SBMA) and carboxybetaine methacrylate as protein resistant agents have been explored. Many of these studies have involved the use of SBMA as a surface modifying coat on other materials with sufficient mechanical strength to improve the low mechanical strength of SBMA as a

homopolymer. (Ashtiani et al., 2018) Some studies in which zwitterionic polymers were used in combination with other polymers also identified the softening effect of the zwitterionic polymer. (Zhang et al., 2017) As a panacea to a major drawback to the stand-alone use of zwitterionics in medical devices and implants (limited mechanical robustness), Carr and co-workers synthesized and used a crosslinker with a structural resemblance to the zwitterionic. Their work showed an improvement in the mechanical properties of hydrogels formed using the new zwitterionic crosslinker over the hydrogels prepared with the traditional methylene bisacrylamide (MBAA). This improvement was ascribed to the improved solubility of the synthesized zwitterionic crosslinker at all concentrations over that of MBAA. (Carr et al., 2011) Unfortunately, the added synthesis of the zwitterionic crosslinker was complex. Even though surface modification with other hydrophilic polymers and zwitterionics had yielded protein resistant biomaterials, the durability of these coating is still a concern particularly due to the dynamic nature of the environment for specific ocular applications. (Uwaezuoke et al., 2021)

Polyvinyl alcohol (PVA) is one of the polymers that have been used in surface modification of commercially available contact lenses where its hydrophilicity was exploited to impart protein resistance. Researchers had reported the potential use of PVA as a stand-alone hydrogel for ocular application with appropriate mechanical strength. (Kita et al., 1990) The hydrophilicity and high swelling of PVA hydrogels has also great implications for its mechanical strength hence Tummala and coworkers (following the method of Kita and co-workers (Kita et al., 1990)) explored its use in a contact lens but with reinforcement with carboxylated nanocellulose whiskers. (Tummala et al., 2016) Another drawback to the use of PVA in ocular application particularly for contact lens application is its lack of adhesiveness hence if used in an application such as lens or patch, it may not adhere to the ocular surface. Additionally, traditional methods of crosslinking PVA involving the physical process of freeze-thaw cycles and the chemical crosslinking using glutaraldehyde are both time consuming, tedious, and may have implications for safety (chemical method). Methacrylation of PVA enables the photo-polymerization process which has been proposed as a better method for the fabrication of hydrogels for biomedical applications in view of the shorter time periods of exposure and amenability to room temperatures operations and the availability of biocompatible photo-initiators. (Zhang et al., 2019) (Shin et al., 2012)

Herein, the fabrication of an ocuterial in the form of a hydrogel using two highly hydrophilic polymers is reported. A synergistic potentiation in the hydrophilicity of the expected hydrogel was hypothesized *ab initio* with a view to maximally limit protein adhesion to the surface of the hydrogel

with maximized hydrophilicity. With the expected possible mechanical deficit, this work set out to exploit the possible synergy of two hydrophilic polymers, polyvinyl alcohol (PVA) and sulfobetaine methacrylate (SBMA) in developing a super-hydrophilic protein resistant ocular hydrogel. PVA was first methacrylated to make it photo-cross linkable while improving its adhesiveness. In a facile, one step process, SBMA monomer was grafted as polymers onto PVA methacrylate by photo-initiated crosslinking polymerization. Serendipitously, concentration dependent mechanical strength improvement from an apparently mechanical strength-deficit polymer, SBMA was developed.

3.2 Materials and methods

3.2.1 Materials

Poly (vinyl alcohol) (PVA) (Mw 89000-98000 m/mol, 98+% hydrolysed) Irgacure 1929, Polyethylene glycol dimethacrylate Average M_n 750, 1,3-propane sultone, Dimethylaminoethyl methacrylate (DMAEMA), Glycidyl methacrylate (GMA), and Dimethylaminopyridine (DMAP) were all purchased from Sigma-Aldrich (St Louis, MO, USA). All other reagents were of highest laboratory standards and used as received.

3.2.2 Synthesis of the sulfobetaine methacrylate

Sulfobetaine methacrylate monomer was synthesized following a previously reported method in which equimolar concentrations of 1,3-propane sultone and DMAEMA were reacted together. (Xiang et al., 2016) Briefly, a solution of propane sultone in about 50 mL of acetone was introduced to a round bottom flask to which a dropping funnel was attached and placed on a magnetic stirrer set at 40 rpm. A solution of DMAEMA (passed through basic alumina to remove inhibitor) was introduced into the dropping funnel and allowed to drop into the round bottom flask over a period of 1 hour. The reaction flask was kept in the dark for 48 hours. Thereafter, the resulting white precipitate was collected by filtration and purified by recrystallization from an acetone methanol solvent mixture.

3.2.3 Synthesis of the GMA modified PVA (PVAGMA)

Polyvinyl alcohol solution (10 % w/v) was prepared in anhydrous DMSO in a 2-arm round bottom flask following a modified method from previous reports. (Zhang et al., 2019). DMAP (0.22g) and 0.6 mL of GMA were introduced into the flask which was stirred under nitrogen at 60 ^{o}C for 1 hours. PVAGMA was recovered from the reaction mixture using a large excess of acetone. The

resulting white precipitate was washed twice with acetone and dried under vacuum for 48 hours. The concentration of GMA was varied to achieve different degrees of methacrylation.

3.3.4 Zwitterionization and photoinitiated crosslinking copolymerization of PVAGMA and SBMA

Required quantities of PVAGMA and SBMA were dissolved in about 6 mL mixed solvent system containing 80% DMSO in deionized water. The ratio of PVAGMA to SBMA was varied from 1: 0 to 1: 0.25. PEGDMA (varied between 3% and 5% w/w and Irgacure 1929 (1% w/w) were added to the polymer solution and stirred. Air bubbles were removed by ultrasonication in a bath sonicator at 27 ^{o}C for 5 minutes. Crosslinking polymerization was afterwards carried out in a UV chamber powered by a 365 nm light for 10 minutes. The resulting hydrogels were immersed in excess amount of deionized water over 72 hours with daily water changes for rehydration and to get rid of unreacted components.

3.2.5 Characterization of the PVAGMA base material and ocular hydrogel

3.2.5.1 Determination of the molecular transitions in the pristine and modified starting materials

Attenuated total reflectance-Fourier transform infrared spectroscopy to determine the molecular transitions within the pristine and modified components was carried out on all starting materials and hydrogels using Perkin Elmer Spectrum 2000 ATR-FTIR spectrometer (PerkinElmer 100, Llantrisant, Wales, UK) fitted with a single-reflection diamond MIRTGS detector. Analysis was obtained in the 4000–650 cm^{-1} range after 60 scans.

Proton Nuclear Magnetic Resonance (^{1}HNMR) was undertaken on both the pristine and modified PVA. Spectra was obtained at 90°C in deuterated DMSO on a BRUKER–200 MHz Varian spectrometer.

Percent Transmittance was determined by scanning on a Varian Cary 4000 UV–vis spectrophotometer in the wavelength range 200 – 800 nm. Deionized water was used as a blank for all determinations.

Thermal properties and thermogravimetric analysis were undertaken on the Mettler Toledo, DSC, STARe System, (Swchwerzenback, ZH, Switzerland) and PerkinElmer, TGA 4000, (Llantrisant, UK). For DSC measurements, between 3 to 10 mg of the sample to be analysed was sealed in aluminium crucibles and heated over a temperature range of 20 to 300 °C at a heating rate of

10 °C/min under a N_2 atmosphere. DSC curves were obtained as plots of heat flow against temperature. For TGA, samples were heated at a rate of 10 °C/min from 30 to 900 °C under continuous nitrogen purging. Thermograms were generated as percentage weight loss vs. temperature.

X-ray powder diffraction to delineate the crystallinity of the individual modified and unmodified components of the hydrogel and the hydrogel was determined on benchtop (Rigaku Miniflex 600, Rigaku Corporation, Matsubara-cho, Akishima-shi, and Tokyo, Japan) diffractometer using *CuK*α radiation at 40 kV and 15 mA. The diffractograms were obtained at a scanning 2θ range between 5 to 90 degrees at a scan rate of 10 degrees/minute. The scan step of 0.02 °C was used throughout.

The surface area and porosity of the dried hydrogel sample was undertaken using the BET and BJH principles of the Porositometric analyser (Micromeritics ASAP 2020, Norcross, GA, USA). A minimum of 100 mg sample of the dried hydrogel was initially degassed and subsequently subjected to analysis at an evacuation rate of 50 Hg/second and temperature ramp of 10°C/ minute. The targeted temperature was 115 °C which was maintained for 900 minutes till the end of the analysis.

3.2.6 Morphological Analysis of prepared hydrogels

The morphology of the hydrogels obtained from the photo initiated crosslinking polymerisation of PVAGMA and SBMA was characterized using Field Emission Scanning Electron Microscopy of ZEISS Sigma 300 VP with a ZEISS 'smart SEM' software (Field Emission Scanning Electron Microscope, FEI, Orlando, Florida, USA). Dried hydrogel samples were fractured in liquid nitrogen and mounted on aluminium stubs to view the planar and cross sections of each dried hydrogel which was coated with palladium/gold prior to SEM analysis at an accelerating voltage from 10 t0 15 kV.

3.2.7 Mechanical and viscoelasticity profiling

The mechanical characteristics of sample hydrogels swollen in artificial tear fluid was studied using the compression mode of the texture analyser (TA. XT plus texture analyser, Stable Microsystems, Surrey, UK) at room temperature fitted with the compression platen probe (0.5r) at different strain percent. The diameter and height of a cylindrical sample punched with a 6 mm skin biopsy punch was measured using a digital vernier caliper (Krafft, DV150GW, Schoellerstr Düren, German). Each sample disc was first subjected to 10 compression cycles at a 40 %

strain and afterwards compressed to failure at 70 % strain using an auto trigger force of 0.001 kg at room temperature.

The shear storage modulus, Shear loss modulus, compressive modulus, and tan d of equilibrium swollen hydrogel discs were determined on the ElastoSens™Bio (Rheolution instruments, Canada). For each analysis, a hydrated disc of the hydrogel designed to fit into the sample holder is used. The system is first calibrated with the sample holders before each determination. A single measurement with temperature profile from 25 °C to 37 °C was undertaken to determine viscoelastic properties between the handling temperature and the body temperature. The temperature step was set at 5 °C.

3.2.8 Surface porosity analysis of the hydrogel samples by Brunauer-Emmett-Teller (BET) Theory

The porositometric analyser (Micromeritics ASAP 2020, Norcross, GA, USA) was employed for the evaluation of the surface area, pore size, and pore volume of the hydrogel sample. The dried hydrogel sample cut to meet the minimum weight requirement for the porositometric analyser was introduced into the sample tube and degassed. Surface parameters were determined using the BET and BJH models on the instrument software. An evacuation rate of 50 mm Hg/s, a temperature ramp rate of 10 °C/minute, target and holding temperatures of 115 °C and 30 °C respectively was employed for a duration of 900 minutes to complete the analysis.

3.2.9 Determination of Equilibrium water uptake (EWU)

To determine the percent swelling of the hydrogel, the initial weigh of an equilibrium swollen hydrogel was determined. Subsequently, the hydrogel is dried in a vacuum oven set at 90 °C to a constant weight. The percent swelling is subsequently determined using **Equation 3.1**

Equation 3.1

$$\%Swelling = \frac{Weight\ of\ swollen\ hydrogel - Weight\ of\ dried\ hydrogel}{Weight\ of\ dried\ hydrogel}\ x\ 100.$$

3.2.10 Determination of the water contact angle measurement

Water contact angle is usually used as an indication of the hydrophilicity of any material and by extension its protein resistance potential. The water contact angle of a sessile water drop of

distilled water on an equilibrium swollen hydrogel was determined on a DataPhysics Instruments contact angle goniometer. Each sample was wiped with filter paper to remove excess water from the surface of the hydrogel and mounted on a stage. 1 µL of distilled water was delivered on the surface using a Hamilton syringe at a dosing rate of 1 µL/s. The digital picture of the stabilized droplet is subsequently recorded using the camera software while the contact angle was measured using SCA202 version 4.1.12 build software. The procedure was repeated on three different points on each sample.

3.2.6. In vitro assessment of protein adhesion to the hydrogel samples

The amount of protein adsorbed unto the hydrogel was quantified using the Micro BCA™ protein assay kit. For the adsorption study, discs were punched out of the hydrogel and the dimensions noted. For each hydrogel formulation, 3 such discs were punched and immersed in a protein solution and thereafter incubated in an orbital shaker set at 37° C for 1 hour. The artificial tear fluid (ATF) containing a mixture of proteins was made by dissolving lysozyme, mucin, bovine serum albumin (BSA) and calcium chloride in phosphate buffered saline (PBS) pH 7.4 and used for constructing the calibration curve. After the incubation, the discs were washed in PBS 3 times and subsequently, a 1 % sodium dodecyl sulfate solution was used to detach the protein adsorbed to each of the disc. The amount of protein adsorbed to each disc was measured using the Implen NanoPhotometer® according to the protocol of the Micro BCA™ protein assay kit.

3.2.7 Cytotoxicity evaluation of the hydrogel extract using MTT assay

MTT assay to determine the cytotoxicity of extractables from the hydrogel was carried out using 3T3 fibroblast, HEK 293 cells and an ocular cell line, human retinal epithelial primary (HREP) cell lines. RPMI medium supplemented with 10 % fetal bovine serum (FBS) and 1% penicillin/streptomycin was used as the culture medium for 3T3 and HEK 293 cells while HREP cells were grown in DMEM: Ham's F-12 (50: 50) supplemented with 10 % FBS and 1 % penicillin/streptomycin. The cells were grown to 80 to 90 % (about 48 hours incubation) confluence in an incubator set at a temperature of 37°C with 5% CO_2. Thereafter, the cells were detached using about 2 mL of 1% trypsin. 90 µL of the cell suspension were thereafter seeded per well in two 96-well plate from a cell suspension at a cell density of 30000 cells/mL for 3T3 and HEK 293 cells and 40000 cells/mL for HREP cells. The plates were further incubated for 24 hours and thereafter, each well was treated with 10 µL of the extract from the hydrogel prepared by incubating each hydrogel formulation in ATF at 37°C for 7 days. After 24 and 48 hours respectively, each well plate was treated with 10 µl of (3-[4,5- dimethylthiazol-2-yl]-2,5-

diphenyltetrazolium bromide) (MTT) at a final concentration of 5 mg/ml. Each plate was further incubated for 4 hours in a humidified atmosphere at 37° C and 5 -6 % CO_2. 100µl of solubilization reagent was then added and the plate allowed to stand overnight in the incubator. The absorbance of the developed purple formazan crystals was then read in a VX3 microplate reader at 570 nm. The percent viability of the cells was subsequently calculated using **Equation 3-2.**

$$\%\, Viability = \frac{Absorbance\ of\ treated\ well - absorbance\ of\ blank}{Absorbance\ of\ control - absorbance\ of\ blank} x\ 100 \quad \textbf{(3.2)}$$

ATF was used as the negative control; 5 fluorouracil was used as the positive control and untreated cells were used as the blank. Percent viability will be Viability will be plotted as a bar graph.

3.2.8 Statistical analysis

Results were reported as the mean ± standard deviation of triplicate readings. Where necessary, comparisons between means are made using the student t-test and one way analysis of variance using Microsoft Excel 2016 (Microsoft Corp, WA, USA) and GraphPad by Dotmatics (Boston, Massachusetts).

3.3. Results and Discussion

3.3.1 Synthesis and spectral characterization of PVAGMA and the hydrogels

PVAGMA was synthesized by the grafting of a methacrylic moiety to PVA via the ring opening reaction of GMA in the presence of PVA. The SBMA was added as a monomer in the hydrogel forming mixture with the expectation that polymerization will take place simultaneously with the crosslinking. Different characteristics of the formed hydrogel was optimized by varying different components. A general nomenclature was used to name each formulation based on the 2-constituent polymer, PVAGMA and SBMA, coded PM and SM respectively and the numbers following immediately after each component representing the percentage content of that polymer relative to the second polymer. As an example, PM90-SM10 codes for a formulation in which the ratio of the PVGMA: SBMA is 90 :10.

ATR-FTIR being an excellent tool for the delineation of the vibrational patterns of dipole moments of compounds that result from infrared absorption or transmittance was used in analysing the molecular transitions occurring at every step of the synthesis. Analysis shown in **Figure.3.1**

confirmed the molecular transitions brought about by the methacrylation of PVA. **Table 3.1** is a summary of the various peaks that appeared in the modified PVA and their absorption wavenumbers. The characteristic C= O stretching of the methacrylates appeared at

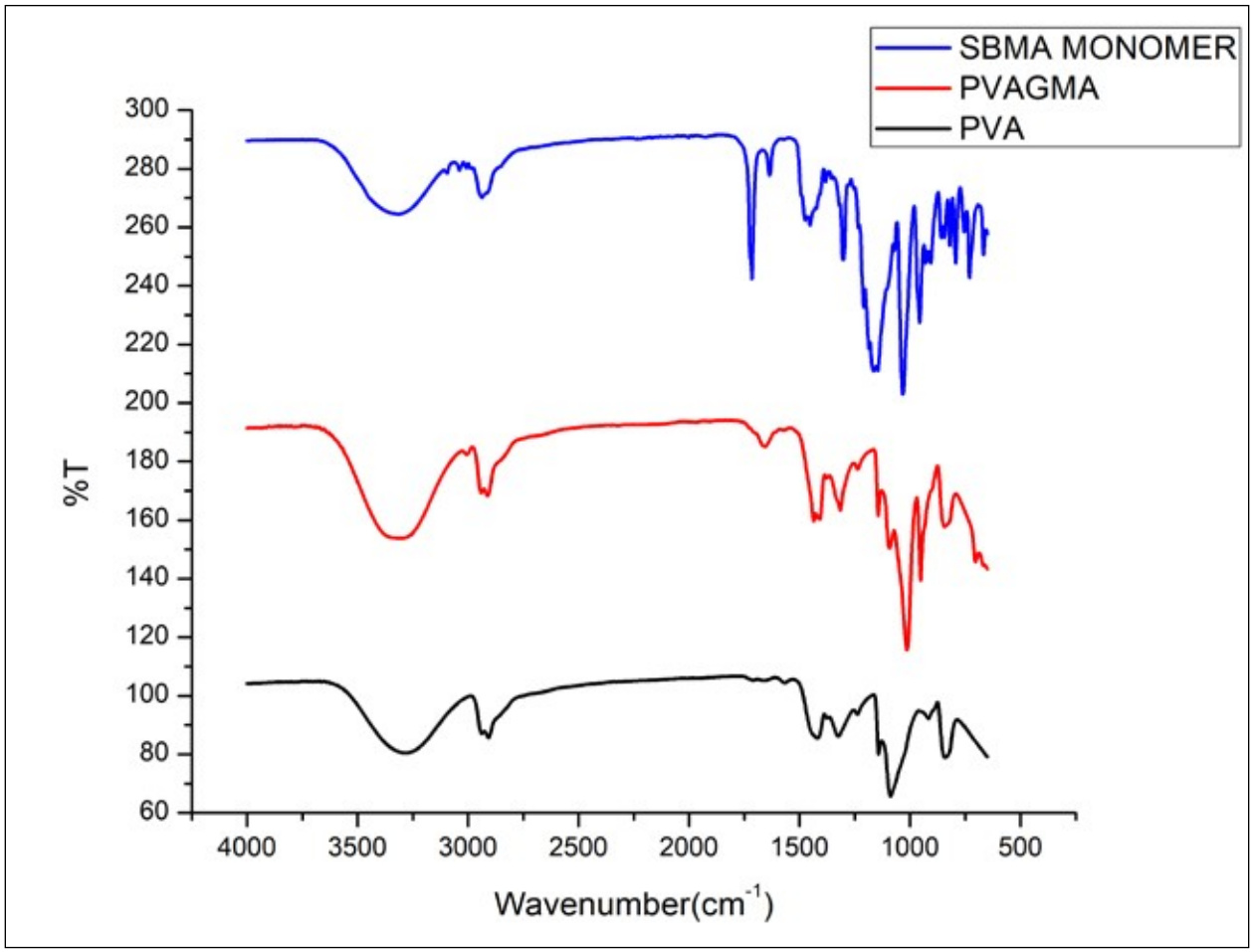


Figure 3.1 FTIR spectra of SBMA monomer, PVA, and PVAGMA.

1708.15 cm-1 while the C = C stretch appeared at 1642.96 cm -1. Previous studies had assigned the OH stretch of PVA FTIR spectra to the peak at 3280, the CH2 – CH3 stretch to the peak at 2917 cm -1 and 3001 cm -1 respectively. (Huszank et al., 2019) The peak at 1690 cm -1 is assigned to the C = O, CH bending vibration assigned at 1425 cm-1, C- H deformation vibration at 1324 cm^{-1}, C-O stretching of acetyl group at 1081 cm^{-1} and C-C stretching at 839 cm^{-1}. (Kharazmi et al., 2015). Zhou and coworkers, in their work, in which, SBMA was grafted to

Table 3.1 FTIR Wave number assignments in PVA and PVAGMA.

Assignments	PVA Absorption wavenumber (Omkaram et al., 2007)	PVA Absorption wavenumber	PVAGMA Absorption Wavenumber
OH stretching	3340	3283	3319
CH_3 stretching		-	3001
CH_2 stretching	2942	2907	2913
C = O from ester			1708
C = C stretching			1642
CH_2 bending	1430	1420	1452
C – O -C stretching	1141	1142	
C = O stretching	1096	1087	1093
CH_2 vibrations	916	918	952
C – C stretching	850	848	845

chitosan, assigned the stretching vibrations appearing at 2934 cm^{-1}, 1750 cm^{-1}, and 1150 cm^{-1} to the stretching vibrations of -CH_2, -C=O and -S=O bonds resulting from SBMA grafting. (Zhou et al., 2015) Likewise, Lalani and Liu assigned the FTIR peaks appearing at 1160 cm^{-1} and 1032 cm^{-1} respectively to the asymmetric and symmetric S=O of the sulfonate group while assigning the peak at 1480 cm^{-1} to the quaternary ammonium bond in the poly sulfobetaine spectrum. (Lalani & Liu, 2011) In this work therefore, the peaks appearing 1161 cm^{-1} and at 1034 cm^{-1} in the SBMA monomer spectrum are assigned respectively to the asymmetric and the symmetric S = O bonds of the sulfonate group while the peak at 1418 cm^{-1} is assigned to the quaternary ammonium group.

In **Figure 3.2**, the FTIR spectra of the lyophilised PVAGMA hydrogels copolymerized with 20 % w/w (PM-80SM-20), 11 % w/w SBMA ((PM-89SM-11) and the hydrogel made from PVAGMA alone (PM-100) are shown. The peaks appearing in the range 2943 cm^{-1}- 3043 cm^{-1}

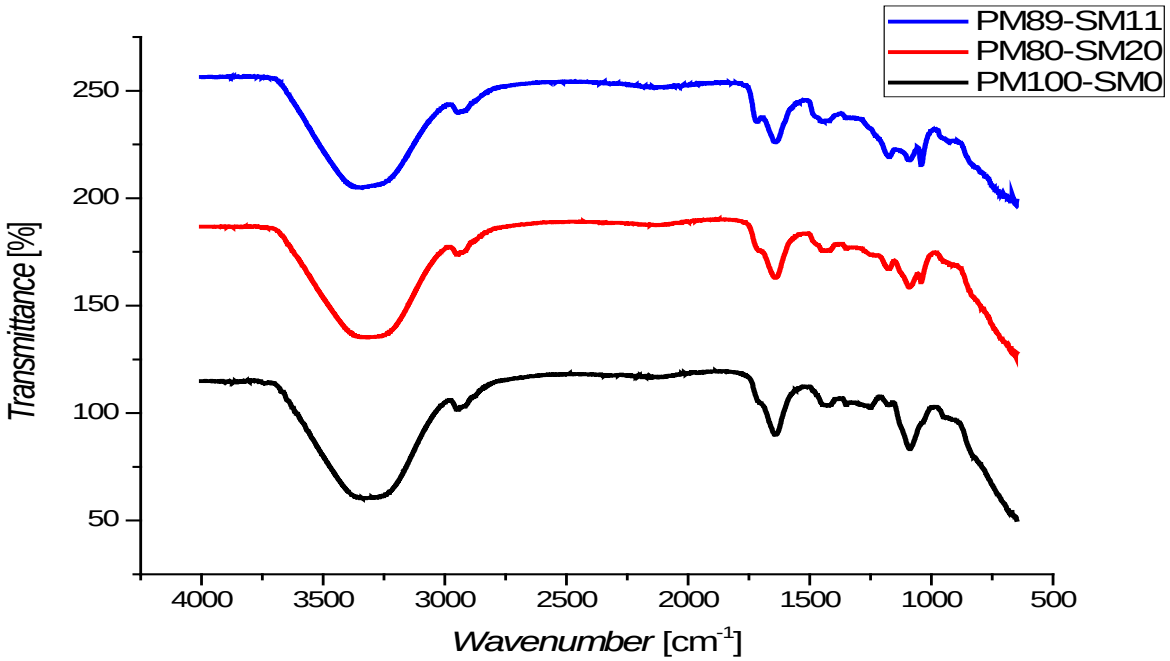


Figure 3.2 Comparative FTIR spectra of PVAGMA hydrogel with varying content of SBMA.

representing respectively the CH_2 and methyl groups of the methacrylate in the SBMA monomer and which also appeared in the PM-100-SM0 hydrogel in **Figure 3.1** disappeared in the hydrogels in which SBMA had been copolymerized with PVAGMA, (PM-80SM-20 and PM-89SM-11) in **Figure 3.2** and possibly represents the crosslinking points. Additionally, the appearance of the peak at 1170 confirmed the presence of the stretching vibrations of S = O of the SBMA thus confirming the copolymerization of SBMA with the PVAGMA hydrogel. The C = O band confirming the presence of the ester group appeared at 1708 cm^{-1} and between 1716 -1722 cm^{-1} of PVAGMA and SBMA spectrum respectively. The stretching vibrations that appeared at 2997 cm^{-1} and 3001 cm^{-1} of PVAGMA and SBMA belonged to the CH stretching of the methacrylate group. In addition, the peak occurring around 1640 cm^{-1} was used to confirm the polymerization of methacrylates (Delgado & Young, 2021) and the shift of the wavenumber and the intensity was used to confirm the polymerization of SBMA in the hydrogel. These confirm the polymerization of SBMA and its crosslinking with PVAGMA.

The chemical shifts of the different protons occurring in PVA was obtained though proton NMR using deuterated DMSO as the solvent and was used to further confirm the methacrylation of PVA. In addition, the effect of doubling the concentration of glycidyl methacrylate during the methacrylation of PVA was also confirmed using ^{1}H NMR. **Figure 3.3** shows the spectra of pristine PVA and methacrylated PVA. The occurrence of singlet proton signals at the chemical shifts of 5.65 ppm and 6.0 ppm. The group of protons occurring at chemical shift of 1.5 ppm belonged to the CH_2 of the PVA backbone. These protons are mixed up of doublets and triplets arising from the varied nature of their chemical environment. The doublet proton signal occurring downfield at chemical shift of 3.9 ppm has been assigned to the CH group attached to the oxygen atom of the PVA. The degree of methacrylation is found by determination of the integration of the peaks arising from the methacrylate group occurring at chemical shifts 5.65 ppm and 6.0 ppm. By visual inspection of the NMR spectra comparing the PVAGMA with lower concentration of GMA and that with higher GMA shown in **Figure 3.4A**, it is obvious that these peaks at chemical shifts 5.65ppm and 6.0 ppm became more visible in the NMR spectra of the PVGMA prepared with higher concentration of GMA, (**Figure 3.4B).**

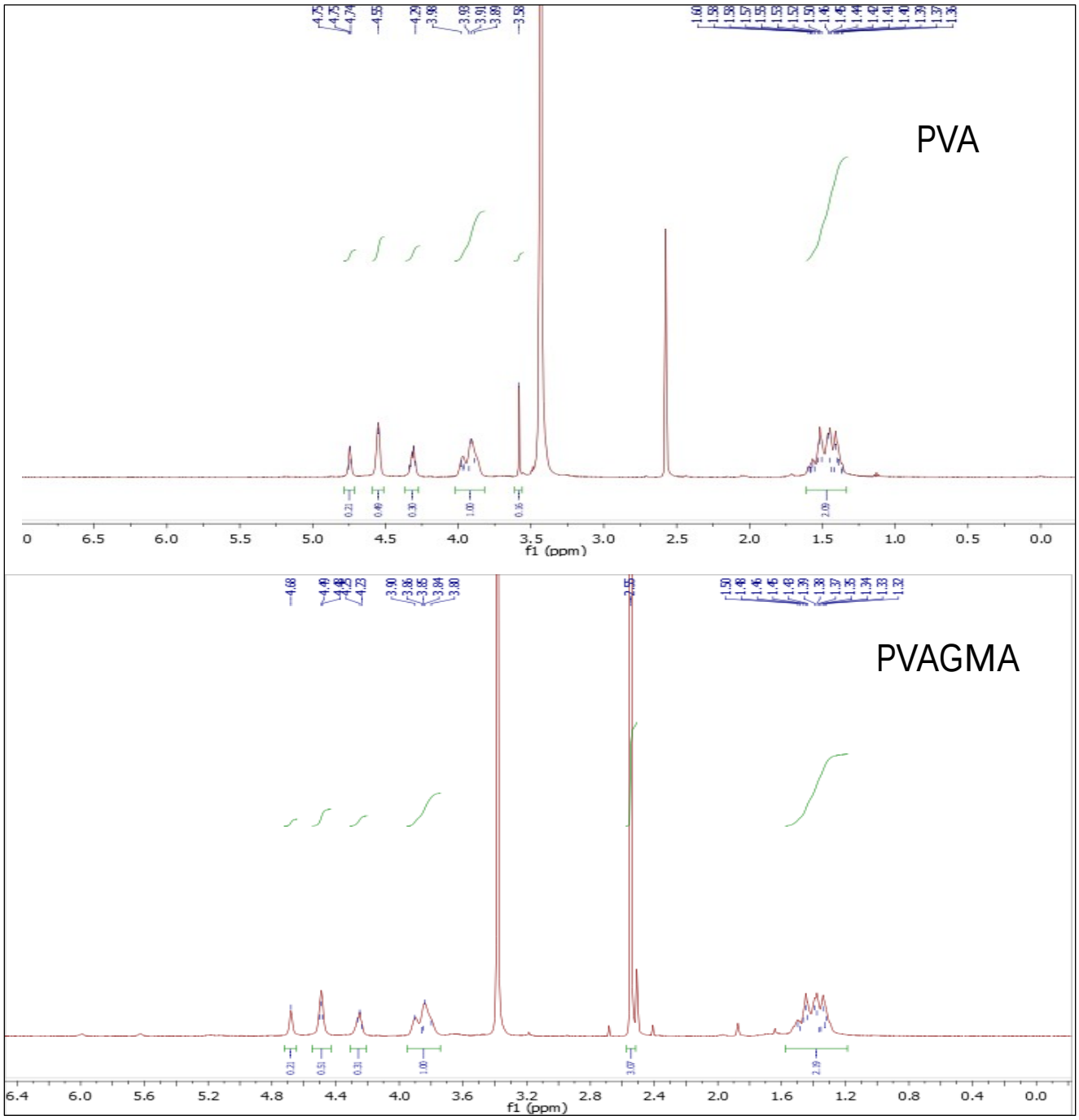


Figure 3.3 1HNMR of pristine PVA and methacrylated PVA.

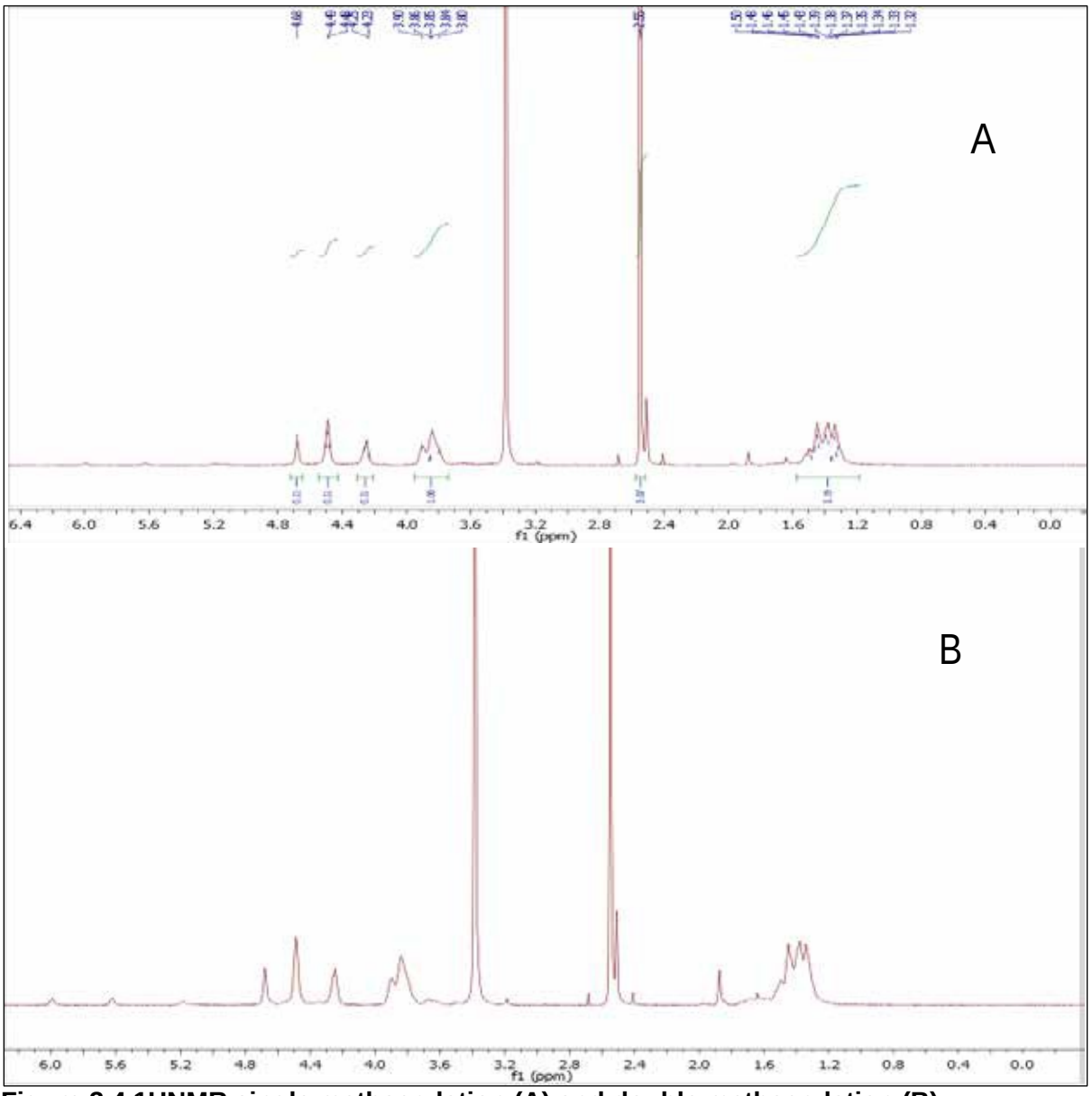


Figure 3.4 1HNMR single methacrylation (A) and double methacrylation (B).

3.3.1. Thermal analysis of PVAGMA and the hydrogels

The thermal events that occurred when the polymers were subjected to heat flow in a DSC furnace is shown in **Figure 3.5 (**A – D).

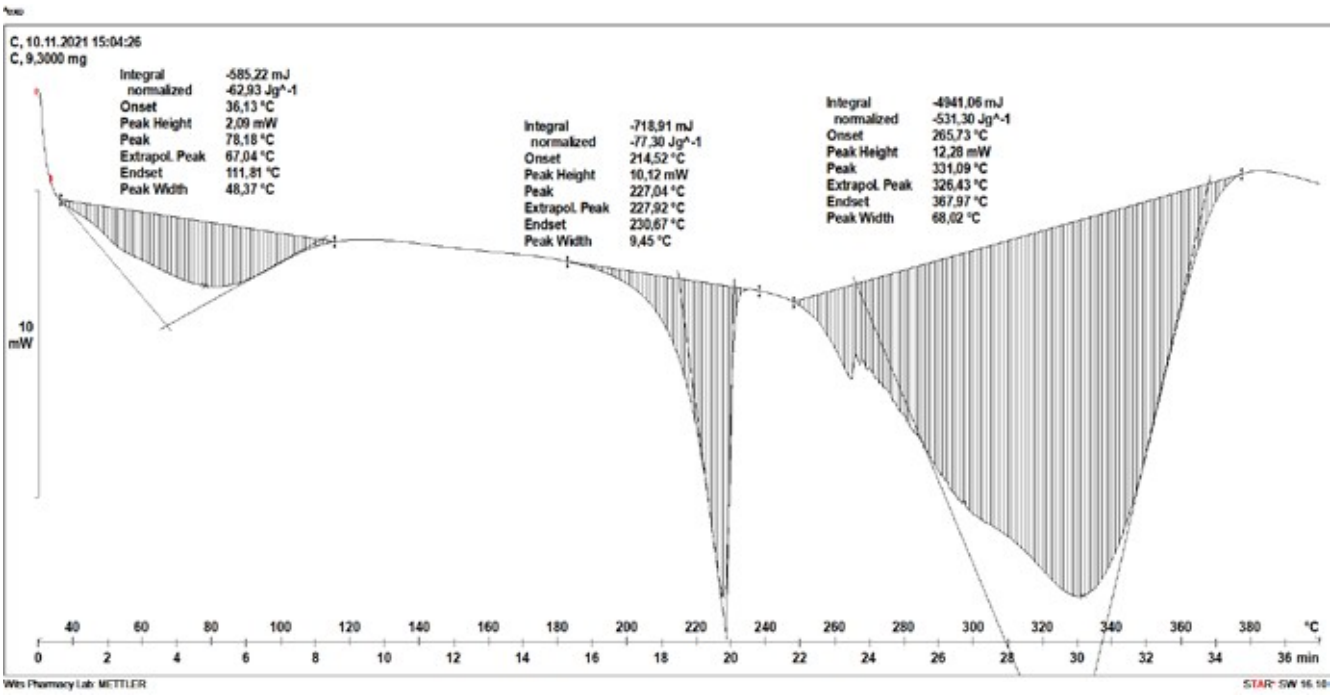


Figure 3.5A DSC thermograms of A pristine PVA.

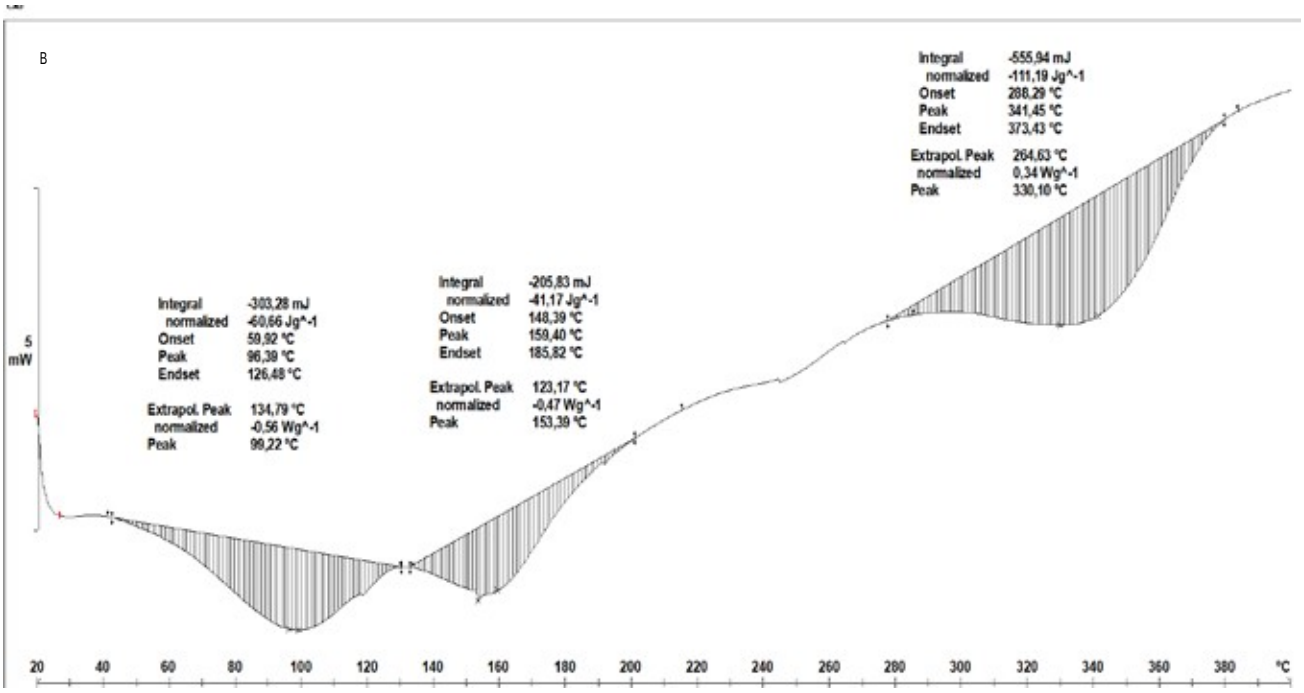


Figure 3.5B1 DSC thermograms of PVAGMA.

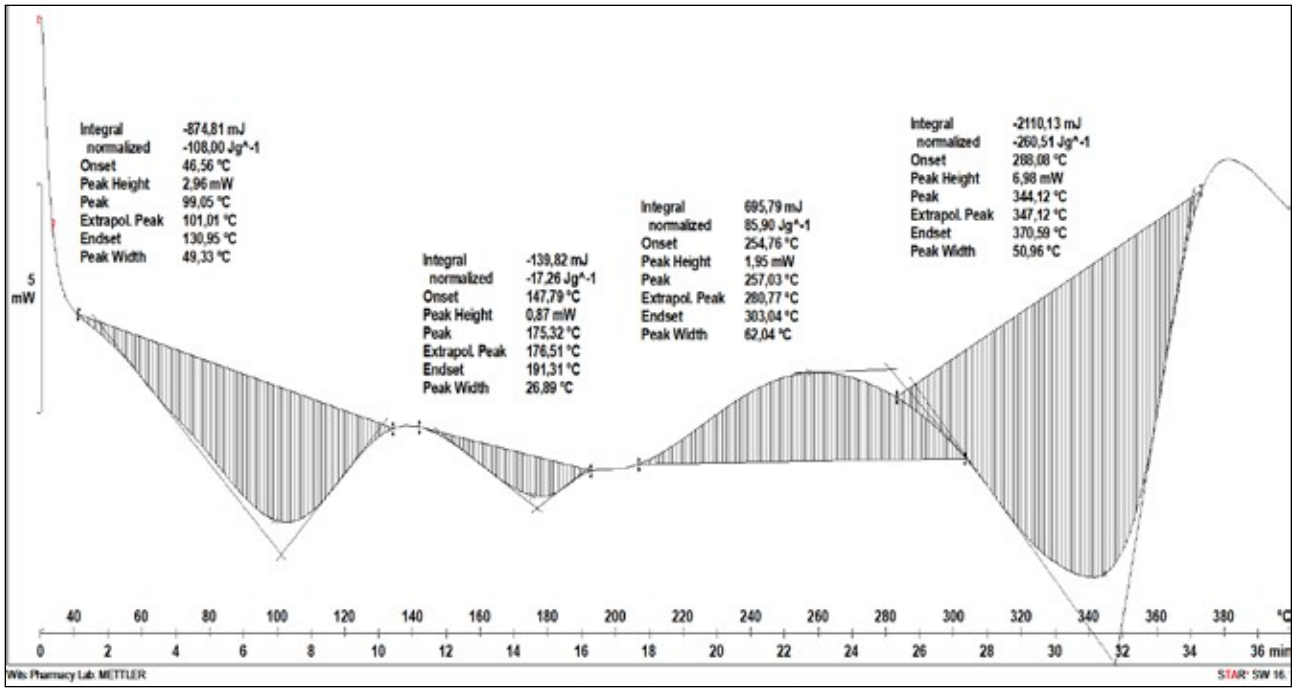


Figure 3.5B2 DSC thermograms of PVAGMA with higher methacrylation.

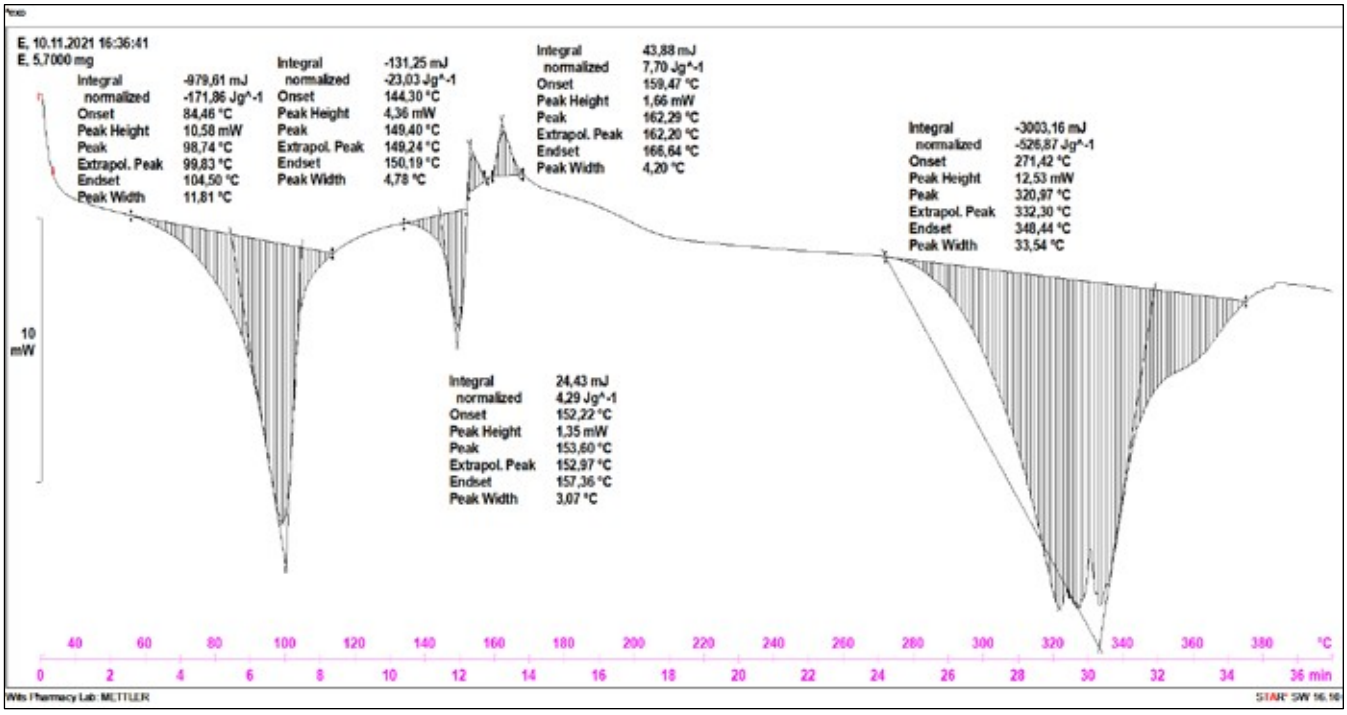


Figure 3.5C DSC thermograms of SBMA monomer.

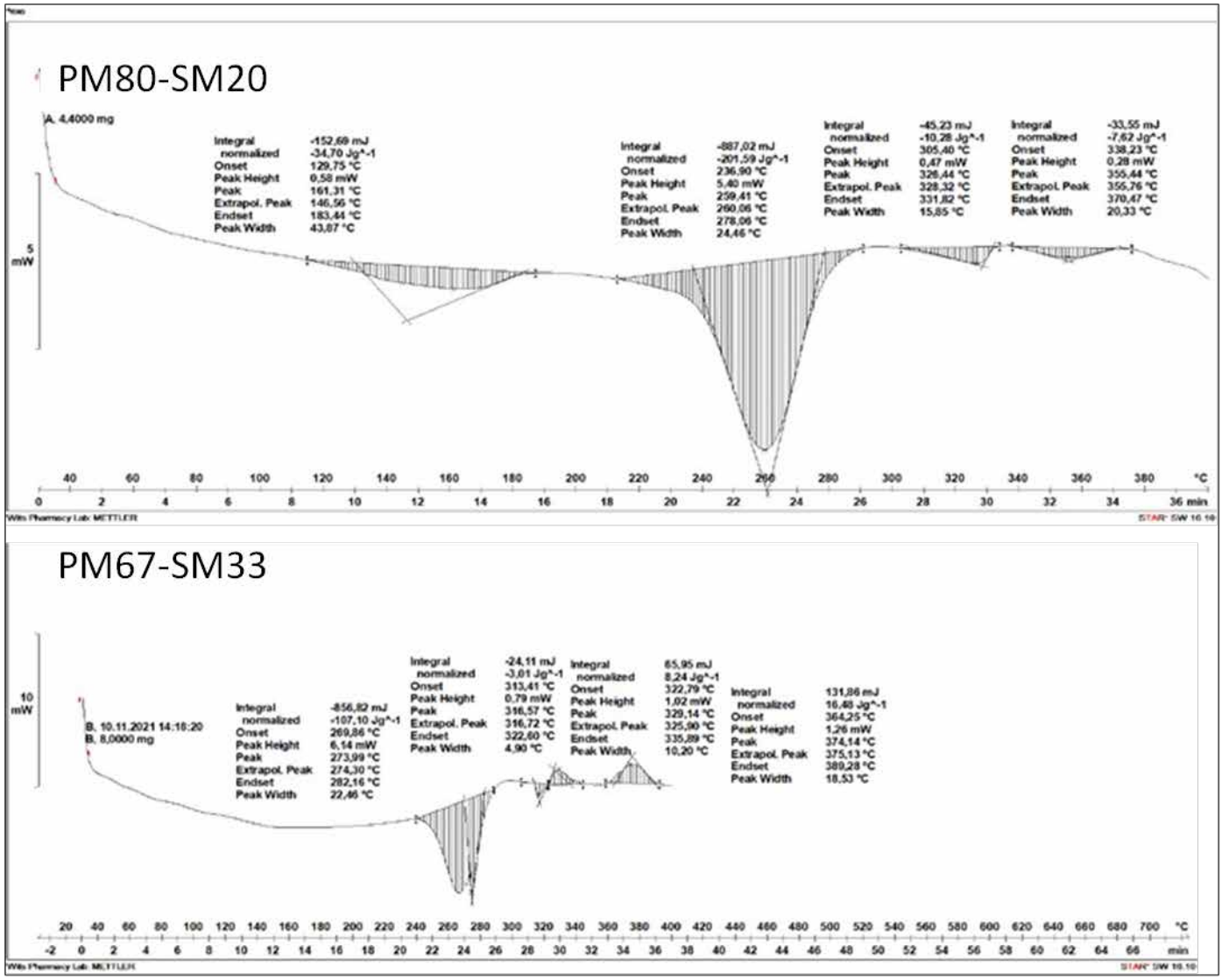


Figure 3.5D DSC thermograms of PVAGMA hydrogels with different SBMA content.

From **Figure 3.5** A, the glass transition temperature (Tg) and melting point of the PVA used in this work was determined at 80.81 °C and 208.08 °C and melting point of the PVA used in this work was determined at 80.81 °C and 208.08 °C respectively. Although this varied by 0.81 °C and 8 °C with that reported in literature for reference samples (Schindler and Hauser 2004), different studies had shown glass transition temperatures of 85 °C (Fathi et al., 2011) and 70 °C (Strawhecker & Manias, 2000). Strawhecker and Manias, additionally reported a melting point of 225 °C (Strawhecker & Manias, 2000). These differences have been attributed to the variability in the degree of crystallinity obtained from different batches of PVA, the degree of hydrolysis and the determination technique or operation. The melting temperature was associated with

$Jg.^{-1}$ and an endothermic peak 228.75 °C. The small shoulder occurring at 265.48 °C could be attributed to crystallisation occurring very close to melting. Decomposition started around 344 °C. Methacrylation of PVA resulted in a polymer with a higher Tg of 99.22 °C, a melting endotherm of 153.7 °C and a decomposition peak at 330.9 °C as can be seen in **Figure 3.5** B 1. **Figure 3.5** B2 shows that increasing the degree of methacrylation shifted the Tg and melting point even further. This differed greatly from 66.1 °C observed by Zhou and coworkers (Zhou et al., 2019). The difference is not surprising since the PVA used in their study was of different molecular weight and degree of hydrolysis. In addition, the melting peaks of partially crystalline polymers depends on the distribution of crystallinities within the bulk of the polymer. Many other parameters such as degree of methacrylation will also determine the Tg of the modified polymer. The thermogram of SBMA monomer did not show any glass transition temperature. This agrees with the crystalline nature of the monomer. In addition, Lalani and coworkers also did not observe a glass transition temperature from the DSC of the SBMA polymers but rather observed a broad endothermic peak that peaked at 122 °C, 137 °C and 150 °C depending on the molecular weight of the polymer (Lalani & Liu, 2011). In this work, however, the DSC thermogram of SBMA monomer shown in **Figure 3.5**C shows a melting endotherm at 146.3 °C closely followed by two peak resembling that of cold crystallisation at 153.50 °C and 163.29 °C. In other thermograms (not shown), these two peaks appeared as one peak at 157 °C implying the presence of a polymorph in the sample showing two peaks. The decomposition temperature showed at 326.17°C. On the other hand, the DSC curve of a hydrogel sample containing SBMA (shown in **Figure 3.5**D) portrayed major thermal events at 71.36 °C, 187.16 °C, 261.34 °C, and 258.5 °C corresponding to the Tg, melting point, and decomposition temperatures. It is observed that the crystallinity of the SBMA monomer did not reflect in the hydrogel. This is likely because the SBMA monomer polymerised and crosslinked in the hydrogel as will be later seen from the XRD result. The degree of crystallinity of the polymerised SBMA is lower than that of the monomer. Crosslinking polymerisation led to the formation of amorphous areas as Fathi and coworkers observed the same effect while working with PVA xerogels. The physical crosslinking process involved in the xerogel formation caused a significant reduction in the melting endotherm attributed to the ordering effect which resulted in more closely packed PVA crystals. (Fathi et al., 2011)

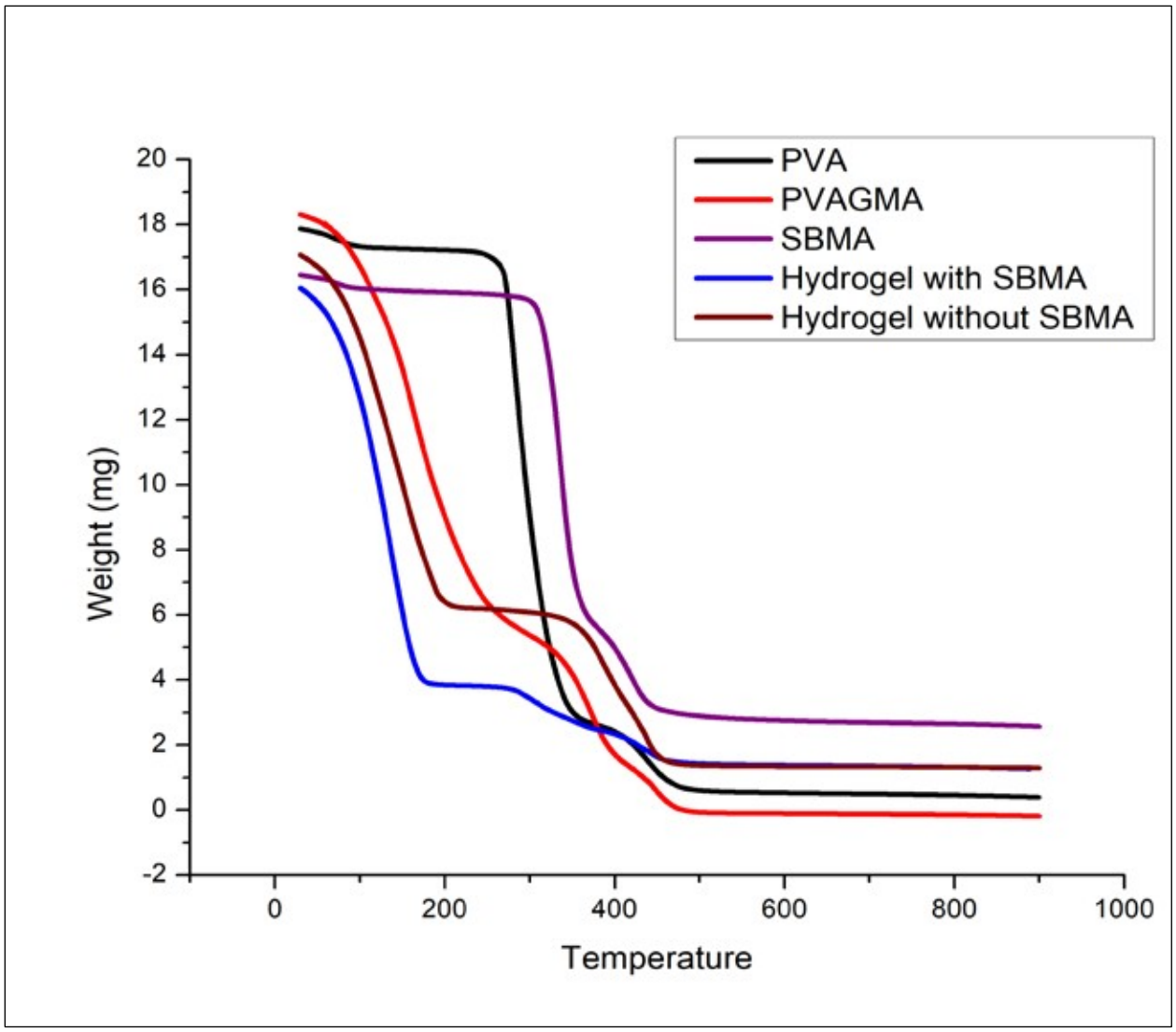


Figure 3.6 TGA of the starting materials and hydrogels.

Thermogravimetric analysis usually shows how substances decompose under the influence of temperature. The decomposition of PVA will yield varied products that may include alcohols, acetone, acetaldehyde, and water depending on the starting material. (Fathi et al., 2011). **Figure 3.6** shows two distinct degradation phases from TGA of PVA. Weight derivative curve shown in **Figure 3.7** shows a third phase with temperature of approximately 77 °C that rather represents probably the Tg of PVA since the weight loss associated with that phase is minimal. The bulk of the decomposition occurred at around 277 °C that almost corresponds to the temperature of the shoulder observed in the DSC curve. The onset temperature of the final decomposition phase was around 350 °C peaking at 434 °C.

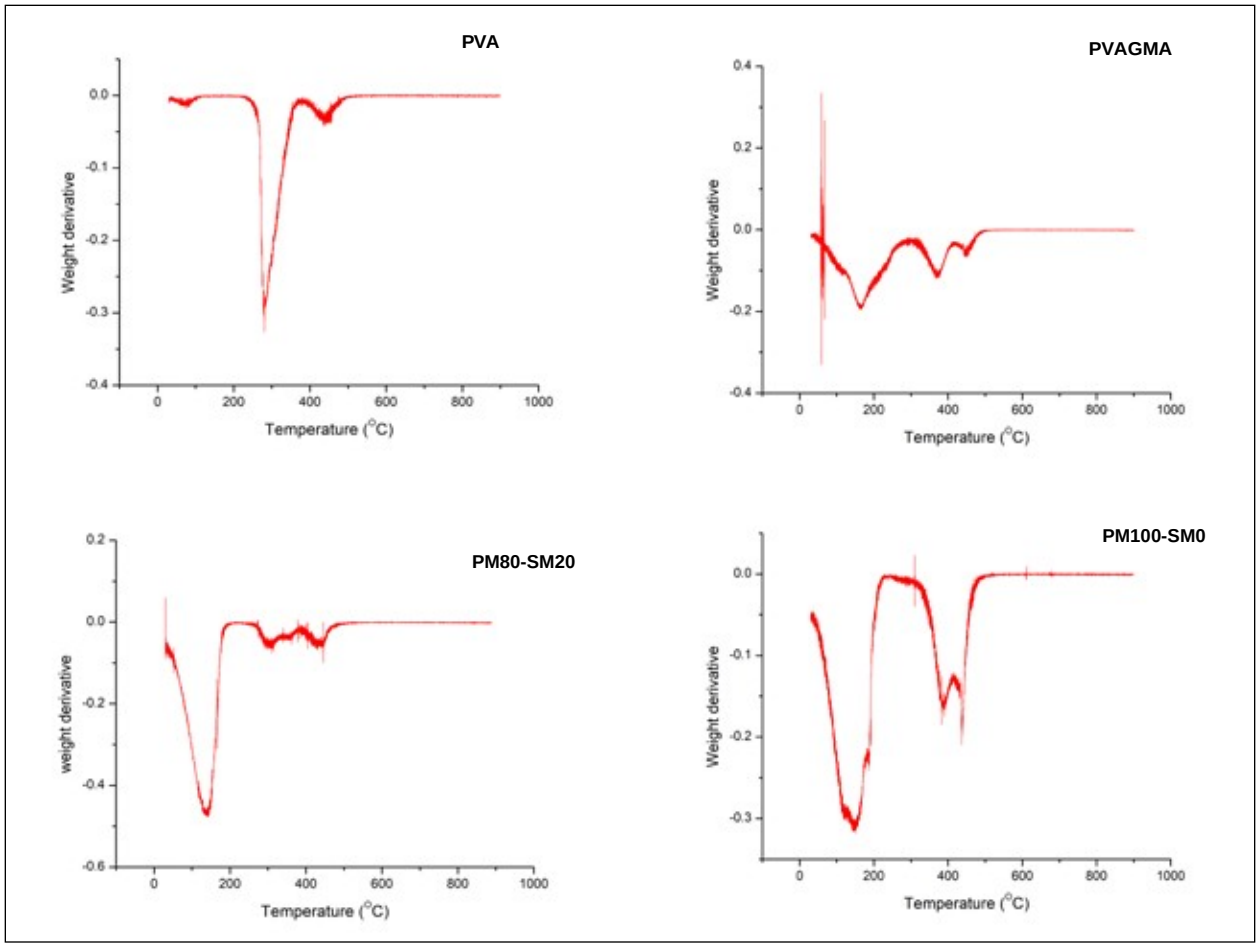


Figure 3.7 TGA weight derivative of PVA, PVAGMA and the hydrogels.

The TGA curve of methacrylated PVA, PVAGMA, was very different from that of PVA with the weight derivative curve showing 3 peaks in which the weight loss was more fairly distributed when compared to that of PVA. The first phase of the weight loss (over 60 %) occurred at a higher peak temperature (compared to PVA) of 164 °C while the second phase (involving 28 % weight loss) occurred at a peak temperature of 367 °C. The last phase of decomposition for the PVAGMA peaked at around 450 °C. These shows the temperature stabilizing effect of methacrylation on PVA. The TGA and weight derivative curves of pure PVAGMA hydrogel also shown in **Figure 3.6** and **Figure 3.7** respectively differed from that of uncrosslinked PVAGMA in terms of intensity of the weight derivative peaks and a slight shift in the corresponding peak temperatures. In addition, the peaks in the weight derivative curve depicting the second and the third phase of the decomposition is not clearly separated at the baseline. This means that the third phase of the decomposition started while the second phase was yet to end. The peak temperatures for these

phases were 148 °C, 388 °C and 437 °C. These difference may have resulted due to the higher water content of the hydrogels. The TGA curve of the hydrogel containing SBMA also differed visibly from that without SBMA. The intensities of the second and third phases of the TGA weight derivative curves were very low. The peaks for the thermal events occurred at 140 °C, 298 °C, and 358 °C.

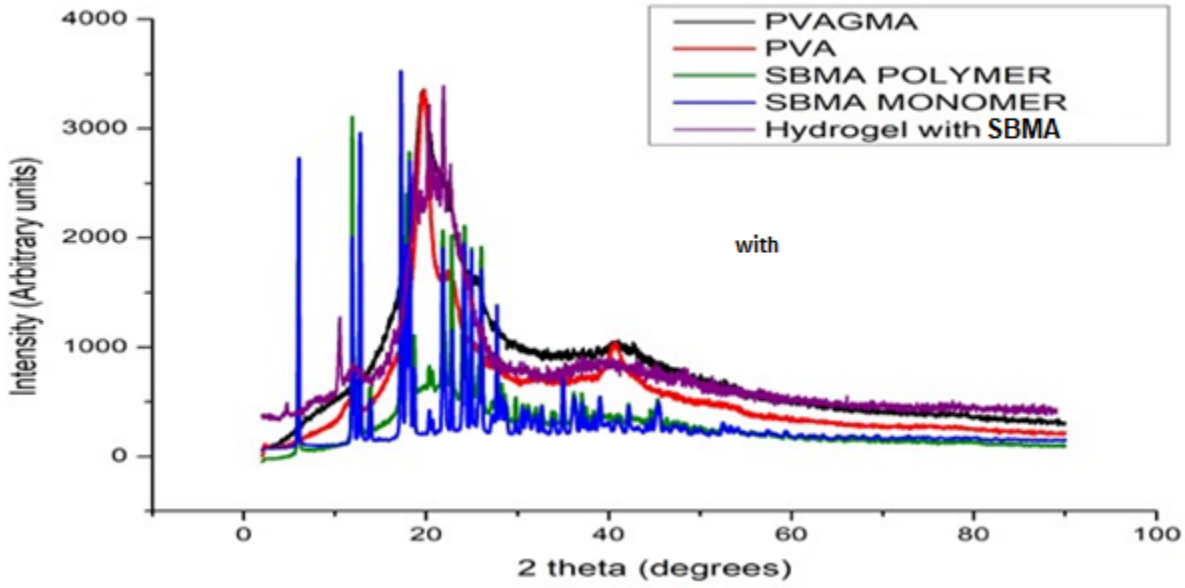


Figure 3.8 Comparative XRD spectra of PVA, PVAGMA, SBMA and a hydrogel sample.

3.3.3 Crystallinity of PVA, PVAGMA and the hydrogel samples

The contributions and presence of both crystalline and amorphous regions in various samples were studied using XRD powder diffraction. The diffractograms of the PVA, PVAGMA, SBMA (polymer and monomer) and a hydrogel sample with SBMA is shown in **Figure 3.8**. PVA being semi crystalline exhibited peaks at 2θ = 19.8 ° and 40.4 ° close to the 20 ° and 40 ° values previously reported. (Yang & Wu, 2009) An additional peak which disappeared in the PVAGMA diffractogram was recorded for PVA at 2θ = 11 ° (**Figure 3.9**) and further confirms modifications in the pristine PVA. In addition, the visible reduction in the intensities of the peaks occurring at 2θ = 19.8 ° and 40.4 ° in PVA from 6641 and 2085 arbitrary units to 3378 and 1057 arbitrary units

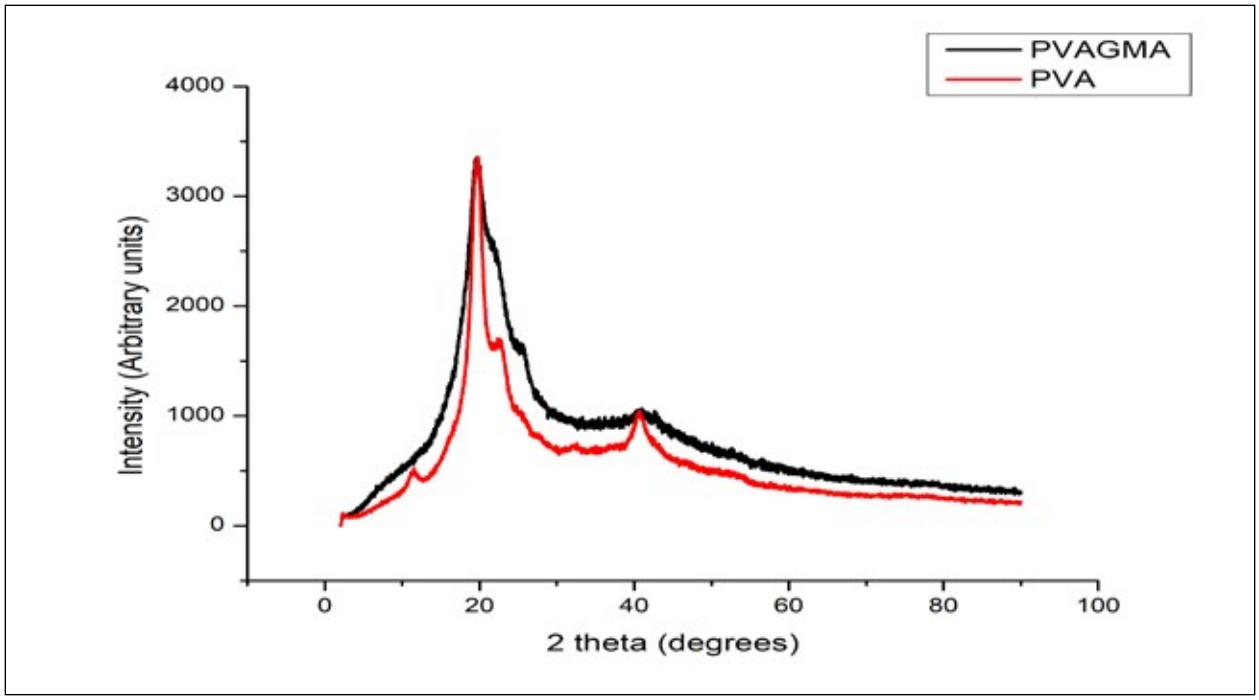


Figure 3.9 Comparative XRD of PVA AND PVAGMA.

in the PVAGMA respectively represents the introduction of disordered amorphous regions or cavities in the PVAGMA. The exact size of the reduction, as shown in **Figure 3.10** and **Figure 3.11**, is represented by an increase in the value of the full width at half maximum (FWHM) calculated for PVA and PVAGMA from 5.864 nm to 8.417 nm respectively. FWHM varies inversely with the crystallite size as shown by the Scherrer's equation. (Muniz et al., 2016) This means that the methacrylation of PVA either led to the smaller crystallite sizes within the PVAGMA or the creation of a more ordered packing of the crystals leading to free spaces within the PVAGMA structure. Zhang and colleagues made a similar observation for a composite hydrogel of PVAGMA and cellulose nanofibrils (CNF). They reported that inclusion of CNF affected the crystallinity of PVAGMA (Zhang et al., 2019). They reported only one peak appearing at $2\theta = 19.4$ in the XRD of PVAGMA which they attributed as arising from the orthorhombic lattice of semi-crystalline PVA. In like manner, the XRD curve for both polymerized SBMA and the monomer were compared to enable the elucidation of the contributions of SBMA in the resultant hydrogel.

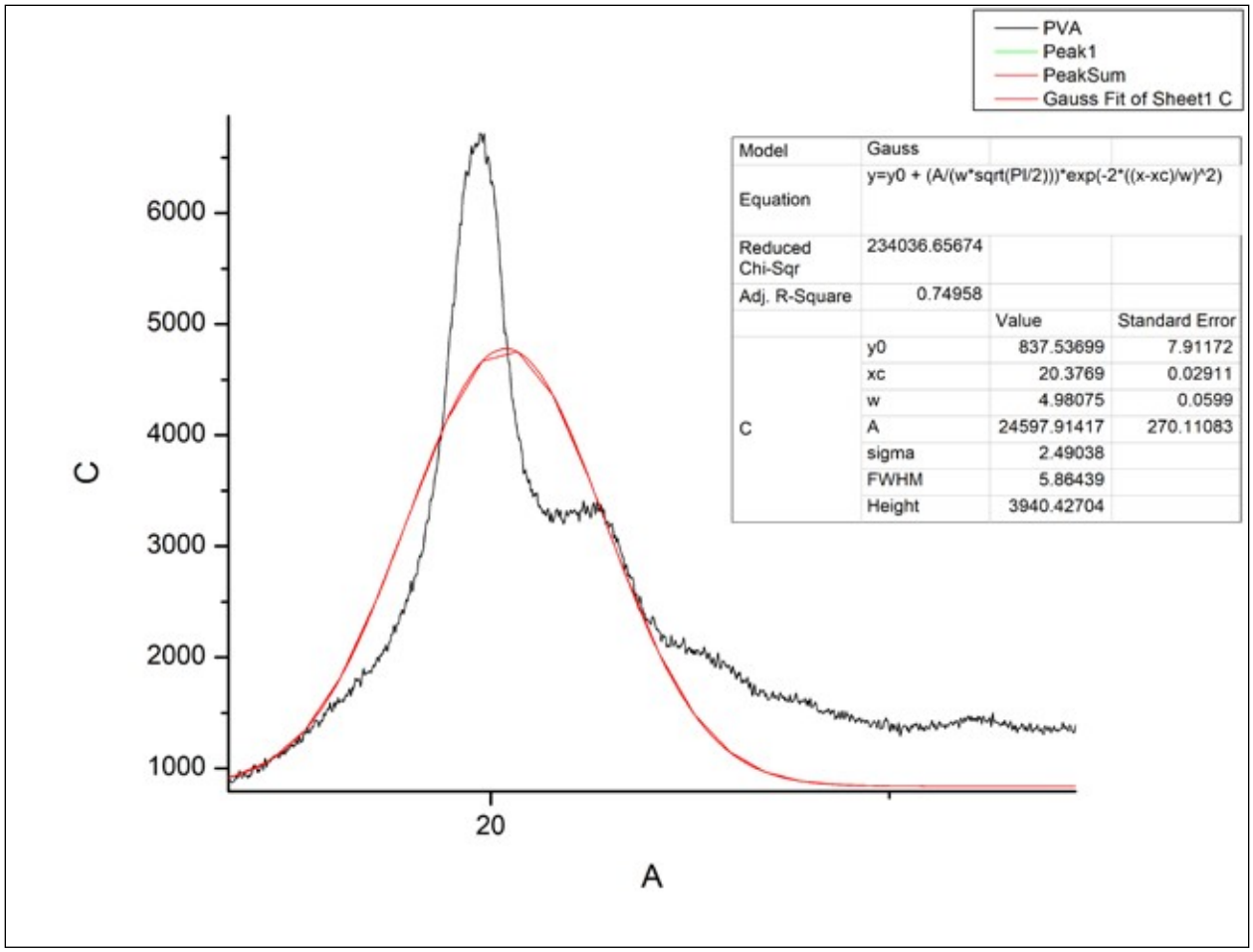


Figure 3.10 FWHM for PVA.

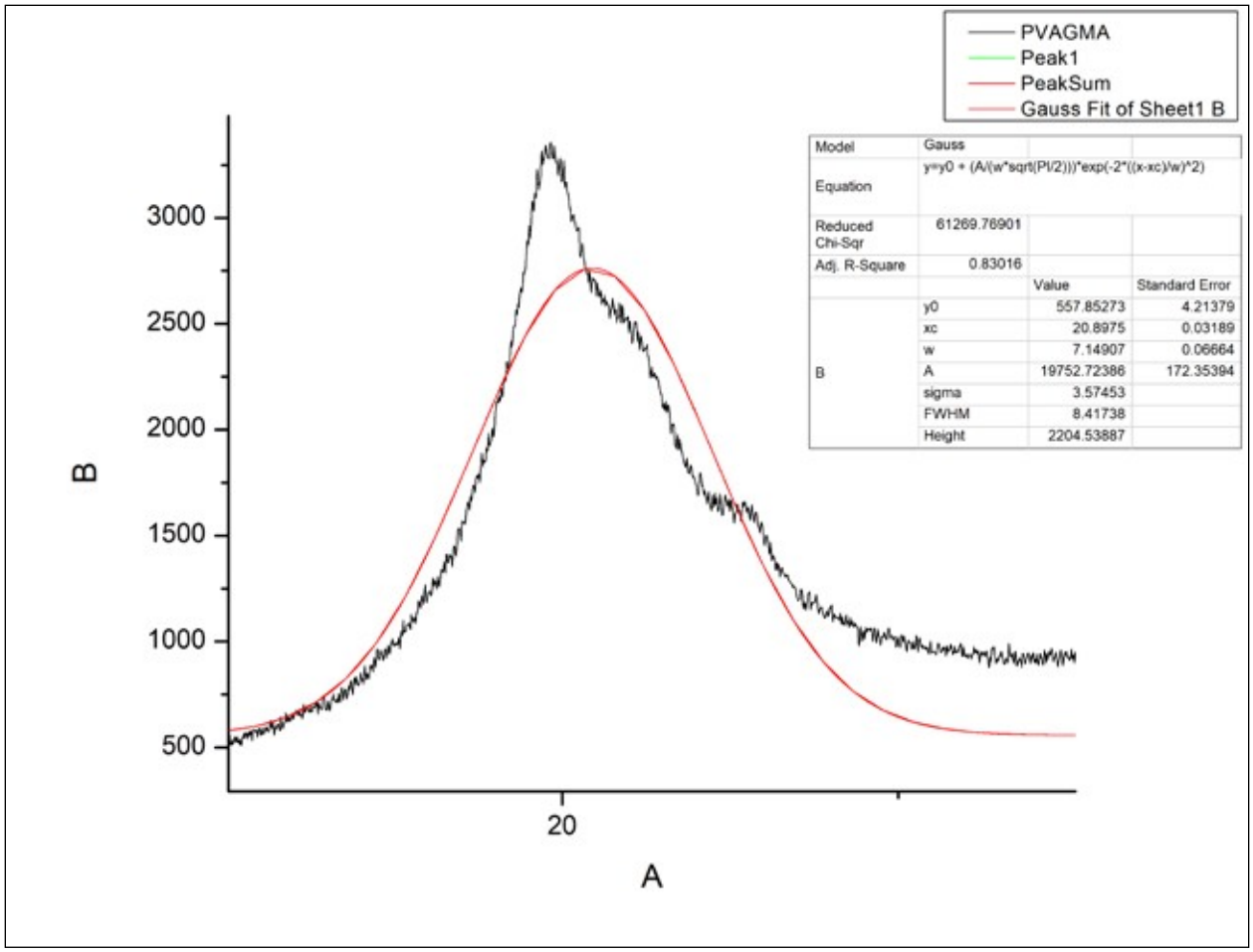


Figure 3.11 FWHM for PVAGMA.

The peaks for both the monomer and polymer of SBMA occurred at the same 2θ positions but only differed in intensities. Since the peak intensities represent the magnitude of the contributions of each crystal to the crystallinity of that phase, (El-Shamy et al., 2014), it then means that the crystallinity of SBMA reduced with polymerization. In the synthesis of the hydrogel, SBMA was added in the monomeric form. The XRD of the resulting hydrogel (**Figure 3.8**) confirms the disappearance of the crystallite peaks that were so prominent for SBMA monomer and with reduced intensity in the SBMA polymer diffractogram. **Table 3.2** outlines the full width at half maximum (FWHM) for the first 5 peaks in SBMA monomer, SBMA polymer, and a hydrogel sample, PM89-SM11. The hydrogel showed a single peak of very low intensity at 2θ = 10.5 and FWHM of 6.909 nm. Peaks 2 to 5 in the PM100-SM0 hydrogel originated as a single broad peak at 2θ = 20.33 ° and only split at the top into 4 different peaks which is recorded in **Table 3.2**. This represents a further increase in the amorphous regions in the hydrogel.

Table 3.2 The FWHM for the component peaks in SBMA monomer, SBMA polymer, PVAGMA and PM89-SM11.

2θ (°)	**Full width at half maximum (FWHM)(nm)**			
	SBMA monomer	SBMA polymer	Hydrogel with SBMA	PVAGMA
6.11	1.342	13.855	-	-
10.52	-	-	6.909	-
11.57	1.295	1.076	-	-
12.81	0.151	12.318	-	-
17.25	0.223	-	-	-
17.86	0.196	17.472	-	-
18.20	0.178	33.800	-	-
18.78	-	-	3.762	-
20.33	-	-	38.919	8.417
21.93	-	-	5.382	-
22.71	-	-	33.370	-

3.3.4 Mechanical properties of the synthesized hydrogels

The mechanical robustness of hydrogels is an important attribute that dictates to a large extent its usability for each application. Hydrogels, by virtue of their high-water content, are usually soft materials. Their elastomeric inclination makes them attractive alternatives in many soft tissue applications. Despite their soft nature, hydrogels are required to exhibit a measure of strength

that will make handling possible. In certain ocular application such as the contact lens and scleral patch, the hydrogel should be strong enough to withstand shearing brought about by blinking in addition to being handled during insertion by the patient. This may be a big challenge considering that the water content, which varies inversely with the mechanical strength, is very important as it contributes heavily to the oxygen permeability in such applications. All prior studies involving UV-cross linkable PVAGMA hydrogels (where not used alone) had involved the use of materials such as cellulose nanofibrils (Zhang et al., 2019), hydroxyapatite (Zhou et al., 2019), and chondroitin sulphate (Crispim et al., 2012), aimed at reinforcing the mechanical robustness of PVAGMA hydrogels. In other studies, it was a symbiotic approach by which the mechanical robustness of polysulfobetaine methacrylate was improved by grafting with polymers such as chitosan while chitosan ability to resist protein adsorption was improved. (Zhou et al., 2015) Rarely has polysulfobetaine methacrylate been used alone mainly because of its deficit in mechanical robustness. Only one such study was found (within the limits of literature available so far) in which electrospun fibres from polysulfobetaine methacrylate were explored for wound healing applications. (Lalani & Liu, 2011) This is not surprising as the mechanical robustness demands on hydrogels for wound healing applications is minimal. In a similar study involving sulfobetaine acrylamide, nanoclay was employed as a reinforcing crosslinker. (Huang et al., 2016) Representative graphs of the results obtained from the compressive stress-strain cycles (series A) and compression to failure (series B) of some of the samples are shown in **Figure 3.12**. Compressive stress-strain curves were obtained in cyclic mode for 10 cycles, on each sample before being compressed to failure. A 40 % strain was used for each compressive cycle while a 70 % strain was used for compression to failure. In some of the samples, stain higher than 80 % was required to deform the samples to failure while the sample without SBMA failed with a 50 % strain. Compression to failure was required to determine the strength of the hydrogels. All the samples (some results not shown) withstood 10 compressive cycles. The graph appeared as that of a single cycle with no shifts in going from one cycle to the other for samples containing SBMA. This represents the stability of the hydrogels and their ability to recover uniformly when subjected to a shearing stress of such magnitude. In addition, the size of the hysteresis represents the energy dissipated by the hydrogel in the form of heat while unloading. Hard materials are known to have minimal hysteresis while elastomers with high elongation potential exhibit large hysteresis. A visual comparative analysis of the graphs in **Figure 3.12** (series A) for samples containing 0 % w/w SBMA, 33 % w/w SBMA, and 12 % w/w SBMA with respect to PVAGMA) show that the size of the elastic hysteresis is least in the hydrogel sample composed of 100 %w/w PVAGMA.

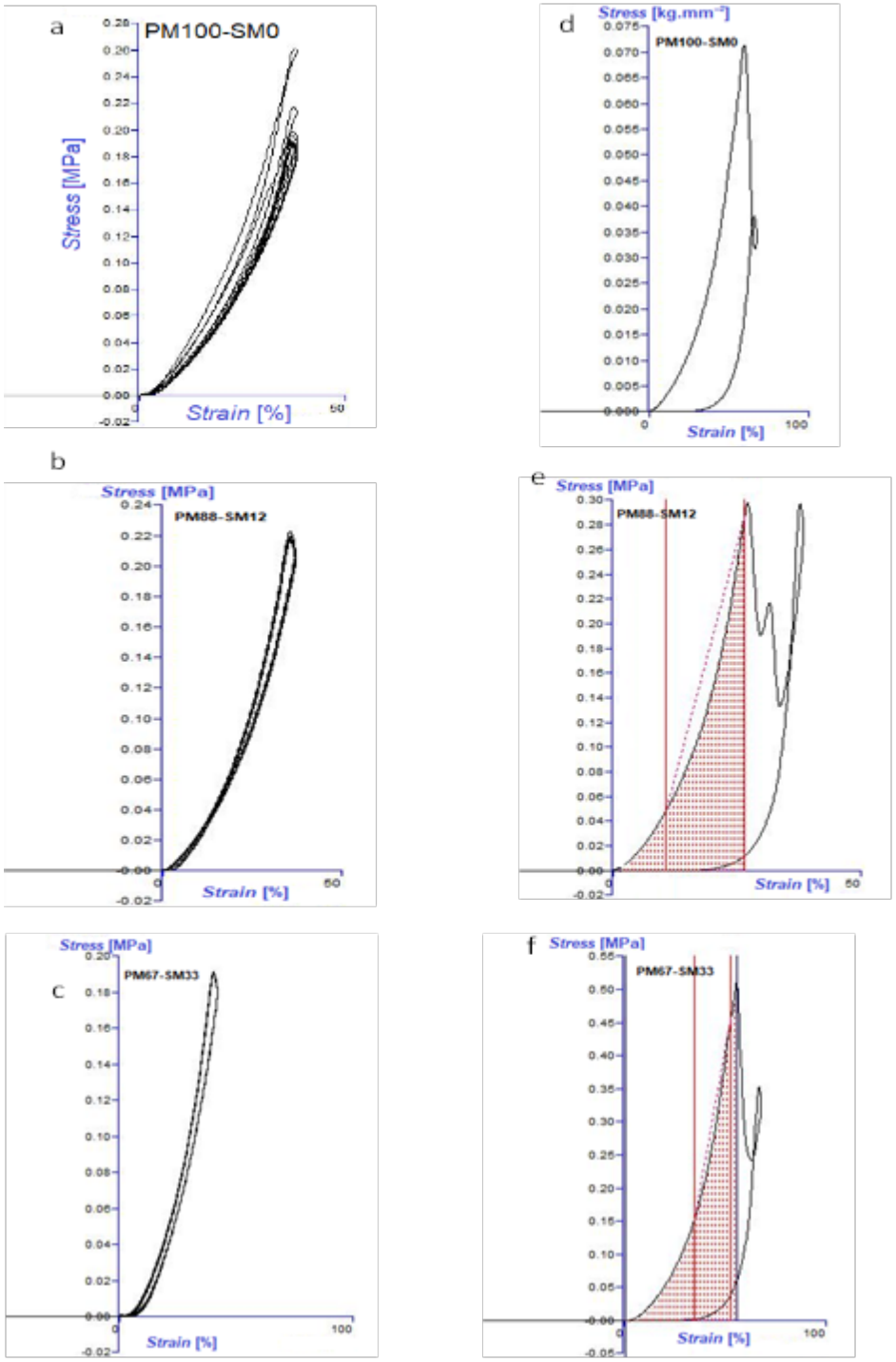


Figure 3.12 Compression stress-strain curves for cyclic (A) at 40% strain and compression to failure (B) at 70% strain for hydrogels.

In addition, the displacement of each cycle graph downward from the first curve shows the reduction in the elasticity of the hydrogel with each cycle. This is different for the curve of samples containing about 33 % w/w and 12 % w/w of SBMA respectively.

Table 3.3 Mechanical parameters of the hydrogel samples compressed to failure at 70% strain.

Sample name	SBMA content (% relative to PVAGMA)	Young modulus (Mpa%)	Peak (Mpa)	Compressive strength (area under the curve) (Mpa%)
PM100-SM 0	0	0.015*	0.1992	7.63
PM 67-SM 33	33	0.015	0.46	7.37
PM 88-SM 12	12	0.013	-	3.12
PM 80-SM 20	20	0.020	1.224	21.66

The darkening of the curve for PM88-SM12 represents a very slight displacement in each cyclic curve over the 10 cycles. This darkening is not visible in the curve for PM67-SM33 hydrogel. This observation may translate to the contributions of SBMA to the degree of elasticity. The recorded mechanical strengths determined in this study more than matched those obtained for PVA hydrogels reinforced with carboxylated nanocellulose whiskers. (Tummala et al., 2016) **Table 3.3** outlines the derived parameters from the stress strain curve of selected samples. There was an initial reduction in the compressive strength of PVAGMA hydrogel with addition of SBMA (12 %). The compressive strength subsequently increased with increasing content of SBMA up to a limit. Similarly, Young's modulus increased with increasing content of SBMA. These results obtained are comparative to results of previous studies that used hydroxyapatite for reinforcement and in which a peak stress of 2.3 Mpa at 90 % compression strain was recorded. (Zhou et al., 2019)

Though the highest peak stress recorded in our study, 1.2 Mpa, is lower than the 2.3 Mpa recorded by Zhou and colleagues, these values may still be comparable considering that hydroxyapatite was used at 40 % for mechanical reinforcement before such value could be obtained. Moreover, SBMA used in this study is considered a mechanically non-robust polymer and was not expected to contribute to the mechanical robustness of the composite hydrogel in the manner it did.

3.3.5 Viscoelastic properties of the plain and composite hydrogels

The Elastosens™ Bio, an instrument that uses laser light to non-destructively explore the transitions in the microstructure of a sample, was used to study the viscoelastic properties of the hydrogels over a temperature range of 25 °C to 37 °C to represent transitions between the room and the body temperatures, respectively. At each of these temperatures, the interplay between the shear storage modulus', shear loss modulus, G'', shear complex modulus, G*, and tan d for each of the hydrogels is shown in. **Figure 3.13** - **Figure 3.16.**

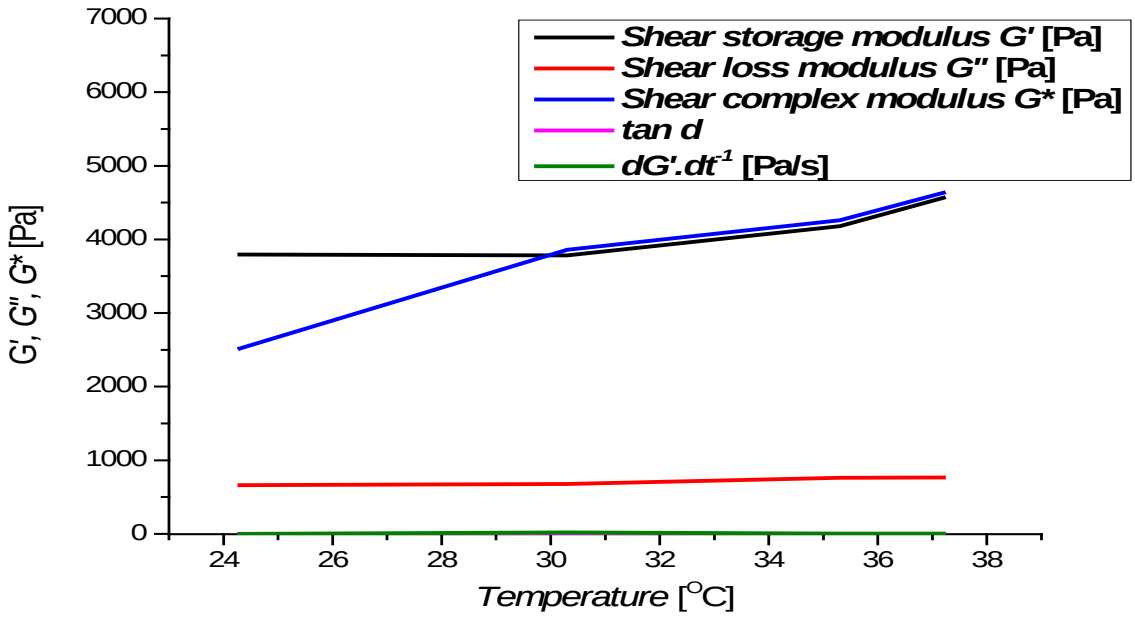


Figure 3.13 Graph displaying the inter-relationship between the G', G'', G*, and tan d of hydrogel PM100-SM0.

The shear complex modulus defines the viscoelastic behaviour of the hydrogels and represents the degree of elasticity with respect to the viscosity of the polymer chains. The hydrogel sample containing about 20 %w/w SBMA had the highest viscoelastic behaviour. This observation corelates well with what was observed in the experiments involving the mechanical properties. Above and below 20 % w/w SBMA, the viscoelastic properties declined as was observed for the mechanical properties. The shear complex modulus for hydrogel PM100-SM0 increased with every step increase in temperature while the reverse was the case for other hydrogels containing SBMA. The storage modulus of a polymer is a measure of the stiffness or solid-like properties of a polymer and represents the amount of energy input required to disrupt the solid structure. Shear loss modulus, conversely, is a measure of the liquid like property of a polymer. When the G' is higher than the G'' in a polymer, it means that the polymer exists in a stiff or solid-like state. G' was higher than G'' for all hydrogel samples showing the stiff nature of the hydrogels.

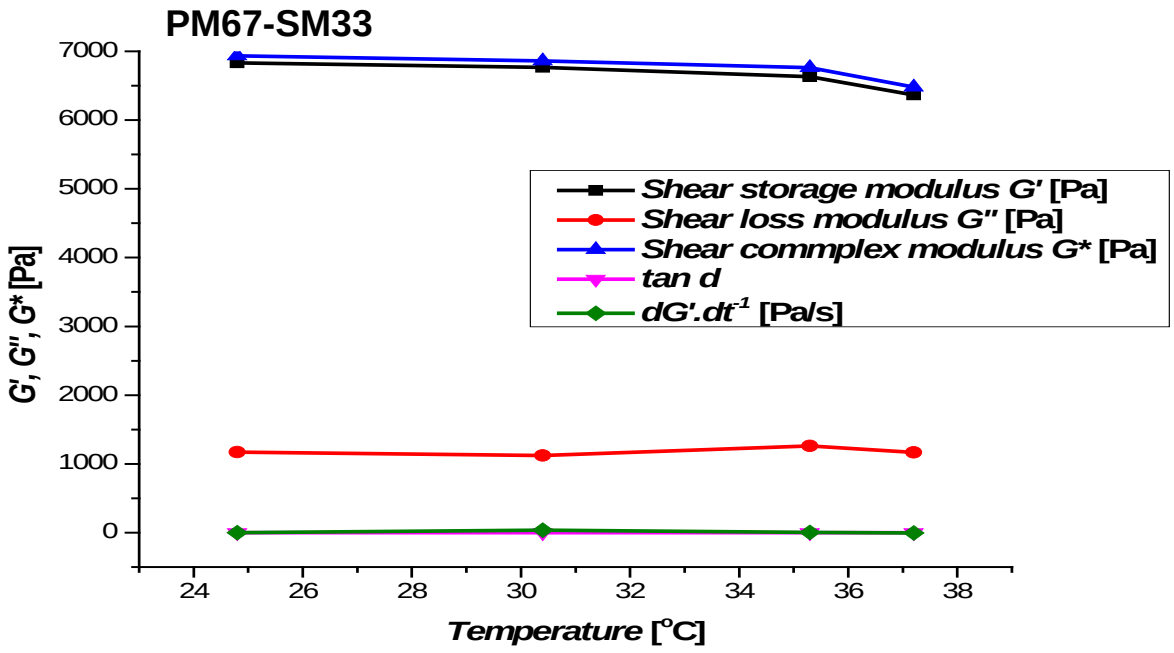


Figure 3.14 Graph displaying the inter-relationship between the G', G'', G*, and tan d of hydrogel PM67-SM33.

For PM100-SM0 containing only PVAGMA, the G' was lowest and increased slightly from 4 Kpa to 4.5 Kpa in going from 25 ºC to 37 ºC respectively. For the samples containing SBMA, the G' increased as the percentage of SBMA increased from 0 % to 20 % and afterwards decreased. In addition, there was a negligible decrease in the G', contrary to what was seen in the PVAGMA hydrogel, for all samples containing SBMA as the temperature increased to 37 ºC. This decrease was least in the hydrogel sample with the highest G', PM80-SM20. In like manner, tan d, also known as damping, which is a measure of the energy dissipating ability of a material, varied across the hydrogels. In compression tests, tan d is derived from the area enclosed by the loading and unloading curve.

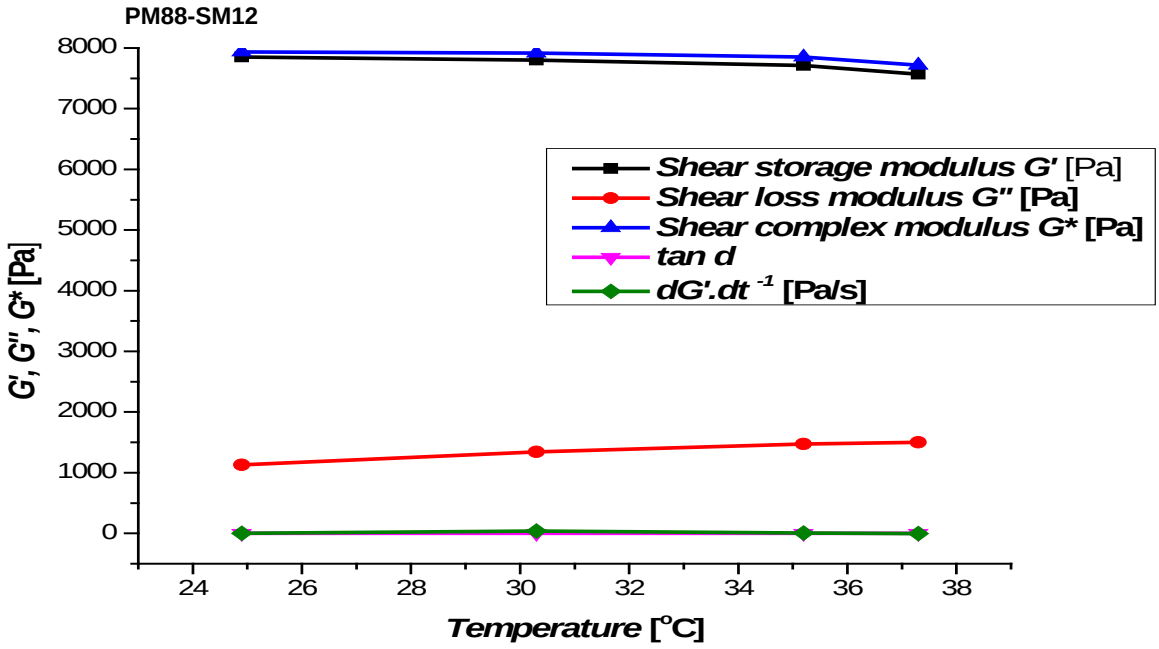


Figure 3.15 Graph displaying the inter-relationship between the G', G'', G*, and tan d of hydrogel PM88-SM12.

Figure 3.17 shows the graph analysing the damping potential of the hydrogels across different temperatures. Hydrogel PM88-SM12 noticeably had the best damping potential even though it had the least compressive strength while hydrogel PM80-SM20 that had the highest shear storage modulus and compressive strength showed the least capacity for damping.

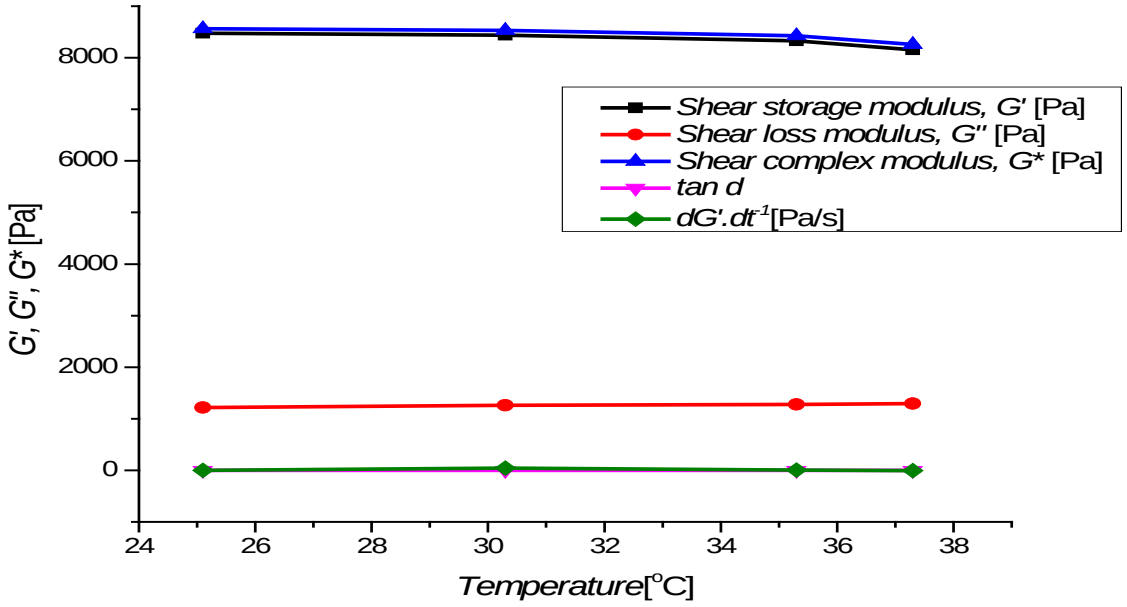


Figure 3.16 Graph displaying the inter-relationship between the G', G'', G*, and tan d of hydrogel PM80-SM20.

This observation is in line with the narration that two materials with the same shear storage modulus may have different capacity for damping. The shear storage modulus, G', which is a measure of the elasticity or solidity of the hydrogels varied in like manner as the shear complex modulus across the formulations. As noted earlier, PM80-SM20 has the highest value of shear modulus 8.48 kPa ± 0.93 kPa. In sample PM100-SM0 containing only PVAGMA, the shear storage modulus increased with temperature contrary to what was observed for other samples. This means that the samples stiffened as temperatures approached body temperature. This observation may be particularly important as the compatibility of any biomaterial with body tissues depends very much on the stiffness or softness of the material under use conditions. All other samples got softer with temperature though the decrease in the shear storage modulus was not as dramatic as that observed for hydrogel PM100-SM0.

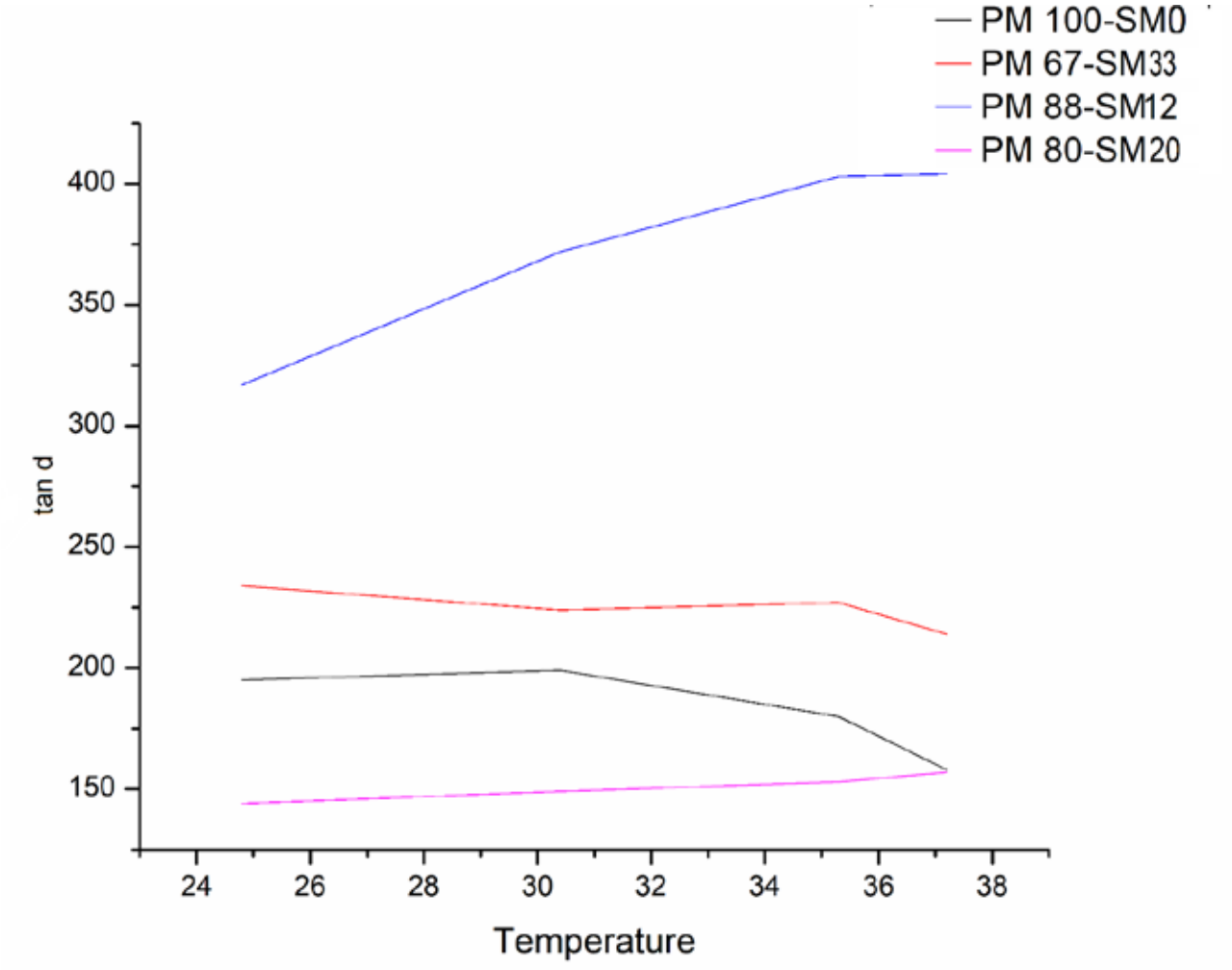


Figure 3.17 Damping potential of the hydrogels.

3.3.7 Surface morphology and characterization

The scanning electron micrographs showing the surface morphology of planar, and cross-sections of hydrogel samples freeze fractured in liquid nitrogen are shown in **Figure 3.18**. Different morphologies have been reported for PVAGMA hydrogel samples crosslinked by different crosslinkers. Zhang and co-workers prepared PVAGMA hydrogels (with and without cellulose nanofibrils) using a photo initiator. (Zhang et al., 2019) They reported a densely porous morphology for all lyophilized hydrogel samples. Zhou and co-workers, on the other hand, while working on similarly prepared PVAGMA hydrogels (prepared with photoinitiators) but containing hydroxyapatite nanoparticles reported a dense non-porous morphology which they attributed to the collapse of the hydrogel structure occasioned by lyophilization.

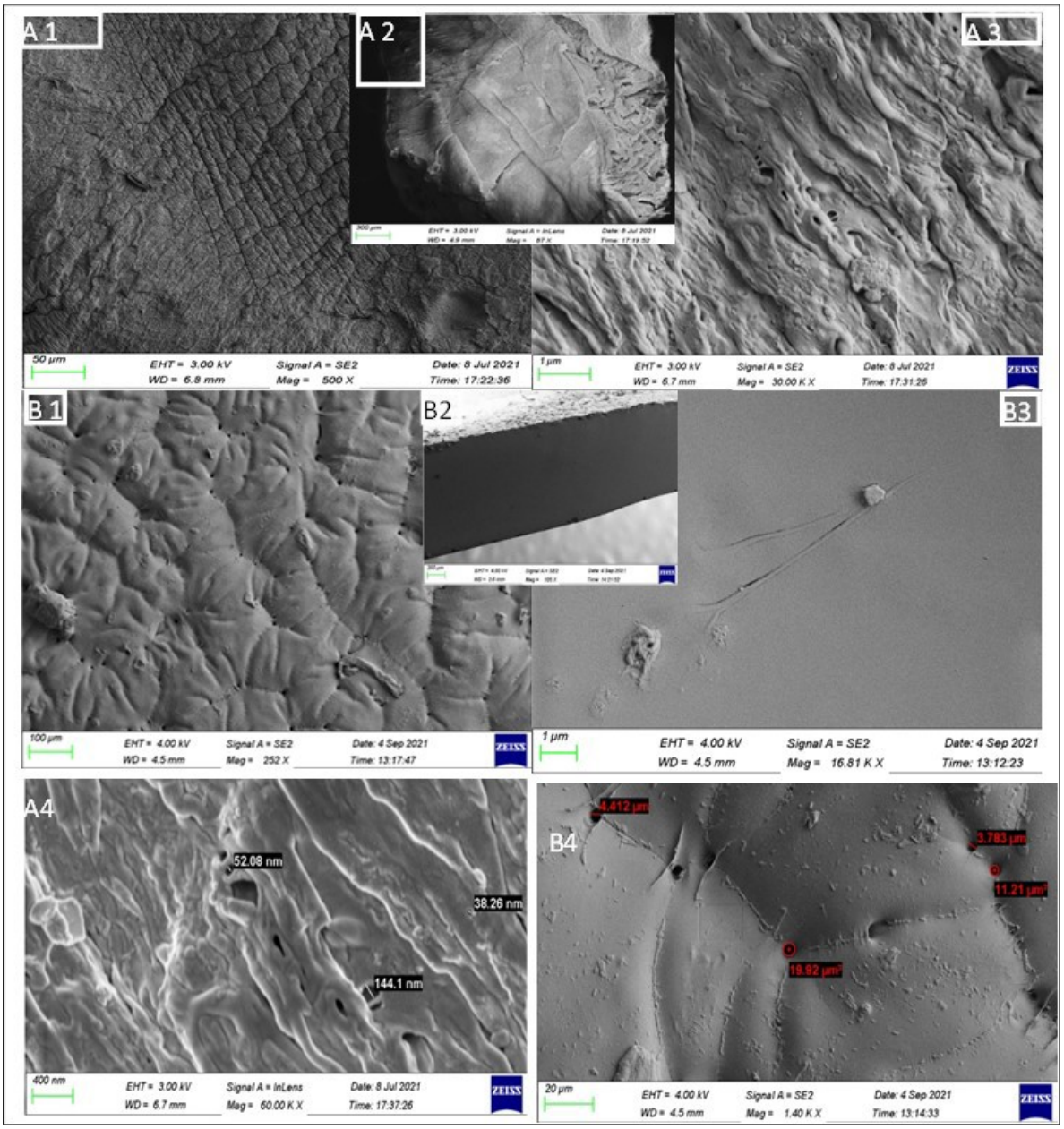


Figure 3.18 SEM digital images of the planar and cross-sectional surface of dried hydrogels with SBMA: A (1-4) and without SBMA: B (1 -4).

The surfaces of the hydrogels in this study displayed dimpled and rough surfaces with pore-like structure. In **Figure 3.18**A (1-3), and **Figure 3.18**B (1-3) the morphologies of hydrogel sample containing SBMA and that without SBMA are respectively shown at different magnifications while A4 and B4 captured the different pore sizes occurring in the hydrogel sample with SBMA and without SBMA respectively measured by the SEM.

In contrast to the observations of these previous studies, the morphologies observed in this study were that of dense rough layers spurted with pores of non-uniform sizes. Morgacheva and co-workers discussed the effect of crosslinking temperature on the porosity of PVAGMA hydrogels. (Morgacheva et al., 2015) In their work in which hydrogels were crosslinked with potassium persulfate and ascorbic acid, freezing conditions yielded macroporous gels while room temperature yielded isotropic gels. The photo initiated crosslinking process may have contributed to the variability in the pore sizes encountered in this study. The nature of the pores encountered in hydrogels have been reported to contribute to the swelling. These may have additional implication for the fast release of medicaments incorporated into such hydrogels. The presence of nanosized pores may hinder the rapid release of enclosed medicaments particularly as it is known that many hydrogels release their medication by swelling. The presence of pores in the hydrogels was further affirmed by the porositometric analysis of some of the hydrogel samples. The presence of roughened surfaces could contribute to the hydrophilicity or hydrophobicity of a hydrogel material depending on the leanings of the hydrogel material. (Zhao et al., 2014) The observed surface morphology may, therefore, contribute to the hydrophilicity of the hydrogels. According to the Wenzel model, the presence of nanostructures or surface roughness can contribute to the degree of hydrophilicity or hydrophobicity of a hydrophilic or hydrophobic material respectively. (Ying et al., 2020) These structures presenting as troughs may play a role in complementing the hydrophilicity imparted by the zwitterionic polymer and its consequent effect on protein adsorption. (Askari et al., 2019)

3.3.8 Surface porosimetric analysis of the hydrogels

The porositometric analysis of lyophilized hydrogel samples (**Table 3.4)** showed the presence of pores in the nanometric size region. This goes further to confirm the presence of pores reported from the SEM images. The average BET pore size was determined to be 93.8602 Å. The presence of these pores will additionally facilitate the diffusion of oxygen through the hydrogel in the event it is used as a contact lens. If per adventure, an implantable device is decided, the presence of the pores, their size, and volume will be ultimate contributors and determinants to the nature and mechanism of the drug release process. **Table 3.4** shows an interesting relationship between the pore size and the content of the zwitterionic monomer in the hydrogels. The surface area and the average pore width of the pores increased with increasing content of zwitterionic component. whereas the adsorption pore volume decreased with increasing zwitterionic component content up to 20 % w/w. The implications of these for the ultimate application of these

hydrogels deserve further studies with a view to harnessing the potentials it portends. The presence of these pores can additionally contribute to protein adsorption. Ishihara and coworkers (2021) demonstrated that the adsorption of low molecular weight protein such as lysozyme depends, in addition to hydrophilicity, on its diffusion into the hydrogel. (Ishihara et al., 2021) This implies that the presence of bigger pores may contribute to the diffusion of higher molecular weight proteins into the hydrogels hence compromising the effect of hydrophilicity.

Table 3.4 Porosity analysis for selected hydrogels.

Name	**Surface area**	**Pore volume**	**Pore size**		
	Single point surface area at P/Po = 0.200129527	**Single point Adsorption total pore vol of pores less than 784.406 Å diameter P/Po = 0.974687626**	**Adsorption average pore width (4 V/A by BET)**	**BJH Adsorption average pore diameter (4 V/A)**	**BJH Desorption average pore diameter (4 V/A)**
PM100-SM0	0.0558 m^2/g	0.000166 cm^3/g	-530.836 Å	1200.676 Å	746.258 Å
PM67-SM33	0.3778 m^2/g	0.0002929 $cm^3/$	205.1014 Å	249.447 Å	210.834 Å
PM88-SM12	0.1142 m^2/g	0.000523 cm^3/g	93.8602 Å	168.240 Å	37.648 Å
PM80-SM20	0.1644 m^2/g	0.000863 cm^3/g	126.7948 Å	675.542 Å	248.867 Å

3.3.9 Water contact angle (WCA) and hydrophilicity of hydrogels

The water contact angle is a measure of the hydrophilicity of any material and its propensity to limit protein adhesion. The mean water contact angle of a sessile drop of distilled water on equilibrium swollen hydrogel samples is shown in **Table 3.5** while the digital images are captured in **Figure 3.19.** Though the mean values of the measurements showed a highly hydrophilic surface, the standard variations showed the polydisperse distribution of this hydrophilicity across each surface. This may be as a result of the heterogeneity in the distribution of crosslinks within the hydrogel (particularly common with UV crosslinks) with areas of dense and sparse crosslinks as reported by Eke and coworkers. (Eke et al., 2017) Though in their study, the crosslink's distribution was related to the mechanical performance of the hydrogel, crosslink distribution can also be related to the hydrophilicity of the hydrogels. The variability in the WCA of some hydrogels (results not shown as this was part of the optimization process) suggested that the distribution of the modifying zwitterionic SBMA across the two surfaces may differ contributing to this variability. It was posited that the open nature of the glass tube mould additionally contributed to this variability hence an alternate mould consisting of two glass plates separated by 0.75 mm spacer. The results obtained thereafter showed that both surfaces were superhydrophilic with a WCA below 10 ^{o} for both surfaces (not shown). There was a progressive decrease in the water contact angles of the hydrogels as the concentration of SBMA increased as shown in **Table 3.5**. Additionally, the non-zwitterionized PM100-SM0 hydrogel had a very low WCA as a standalone hydrogel. It was found (not shown) that increasing the PVAGMA content of zwitterionized hydrogel also caused a reduction in the WCA and a consequent increase in hydrophilicity. The WCA angle has been used as a measure of the surface hydrophilicity of hydrogels which in turn depends on the chemistry of groups accumulating on the surface of the hydrogels. (Pop-Georgievski et al., 2013; Rostam et al., 2016) The contributions of the zwitterionic SBMA to the hydrophilicity of the hydrogels arises from the nature of its interaction with water molecules via ionic solvation. It is hypothesized that this, in addition to, the contributions of the interactions of PVAGMA with water through hydrogen bonding resulted in superhydrophilicity. Goda and group had previously reported no dependency between the WCA and water content. (Goda et al., 2009)

Table 3.5 Water contact angle of sample hydrogels.

Sample	Water contact angle (°)
PM100-SM0	27.69 ± 6.56
PM88-SM12	15.8 ± 5.89
PM80-SM20	13.70 ± 6.93
PM67-SM33	9.76 1.04

3.3.10 Equilibrium water uptake (EWU) of the hydrogels

The very high application rate of hydrogels in biomedical fields derives partly from their high-water content which makes them resemble biological environments. In addition, the rate and extent of swelling in hydrogels underpins certain of their abilities to act as drug delivery platforms. In ocular applications such as contact lenses, high water content is additionally desirable since high water content translates to the oxygen permeability which is a core requirement for corneal health in such applications. The results of the EWU of the samples are represented in **Figure 3.20.**

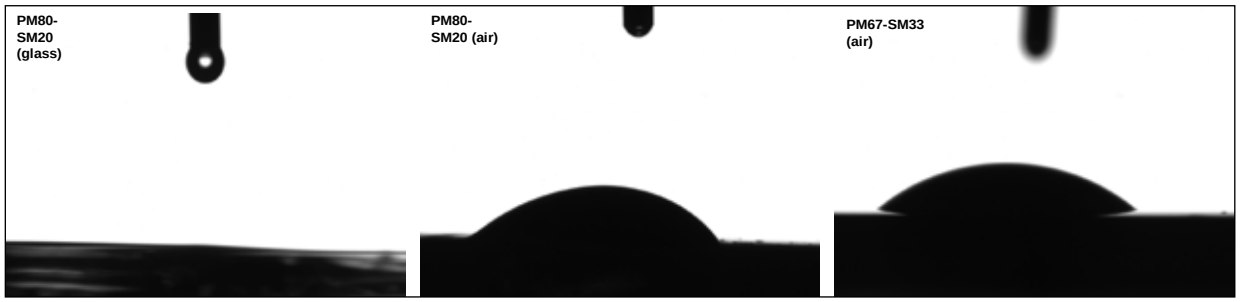


Figure 3.19 Digital images of a sessile drop of water on some hydrogel samples.

Percent swelling was observed to depend on the degree of methacrylation of the PVAGMA, its concentration and the concentration of the crosslinking agent. Previous studies have reported the rapid and high swelling capacity of PVAGMA hydrogels. (Zhou et al., 2019) (Cavalieri et al., 2004) Results shown in **Figure 3.20** confirm that as the degree of methacrylation increased, the degree of swelling reduced. Inclusion of SBMA increased the degree of swelling for all hydrogel

samples up to a limit. Beyond 20 % w/w content of SBMA, percent swelling decreased. This observation may not be unconnected to the presence of structured water around the zwitterionic group of SBMA. Some other researchers also made a similar observation about a different zwitterionic polymer, 2-methacryloyloxyethylphosphorylcholline. (Goda et al., 2009) (Carr et al., 2011) At all concentrations, the degree of swelling was lower in hydrogels with PVAGMA with higher methacrylation (HM). This is expected since higher methacrylation will result in higher crosslinking density and reduced swelling. The degree of swelling is a very good index for the equilibrium water content in hydrogels. It also correlates well with the oxygen permeability in hydrogels for ocular application. In hydrogels designed for contact lens application, it has been reported that the oxygen permeability increases with the equilibrium water content of the hydrogel. In such application, swelling becomes an important index in establishing the ability of the cornea to get oxygenated while the contact lens is worn. In this context, the hydrogels from this study outperformed many hydrogels from regular contact lenses polymers. In addition, it is expected that the mechanical robustness of hydrogels will decrease with high water content. It was interesting to note that the mechanical robustness of the prepared hydrogels was not compromised (at least within the possible potential ocular uses) with the high-water content as was observed in some other hydrogels when water content was high (Goda et al., 2009).

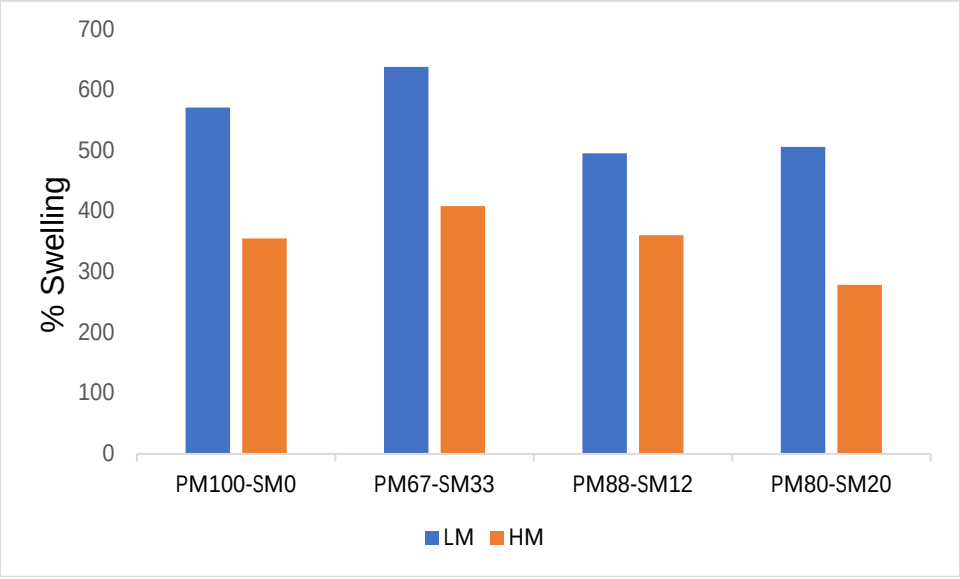


Figure 3.20 Chart of percent water uptake as a function of degree of methacrylation.

3.3.11 Transmittance of the hydrogels

The results of percent transmittance obtained from the hydrogels are show numerically in **Table 3.6** while **Figure 3.21** shows a digital image of hydrogels showing their transparency. The transmittance shows the ability of the hydrogels to transmit visible light. For ophthalmological hydrogels, transmittance is very important for clear vision. All the hydrogels studied had over 98 % transmittance. This result is similar to what has previously been reported for PVAGMA hydrogel. The digital image of a 0.4 cm thick hydrogel in **Figure 3.21** shows how transparent the hydrogels are. This result is not surprising since the hydrogel absorbs over 200 % of its weight of water in the swollen state. The transmittance of the hydrogels was positively enhanced by the inclusion of SBMA as the transmittance increased with increasing SBMA content. The effect of SBMA may result from unique hydration states in which molecules of water is bound to the SBMA as a hydration layer.

Table 3.6 Percent transmittance of hydrogels.

Sample	% Transmittance
PM100-SM0	98.02
PM67-SM33	99.68
PM88-SM12	99.12
PM80-SM20	99.17
PM94-SM06	98.07

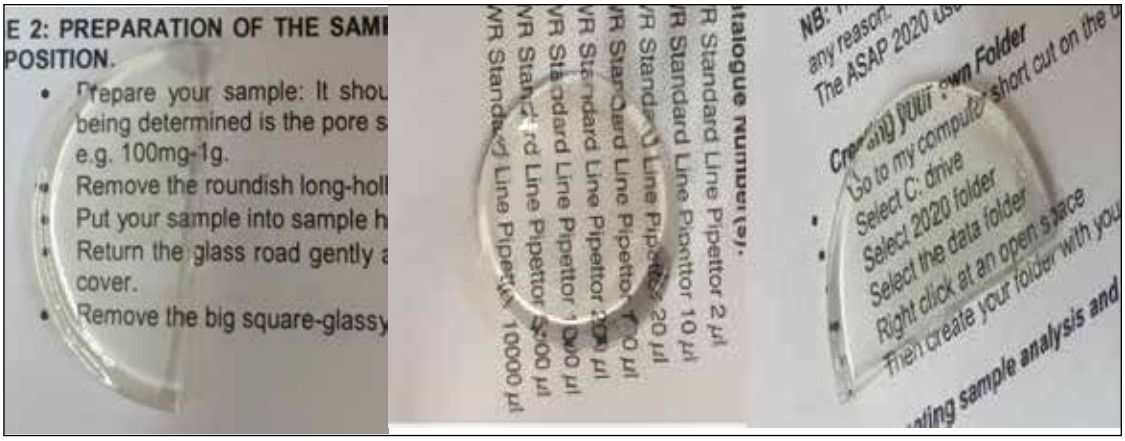


Figure 3.21 Digital images of some hydrogels displaying their transparency.

3.3.12 Protein adsorption onto the PVA-hydrogel samples

Within minutes of contact with biological fluids, proteins and lipids adsorb unto the implant material. For ocular devices such as contact and intraocular lenses, the initial protein adsorption may lead to opacification, blurring, biofilm formation, pro-inflammatory response, consequent full blown foreign body response and even ultimate failure of the implant. Many attempts at limiting the initial protein adsorption for ocular biomaterials have predominantly involved surface modification with hydrophilic and zwitterionic polymers. The results obtained from protein adsorption studies are shown in **Figure 3.22**. Previous studies have used single protein solutions in the determination of protein adhesion to biomaterials. Unfortunately, these do not adequately represent the complex protein components of biological systems. In this report, the calibration curve for determination of adsorbed protein on the hydrogels was determined using an ATF made up of 3 major proteins found in tear fluid, lysozyme, bovine serum albumin (BSA), and mucin. Determination of the total protein adsorbed unto the hydrogel samples were subsequently evaluated using the same protein solution. The total adsorbed protein per unit area of the hydrogel disc across both pristine and zwitterionized hydrogels were below 0.6 µg/cm^2. Hydrogel PM67-SM33 containing the highest amount of SBMA had the least protein adsorption (0.370 ± 0.077 µg/cm^2). Zwitterionization resulted in a statistically significant (at 90 % confidence interval) reduction (31.70 %) in the level of adsorbed protein when compared to the non-zwitterionized hydrogel (0.541 ± 0.002 µg/cm^2). The concentration of SBMA however, did not contribute to a statistically significant difference when the protein adsorption capacity amongst the zwitterionized hydrogels were analyzed using one way ANOVA at 95 % confidence interval. Different studies have reported the protein adsorption resistant properties of SBMA modified materials. However, the reduction in protein adsorption reported in some of these previous studies approaches a 50 % decrease when compared to the current study for all hydrogel samples.

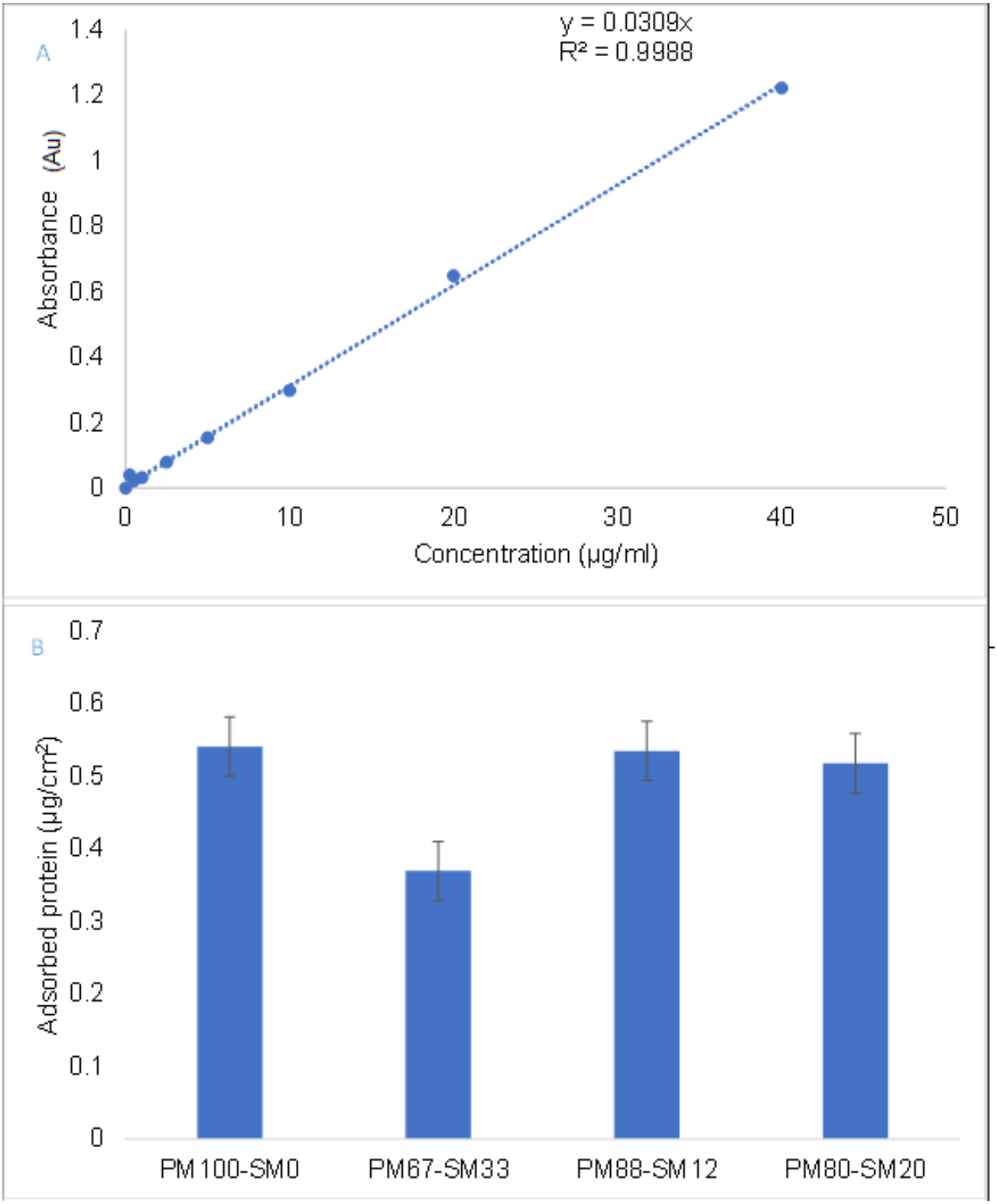


Figure 3.22 Calibration curve (A) and a chart of total adsorbed protein on the hydrogels (B).

Zhang and colleagues reported a protein adsorption of approximately 0.4 µg/mL and 0.9 µg/mL respectively for BSA and lysozyme from single protein solutions using BCA assay kit. (Zhang et al., 2017) The current study however, studied protein adsorption from a mixed protein solution using a micro-BCA assay kit that had a higher sensitivity. The protein adsorbed on the best modified hydrogel sample was below the limit of detection by the micro-BCA assay kit and hence was calculated from the absorbance values using the equation generated from the standard curve of the protein solution. PVA has previously and severally been used as a stand-alone agent for imparting hydrophilicity to materials. (Winterton et al., 2007) In addition, certain already marketed contact lenses are made from PVA as a base polymer including already marketed products. Likewise, zwitterionic polymers such as 2-methacryloyioxyethyl phosphoryl choline has previously been used alone as a surface modifying agent to limit protein adsorption. (Goda & Ishihara, 2006; Shi et al., 2021) The results obtained implies a synergistic superhydrophilicity arising from the combination of PVA and the zwitterionic SBMA resulting in a higher capacity to limit protein adhesion in the developed biomaterial. Against the traditional surface modification to which zwitterionics have previously been applied, SBMA was incorporated in the structure of the base PVAGMA polymer through a crosslinking process that potentially maintain the lifetime of the protein resistance of the developed material.

3.3.13 Cytotoxicity assay of the hydrogel extract

MTT assay has variously been used to assess the toxicity of different compounds to ocular cell lines. Primary human retinal epithelial cells were included in this study as they represent the most sensitive, among ocular cells, to extraneous substances. The results shown in **Figure 3.23** represent the percent viabilities of 3T3 (A), HEK 293 (B), and HREP (C) cells at 24 and 48 hours. These confirm generally the non-toxicity of the leached extract from the hydrogels across all cell lines used. More specifically, the viabilities at 48 hours were significantly higher than the viabilities at 24 hours across most cell lines for all the formulations. This may signify that the cells quickly adjusted to the presence of these extracts over the 24-hour period. In addition, the viabilities at all time points showed a graded response with viabilities increasing proportionately to an increasing concentration of SBMA in the hydrogels in 3T3 cell lines. This effect may relate to the similarity of SBMA to membrane proteins hence contributing the safety and comfortability of the cells to its presence in the hydrogels. Interestingly, the over 100 % viabilities obtained at all sampling time points showed that the extracts rather had a proliferative effect on all cells.

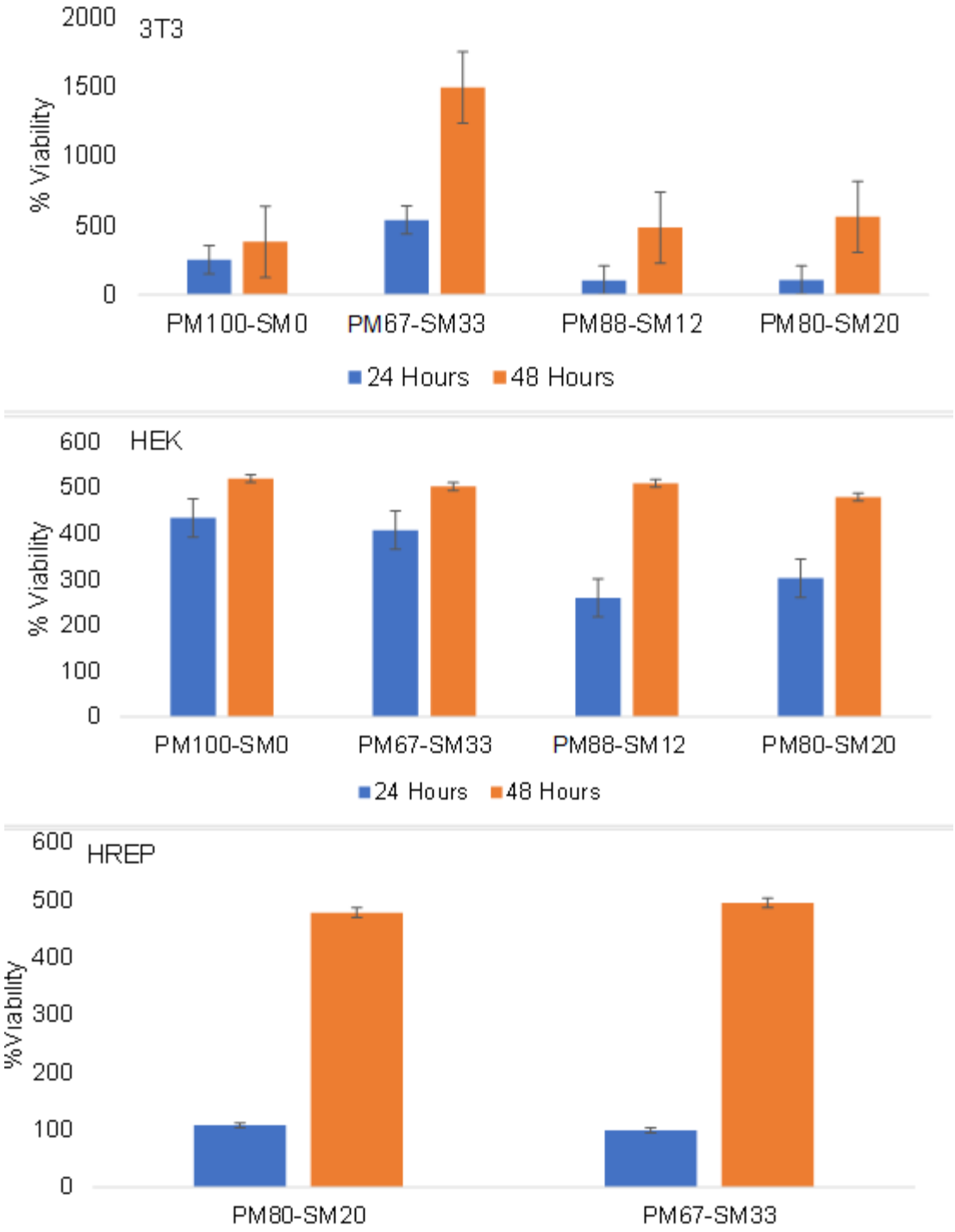


Figure 3.23 MTT assay against 3T3, HEK 293, and HREP cells at 24 and 48 hours.

Likewise, the morphology of HREP cells is captured in **Figure 3.24.** It is known that the morphology of cells shows how stressed cells are under any given condition. The results obtained for the morphologies before (**Figure 3.24)** and after 48 hours treatment with hydrogel extract indicates a normal morphology. A high mitotic index usually indicated by high viability demonstrates the ability of cells to repair after injury. (Edelhauser, 2006) The implication may be enormous in instances where the developed hydrogel is used in procedures that entail wound healing. It is important to note that a previous work on ocular hydrogel contact lens recorded similar viabilities. (Tran et al., 2020) Overall, these results speak to the safety of the developed biomaterial to ocular cell lines.

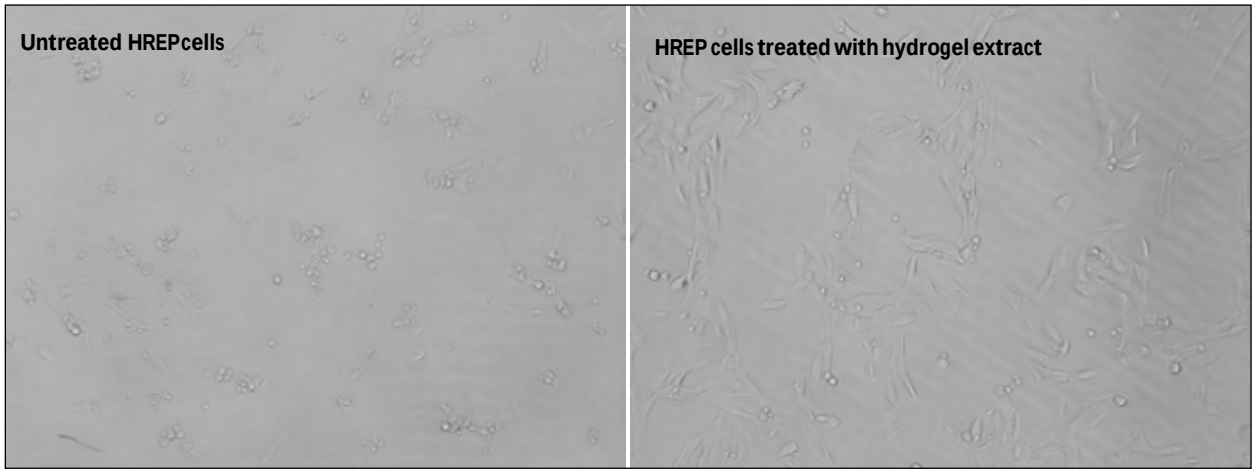


Figure 3.24 Morphology of HREP cells before and after 24 hours of treatment with hydrogel extract.

3.4 Conclusions

Herein has been outlined the facile synthesis of a PVAGMA hydrogel modified by a photo-initiated crosslinking polymerization with SBMA. Physicochemical characterization confirmed the synthesis and chemical stability of PVAGMA from PVA and GMA. Beyond surface modification, and the impediments to efficient copolymerization of zwitterionics with regular crosslinkers, the zwitterionic SBMA was incorporated as an integral part of the ocular hydrogel. The properties of the synthesised hydrogel in terms of mechanical strength, equilibrium water content, hydrophilicity, and transparency were robust. The prepared hydrogel by virtue of its hydrophilicity, morphology, and mechanical properties additionally had a limiting effect on the

protein resistance ability of the hydrogels. These attributes have previously been linked to the ability of biomaterial to limit inflammatory responses to the biomaterial and was demonstrated for the particular case of ocular application in chapter 5 of this dissertation. Additionally, the ability of the hydrogel to serve as a drug delivery implant is explored in chapter 5 using both a nano-vesicular system (developed in chapter 4) and drug solution.

3.5 References

Ashtiani, M. K., Zandi, M., Shokrollahi, P., Ehsani, M., & Baharvand, H. (2018). Surface modification of poly(2-hydroxyethyl methacrylate) hydrogel for contact lens application. *Polymers for Advanced Technologies*, *29*(4), 1227–1233. https://doi.org/10.1002/pat.4233

Askari, F., Zandi, M., Shokrolahi, P., Tabatabaei, M. H., & Hajirasoliha, E. (2019). Reduction in protein absorption on ophthalmic lenses by PEGDA bulk modification of silicone acrylate-based formulation. *Progress in Biomaterials*, *8*(3), 169–183. https://doi.org/10.1007/s40204-019-00119-x

Carr, L. R., Xue, H., & Jiang, S. (2011). Functionalizable and nonfouling zwitterionic carboxybetaine hydrogels with a carboxybetaine dimethacrylate crosslinker. *Biomaterials*, *32*(4), 961–968. https://doi.org/10.1016/j.biomaterials.2010.09.067

Cavalieri, F., Miano, F., D'Antona, P., & Paradossi, G. (2004). Study of Gelling Behavior of Poly(vinyl alcohol)-Methacrylate for Potential Utilizations in Tissue Replacement and Drug Delivery. *Biomacromolecules*, *5*(6), 2439–2446. https://doi.org/10.1021/bm049654g

Chen, S., Zheng, J., Li, L., & Jiang, S. (2005). Strong Resistance of Phosphorylcholine Self-Assembled Monolayers to Protein Adsorption: Insights into Nonfouling Properties of Zwitterionic Materials. *Journal of the American Chemical Society*, *127*(41), 14473–14478. https://doi.org/10.1021/ja054169u

Crispim, E. G., Piai, J. F., Fajardo, A. R., Ramos, É. R., Nakamura, T. U., Nakamura, C., Rubira, A. F., & Muniz, E. (2012). *Hydrogels based on chemically modified poly(vinyl alcohol) (PVA-GMA) and PVA-GMA/chondroitin sulfate: Preparation and characterization*. https://doi.org/10.3144/EXPRESSPOLYMLETT.2012.41

Delgado, A. H. S., & Young, A. M. (2021). Methacrylate peak determination and selection recommendations using ATR-FTIR to investigate polymerisation of dental methacrylate mixtures. *PLOS ONE*, *16*(6), e0252999. https://doi.org/10.1371/journal.pone.0252999

Edelhauser, H. F. (2006). The Balance between Corneal Transparency and Edema The Proctor Lecture. *Investigative Ophthalmology & Visual Science*, *47*(5), 1755–1767. https://doi.org/10.1167/iovs.05-1139

Eke, G., Mangir, N., Hasirci, N., MacNeil, S., & Hasirci, V. (2017). Development of a UV crosslinked biodegradable hydrogel containing adipose derived stem cells to promote vascularization for skin wounds and tissue engineering. *Biomaterials*, *129*, 188–198. https://doi.org/10.1016/j.biomaterials.2017.03.021

El-Shamy, A. G., Attia, W., & Abd El-Kader, K. M. (2014). The optical and mechanical properties of PVA-Ag nanocomposite films. *Journal of Alloys and Compounds*, *590*, 309–312. https://doi.org/10.1016/j.jallcom.2013.11.203

Fathi, E., Atyabi, N., Imani, M., & Alinejad, Z. (2011). Physically crosslinked polyvinyl alcohol–dextran blend xerogels: Morphology and thermal behavior. *Carbohydrate Polymers*, *84*(1), 145–152. https://doi.org/10.1016/j.carbpol.2010.11.018

Goda, T., & Ishihara, K. (2006). Soft contact lens biomaterials from bioinspired phospholipid polymers. *Expert Review of Medical Devices*, *3*(2), 167–174. https://doi.org/10.1586/17434440.3.2.167

Goda, T., Matsuno, R., Konno, T., Takai, M., & Ishihara, K. (2009). Protein adsorption resistance and oxygen permeability of chemically crosslinked phospholipid polymer hydrogel for ophthalmologic biomaterials. *Journal of Biomedical Materials Research. Part B, Applied Biomaterials*, *89*(1), 184–190. https://doi.org/10.1002/jbm.b.31204

Huang, K.-T., Fang, Y.-L., Hsieh, P.-S., Li, C.-C., Dai, N.-T., & Huang, C.-J. (2016). Zwitterionic nanocomposite hydrogels as effective wound dressings. *Journal of Materials Chemistry B*, *4*(23), 4206–4215. https://doi.org/10.1039/C6TB00302H

Huszank, R., Szilágyi, E., Szoboszlai, Z., & Szikszai, Z. (2019). Investigation of chemical changes in PMMA induced by 1.6 MeV He+ irradiation by ion beam analytical methods (RBS-ERDA) and infrared spectroscopy (ATR-FTIR). *Nuclear Instruments and Methods in Physics Research Section B: Beam Interactions with Materials and Atoms*, *450*, 364–368. https://doi.org/10.1016/j.nimb.2018.05.016

Ishihara, K., Fukazawa, K., Sharma, V., Liang, S., Shows, A., Dunbar, D. C., Zheng, Y., Ge, J., Zhang, S., Hong, Y., Shi, X., & Wu, J. Y. (2021). Antifouling Silicone Hydrogel Contact Lenses with a Bioinspired 2-Methacryloyloxyethyl Phosphorylcholine Polymer Surface. *ACS Omega*, *6*(10), 7058–7067. https://doi.org/10.1021/acsomega.0c06327

Kharazmi, A., Faraji, N., Mat Hussin, R., Saion, E., Yunus, W. M. M., & Behzad, K. (2015). Structural, optical, opto-thermal and thermal properties of ZnS-PVA nanofluids synthesized through a radiolytic approach. *Beilstein Journal of Nanotechnology*, *6*, 529–536. https://doi.org/10.3762/bjnano.6.55

Kita, M., Ogura, Y., Honda, Y., Hyon, S.-H., Cha, W.-I., & Ikada, Y. (1990). Evaluation of polyvinyl alcohol hydrogel as a soft contact lens material. *Graefe's Archive for Clinical and Experimental Ophthalmology*, *228*(6), 533–537. https://doi.org/10.1007/BF00918486

Lalani, R., & Liu, L. (2011). Synthesis, characterization, and electrospinning of zwitterionic poly(sulfobetaine methacrylate). *Polymer*, *52*(23), 5344–5354. https://doi.org/10.1016/j.polymer.2011.09.015

Morgacheva, A. A., Artyukhov, A. A., Panov, A. V., Gordienko, M. G., Shtil'man, M. I., & Mezhuev, Ya. O. (2015). Synthesis of polyvinyl alcohol with methacrylate groups and of hydrogels based on it. *Russian Journal of Applied Chemistry*, *88*(4), 617–621. https://doi.org/10.1134/S1070427215040102

Muniz, F. T. L., Miranda, M. a. R., Morilla dos Santos, C., & Sasaki, J. M. (2016). The Scherrer equation and the dynamical theory of X-ray diffraction. *Acta Crystallographica Section A: Foundations and Advances*, *72*(3), 385–390. https://doi.org/10.1107/S205327331600365X

Omkaram, I., Sreekanth Chakradhar, R. P., & Lakshmana Rao, J. (2007). EPR, optical, infrared and Raman studies of VO2+ ions in polyvinylalcohol films. *Physica B: Condensed Matter*, *388*(1), 318–325. https://doi.org/10.1016/j.physb.2006.06.134

Poly(vinyl alcohol). (n.d.). Retrieved 19 September 2021, from http://polymerdatabase.com/polymers/polyvinylalcohol.html

Pop-Georgievski, O., Rodriguez-Emmenegger, C., Santos Pereira, A. de los, Proks, V., Brynda, E., & Rypáček, F. (2013). Biomimetic non-fouling surfaces: Extending the concepts. *Journal of Materials Chemistry B*, *1*(22), 2859–2867. https://doi.org/10.1039/C3TB20346H

Rostam, H. M., Singh, S., Salazar, F., Magennis, P., Hook, A., Singh, T., Vrana, N. E., Alexander, M. R., & Ghaemmaghami, A. M. (2016). The impact of surface chemistry modification on macrophage polarisation. *Immunobiology*, *221*(11), 1237–1246. https://doi.org/10.1016/j.imbio.2016.06.010

Schindler, W. D., & Hauser, P. J. (2004). 4—Hand building finishes. In W. D. Schindler & P. J. Hauser (Eds.), *Chemical Finishing of Textiles* (pp. 43–50). Woodhead Publishing. https://doi.org/10.1533/9781845690373.43

Shi, X., Cantu-Crouch, D., Sharma, V., Pruitt, J., Yao, G., Fukazawa, K., Wu, J. Y., & Ishihara, K. (2021). Surface characterization of a silicone hydrogel contact lens having bioinspired 2-methacryloyloxyethyl phosphorylcholine polymer layer in hydrated state. *Colloids and Surfaces B: Biointerfaces*, *199*, 111539. https://doi.org/10.1016/j.colsurfb.2020.111539

Shin, H., Olsen, B. D., & Khademhosseini, A. (2012). The mechanical properties and cytotoxicity of cell-laden double-network hydrogels based on photocrosslinkable gelatin and gellan gum biomacromolecules. *Biomaterials*, *33*(11), 3143–3152. https://doi.org/10.1016/j.biomaterials.2011.12.050

Strawhecker, K. E., & Manias, E. (2000). Structure and Properties of Poly(vinyl alcohol)/Na+ Montmorillonite Nanocomposites. *Chemistry of Materials*, *12*(10), 2943–2949. https://doi.org/10.1021/cm000506g

Tran, N.-P.-D., Ting, C.-C., Lin, C.-H., & Yang, M.-C. (2020). A Novel Approach to Increase the Oxygen Permeability of Soft Contact Lenses by Incorporating Silica Sol. *Polymers*, *12*(9), 2087. https://doi.org/10.3390/polym12092087

Tummala, G. K., Joffre, T., Lopes, V. R., Liszka, A., Buznyk, O., Ferraz, N., Persson, C., Griffith, M., & Mihranyan, A. (2016). Hyperelastic Nanocellulose-Reinforced Hydrogel of High Water Content for Ophthalmic Applications. *ACS Biomaterials Science & Engineering*, *2*(11), 2072–2079. https://doi.org/10.1021/acsbiomaterials.6b00484

Uwaezuoke, O. J., Kumar, P., Pillay, V., & Choonara, Y. E. (2021). Fouling in ocular devices: Implications for drug delivery, bioactive surface immobilization, and biomaterial design. *Drug Delivery and Translational Research*. https://doi.org/10.1007/s13346-020-00879-1

Winterton, L. C., Lally, J. M., Sentell, K. B., & Chapoy, L. L. (2007). The elution of poly (vinyl alcohol) from a contact lens: The realization of a time release moisturizing agent/artificial tear.

Journal of Biomedical Materials Research Part B: Applied Biomaterials, *80B*(2), 424–432. https://doi.org/10.1002/jbm.b.30613

Xiang, T., Lu, T., Xie, Y., Zhao, W.-F., Sun, S.-D., & Zhao, C.-S. (2016). Zwitterionic polymer functionalization of polysulfone membrane with improved antifouling property and blood compatibility by combination of ATRP and click chemistry. *Acta Biomaterialia*, *40*, 162–171. https://doi.org/10.1016/j.actbio.2016.03.044

Yang, C.-C., & Wu, G. M. (2009). Study of microporous PVA/PVC composite polymer membrane and it application to MnO2 capacitors. *Materials Chemistry and Physics*, *114*(2), 948–955. https://doi.org/10.1016/j.matchemphys.2008.11.009

Ying, T., Su, J., Jiang, Y., Ke, Q., & Xu, H. (2020). A pre-wetting induced superhydrophilic/superlipophilic micro-patterned electrospun membrane with self-cleaning property for on-demand emulsified oily wastewater separation. *Journal of Hazardous Materials*, *384*, 121475. https://doi.org/10.1016/j.jhazmat.2019.121475

Zhang, J., Liu, T., Liu, Z., & Wang, Q. (2019). Facile fabrication of tough photocrosslinked polyvinyl alcohol hydrogels with cellulose nanofibrils reinforcement. *Polymer*, *173*, 103–109. https://doi.org/10.1016/j.polymer.2019.04.028

Zhang, W., Li, G., Lin, Y., Wang, L., & Wu, S. (2017). Preparation and characterization of protein-resistant hydrogels for soft contact lens applications via radical copolymerization involving a zwitterionic sulfobetaine comonomer. *Journal of Biomaterials Science, Polymer Edition*, *28*(16), 1935–1949. https://doi.org/10.1080/09205063.2017.1363127

Zhao, M.-H., Chen, X.-P., & Wang, Q. (2014). Wetting failure of hydrophilic surfaces promoted by surface roughness. *Scientific Reports*, *4*(1), 5376. https://doi.org/10.1038/srep05376

Zhou, D., Dong, Q., Liang, K., Xu, W., Zhou, Y., & Xiao, P. (2019). Photocrosslinked methacrylated poly(vinyl alcohol)/hydroxyapatite nanocomposite hydrogels with enhanced mechanical strength and cell adhesion. *Journal of Polymer Science Part A: Polymer Chemistry*, *57*(18), 1882–1889. https://doi.org/10.1002/pola.29263

Zhou, Y., Dong, P., Wei, Y., Qian, J., & Hua, D. (2015). Synthesis of poly(sulfobetaine methacrylate)-grafted chitosan under γ-ray irradiation for alamethicin assembly. *Colloids and Surfaces B: Biointerfaces*, *132*, 132–137. https://doi.org/10.1016/j.colsurfb.2015.05.019

CHAPTER FOUR

LINOLEIC ACID BASED TRANSFEROSOMES FOR TOPICAL OCULAR DELIVERY OF CYCLOSPORINE A

pharmaceutics

MDPI

Article

Linoleic Acid-Based Transferosomes for Topical Ocular Delivery of Cyclosporine A

Onyinye Uwaezuoke [1], Lisa C. Du Toit [1], Pradeep Kumar [1], Naseer Ally [2] and Yahya E. Choonara [1,*]

[1] Wits Advanced Drug Delivery Platform Research Unit, Department of Pharmacy and Pharmacology, School of Therapeutic Sciences, Faculty of Health Sciences, University of the Witwatersrand, 7 York Road, Parktown, Johannesburg 2193, South Africa
[2] Department of Neurosciences, Division of Ophthalmology, University of the Witwatersrand, 7 York Road, Parktown, Johannesburg 2193, South Africa
* Correspondence: yahya.choonara@wits.ac.za; Tel.: +27-11-717-2274

Abstract: Delivering high-molecular-weight hydrophobic peptides, such as cyclosporine A, across the corneal epithelium remains a challenge that is complicated by other physio-anatomical ocular structures that limit the ocular bioavailability of such peptides. Transferosomes have previously been used to improve transdermal permeability, and have the potential for improving the ocular corneal permeability of applicable drugs. In this study, transferosomes for the potential ocular delivery of cyclosporine A were investigated. Linoleic acid was evaluated for its effect on the stability of the transferosomes and was substituted for a portion of the cholesterol in the vesicles. Additionally, Span® 80 and Tween® 80 were evaluated for their effect on transferosome flexibility and toxicity to ocular cells as edge activators. Attenuated Total Reflectance–Fourier Transform Infrared spectroscopy (ATR-FTIR), differential scanning calorimetry (DSC), and dynamic light scattering (DLS) were used to evaluate the physicochemical parameters of the blank and the cyclosporine A-loaded transferosomes. Cyclosporine A release and corneal permeability were studied in vitro and in a New Zealand albino rabbit corneal model, respectively. The linoleic acid contributed to improved stability and the nano-size of the transferosomes. The Tween®-based formulation was preferred on the basis of a more favorable toxicity profile, as the difference in their corneal permeability was not significant. There was an initial burst release of cyclosporine A in the first 24 h that plateaued over one week. The Tween®-based formulation had a flux of 0.78 μg/cm^2/h. The prepared transferosomes demonstrated biocompatibility in the ocular cell line, adequately encapsulated cyclosporine A, ensured the corneal permeability of the enclosed drug, and were stable over the period of investigation of 4 months at −20 °C.

Keywords: topical ocular drug delivery; transferosomes; linoleic acid; cyclosporine A; nanoparticle drug-delivery systems

check for updates

Citation: Uwaezuoke, O.; Du Toit, L.C.; Kumar, P.; Ally, N.; Choonara, Y.E. Linoleic Acid-Based Transferosomes for Topical Ocular Delivery of Cyclosporine A. *Pharmaceutics* **2022**, *14*, 1695. https://doi.org/10.3390/pharmaceutics14081695

Academic Editors: Hugo Almeida and Ana Catarina Silva

Received: 30 June 2022
Accepted: 5 August 2022
Published: 15 August 2022

Publisher's Note: MDPI stays neutral with regard to jurisdictional claims in published maps and institutional affiliations.

Copyright: © 2022 by the authors. Licensee MDPI, Basel, Switzerland. This article is an open access article distributed under the terms and conditions of the Creative Commons Attribution (CC BY) license (https://creativecommons.org/licenses/by/4.0/).

1. Introduction

Topical ocular delivery is fraught with numerous challenges, arising mainly from the physio-anatomical barriers posed by ocular structures in their normal physiological line of duty [1]. A formidable barrier to topically applied substances is regularly presented by the corneal epithelium, barely permitting the passage of low molecular weight substances by diffusion [2]. The corneal epithelial cells allow the passage of lipophilic drugs that then is barred by the corneal stroma, which is hydrophilic [3]. In addition, the paracellular passage of substances is heavily challenged by the tight junctions presented by the cornea [4]. Consequently, the drive to deliver drugs across the cornea via topical ocular formulations is a continuing venture. There is also the additional challenge of increasing the time that such formulations stay on the ocular surface. This surface residence time is shortened by the blink reflex, as well as the constant flow of the tear film. Various colloidal systems,

4.1 Introduction

Topical ocular delivery is fraught with numerous challenges, arising mainly from the physio-anatomical barriers posed by ocular structures in their normal physiological line of duty (Uwaezuoke et al., 2021). A formidable barrier to topically applied substances is regularly presented by the corneal epithelium, barely permitting the passage of low molecular weight substances by diffusion (Mun et al., 2014). The corneal epithelial cells allow the passage of lipophilic drugs that then is barred by the corneal stroma, which is hydrophilic (Grass and Robinson, 1988). In addition, the paracellular passage of substances is heavily challenged by the tight junctions presented by the cornea (Ramsay et al., 2018). Consequently, the drive to deliver drugs across the cornea via topical ocular formulations is a continuing venture. There is also the additional challenge of increasing the time that such formulations stay on the ocular surface. This surface residence time is shortened by the blink reflex, as well as the constant flow of the tear film. Various colloidal systems, such as polymeric micelles (Di Tommaso et al., 2012), nanoparticles (Sharma et al., 2012) nanocapsules (Calvo et al., 1997), microemulsions (Ibrahim et al., 2020) and vesicular systems, have been explored to overcome many of these challenges. Among these, vesicular systems such as liposomes have stood out, overcoming the polarity issues associated with many of the new chemical entities (and which limit their passage through many biological membranes) and bringing biocompatibility, extended release, reduced systemic side-effects, and improved ocular biodistribution to topical ocular delivery (Urtti and Salminen, 1993).

Many of the ocular conditions require the topical application of medicaments for their treatment. Among these, the most frequently occurring are dry eye syndrome (keratoconjunctivitis sicca), keratoconus, and keratitis (Moiseev et al., 2019). Cyclosporine A (CysA) is a strong immune suppressive oligopeptide with 11 amino acid residues that has found use in many inflammatory conditions of the eye, such as non-infectious uveitis and vernal keratoconjunctivitis corneal healing (Lallemand et al., 2017). Even though the systemic administration of CysA, which was the initial mode of administration for ocular interventions, achieves high concentrations in ocular tissues, the high incidence and level of side effects arising from such a systemic administration is driving the search for topical formulations that could achieve the same therapeutic concentrations in the ocular tissues (Utine et al., 2010). Unfortunately, the high molecular weight (1202.6 Da), strong hydrophobicity (Log P lies between 1.4 and 3 depending on the solvent), and the presence of formidable barriers leaves little room for flexibility in terms of formulation maneuvers to achieve the optimum availability in ocular tissues from topical applications (Lallemand et al., 2017) (Daull et al. 2021). Nevertheless, various nanoplatforms have been explored for overcoming some of these issues with the physicochemical properties of CysA. Many of these platforms utilized excipients, to

enable the solubilization and stabilization of CysA, some of which may be contraindicated in the disease conditions which these formulations are intended to treat, as a result of the additional disruptions brought about on the corneal surface (Di-Tommaso et al., 2012) (Jumelle et al.,2020). Allergan Inc., USA (now AbbVie) was the first company to push a nanoemulsion formulation of CysA to the market. Most of the other marketed CysA topical drops are micellar solutions in which various surfactants, alcohols, co-solvents, and even some excipients that have been shown to be harmful to ocular health, were used. One such excipient is EDTA, which is employed for the solubilization of CysA (Ramsay et al., 2018, Burstein et al.,1980).

Transferosomes were introduced three decades ago to further expound the capabilities of the liposomal systems though directed to improve the delivery via the stratum corneum of the skin (Cevc and Blume, 1992). Transferosomes as ultra-elastic lipid vesicles have, since inception, been exploited in transdermal delivery for their exceptional permeability and the deformability properties imparted to the bilayer of regular vesicles, due to the presence of edge activators, such as Tween® 80, Span® 80, and sodium cholate (Opatha et al., 2020). Transferosomes are currently being deployed to improve the permeability of the stratum corneum to a variety of drugs. The success of transferosomes as a transdermal delivery system has been attributed partly to the osmotic gradient that exists across the outer and inner skin layers, and partly to the ability of transferosomes to deform while passing pores that are much smaller than them. This understanding and the existence of similar gradients across the corneal epithelium and stroma suggest that the same possibilities may exist for the permeation of large molecules across the tight junctions of the eye cornea. One major challenge that may deter the use of transferosomes in the corneal drug delivery has to do with the possible toxicity of the surfactants employed as the edge activators to ocular cells and therefore, requires a careful selection of, and delicate balance between, the edge activators and their use level. A major challenge in dry eye disease is the instability in the tear film as a result of sub-optimal tear volume and function (Moiseev et al., 2019). While CysA has a strong stimulating effect on tear fluid production, the excipients that will adequately stabilize the produced tear fluid are still lacking in many commercial formulations. As a result of these considerations, linoleic acid was introduced as a vesicle component to complement the pharmacological action of cyclosporine A in the treatment of the targeted ocular condition. Linoleic acid is an essential fatty acid that has been shown to stabilize the tear film when applied topically (Mudgil, 2020), and could therefore contribute to the therapeutic experience in patients with dry eye syndrome, in whom tear film stability is a major challenge contributing to the discomfort from the disease (Yokoi et al., 2015). Daull and co-workers (Daull et al., 2021) had earlier concluded, after reviewing many formulations of cyclosporine A currently on the market,

that the vehicle carrier in cyclosporine A topical formulations could contribute to a significantly improved performance.

The benefits of transferosomes that have chronicled its application in transdermal delivery underscore their potential in topical ocular delivery. Thus far, no study has explored the possibility of transferosomes in ocular applications; hence, in this investigation, a topical transferosomal formulation was proposed and explored as an alternative topical formulation for CysA, particularly in the treatment of dry eye disease. In this investigation, transferosomes, which are generally composed of phospholipids and an edge activator as a membrane-softening agent, were formulated. Both Tween® 80 and Span® 80 were selected for investigation, based on their demonstrated efficacy in facilitating the deformability of the transferosomes. The additional challenge of tear film stability that accompanies and complicates ocular conditions, such as dry eye, informed the decision to include linoleic acid in the formulation. Linoleic acid has been found to have a stabilizing effect on tear film. In addition, linoleic acid can contribute to permeation enhancement as a fatty acid since other fatty acids, such as oleic acid, have demonstrated potential as permeation enhancers in dermal formulations (Hashmat et al., 2020). Additionally, linoleic acid was explored for its effect on stabilizing the lipid bilayer of the transferosome, thereby acting as both an excipient and an active ingredient. Spectroscopic methods were used to characterize and confirm the inclusion of CysA in the form of transferosomes. Further physicochemical parameters, such as size and zeta potential, were studied, as well as the biocompatibility in an ocular cell line. In addition, the ex vivo corneal permeability of the developed transferosomes were assessed, employing rabbit corneal tissue.

4.2 Materials and Methods

4.2.1 Materials

The cyclosporine A was purchased from LEAP pharma (DLD Scientific, South Africa). The Tween® 80, Span® 80, linoleic acid, soy phosphatidylcholine, cholesterol, and the MTT assay kit were purchased from Sigma-Aldrich (St. Louis, MO, USA). The ultrapure water (Milli Q, water, Sigma-Aldrich, Massachusetts, MA, USA) was used. All of the other solvents were obtained and used without further purification.

4.2 Materials and Methods

4.2.1 Materials

Cyclosporin A was purchased from LEAP pharma (DLD Scientific, South Africa). L-α-soy Lecithin

was purchased from EMD Millipore Corp. (290 Concord Road, Ballerica, MA, USA). Tween® 80, Span 80®, linoleic acid, cholesterol and MTT assay kit were purchased from Sigma (St. Louis, MO, USA). All other solvents were obtained from and used without further purification.

Table 4.1 Composition of transferosomes.

Component	Composition	Function
Soy Lecithin	180 mg	Lipid
Cholesterol	20 mg	Lipid
Linoleic acid	20 mg	Stabilizer/moisturizer
Tween® 80	1–2% *v*/*v*	Edge activator
Span® 80	1–2% *v*/*v*	Edge activator
CysA	60 mg	Active ingredient
Sucrose	2% w/v	Cryoprotectant

4.2.2 Preparation of the cyclosporine-A loaded transferosomes

The thin film method was employed in the preparation of blank and CysA-loaded transferosomes, using the formulation variables outlined in **Table 4 1**. The lipids, cholesterol, and linoleic acid were dissolved in an appropriate volume of chloroform–methanol solution, mixed in a ratio of 3:1. For the CysA-loaded transferosome, the cyclosporine was added in the film-forming solution. The resulting solution was evaporated in a rotary shaker (Rotavapor1 RII, Büchi Labortechnik AG, Flawil, Switzerland) to obtain a thin film which was subsequently hydrated using either a Tween® or Span® solution constituted in artificial tear fluid (ATF) of pH 7.4. The concentration of the Tween® or Span® solution was varied, as shown in **Table 4.1,** and incorporated either as part of the hydrating fluid or as part of the lipid film. The resulting multilamellar vesicles were ultrasonicated for 5 min in ice using a probe sonicator (Sonics Vibra cell, Newtown, CT, USA) set at a 20 s on and 5 s off cycle, and an amplitude of 50%. The obtained nanovesicles were subsequently lyophilized (Freezone 12 freeze drier, Labonco, Kansas City, KS, USA) and characterized appropriately. A 2% sucrose solution was used as a

cryo-protectant. The effect of the linoleic acid inclusion on the physicochemical characteristics of the transferosomes was also evaluated by preparing Tween® 80-based transferosomes, with and without linoleic acid.

4.2.3 Characterization of the transferosomes

The size, zeta potential, and polydispersity index of the prepared transferosomes were determined in triplicate, using dynamic light scattering (DLS) on the ZetaSizer NanoZS (Malvern Instruments, Malvern, UK). These measurements were undertaken shortly after sonication and after 4 months of storage at −20 °C in a freezer (GL I472QPZX, LG Korea) (Sydykov et al., 2018).

A FEI Tecnai T12 transmission electron microscope (TEM, Hillsboro, OR, USA) and the ZEISS Sigma 300 VP with a ZEISS 'smart SEM' software (Field Emission Scanning Electron Microscope, SEM, FEI, Orlando, FL, USA) were used to characterize the morphology of the transferosomes. A dispersion of the lyophilized transferosomes was prepared in deionized water to a concentration of 0.5 mg/mL and dropped on a copper grid. The excess was dabbed with a filter paper and the dispersion allowed to dry. The grid was subsequently covered by a drop of 2% v/v phosphotungstic acid and imaged with the FEI Tecnai T12 transmission electron microscope. For the SEM imaging, a drop of the dispersion was dropped onto a two-sided carbon tape mounted on an aluminum stub. The dispersion was dried, and sputter-coated with gold/palladium before imaging.

Differential scanning calorimetry (DSC) was undertaken (Mettler Toledo, DSC, STARe System, Swchwerzenback, ZH, Switzerland) to study the heat transitions in both the CysA-loaded and unloaded vesicles.

Attenuated Total Reflectance–Fourier Transform Infrared spectroscopy was undertaken on a Perkin Elmer Spectrum 2000 ATR-FTIR spectrometer (PerkinElmer 100, Llantrisant, Wales, UK), fitted with a single-reflection diamond. A MIRTGS detector was used to study the surface transitions and functional groups on both the cyclosporine A-loaded and unloaded transferosomes.

The stability of the transferosomes was assessed by storing lyophilized transferosomes at a representative storage temperature of −20 °C over a period of 4 months. At specified time intervals, the size distribution, polydispersity index, and zeta potential of the samples were measured.

The elasticity of the transferosomes was studied, using a modified method as applied by Jain and coworkers (Jain et al., 2003). An appropriate amount of the lyophilized transferosomes was dispersed in artificial tear fluid (ATF) to formulate a stock suspension that was diluted appropriately before analysis. The stock suspension (one part) was diluted with nine parts of

ATF and the particle size determined. Subsequently, 1 mL of the diluted system was extruded through a 100 nm polycarbonate filter. The volume extruded was noted, as well as the hydrodynamic size of the extruded dispersion. The extrusion process was repeated five times.

4.2.4 Encapsulation efficiency (EE%) and in vitro release of cyclosporine A from the transferosomes

The direct method was employed in determining the quantity of the drug encapsulated in the transferosomes (Yu et al., 2018). To this end, a dispersion of the lyophilized CysA-loaded transferosomes was prepared in ATF and the absorbance read at a wavelength of 207 nm on an IMPLEN NanoPhotometer®, (Implen GmbH, Munchen, Germany) The concentration was subsequently determined from a standard calibration curve of cyclosporine A, prepared using methanol: ATF (9:1) solution as solvent. The encapsulation efficiency (EE%) was subsequently calculated using **Equation 4.1.**

$$EE\% = \frac{\boldsymbol{Actual\ amount\ of\ drug}\ entrapped\ \boldsymbol{in\ the\ transferosome}}{\boldsymbol{Amount\ of\ drug\ incoporated\ in\ the\ transferosome}} \times 100 \qquad \textbf{(4.1)}$$

In a similar process, the drug release from the transferosomes was determined, using a modified USP dissolution apparatus, commonly applied as an in vitro drug release test for colloidal drug carriers (Abdel-Mottaleb and Lamprecht, 2011). Briefly, one end of a glass tube (open at both ends) was covered with dialysis tubing (12,000–14,000 MWCO), which had initially been equilibrated in ATF at 37 °C. The prepared transferosome dispersion in ATF (1 mL) was introduced from the other open end and suspended in 100 mL of ATF of pH 7.4 as the dissolution medium. The dissolution medium was stirred at 50 rpm and maintained at 37 °C ± 1 °C. At scheduled time intervals, a 1 mL sample was withdrawn from the dissolution medium and replaced with an equivalent volume of ATF and the drug content subsequently calculated from the absorbance reading acquired from the Implen NanoPhotometer™ (Implen GmbH, Munchen Germany.

4.2.5 *Ex vivo* corneal permeability of the transferosomes

The corneal permeability of the formulations was determined, using the cornea from New Zealand albino rabbits. The rabbits were selected because the size of the rabbits' cornea is

similar to that of humans. The eyes of the rabbits were enucleated, and the cornea removed accompanied by about 3 mm of scleral tissue. These were immediately rinsed with ATF and wrapped with film to prevent dehydration. Subsequently, they were stored at 4 °C until used within 4 h of harvest [25,4]. The permeability study was undertaken in a Franz diffusion cell (PermeGear Inc. Bethlehem, PA, USA) with three cells. The cornea was used as the separating membrane between the donor and receptor chamber (enclosed in silicon rings) with the epithelial surface facing upward to the donor chamber. The receptor chamber was filled with 12 mL of degassed ATF, stirred at 60 rpm, and the system temperature maintained at 36 °C by means of a circulating water bath. A transferosomal dispersion in ATF was made and 1 mL introduced into the donor chamber. At 3, 6, and 24 h, 0.4 mL was withdrawn from the receptor chamber and replaced with an equal volume of degassed ATF. These were subsequently analysed and the amount of drug that had passed through was determined from the cyclosporine A calibration curve.

4.2.6 *Ex vivo* corneal permeability of the transferosomes

The corneal permeability of the formulations was determined, using the cornea from New Zealand albino rabbits. The rabbits were selected because the size of the rabbits' cornea is similar to that of humans. The eyes of the rabbits were enucleated, and the cornea removed accompanied by about 3 mm of scleral tissue. These were immediately rinsed with ATF and wrapped with film to prevent dehydration. Subsequently, they were stored at 4 °C until used within 4 h of harvest (Ramsay et al., 2018) (Pescina et al., 2015) The permeability study was undertaken in a Franz diffusion cell (PermeGear Inc. Bethlehem, PA, USA) with three cells. The cornea was used as the separating membrane between the donor and receptor chamber (enclosed in silicon rings) with the epithelial surface facing upward to the donor chamber. The receptor chamber was filled with 12 mL of degassed ATF, stirred at 60 rpm, and the system temperature maintained at 36 °C by means of a circulating water bath. A transferosomal dispersion in ATF was made and 1 mL introduced into the donor chamber. At 3, 6, and 24 h, 0.4 mL was withdrawn from the receptor chamber and replaced with an equal volume of degassed ATF. These were subsequently analysed and the amount of drug that had passed through was determined from the cyclosporine A calibration curve.

4.2.7 Cytotoxicity studies of the transferosomes in human retinal epithelial cell line

The MTT, (3-[4,5- dimethylthiazol-2-yl]-2,5-diphenyltetrazolium bromide), assay to determine the

cytotoxicity of the transferosomes was carried out using an ocular cell line, human retinal epithelial primary (HREP) cells. The HREP cells were grown in DMEM: HAM's F12 (50:50) medium supplemented with 10% FBS and 1% penicillin/streptomycin. The cells were grown until they were 80 to 90% (about 48 h incubation) confluent in an incubator set at a temperature of 37 °C with 5% CO_2. Thereafter, the cells were detached using 2 mL of 1% trypsin. The cells were thereafter seeded in two 96-well plates using 90 µL of cell suspension at a cell density of 40,000 cells/mL for the HREP cells and further incubated for 24 h. The wells were thereafter treated with 10 µL of a 5 mg/mL transferosome dispersion. After the treatment, the plates were incubated at a temperature of 37 °C with 5 % CO_2. At 24 and 48 h, respectively, each well was treated with 10 µL of (3- [4,5- dimethylthiazol-2-yl]-2,5-diphenyltetrazolium bromide) (MTT) at a final concentration of 5 mg/mL. Each plate was further incubated for 4 h in a humidified atmosphere at 37 °C and 5 – 6 % CO_2. A solubilization reagent (100 µL) was then added and the plate allowed to stand overnight in the incubator. The absorbance of the developed purple formazan crystals was then read in a VX3 microplate reader at 570 nm. The percent viability of the cells was subsequently calculated using **Equation 4.2.**

$$\%\, Viability = \frac{Absorbance\ of\ treated\ well - absorbance\ of\ blank}{Absorbance\ of\ control - absorbance\ of\ blank} \times 100 \qquad (4.2)$$

The ATF was used as the negative control, the 5-fluorouracil and DMSO were used as the positive controls, and the untreated wells were used as the blank.

4.2.8 Statistical analysis

The continuous variables with a normal distribution, such as particle size, size distribution, zeta potential, etc., are reported as mean ± SD. Comparisons to establish the statistical significance where needed were undertaken using one way ANOVA and Student's t-test at $p < 0.05$. All of the statistical analyses were performed using Microsoft Excel 2016 (Microsoft Corp, Redmond, WA, USA) and GraphPad by Dotmatics (Boston, MA, USA).

4.3 Results and Discussion

4.3.1 Formulation and characterization of transferosomes

The hydrodynamic diameter, polydispersity index, and zeta potential transferosomes prepared using 1% v/v Span® 80 or Tween® 80, together with linoleic acid, are displayed in **Table 4.2**.

During preliminary studies, the concentration of the surfactants employed was varied between 1% v/v and 2% v/v to establish a compromise between toxicity, and elasticity/deformability. A concentration of 1% v/v of Span® 80 or Tween® 80 was employed in the ensuing investigations, based on the ability to form stable, deformable transferosomes of adequately low toxicity. The results displayed in **Table 4. 2** indicate that the hydrodynamic diameter of the transferosomes formed using the Span 80® was higher than that formed by the Tween 80®. Contrary to the norm, loading CysA seemed to yield smaller sized transferosomes. The hydrodynamic diameters obtained in this study are congruent with those observed in previous studies (Ahad et al., 2017). The linoleic acid was incorporated to replace a portion of the cholesterol as part of the lipid concentration for the membrane stabilization. Cholesterol is known to contribute to the membrane thickness and hence the increased size of the vesicles (Nakhaei et al., 2021). The replacement of a part of the cholesterol with linoleic acid and the CysA-loading that improves membrane fluidity all con-tributed to a reduction in the hydrodynamic size of the prepared transferosomes. Most of the studies report an increase in the size of the vesicles after drug loading. Shen and co-workers reported a slight decrease in the size of paclitaxel-loaded micelles, although this decrease was not consistent across all of their formulations (Shen et al., 2009). The reduction in size observed in this study may have resulted from an effect of the CysA on the membrane packing. The defects in the lipid membrane are an important factor modulating the binding of different peripheral proteins (Tripathy et al., 2020), that in turn affects fluidity, and membrane thickness (Huang et al., 2017). Pezeshky and co-workers (Pezeshky et al., 2016) described the effect of cholesterol, for example, on the size of vesicles after 30 days of storage. The membrane thickness has been identified as one parameter that affects the size of vesicles (Huang et al., 2017). According to Huang and others, an in-crease in the membrane thickness leads to an increase in the vesicle size (Huang et al., 2017). It can be inferred that CysA, being hydrophobic, is loaded into the lipid bilayer and facilitates the compact packing that reduces the thickness of the membrane, and therefore the vesicles size. The level of surfactants incorporated into ophthalmic products is critical for both the ocular cell toxicity and formulation stability. In transferosomes, an additional demand is placed on the surfactant for effective flexibility and deformability. The transferosomes enable the effective deposition of the contained drug at the site of physiological action possessing the potential to migrate through orifices smaller than their size. Tween® 80 was selected because it has found use in ophthalmic products on the market due to its acceptable safety profile.

Lyophilization had a potentially stabilizing effect on all of the vesicles. This is evident from the results of the zeta potential, which depict the magnitude of charges that tend to cause repulsion

Table 4.2 Size distribution and polydispersity of blank and loaded transferosomes.

Parameter	Non-lyophilized Tween® 1%		Lyophilized Tween® 1%		Non-lyophilized Span® 1%		Lyophilized Span 1%	
	loaded	blank	Loaded	Blank	Loaded	Blank	Loaded	Blank
Size (nm)	64.68 ± 0.14	69.33 ± 0.31	183.67 ± 0.62	243.01 ± 1.61	104.87 ± 0.8	159.37 ± 0.63	246.5 ± 3.09	315.7± 4.41
Polydispersity index	0.209± 0.005	0.223± 0.004	0.367 ± 0.01	0.388 ± 0.01	0.127 ± 0.01	0.244 ± 0.01	0.305 ± 0.02	0.388 ± 0.05
Zeta Potential	-18.9 ± 1.6	-26.23 ± 1.3	-24.43 ± 2.88	-20.2 ± 2.90	-35.5 ±.1.26	-43.6 ± 4.29	- 4.77 ± 0.58	-35.5 ± 3.05

between two vesicles in close proximity. The values above +30 mV and below −30 mV are considered acceptable for the stability of the colloids (Danaei et al., 2018). Even though the zeta potentials for all of the formulations were initially within an acceptable range, they all somewhat increased after lyophilization.

Nanovesicles, by default, are prone to membrane destabilization that result from the double effect of environmental factors, such as moisture, oxygen, and the presence of large quantities of unsaturated fatty acids in an aqueous environment (Yang et al., 2021). Lyophilization, which is often employed as one of the methods to limit this form of instability, can fracture the delicate vesicle membrane as a result of the effect of ice crystals. The stabilization can, therefore, be the result of an intricate interplay between the concentration and type of cryoprotectants used and the fracturing effect of lyophilization (Almalik et al., 2017). For Tween® 1% formulations, the stabilization effect is noted in the form of a favorable shift from a value of −18.9 ± 1.6 to −24.43 ± 2.88 for the CysA-loaded formulation. To study the effect of linoleic acid, the preliminary formulations were prepared with and without linoleic acid. In all of the formulations studied, the zeta potential and, thus, the stability to aggregation was improved by the addition of linoleic acid

Table 4.3 Effect of incorporation of linoleic acid on the stability of transferosomes.

Formulation	Size (nm)	Polydispersity Index	Zeta potential
With Linoleic acid	125.33 ± 1.60	0.319 ± 0.32	-13.4 ± 1.00
Without linoleic acid	150.17 ± 1.20	0.382 ± 0.01	-5.71 ± 0.17

both for the CysA-loaded and blank Tween® 80 transferosomes. The size of the transferosomes was also comparatively reduced. The results from a representative lyophilized Tween® 80 1% v/v CysA-loaded formulation are shown in **Table 4.3**. The two-tailed *p*-value for size and the zeta potential comparison between the representative formulations determined by GraphPad were less than 0.0001 and 0.0002, respectively, thus notably significant.

4.3.2 Physicochemical characterization of the transferosomes

Fourier-transform infrared spectroscopy is usually used to study and characterize the nature of functional groups occurring at molecular surfaces. The results displayed in **Figure 4. 1** depict the FTIR fingerprints for pure CysA, blank transferosomes, and CysA-loaded transferosomes. The FTIR of both the blank and CysA-loaded transferosomes are identical, showing the same band intensities for identified functional groups occurring at the same wave numbers. None of the characteristic bands for CysA could be detected in the CysA-loaded transferosomes. This confirms the encapsulation of CysA within the transferosome vesicles and that no new bonds were formed when CysA was loaded into the transferosomes (Wagh and Apar, 2014).

Figure 4. 2 depicts the thermograms derived from the differential scanning calorimetric analysis performed on pure CysA, the unloaded transferosomes prepared with and without linoleic acid, and the transferosomes loaded with CysA. DSC was applied to characterize the thermal transitions between phases that occur in materials, resulting from temperature changes as directed by heat flow. The thermogram of bilayers of pure lipids generally depicts the transition temperature at which the lipid transforms from gel to a liquid crystalline phase. (Demetzos, 2008).

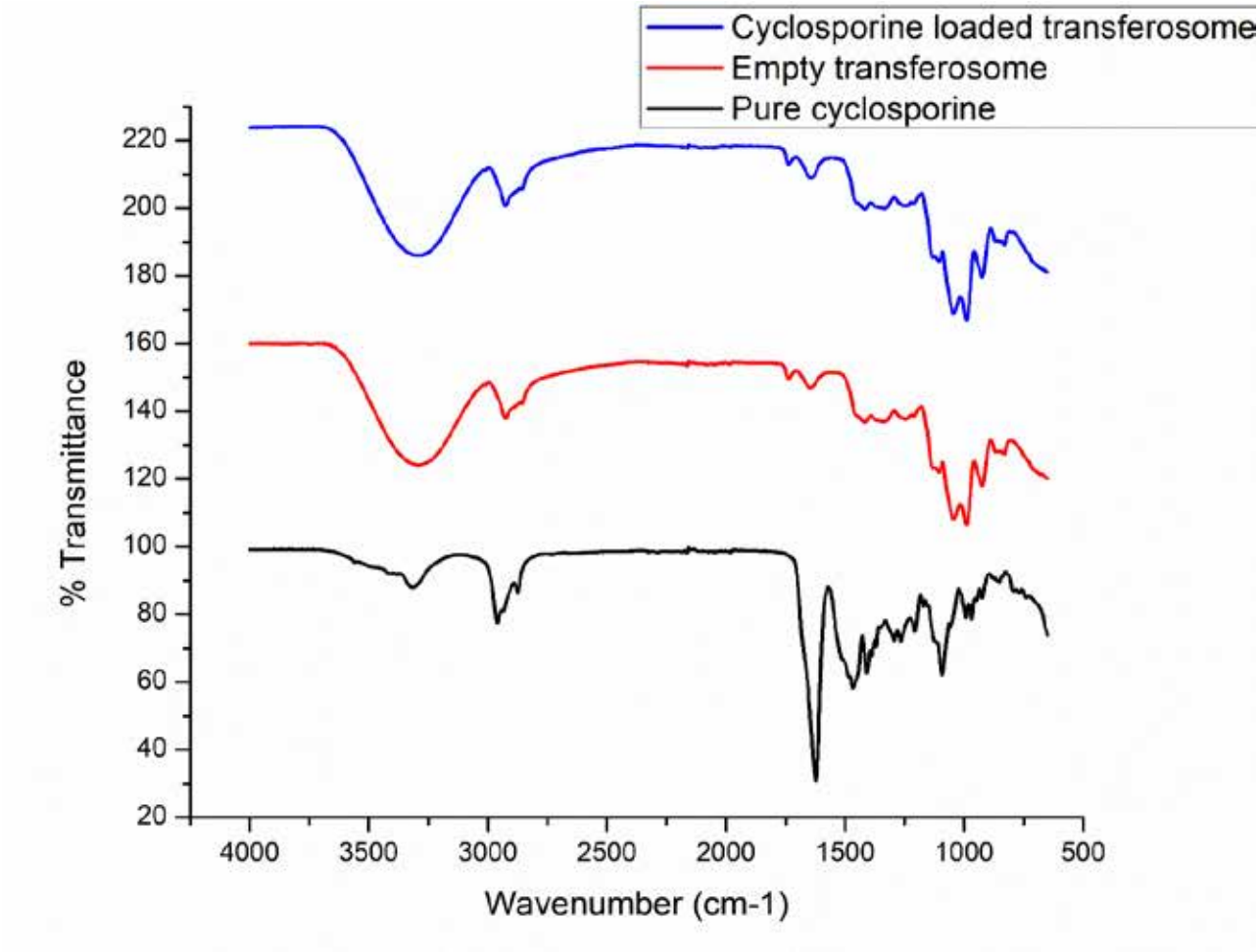


Figure 4.1 FTIR analysis of unloaded and CysA-loaded transferosomes.

In **Figure 4.2**, the thermal transitions occurring in the lipid vesicles prepared in this study are evident. These vesicles were cryo-protected with a 2% sucrose solution before being lyophilized. The exothermic peaks that occurred at ~132 °C in all of the transferosomes represented the glass transition temperature. In the melting peaks occurring at 170.97 °C and 172.50 °C, respectively, for the transferosomes with and without linoleic acid; there was a slight depression in the melting temperature with respect to the transferosomes without linoleic acid. Londoño and coworkers (Londoño et al., 2019) studied the thermal transitions in soy phosphatidylcholine-based ethosomes and observed peaks at 187.5 °C, which they attributed to the interdigitation of lipid chains that represents the presence of crystalline structures through which the heat flux is constant. The peaks, observed between 170.97 °C and 172.50 °C for the vesicles in the current study, can thus be attributed to such interdigitation of the vesicle chains.

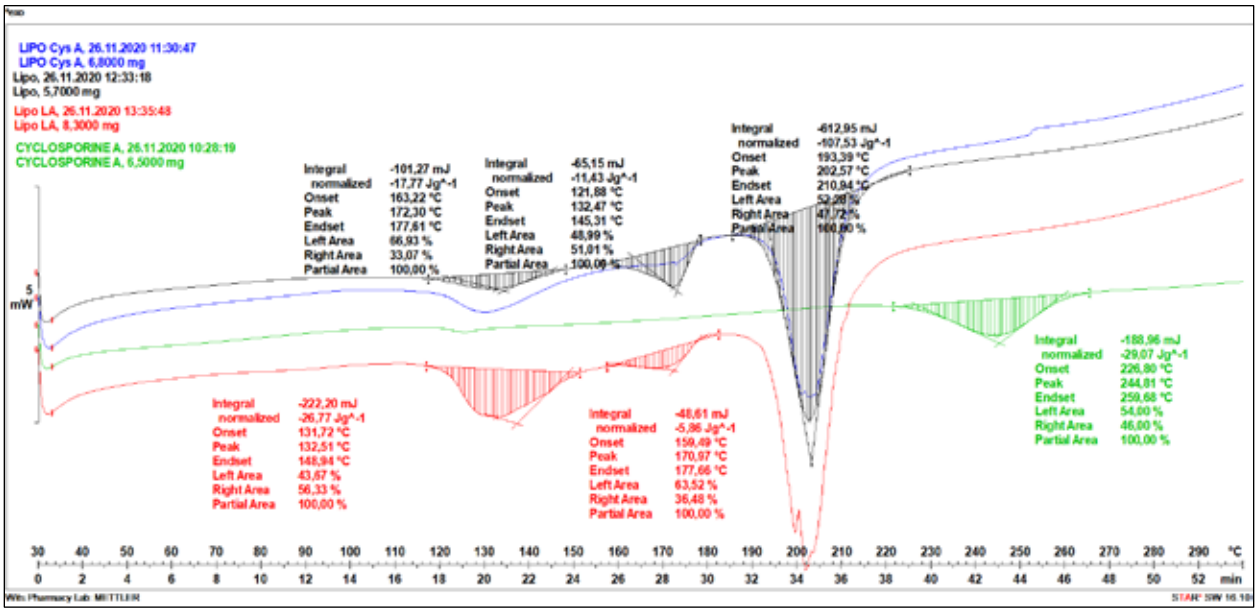


Figure 4.2 Differential scanning calorimetry of pure CysA, blank transferosomes, and CysA-loaded transferosomes.

The melting endotherm for pure CysA in this study was found at ~130 °C (the melting point is reported as 148–151 °C ("The Merck index: an encyclopaedia of chemicals, drugs, and biologicals (Book, 2006) [WorldCat.org]," n.d.)) and the decomposition started at 226.80 °C. These peaks, however, disappeared completely from the thermogram of the CysA-loaded transferosome, thus indicating the efficacy and stability of the encapsulation process. Similar observations were previously reported (Wagh and Apar, 2014). For the soy phosphatidylcholine employed in this investigation, the phase transition temperature was previously determined to be 58.1 °C in other studies (Londoño et al., 2019). Shalaev and Steponkus had earlier studied the influence of sugar concentration and hydration states in DOPE-based vesicles and found that both the presence of sucrose and hydration states modified the phase transition temperature. In addition, they found that the physical state of the sugar matrix at the transition point affected the temperature of the transition and that the depression of the transition temperature for lipid vesicles always occurred if the glass transition temperature of the sugar is higher than that of the lipid used (Shalaev and Steponkus, 2001). The peaks observed between 170.97 °C and 172.50 °C for the vesicles can thus be attributed to such an interdigitation of the vesicle chains. The melting endotherm for pure CysA was found at ~130 °C and the decomposition started at 226.80 °C. These peaks disappeared completely from the thermogram of the CysA-loaded transferosomes, thus indicating the efficacy and stability of the

encapsulation process. Wagh and colleagues (Wagh and Apar, 2014) made a similar observation while working with CysA nanoparticles prepared with PLGA and Eudragit 100®. The melting peak that appeared in the thermogram of CysA completely disappeared from the thermogram of the optimized formulation, signifying the efficacy of the encapsulation process.

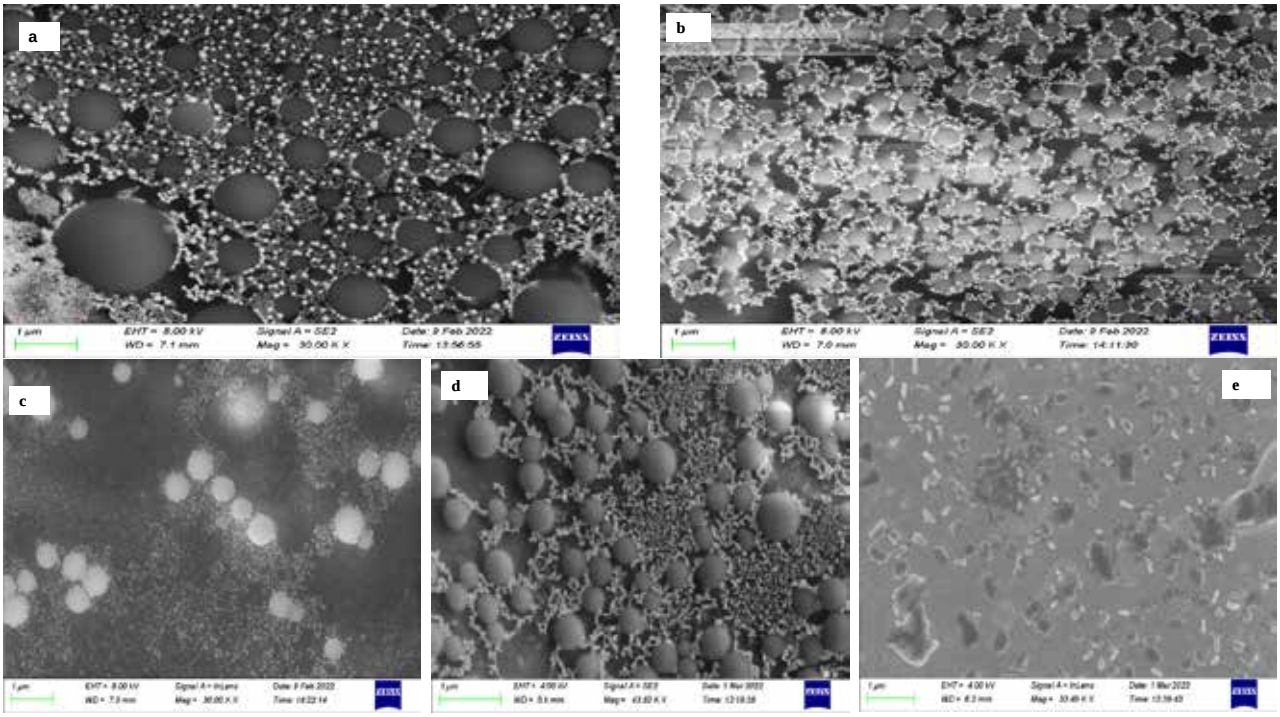


Figure 4.3 SEM images of transferosomes reflecting the impact of drug loading on the polydispersity and size for. (a) blank Span® transferosomes; (b) CysA-loaded Span® transferosomes; (c) blank Tween® transferosomes; (d) CysA -loaded Tween® transferosomes; and (e) lyophilized Tween® transferosomes. Scale bar represents 1 µm.

The representative SEM images shown in **Figure 4.3** confirm the polydisperse nature of the prepared transferosomes obtained during DLS size analysis. The approach employed for the incorporation of the edge activators was explored for the possible effects on the morphology of the transferosomes. The morphology of the transferosomes prepared with Span® 80 as part of the hydrating fluid is shown in **Figure 4.3a.** The stabilizing effect of CysA loading into the transferosomes (**Figure 4.3b**) is noted as more uniformly distributed spheres of smaller diameters when compared with the blank. This effect corroborated the reduction in the hydrodynamic size with CysA loading, observed following the DLS size analysis. While **Figure 4.3c** represents the transferosomes prepared via the incorporation of Tween® 80 as a

constituent of the hydration fluid, Figure 3d depicts the morphology of the CysA-loaded Tween® 80 transferosomes, resulting from incorporating the edge activator, Tween® 80, into the film-forming solution. Apart from a visually imperceptible difference in the size, the morphology is the same. This indicates that the method of incorporation of the edge activator had a minimal impact on the size and size distribution. A representative image of the morphology of the lyophilized samples is depicted in **Figure 4.3e**. The effect of lyophilization and the cryoprotectant used were obvious, as the spheres developed an elongated shape. This morphology was also observed in the TEM images obtained for the lyophilized samples prepared with Tween® 80.

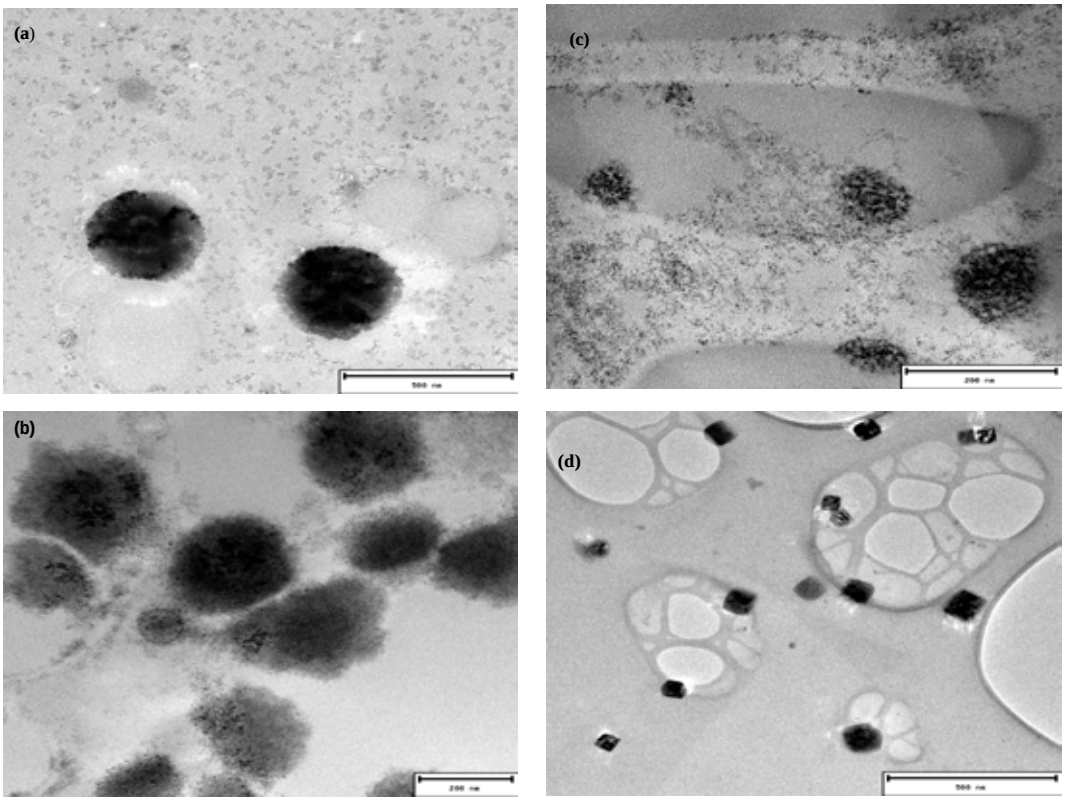


Figure 4.4. TEM images of lyophilized (a) blank Span 80® transferosomes; (b) CysA-loaded Span 80®; (c) blank Tween 80® transferosomes; and (d) un-lyophilized Tween 80® transferosomes. The scale bars for (a, d) are 500 nm, while those for (b, c) are 200 nm

The TEM images depicted in **Figure 4.4** were obtained from the lyophilized samples reconstituted in PBS and dried on a copper grid. The images highlight the spherical nature of the transferosomes. The mean sizes, determined from an analysis of the TEM images for the

drug-loaded Span® 80 transferosomes, were about 200 nm, while the sizes of the blanks were in the range of 300 to 400 nm. The TEM-determined sizes for the blank Tween® 80 transferosomes were between 100 and 150 nm for the lyophilized samples, while that of the drug-loaded un-lyophilized sample was in the range of 100 nm. The TEM images in **Figure 4.4** corroborate the morphology observed from the SEM. The samples also showed a somewhat elongated morphology approaching cuboids for the non-lyophilized Tween® samples, as observed in the SEM images. The size measurements from TEM varied slightly from the DLS-determined sizes. The dehydration process may have accounted for the slight disparity in size obtained from the DLS, TEM, and SEM, as observed by Carreras and co-workers (Carreras et al., 2020)

Table 4.4 shows the results of the stability evaluations obtained from the representative Tween®-based transferosome samples. The differences in the size, size distribution, and zeta potential were statistically different, but all in favour of stability. Even though the average hydrodynamic size of the transferosomes was smaller at the beginning, the poly-dispersity index was high, showing a high variability in the size distribution. The presence of polydisperse vesicles could have resulted from the method of vesicle formation, since the thin film method is known for the production of multilamellar vesicles (Danaei et al., 2018).

Table 4.4 Stability profile of transferosomes.

Time (Months)	Size (nm)	Polydispersity Index	Zeta Potential (mV)
0	76.91 ± 0.81	0.504 ± 0.005	−15.93 ± 0.69
4	113.17 ± 1.11	0.277 ± 0.003	−12.7 ± 1.85

This trend was later reversed, however, evident in the presence of more uniformly distributed larger spheres, that could be due to the effect of annealing that results from the reassembly into bigger vesicles following the disruption in the lamellar membrane by the ice crystals during freezing (Gonzalez Gomez et al., 2019). The contributions of drug loading towards stability were also observed in terms of increased zeta potential values (−19.07 ± 1.22 mV) when compared to the blank vesicles. This corresponds with the observation from previous investigations involving lipid nanocapsules (Urimi et al., 2021).

The results of the flexibility studies undertaken with both blank and CysA-loaded transferosomes are shown in **Table 4.5**. Jain and coworkers had previously established the inverse relationship that exists between the volume reduction after extrusion and flexibility (Jain et al., 2003). Even though the percentage reduction in size for the drug-loaded vesicles was high, these results

Table 4.5 Flexibility analysis of transferosomes.

Formulation	Size before Extrusion (nm)	Size after Extrusion (nm)	% Decrease in Size	Volume Loss (%)
Blank Span® 80	315.77 ± 4.41	140.07 ± 2.08	55.60 ± 0.78	8 ± 1.58
CysA-loaded Span® 80	246.57 ± 3.65	158.8 ± 0.59	35.72 ± 1.38	13 ± 1.05
Blank Tween® 80	243.07 ± 1.61	132.77 ± 0.37	45.37 ± 0.25	6 ± 2.02
CysA-loaded Tween® 80	183.17 ± 0.62	120.13 ± 0.90	34.42 ± 0.34	14 ± 1.02

represent some degree of fluidity when the molecular size cut-off of the polycarbonate membrane (100 µm) used in the extrusion is considered. Statistically significant differences were obtained ($p < 0.05$) when the means of the percent decrease in the size of the blank and drug-loaded vesicles were compared, indicating that the CysA-loaded vesicles were in a more fluid state than the blank vesicles for both of the surfactants studied. The size and stability of the lipid vesicles were shown to depend on membrane packing, and this in turn depends on the interaction of the proteins and peptide molecules with the lipid bilayer (Abdel-Mottaleb, and Lamprecht, 2011) Likewise, the blank vesicles based on Tween® 80 were more deformable than those based on Span® 80 for the blank vesicles based on consideration of the percent decrease in the size of vesicles. This observation is further confirmed by the volume reduction result, which showed a statistically insignificant difference. On the other hand, the difference in size reduction between the CysA-loaded transferosomes based on Tween 80® and those based on Span 80® were statistically not significant. This observation may have serious implications for the contributions of the drug to the membrane stability and fluidity, as was also observed from the dynamic light scattering experiments.

4.3.4 Ocular cytocompatibility of the transferosomes

In order to evaluate the safety of use of the prepared transferosomes in the eye, a toxicity assay was undertaken in a human retinal epithelial primary cell line (HREP). This cell line was selected because of the very high sensitivity of retinal epithelial cells to exogenous substances. The viability

of the cells tested with 3.5 mg/mL stock dispersions of the transferosomes hydrated with surfactant concentrations of 1% v/v were similar to the viability of the negative control, as displayed in **Figure 4.5**. The % viability of the Tween®-based transferosomes was higher than the % viability of the Span®-based transferosomes at all of the concentrations tested. The viability of the HREP cells to the blank transferosomes was, likewise, similar to the viability of the CysA-loaded transferosomes.

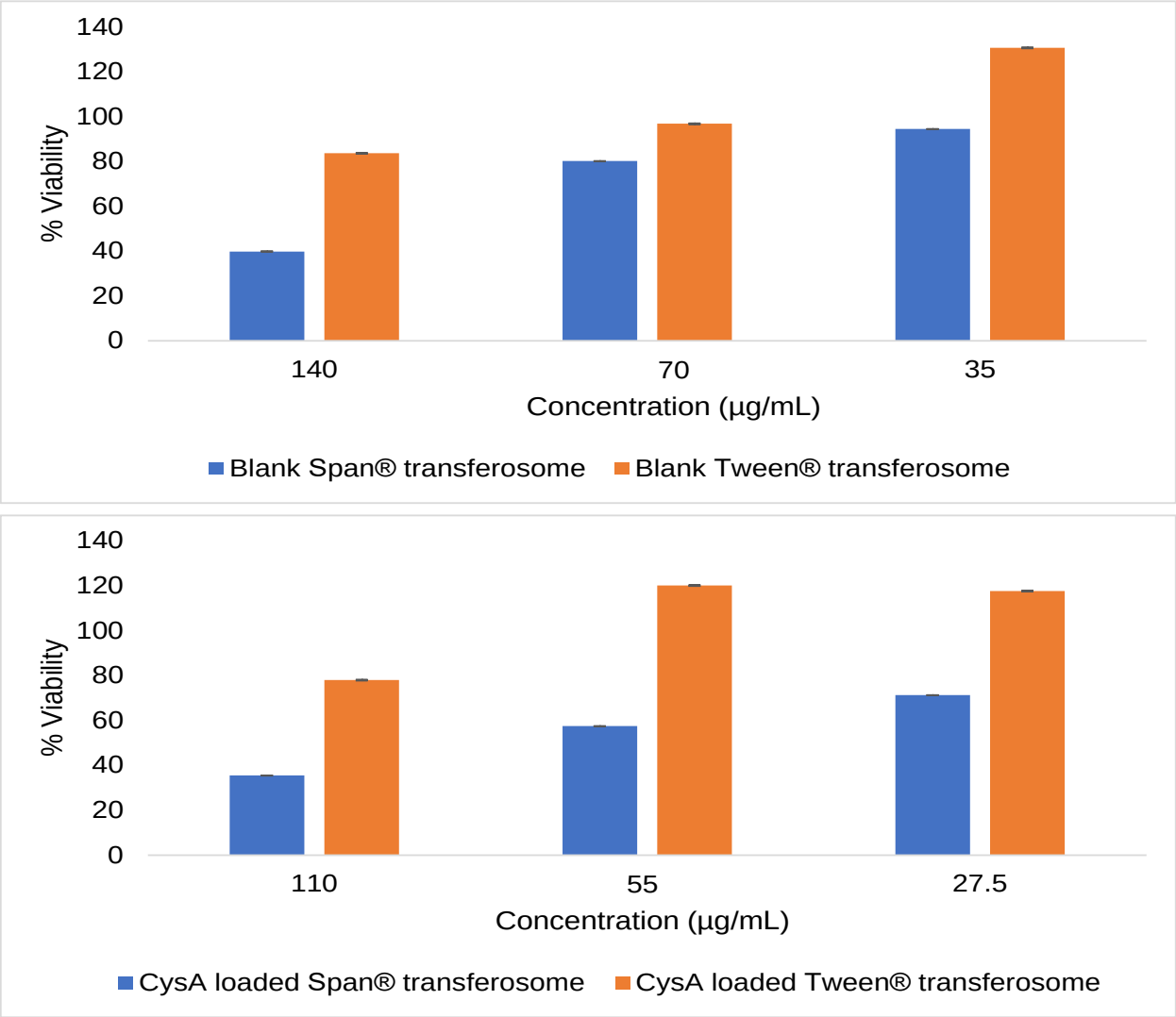


Figure 4.5 Viability of HREP cells against CysA-loaded transferosomes and blank transferosomes.

Figure 4.6 shows the morphology of the HREP cells treated with the dispersions of the Span® 80 and Tween® 80-based transferosomes. The morphology of the cells reflects the environment in which the cells are growing. The abnormalities in the morphology can thus be a stress response to

the toxic elements in the growth medium (Sassine et al., 2020). The morphology of the cells shown in **Figure 4.6** was normal and thus confirms the safety of the transferosomes. Therefore, at the concentrations evaluated, the transferosomes formulated in this study can safely be applied to ocular cells.

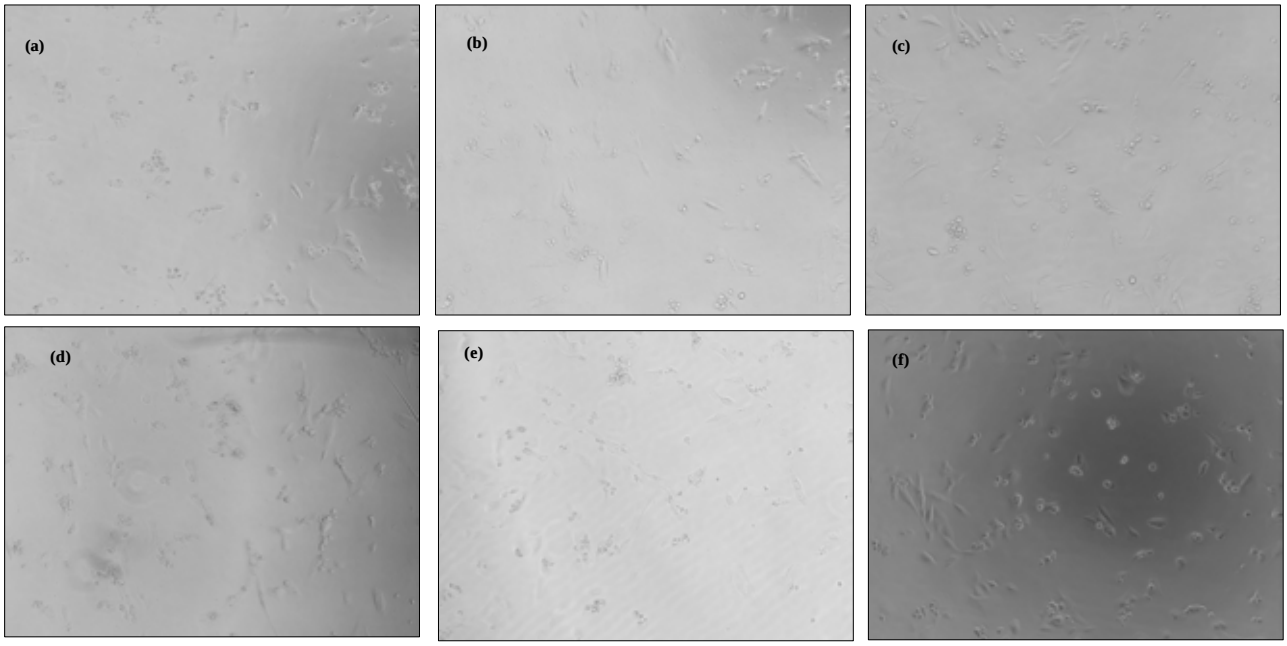


Figure 4.6 Morphology of HREP cells treated with (a)CysA-loaded Span® transferosome; (b) blank Span® transferosomes, (c) blank Tween® transferosomes, (d) CysA-loaded Tween® transferosomes, (e) ATF, and (f) before treatment.

4.3.4 Encapsulation efficiency and *in vitro* release profile of CysA from loaded transferosomes prepared with Tween 80®

The encapsulation efficiency is a measure of the amount of drug loaded into the vesicles and represents the ability of the nanocarriers to encapsulate the enclosed drug. The encapsulation efficiency obtained from the transferosomes prepared using Tween® 80 included in the hydrating fluid was 52.05% ± 2.06%, while that obtained when the Tween® was included in the lipid film former before evaporation was 44.06% ± 3.01%. The edge activators were incorporated using two different approaches to delineate the effect of the incorporation method on the properties of the formed transferosomes. The EE% obtained by including the Tween® 80 in the hydrating fluid was much higher than that from the alternate method. Increasing the cholesterol content, which is important for maintaining the rigidity and hence, the stability of the vesicles, has been shown to decrease the inclusion of CysA into the phospholipid membrane (Ouyang et al., 1995).

Additionally, CysA has been shown to partly partition between the aqueous core and the phospholipid membrane (Czogalla, 2008).

The *in vitro* release profile (**Figure 4.7a**) of the transferosomes was obtained for the Tween®-based formulation since it had a more favorable toxicity profile. In vitro release studies have variously been applied as an indication of the potential performance of a delivery system *in vivo* (du Toit et al., 2014). The release of CysA was initially rapid with over 15% of the loaded drug being released in the first 24 hours. After this phase, there was a steady gradual increase over the next 72 hours up to the time the release study was terminated. Other investigators have made similar observations with regards to the drug release behavior from other vesicle-based delivery systems (Shashidhar and Manohar, 2018). The release data were fitted to different dissolution models and the Korsmeyer–Peppas model, which describes the release mechanism from polymeric systems, was selected as the best fit, based on the Akaike Information Criterion (AIC) and the Model Selection Criterion (MSC). The calculated Korsmeyer–Peppas constant, Kkp, was 4.106 while the n factor for the release data was 0.36, signifying that a Non-Fickian diffusion was the release mechanism from the transferosomes (Ouyang et al., 1995). **Figure 4.7b** shows the predicted and the observed release data after fitting into the Korsmeyer–Peppas model.

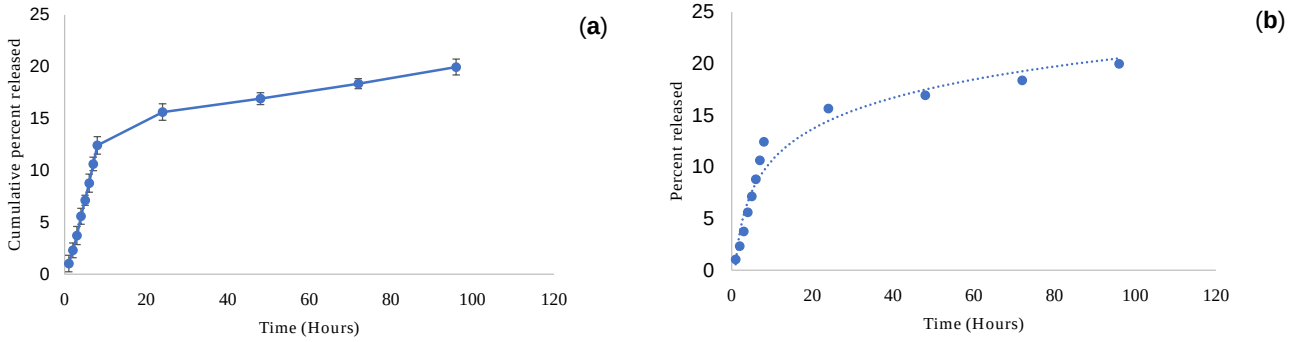


Figure 4.7 Release profile from transferosomes: (a) *In vitro* release of CysA from transferosomes; (b) The predicted release profile based on the Korsmeyer–Peppas model.

The dissolution of pure CysA was discussed and characterized in other investigations, where the poor solubility of CysA was demonstrated. For example, Dubey et al. compared the drug release profiles for the CysA/micelle incorporated nanofibers with that from the corresponding quantity of pure crystalline CysA, which highlighted that there was a complete release of CysA from the nanofiber after 14 min, whereas there was negligible dissolution of the pure drug (Dubey et al.,

2020). Nano-systems, such as those discussed by Dubey et al. and presented herein, serve to improve the dissolution rate of the poorly soluble CysA through various mechanisms (i.e., solubilization, high surface area, improved wetting, and molecular dispersion of the drug); however, the transferosome system also serves to control the release of the drug, thus providing effective CysA levels for an extended period.

4.3.6 *Ex-vivo* corneal permeability and flux across rabbits' cornea

Figure 4.8 shows the results of the corneal permeability studies represented as the cumulative amount of CysA diffusing per unit area plotted against time. In this study, the cumulative amount diffused per unit area increased over time during the 24 h period of investigation. The values were higher for the Tween® based formulation, though the similarity factor between the permeability profiles of the two formulations was close (*F2* = 69.05). Agarwal and colleagues (Agarwal et al., 2018) similarly determined the permeability of CysA across the rabbit cornea, though using formulations based on semi-fluorinated alkanes. According to their study, the best formulation based on perfluorobutylpentane demonstrated a cumulative CysA permeation of 15 µg/g of the cornea over a 4-hour period. Even though this is similar to the value obtained in this study for the Tween® 80 formulation, the volatility of the semi-fluoroalkanes used as a solubilizer in their formulation can lead to precipitation of the dissolved drug. According to Fick's laws of diffusion, that govern the transport of molecules across the corneal surface, the flux across the cornea depends upon the concentration gradient across the corneal barrier and the diffusion or permeability coefficient (Alkilani et al., 2015). The maximum flux is usually determined from the slope of the curve for the cumulative amount permeated/unit area versus the time for the formulations not enclosed in reservoirs. The slope of the linear part of the curve for the Tween®- and Span®-based transferosome formulations were 0.78 µg/cm^2/hour and 0.912 µg/cm^2/hour, respectively, which represents the flux. The Span® 80 transferosomes had a higher flux than the Tween® formulation, even though the cumulative amount permeated per unit time for the Tween® was initially higher. A higher flux from Span® formulation indicates that, over time and at a steady state, the Span® formulation will enable the permeation of higher quantities of CysA. Despite the higher flux from the Span® formulation, the Tween® formulation may still be preferred, considering that this difference in flux is not significant ($p > 0.05$). In addition, the Tween® formulation had a more favorable toxicity profile. The studies that quantitate the amount of CysA released from topical formulations are limited. Most of the studies generally focus on the efficacy of CysA in the ocular condition being targeted for treatment. One study, however, evaluated the blood

concentrations of CysA following the topical application of the usually administered topical doses of 0.05% and 0.1% (Small et al., 2002). Although the ocular concentrations of CysA were not measured, the study established that, at these doses, the 0.05% formulation was below the limit of detection while only 5.5% of the population treated with the 0.1% formulation showed detectable levels of CysA in the blood. Another study evaluated the corneal penetration of CysA from polymeric micelles in a Lewis and Brown Norway rat model (Di Tommaso et al., 2012). The

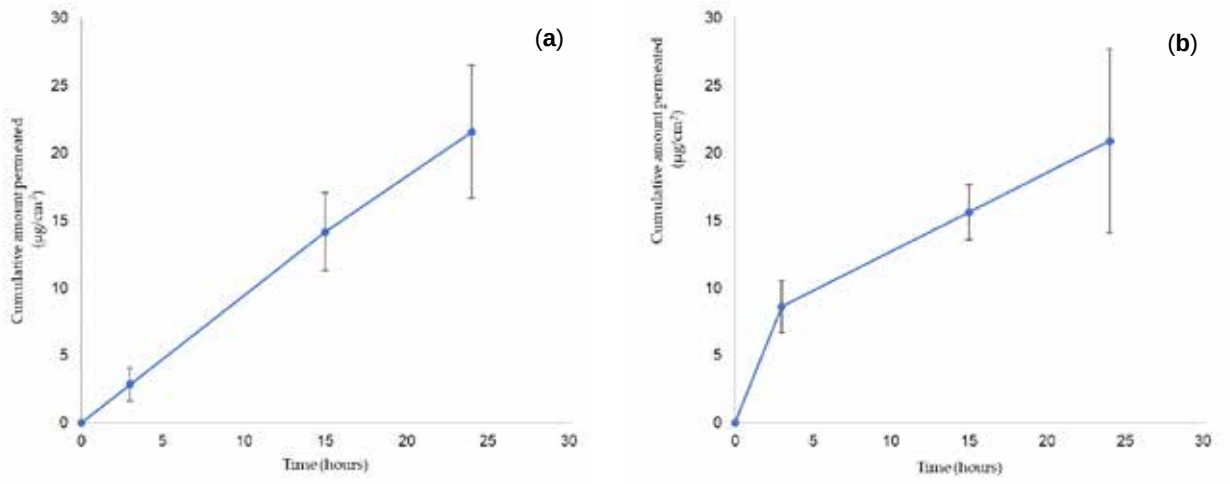


Figure 4.8 Corneal permeability of Span 80® (A) and Tween 80® (B) transferosomes.

corneal CysA levels in the transplanted and healthy rats were 11710 ± 7530 ng/g and 6470 ± 1730 ng/g of tissue, respectively, and implied a superior corneal penetration performance to both a CysA oily solution and normal saline. A similar study compared a CysA micellar formulation with an emulsion formulation (Yu et al., 2018). In their study, and over a 7-day period, 78.36% and 88.87% were released, respectively, from the emulsion and micellar formulation in vitro. The pharmacokinetic profile showed that both of the formulations displayed a similar bioavailability, but with significantly different elimination profiles, resulting in a slower elimination from the micelles. The micellar formulation was thus shown to contribute to maintaining the presence of CysA over a longer period. Even though the current transferosomal formulation presented in this investigation exhibited similar drug delivery profiles, their safety profile was im-proved, which was also a result of the exclusion of the toxic solvents.

The corneal epithelium has been identified as the strongest barrier limiting the passage of topically applied drugs to molecules less than 500 Da and various nano-systems have been explored to overcome this barrier. The contributions of these nano-systems to-wards overcoming the corneal epithelial barrier have mainly been based on the size advantage. However, evidence is also

emerging to underscore the nature of the components of the nano-system viz-à-viz their interaction with the epithelial layer (Calvo et al., 1997), such as interactions with the cholesterol and lipid components of the corneal epithelium, rendering it more permeable to exogenous substances (Morrison et al., 2013).

4.4 Conclusions

The potential for the ocular delivery of CysA using transferosomes was explored in this investigation. The toxicity of the developed transferosomes, which is of major concern, was within acceptable limits. The transferosomes showed potential for sustaining the re-lease of the incorporated CysA in vitro over the time period investigated in this study. The possible interaction of the loaded drug with the lipid membrane, as well as the presence of linoleic acid, may have contributed to the stabilizing effect on the size of the transferosomes over time. The corneal permeability and flux from the Span® and Tween® formulations were similar. A future assessment of the in vivo performance of the developed transferosomes, in terms of toxicity and therapeutic efficacy, is proposed.

4.5. References

Abdel-Mottaleb, M.M.A., Lamprecht, A., 2011. Standardized in vitro drug release test for colloidal drug carriers using modified USP dissolution apparatus I. Drug Dev. Ind. Pharm. 37, 178–184. https://doi.org/10.3109/03639045.2010.502534

Agarwal, P., Scherer, D., Günther, B., Rupenthal, I.D., 2018. Semifluorinated alkane based systems for enhanced corneal penetration of poorly soluble drugs. Int. J. Pharm. 538, 119–129. https://doi.org/10.1016/j.ijpharm.2018.01.019

Ahad, A., Al-Saleh, A.A., Al-Mohizea, A.M., Al-Jenoobi, F.I., Raish, M., Yassin, A.E.B., Alam, M.A., 2017. Formulation and characterization of novel soft nanovesicles for enhanced transdermal delivery of eprosartan mesylate. Saudi Pharm. J. 25, 1040–1046. https://doi.org/10.1016/j.jsps.2017.01.006

Alkilani, A.Z., McCrudden, M.T.C., Donnelly, R.F., 2015. Transdermal Drug Delivery: Innovative Pharmaceutical Developments Based on Disruption of the Barrier Properties of the Stratum Corneum. Pharmaceutics 7, 438–470. https://doi.org/10.3390/pharmaceutics7040438

Almalik, A., Alradwan, I., Kalam, M.A., Alshamsan, A., 2017. Effect of cryoprotection on particle size stability and preservation of chitosan nanoparticles with and without hyaluronate or alginate coating. Saudi Pharm. J. SPJ 25, 861–867. https://doi.org/10.1016/j.jsps.2016.12.008

Burstein, N.L., 1980. Corneal cytotoxicity of topically applied drugs, vehicles and preservatives. Surv. Ophthalmol. 25, 15–30. https://doi.org/10.1016/0039-6257(80)90072-7

Calvo, P., Vila-Jato, J.L., Alonso, M.J., 1997. Evaluation of cationic polymer-coated nanocapsules as ocular drug carriers. Int. J. Pharm. 153, 41–50. https://doi.org/10.1016/S0378-5173(97)00083-5

Carreras, J.J., Tapia-Ramirez, W.E., Sala, A., Guillot, A.J., Garrigues, T.M., Melero, A., 2020. Ultraflexible lipid vesicles allow topical absorption of cyclosporin A. Drug Deliv. Transl. Res. 10, 486–497. https://doi.org/10.1007/s13346-019-00693-4

Cevc, G., Blume, G., 1992. Lipid vesicles penetrate into intact skin owing to the transdermal osmotic gradients and hydration force. Biochim. Biophys. Acta BBA - Biomembr. 1104, 226–232. https://doi.org/10.1016/0005-2736(92)90154-E

Czogalla, A., 2008. Oral cyclosporine A - the current picture of its liposomal and other delivery systems. Cell. Mol. Biol. Lett. 14, 139–152. https://doi.org/10.2478/s11658-008-0041-6

Danaei, M., Kalantari, M., Raji, M., Samareh Fekri, H., Saber, R., Asnani, G.P., Mortazavi, S.M., Mozafari, M.R., Rasti, B., Taheriazam, A., 2018. Probing nanoliposomes using single particle analytical techniques: effect of excipients, solvents, phase transition and zeta potential. Heliyon 4, e01088. https://doi.org/10.1016/j.heliyon.2018.e01088

Daull, P., Baudouin, C., Liang, H., Feraille, L., Barabino, S., Garrigue, J.-S., 2021. Review of Preclinical Outcomes of a Topical Cationic Emulsion of Cyclosporine A for the Treatment of Ocular Surface Diseases. Ocul. Immunol. Inflamm. 0, 1–11. https://doi.org/10.1080/09273948.2021.1957124

Demetzos, C., 2008. Differential Scanning Calorimetry (DSC): A Tool to Study the Thermal Behavior of Lipid Bilayers and Liposomal Stability. J. Liposome Res. 18, 159–173. https://doi.org/10.1080/08982100802310261

Development of a Convenient ex vivo Model for the Study of the Transcorneal Permeation of Drugs: Histological and Permeability Evaluation - Pescina - 2015 - Journal of Pharmaceutical Sciences - Wiley Online Library [WWW Document], n.d. URL https://onlinelibrary.wiley.com/doi/full/10.1002/jps.24231 (accessed 11.11.20).

Di Tommaso, C., Bourges, J.-L., Valamanesh, F., Trubitsyn, G., Torriglia, A., Jeanny, J.-C., Behar-Cohen, F., Gurny, R., Möller, M., 2012. Novel micelle carriers for cyclosporin A topical ocular delivery: In vivo cornea penetration, ocular distribution and efficacy studies. Eur. J. Pharm. Biopharm. 81, 257–264. https://doi.org/10.1016/j.ejpb.2012.02.014

du Toit, L.C., Carmichael, T., Govender, T., Kumar, P., Choonara, Y.E., Pillay, V., 2014. In vitro, in vivo, and in silico evaluation of the bioresponsive behavior of an intelligent intraocular implant. Pharm. Res. 31, 607–634. https://doi.org/10.1007/s11095-013-1184-3

Dubey, P., Barker, S.A., Craig, D.Q.M., 2020. Design and Characterization of Cyclosporine A-Loaded Nanofibers for Enhanced Drug Dissolution. ACS Omega 5, 1003–1013. https://doi.org/10.1021/acsomega.9b02616

Gonzalez Gomez, A., Syed, S., Marshall, K., Hosseinidoust, Z., 2019. Liposomal Nanovesicles for Efficient Encapsulation of Staphylococcal Antibiotics. ACS Omega 4, 10866–10876. https://doi.org/10.1021/acsomega.9b00825

Grass, G.M., Robinson, J.R., 1988. Mechanisms of corneal drug penetration. I: In vivo and in vitro kinetics. J. Pharm. Sci. 77, 3–14. https://doi.org/10.1002/jps.2600770103

Hashmat, D., Shoaib, M.H., Ali, F.R., Siddiqui, F., 2020. Lornoxicam controlled release transdermal gel patch: Design, characterization and optimization using co-solvents as penetration enhancers. PLOS ONE 15, e0228908. https://doi.org/10.1371/journal.pone.0228908

Huang, C., Quinn, D., Sadovsky, Y., Suresh, S., Hsia, K.J., 2017. Formation and size distribution of self-assembled vesicles. Proc. Natl. Acad. Sci. U. S. A. 114, 2910–2915. https://doi.org/10.1073/pnas.1702065114

Huang, Y., Tao, Q., Hou, D., Hu, S., Tian, S., Chen, Y., Gui, R., Yang, L., Wang, Y., 2017. A novel ion-exchange carrier based upon liposome-encapsulated montmorillonite for ophthalmic delivery of betaxolol hydrochloride [WWW Document]. Int. J. Nanomedicine. https://doi.org/10.2147/IJN.S122747

Ibrahim, M.M., Maria, D.N., Wang, X., Simpson, R.N., Hollingsworth, T.J., Jablonski, M.M., 2020. Enhanced Corneal Penetration of a Poorly Permeable Drug Using Bioadhesive Multiple Microemulsion Technology. Pharmaceutics 12, 704. https://doi.org/10.3390/pharmaceutics12080704

Jain, S., Jain, P., Umamaheshwari, R.B., Jain, N.K., 2003. Transfersomes—A Novel Vesicular Carrier for Enhanced Transdermal Delivery: Development, Characterization, and Performance Evaluation. Drug Dev. Ind. Pharm. 29, 1013–1026. https://doi.org/10.1081/DDC-120025458

Jumelle, C., Gholizadeh, S., Annabi, N., Dana, R., 2020. Advances and limitations of drug delivery systems formulated as eye drops. J. Controlled Release 321, 1–22. https://doi.org/10.1016/j.jconrel.2020.01.057

Lallemand, F., Schmitt, M., Bourges, J.-L., Gurny, R., Benita, S., Garrigue, J.-S., 2017. Cyclosporine A delivery to the eye: A comprehensive review of academic and industrial efforts. Eur. J. Pharm. Biopharm. 117, 14–28. https://doi.org/10.1016/j.ejpb.2017.03.006

Londoño, C.A., Rojas, J., Yarce, C.J., Salamanca, C.H., 2019. Design of Prototype Formulations for In Vitro Dermal Delivery of the Natural Antioxidant Ferulic Acid Based on Ethosomal Colloidal Systems. Cosmetics 6, 5. https://doi.org/10.3390/cosmetics6010005

Moiseev, R.V., Morrison, P.W.J., Steele, F., Khutoryanskiy, V.V., 2019. Penetration Enhancers in Ocular Drug Delivery. Pharmaceutics 11, 321. https://doi.org/10.3390/pharmaceutics11070321

Morrison, P.W.J., Connon, C.J., Khutoryanskiy, V.V., 2013. Cyclodextrin-Mediated Enhancement of Riboflavin Solubility and Corneal Permeability. Mol. Pharm. 10, 756–762. https://doi.org/10.1021/mp3005963

M. Shashidhar, G., Manohar, B., 2018. Nanocharacterization of liposomes for the encapsulation of water soluble compounds from Cordyceps sinensis CS1197 by a supercritical gas anti-solvent technique. RSC Adv. 8, 34634–34649. https://doi.org/10.1039/C8RA07601D

Mudgil, P., 2020. Evaluation of use of essential fatty acids in topical ophthalmic preparations for dry eye. Ocul. Surf. 18, 74–79. https://doi.org/10.1016/j.jtos.2019.10.001

Mun, E.A., Morrison, P.W.J., Williams, A.C., Khutoryanskiy, V.V., 2014. On the Barrier Properties of the Cornea: A Microscopy Study of the Penetration of Fluorescently Labeled Nanoparticles, Polymers, and Sodium Fluorescein. Mol. Pharm. 11, 3556–3564. https://doi.org/10.1021/mp500332m

Nakhaei, P., Margiana, R., Bokov, D.O., Abdelbasset, W.K., Jadidi Kouhbanani, M.A., Varma, R.S., Marofi, F., Jarahian, M., Beheshtkhoo, N., 2021. Liposomes: Structure, Biomedical Applications, and Stability Parameters With Emphasis on Cholesterol. Front. Bioeng. Biotechnol. 9.

Opatha, S.A.T., Titapiwatanakun, V., Chutoprapat, R., 2020. Transfersomes: A Promising Nanoencapsulation Technique for Transdermal Drug Delivery. Pharmaceutics 12, 855. https://doi.org/10.3390/pharmaceutics12090855

Ouyang, C., Choice, E., Holland, J., Meloche, M., Madden, T.D., 1995. Liposomal cyclosporine. Characterization of drug incorporation and interbilayer exchange. Transplantation 60, 999–1006.

Pescina, S., Govoni, P., Potenza, A., Padula, C., Santi, P., Nicoli, S., 2015a. Development of a Convenient ex vivo Model for the Study of the Transcorneal Permeation of Drugs: Histological and Permeability Evaluation. J. Pharm. Sci. 104, 63–71. https://doi.org/10.1002/jps.24231

Pescina, S., Govoni, P., Potenza, A., Padula, C., Santi, P., Nicoli, S., 2015b. Development of a Convenient ex vivo Model for the Study of the Transcorneal Permeation of Drugs: Histological and Permeability Evaluation. J. Pharm. Sci. 104, 63–71. https://doi.org/10.1002/jps.24231

Pezeshky, A., Ghanbarzadeh, B., Hamishehkar, H., Moghadam, M., Babazadeh, A., 2016. Vitamin A palmitate-bearing nanoliposomes: Preparation and characterization. Food Biosci. 13, 49–55. https://doi.org/10.1016/j.fbio.2015.12.002

Ramsay, E., del Amo, E.M., Toropainen, E., Tengvall-Unadike, U., Ranta, V.-P., Urtti, A., Ruponen, M., 2018a. Corneal and conjunctival drug permeability: Systematic comparison and

pharmacokinetic impact in the eye. Eur. J. Pharm. Sci. 119, 83–89. https://doi.org/10.1016/j.ejps.2018.03.034

Ramsay, E., del Amo, E.M., Toropainen, E., Tengvall-Unadike, U., Ranta, V.-P., Urtti, A., Ruponen, M., 2018b. Corneal and conjunctival drug permeability: Systematic comparison and pharmacokinetic impact in the eye. Eur. J. Pharm. Sci. 119, 83–89. https://doi.org/10.1016/j.ejps.2018.03.034

Sassine, J., Sousa, J., Lalk, M., Daniel, R.A., Vollmer, W., 2020. Cell morphology maintenance in Bacillus subtilis through balanced peptidoglycan synthesis and hydrolysis. Sci. Rep. 10, 17910. https://doi.org/10.1038/s41598-020-74609-5

Shalaev, E.Y., Steponkus, P.L., 2001. Phase behavior and glass transition of 1,2-dioleoylphosphatidylethanolamine (DOPE) dehydrated in the presence of sucrose. Biochim. Biophys. Acta BBA - Biomembr. 1514, 100–116. https://doi.org/10.1016/S0005-2736(01)00372-8

Sharma, R., Ahuja, M., Kaur, H., 2012. Thiolated pectin nanoparticles: Preparation, characterization and ex vivo corneal permeation study. Carbohydr. Polym. 87, 1606–1610. https://doi.org/10.1016/j.carbpol.2011.09.065

Shen, Y., Tang, H., Zhan, Y., Van Kirk, E.A., Murdoch, W.J., 2009. Degradable Poly(β-amino ester) nanoparticles for cancer cytoplasmic drug delivery. Nanomedicine Nanotechnol. Biol. Med. 5, 192–201. https://doi.org/10.1016/j.nano.2008.09.003

Small, D.S., Acheampong, A., Reis, B., Stern, K., Stewart, W., Berdy, G., Epstein, R., Foerster, R., Forstot, L., Tang-Liu, D.D.-S., 2002. Blood concentrations of cyclosporin a during long-term treatment with cyclosporin a ophthalmic emulsions in patients with moderate to severe dry eye disease. J. Ocul. Pharmacol. Ther. Off. J. Assoc. Ocul. Pharmacol. Ther. 18, 411–418. https://doi.org/10.1089/10807680260362696

Sydykov, B., Oldenhof, H., Sieme, H., Wolkers, W.F., 2018. Storage stability of liposomes stored at elevated subzero temperatures in DMSO/sucrose mixtures. PLOS ONE 13, e0199867. https://doi.org/10.1371/journal.pone.0199867

The Merck index : an encyclopedia of chemicals, drugs, and biologicals (Book, 2006) [WorldCat.org] [WWW Document], n.d. URL https://www.worldcat.org/title/merck-index-an-encyclopedia-of-chemicals-drugs-and-biologicals/oclc/70882070 (accessed 6.16.22).

Tripathy, M., Thangamani, S., Srivastava, A., 2020. Three-Dimensional Packing Defects in Lipid Membrane as a Function of Membrane Order. J. Chem. Theory Comput. 16, 7800–7816. https://doi.org/10.1021/acs.jctc.0c00609

Urimi, D., Widenbring, R., Pérez García, R.O., Gedda, L., Edwards, K., Loftsson, T., Schipper, N., 2021. Formulation development and upscaling of lipid nanocapsules as a drug delivery system for

a novel cyclic GMP analogue intended for retinal drug delivery. Int. J. Pharm. 602, 120640. https://doi.org/10.1016/j.ijpharm.2021.120640

Urtti, A., Salminen, L., 1993. Minimizing systemic absorption of topically administered ophthalmic drugs. Surv. Ophthalmol. 37, 435–456. https://doi.org/10.1016/0039-6257(93)90141-S

Utine, C.A., Stern, M., Akpek, E.K., 2010. Clinical Review: Topical Ophthalmic Use of Cyclosporin A. Ocul. Immunol. Inflamm. 18, 352–361. https://doi.org/10.3109/09273948.2010.498657

Uwaezuoke, O.J., Kumar, P., Pillay, V., Choonara, Y.E., 2021. Fouling in ocular devices: implications for drug delivery, bioactive surface immobilization, and biomaterial design. Drug Deliv. Transl. Res. https://doi.org/10.1007/s13346-020-00879-1

Wagh, V.D., Apar, D.U., 2014. Cyclosporine A Loaded PLGA Nanoparticles for Dry Eye Disease: In Vitro Characterization Studies. J. Nanotechnol. 2014, e683153. https://doi.org/10.1155/2014/683153

Yang, E., Yu, H., Choi, S., Park, K.-M., Jung, H.-S., Chang, P.-S., 2021. Controlled rate slow freezing with lyoprotective agent to retain the integrity of lipid nanovesicles during lyophilization. Sci. Rep. 11, 24354. https://doi.org/10.1038/s41598-021-03841-4

Yokoi, N., Uchino, M., Uchino, Y., Dogru, M., Kawashima, M., Komuro, A., Sonomura, Y., Kato, H., Tsubota, K., Kinoshita, S., 2015. Importance of tear film instability in dry eye disease in office workers using visual display terminals: the Osaka study. Am. J. Ophthalmol. 159, 748–754. https://doi.org/10.1016/j.ajo.2014.12.019

Yu, Y., Chen, D., Li, Y., Yang, W., Tu, J., Shen, Y., 2018. Improving the topical ocular pharmacokinetics of lyophilized cyclosporine A-loaded micelles: formulation, in vitro and in vivo studies. Drug Deliv. 25, 888–899. https://doi.org/10.1080/10717544.2018.1458923

CHAPTER FIVE

IN VITRO AND *IN VIVO* ASSESSMENT OF ANTI-FOULING, AND *IN VITRO* DRUG RELEASE FROM ZWITTERIONIZED PHOTO-CROSSLINKED HYDROGELS

5.1. Introduction

A considerable number of materials have been proposed through different studies for various applications in the ocular field and results from the drive to overcome many challenges, which border on the bioavailability and invasiveness for anterior and posterior target locations, respectively. Incidentally, though certain ocular tissues such as the retina are known to be immune-privileged sites, inflammatory response to implanted devices remain a challenge (Uwaezuoke et al., 2021) which is further complicated by the diverse nature of the ocular tissues existing near each otter. Such ocular implants as intraocular lens, contact lenses, and punctal plugs still suffer from major challenges that border on protein adsorption and the consequent proliferation of cells and biofilm formation. (Uwaezuoke et al., 2021) Biofilm formation is a major concern for implantable ocular devices often leading to infections and sight threatening inflammatory processes such as keratitis. Unfortunately for the eye and due to the proximity of tissues that are widely different, inflammation in one part of the eye always results in adverse effects in sites distant from the site of inflammation. For ocular devices that are handled constantly and frequently by patients such as the contact lens, efforts have been made to limit opportunistic infection using multipurpose cleaning solutions claimed to strip off interfering microbes. Keeping to the routine of constantly dipping such contact lenses in cleaning solution may prove challenging with respect to compliance due to its recurring nature. A contact lens material that can remove this task will be a most desired change.

The design, form, size, structure, components, rigidity, hydrophobicity, and more importantly tissue implantation site, have all been shown to contribute to the type and extent of protein adsorption on any implanted biomaterial and these in turn determine the phenotype of macrophages that will mediate the inflammatory response (Lužajić Božinovski et al., 2022). Xu and colleagues, in their study, established that hydrophobicity was a key factor in determining inflammatory response. (Xu et al., 2021) Ishihara and coworkers pointed out the additional influence of hydrogels porosity as being responsible for increased protein adhesion observed in their study.

They recorded a higher level of protein adsorption on their more hydrophilically modified hydrogel and attributed it to the diffusion of the small molecular weight lysozyme into the gels. (Ishihara et al., 2021) As their hydrogel was surface modified, this observation may also bring to the fore the importance of bulk modification when compared to surface modification. Although several researches have studied the nature of inflammatory response to implanted biomaterials, majority of these studies for ocuterials were studied at sites other than the eyes. (Jansen et al., 2018)

Hydrogels occupy an important place in the drug delivery arsenal of formulation scientist due to their special properties such as biocompatibility, close resemblance to extracellular matrix, ease of fabrication, and versatility in terms of application and manoeuvrability. (Lynch et al., 2020) Hydrogels are prepared from synthetic, semi-synthetic or natural polymers which are either physically or chemically crosslinked to provide a 3-dimensional porous network enclosing a high volume of water. They have been studied extensively for drug delivery for local, targeted, controlled, and smart drug delivery systems. (Vigata et al., 2020) In ocular drug delivery particularly, hydrogels are increasingly being used as a platform to overcome eye specific challenges to drug delivery for both the anterior and posterior segments of the eye. The ability of the blood retinal barrier to keep systemically administered substances away has made intravitreal injections the currently available choice to reach the vitreous. In addition, the chronic nature of diseases requiring these injections and the physicochemical nature of the active ingredients necessitates multiple dosing hence exposing the eye to repeated invasiveness. Conversely for the anterior segment, the trio of corneal epithelial cell barrier, blinking, and rapid tear turnover effectively keeps the residence time and bioavailability of topically applied substances to a meagre 5%. Exploiting various properties of the hydrogels can offer specific solutions to some of these drug delivery challenge. However, limited aqueous solubility and physical incompatibility limits drug loading of hydrophobic drugs to hydrogels. As it stands, over 60% of the drugs in development pipeline are challenged with aqueous solubility. (Larrañeta et al., 2018) The use of hydrophobic crosslinkers or copolymers that introduce hydrophobic domains has been used to improve hydrophobic-drug loading. An alternate approach involves rendering the hydrophobic drug soluble using nanosystems such as micelles. (W. Xu et al., 2019) Kapoor and colleagues exploited the increased solubility of cyclosporine in the hydroxyethyl methacrylate (HEMA) monomer and the subsequent formation of particles during the crosslinking process to load the hydrophobic drug into HEMA hydrogels. (Kapoor et al., 2017)

To achieve sustained release, there is the need to modify hydrogels such as contact lenses, (which must be soaked in contact lens solution after a short wear due to lipid and protein adsorption from the tear fluid) for extended wear. In this report, some relevant properties of the zwitterionized hydrogel ocuterial such as the pore size, which may contribute to the release of the enclosed drug were considered. This report also explored various aspects to achieve the loading of a hydrophobic, high molecular weight drug, cyclosporine A (CysA) into a superhydrophilic hydrogel with no hydrophobic segments. A transferosomal nano system of CysA was one of the aspects exploited. Transferosomes, being ultra-deformable were expected to meander through the pores of the hydrogel and this process could contribute to a sustained release process if the pores in the hydrogel were to be small when compared to the size of the nano system.

5.2 Materials and Methods

5.2.1 Materials

Sulfobetaine methacrylate monomer, polyvinyl alcohol methacrylate, and polyvinyl alcohol methacrylate-co-sulfobetaine methacrylate was synthesized as previously reported in section **3.2.1**. Micro BCA™ Protein Assay Kit (Thermo Fischer Massachusetts, USA), chicken egg lysozyme, mucin, and bovine serum albumin (Sigma Aldrich, Germany). Irgacure 2959, Polyethylene glycol dimethacrylate (Mn 750) were purchased from Sigma (Sigma-Aldrich, St Louis, MO, USA). Cyclosporine A (CysA) was purchased from LEAP pharma (DLD Scientific, South Africa).

5.2.2 Hydrogel preparation by photoinitiated crosslinking polymerization

The hydrogels were prepared based on the composition in **Table 5.1**. Required quantities of SBMA and PVGMA were dissolved in an 80 % solution of DMSO in water. The crosslinker and the photo initiator were added, and the mixture crosslinked under UV light of wavelength 365 nm for 30 minutes in a glass mould separated with 0.75 mm spacers. See section **3.2.4** for a detailed description of the process

5.2.3 *In vitro* quantitative determination of protein adsorption

The BCA micro assay kit was employed in the determination of the quantity of protein adsorbed *in vitro* from a complex protein solution consisting of mucin (0.5 mg/mL), lysozyme (1.2 mg/mL), bovine serum albumin (3.88 mg/mL), and $CaCl_2$ (2 mg), in 100 mL PBS. Briefly, 4 mm discs were punched from the hydrogel samples and equilibrated in ATF. These were subsequently

immersed in 5 mL protein solution, placed in an orbital shaker set at 37 °C and 40 rpm for 1.5 hours. The discs were retrieved thereafter and rinsed three times with PBS. 2 mL of 1 % sodium dodecyl sulphate was used to detach the protein adsorbed on the hydrogels by incubating at 37 °C for 1 hour. The calibration curve was constructed using the complex protein solution in which the discs were subsequently immersed. Quantitation was undertaken by reading off the concentration on an Implen NanoPhotometer® (Implen GmbH, Munchen Germany) using the BCA assay tool.

5.2.4 *Ex vivo* qualitative determination of protein adsorption on hydrogel discs

Discs from both the modified and unmodified hydrogels were punched with a 6 mm biopsy punch. These were incubated in 1 mL aqueous and vitreous humour samples obtained from New Zealand albino rabbits at 37 °C for 90 minutes in an orbital shaker. Subsequently, the discs were washed 3 times with PBS (pH 7.4) The adsorbed protein on the discs were thereafter extracted with a 1 % w/v sodium dodecyl sulphate (SDS) solution. A modified form of the sodium dodecyl sulfate polyacrylamide gel electrophoresis (SDS-PAGE) was used (Zhang *et al*. 2017) to elucidate the pattern of adsorbed proteins on the hydrogel samples. The extract from the 1 % w/v SDS solution is mixed with about 100 µL electrophoresis sample buffer (1 mM EDTA, 10 mM Tris-HCl, pH 8.0, 2.5 % SDS and 5 % β mercaptoethanol) and boiled for 15 minutes and thereafter centrifuged at 9000 rpm for 10 minutes to extract the adsorbed proteins. 10 µL of the supernatant was applied to a 10 % gradient electrophoresis gel and electrophoresis conducted using MINI-PROTEAN® 3 cell (Bio-Rad, USA) at 200 V. The separated protein bands were visualized by staining the gels with about 1 % Coomassie brilliant blue in a 40 % methanol/10 % acetic acid solution for 1 hour and subsequently destained in a solution containing 40 % methanol and 10 % glacial acetic acid.

5.2.5 Determination of cell adhesion using HREP

Cell adhesion studies was undertaken to determine the proliferation capacity of human retinal epithelial cells on the prepared hydrogels. 4 mm x 0.75 mm hydrogel discs were punched in triplicates each from the pristine PVGMA hydrogel (pure), hydrogel with 20 % (PM80-SM20) and 33 % SBMA (PM67-SM33). HREP cells were revived and grown to an 70% confluence in a DMEM: Ham 12 (50:50) medium supplemented with 10 % fetal bovine serum and 1 % penicillin strep. Subsequently, the equilibrium swollen discs were each inserted into a well in a 48 well plate. 300 µL of the HREP cells at a density of 40,000 cells/mL were seeded on top of the hydrogel discs in the well and incubated at 37 °C and 5 % CO_2 for 48 hours. Digital images

were captured both at the centre of the hydrogel and at the boundary between the hydrogel and the well plate. To confirm if the few cells seen on the hydrogel attached on it or on the well plate under the hydrogel, the gels were washed with sterile PBS and fixed with 4% formalin. 4′,6-diamidino-2-phenylindole, DAPI was subsequently used to stain for the nucleus of any cell attached to the hydrogels and visualized with a confocal laser microscope.

5.2.6 Assessment of biofouling potential of hydrogels.

Two bacterial cell lines, a gram positive (*Staphylococcus aureus*) and a gram negative, (*Escherichia coli*) (ATCC25922) known for high contamination potential were used to assess the anti-biofouling capacity of the as modified hydrogels. Hydrogel discs measuring 4mm x 0.75 mm were sterilized by autoclaving and inserted into a sterile suspension of each microbe previously cultured at 37 °C for 24 hours in Luria Bertani medium consisting of 1 % w/w tryptone, 0.5 % w/w yeast extract, 1 % w/w NaCl, and 1.5 % w/w agar in sterile deionized water. The hydrogel disc in the bacterial suspension was incubated at 37 °C for a further 24 hours. The hydrogel discs were removed thereafter, washed 3 times with sterile Dulbecco PBS to remove unattached bacteria, and the bacteria adhering to the disc was detached with a rubber policeman and counted to determine the number of colony forming units, (CFU mL^{-1}).

5.2.7 *In vivo* assessment of cytocompatibility of the hydrogel discs.

Ethics clearance (certificate no 2021-07-03C) (**Appendix A**) for the *in vivo* implantation study in New Zealand albino rabbits was obtained from the Animal Research Ethics Committee of the University of Witwatersrand, Johannesburg, South Africa. A total of 15 male and female rabbits weighing between 2.5 to 3.5 kg were received the Wits Research Animal Facility a week prior to the commencement of the study and acclimatized for 5 days. The animals were housed individually in Wits Research Animal Facility, maintained at a temperature of 25 ℃ ± 2 ℃ and humidity 55 % ± 5 % with a 12-hour light/night cycle and having free access to standard animal food and water. A previously established protocol was followed with modification (Zhang et al., 2009). 4 mm x 0.75 mm hydrogel discs were punched and sterilized and implanted into the sub conjunctival space of the rabbits' right eye (while the left eye served as a control) under aseptic technique by an ophthalmologist following a previous method briefly modified (Acosta et al., 2006). Prior to the procedure, the rabbits were anesthetized with an intraperitoneal injection of a mixture of ketamine (65 mg/Kg) and xylazine (7.5 mg/kg). At 1, 4, and 8 weeks respectively, 5 rabbits were euthanized with an overdose of phenobarbital sodium, and the hydrogel discs explanted. These were fixed in 10 % neutral buffered saline and afterwards, samples were

prepared for SEM viewing using a modified version of a previously applied protocol (Wang et al., 2016). Briefly, a representative explanted disc is dehydrated in a serially concentrated alcohol maintained for 15 minutes at each concentration (50 %, 60 %, 70 %, 80 %, 90 %, and 100 % v/v), air dried, sputter coated with gold/palladium, and examined under the SEM. Sections of representative explanted discs were also stained with haematoxylin-eosin and photographs were taken. Histopathological examination of the capsular tissue surrounding the implanted disc was also undertaken. The SEM images of the implanted discs were compared with that of hydrogel discs that were not implanted.

5.2.8 Cyclosporine A loading into hydrogel discs

Different approaches were used to load cyclosporine into the swollen hydrogel. In the first approach, a 6 mm disc punched out from a swollen hydrogel was dried in the vacuum oven at 40°C to a constant weight. This hydrogel was then allowed to soak in drug solution in the fridge for 48 hours. In the second approach, equilibrium swollen hydrogels were frozen at - 80°C and dried in a lyophilizer over a 4-hour period. Subsequently, the xerogels were soaked in a methanolic water solution of CysA and dried in a vacuum oven. In the third approach, drug solution was incorporated into the hydrogel precursor solution before the photo crosslinking of the hydrogel. In the last approach, the drug formulated into a transferosome was dispersed in the hydrogel precursor mixture before the UV initiated photo crosslinking of the hydrogel. For the transferosome loaded hydrogel, ultrapure water was used as the solvent. 6 mm discs were punched from the hydrogels and subsequently used for release studies.

5.2.9 Characterization of Cyclosporine A loaded hydrogels

Hydrogel-drug interactions were elucidated by studying the molecular transitions of surface functional groups on the unloaded hydrogel, CysA-loaded hydrogels, and pure CysA samples using Attenuated Total Reflectance-Fourier Transform Infrared spectroscopy. Additionally, Differential Scanning Calorimetry was used to study the changes in the thermal properties of the hydrogel because of interaction with CysA. For DSC analysis, a 6mm hydrogel disc was punched and inserted into an aluminium pan and the weight determined. Each was subsequently analysed with the STARe software of the Mettler Toledo.

5.2.10 *In vitro* drug release from Cyclosporine A loaded hydrogels

Three 6 mm drug loaded discs were used for the release studies under a perfect sink condition.

Each loaded disc was put in a 2 mL centrifuge tube containing 1 mL of Simulated tear fluid (ATF) prepared by adding 0.001g of $CaCl_2$ into 100 mL of phosphate buffered saline. These were placed in an orbital shaker set at 37 °C and rotating at 50 rpm. At specific intervals, the 1 mL of the dissolution medium is withdrawn for analysis and replaced with an equal volume of fresh ATF. The collected samples were then read at a wavelength of 213ʎ on an Implen NanoPhotometer® NP80 (Implen GmbH, Munchen Germany) and the concentration calculated from the regression line of cyclosporine A calibration curve obtained by plotting the absorbances of different dilutions of a 2 mg/mL stock solution of cyclosporine in methanol: water (9:1) solvent versus the concentration.

5.3 Results and discussion

5.3.1 Preparation and CysA loading in hydrogels

Zwitterionization was modulated by changing the percentage content of SBMA in the hydrogels and this was done at two levels.

Table 5.1 Composition of the Hydrogels for *in vitro* drug release.

Name	PVGMA (g)	SBMA (g)	CYSA (mg/mL)	VEHICLE (QS)
PM80-SM20(S1)	2	0.5	12	DMSO: H2O
PM67-SM33(S2)	2	1	12	DMSO: H2O
PM80-SM20(L1)	2	0.5	10	DMSO: H2O
PM67-SM33(L2)	2	0.5	10	DMSO: H2O
PLL	2	0.5	50*	H2O
PPD 20	2	0.5	5	DMSO: H2O
PPD 30	2	0.5	10	DMSO: H2O

Note: S= Hydrogels dried in vacuum oven. L= Lyophilized hydrogels. PLL: Transferosome pre-loaded hydrogel. PPD: Pure CysA preloaded hydrogels. * 50 mg/ml of CysA loaded transferosome.

Hydrogel samples prepared with 20 % and 33 % w/w SBMA were used for the assessment of *in vitro*, and *in vivo* cytocompatibility and to evaluate the potential effect of zwitterionization on drug release from the hydrogels. The physicochemical properties of the hydrogel have previously been reported in chapter three. The transparency of the hydrogels preloaded with drugs were reduced. This is line with microphase separation that results as the hydrogel undergoes crosslinking since the solubility limit of CysA has been exceeded in the precursor mixture. Ultrapure water was used as the solvent for the transferosome preloaded hydrogel. Different nanosystems have been employed as a means of increasing the drug loading of hydrophobic drugs into hydrophilic hydrogels.

5.3.2 *In vitro* and *ex vivo* protein adsorption studies result

The results obtained from the BCA assay are displayed in **Figure 5.1**. The level of *in vitro* protein adsorption from across all samples were low with the highest amount of protein (0.1036 ± 0.4224 µg/mm^2) being adsorbed by PM100-SM0 hydrogel. There was a gradual decrease in the level of adsorbed protein as the concentration of modifying monomer, SBMA, in the hydrogel increased. Statistical analysis showed that the addition of SBMA contributed significantly to protein resistance *in vitro* with a p value of 0.000531. The hydrogel with the highest level of SBMA had the least adsorbed protein (0.0487 ± 0.263 µg/mm^2) *in vitro.*

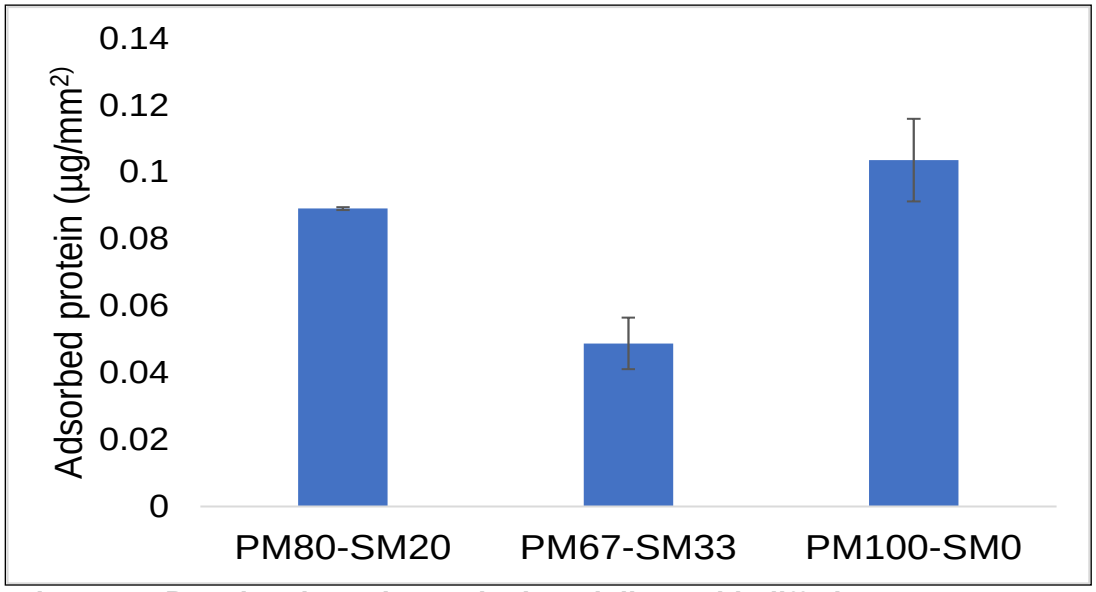


Figure 5.1 Protein adsorption on hydrogel discs with differing SBMA content.

This observation is not different from that of other studies though the level of protein adsorbed in the current study is below that observed in several of these studies (Ramsay et al., 2018), (Ashtiani et al., 2018), (Goda et al., 2009). It is pertinent to note that the protein constitution of theartificial tear fluid used in different studies as well as the evaluation method varied and may have contributed to observed differences in the total adsorbed protein observed for individual studies. In addition, the sensitivity of different methods of evaluation also varies. In this report, the protein solution used represents a complex protein solution constituted from 3 different proteins commonly found in artificial fluid. In addition, during protein evaluation, the calibration curve was constructed using a serial dilution of the same stock solution from which protein adsorption unto the hydrogels were studied and evaluated.

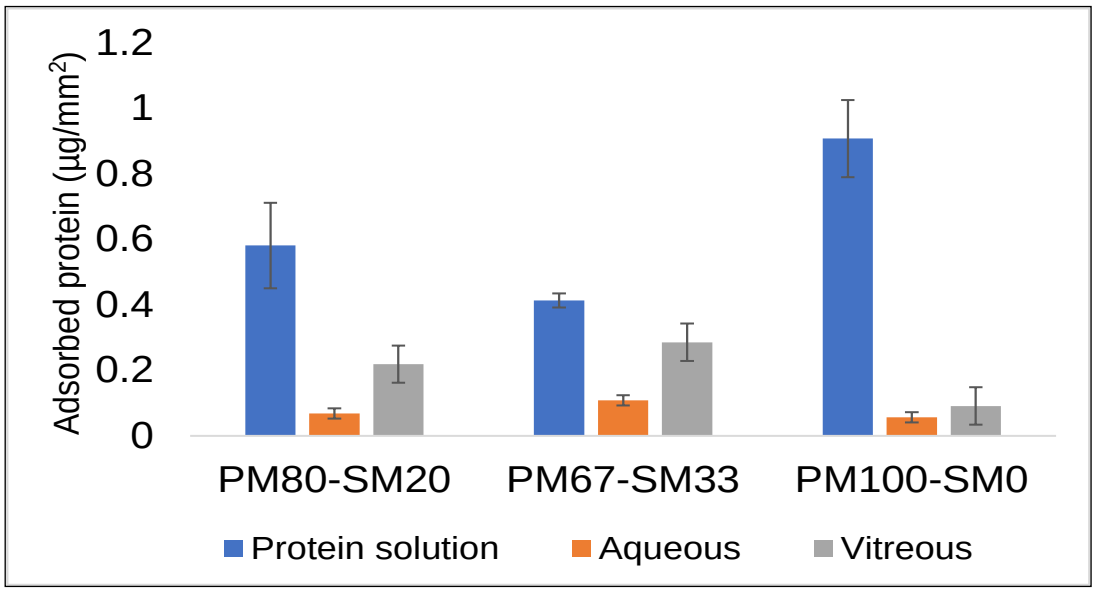


Figure 5.2 *Ex vivo* protein adsorption using aqueous and vitreous humour.

The *ex vivo* protein adsorption determined in aqueous and vitreous humour collected from rabbits is displayed in **Figure 5.2**. The impact of the complex nature of the proteins presented to implants by living systems was evident. The protein adsorption potential of the hydrogels varied inversely with the SBMA content in *ex vivo* fluids. This observation represents the exact opposite of that obtained from *in vitro* experiments with artificial protein solution. The non-zwitterionized hydrogel, PM100-SM0, that had the highest adsorption from *in vitro* protein mixture had the least adsorption from both aqueous and vitreous humour samples. In addition, the total amount of protein adsorbed per unit area of the hydrogel discs were much lower than that adsorbed from the artificial

protein mixture *in vitro*. Different studies had explored the proteomic fingerprint from the aqueous and vitreous humour. The low level of adsorption may reflect the extremely low level of total proteins found in the aqueous and vitreous humour as the total amount of proteins present in the aqueous humour in humans is approximately 500 µg (Skeie et al., 2015) whereas the total amount of protein in the aqueous fluid of rabbits varied between 0.8 and 2.5 mg/mL when determined using the BCA assay (Stastna et al., 2011). In juvenile rabbits however, Young and coworkers found a procedure-dependent protein concentrations varying from 3.6 mg/mL in preoperative conditions to 12.1 mg/mL with IOL insertion hence, bringing to the fore the capacity of an implantable device or biomaterial to stimulate protein release (Young et al., 2020). Even though their study was aimed at investigating the root causes of excessive scarring and immune response in children undergoing cataract surgery, the study relates the possible role that could be played by biomaterials in inducing proteins that can act as cues for pro and anti-inflammatory macrophage polarization. It is important for this research that the total protein adsorbed by the hydrogels from an *in vitro* protein solution was higher than that adsorbed from the rabbit's ocular fluids. It is also important that the nature and type of proteins induced by a biomaterial depends to an extent on the properties of the biomaterial. Though there was a general reduction in the quantity of proteins adsorbed from ocular fluids, the reverse role played by the SBMA content of the hydrogel raises questions as to the nature of the interaction between itself and the proteins in the ocular fluids particularly bearing in mind the unique nature of the ocular environment. Boone and colleagues also noted a difference in the quantity of lysozyme adsorbed from *ex vivo* tear fluid and *in vitro* experiments. (Boone et al., 2009) As with the current study, the total protein deposited in *in vitro* experiments were higher than that from *ex vivo* experiments, which they attributed to the complex nature of *ex vivo* protein creating opportunity for competitive adsorption. Moreover, adsorption of certain types of proteins such as lysosome which has antibacterial effect could serve the purposes of the biological environment at such instance. In addition, the structural resemblance of SBMA to certain cell membrane proteins may contribute to this inverse relationship in terms of total proteins adsorbed as has been observed in this study. Zhang and colleagues previously demonstrated the stabilizing effect of polycarboxybetaine network within which uricase, a protein was encapsulated, (Zhang et al., 2015) to immunogenic attacks that usually result from repeated frequent protein injections. There is therefore the need to explore this interaction with a view to harnessing the potential benefits from biomaterials modified by zwitterionic SBMA. See 3.3.11 for more discussion on *in vitro* protein adsorption.

5.3.3 Qualitative determination of adsorbed protein by SDS-PAGE

Figure 5.3 shows the digital image of a representative run for the qualitative assessment of the protein adsorbed on hydrogel discs. The 2 lanes at the opposite ends of the gel were for the protein stock solution (containing a mixture of the proteins used) and the protein marker, respectively. Each constituent protein sample was put in 2 wells. One protein band was prominent from all the wells containing extracts from the protein was responsible for the adsorption on the gels. An alternative explanation maybe that the level of the other proteins adsorbed on the hydrogel were extremely low and hence could not be resolved by the 10 % acrylamide gel gradient seeing that the limit of detection by SDS-PAGE stained with Coomassie blue is 100 ng. Protein concentration could resolve this, but it is beyond the objectives of the current work. In like manner, proteins adsorbed from the *ex-vivo* experiments with aqueous and vitreous humour were also subjected to analysis by electrophoresis. **Figure 5.4** shows the results of electrophoresis for protein adsorption from aqueous and vitreous humour samples. The results were similar to that obtained from *in-vitro* protein adsorption study and shows only the protein marker lane.

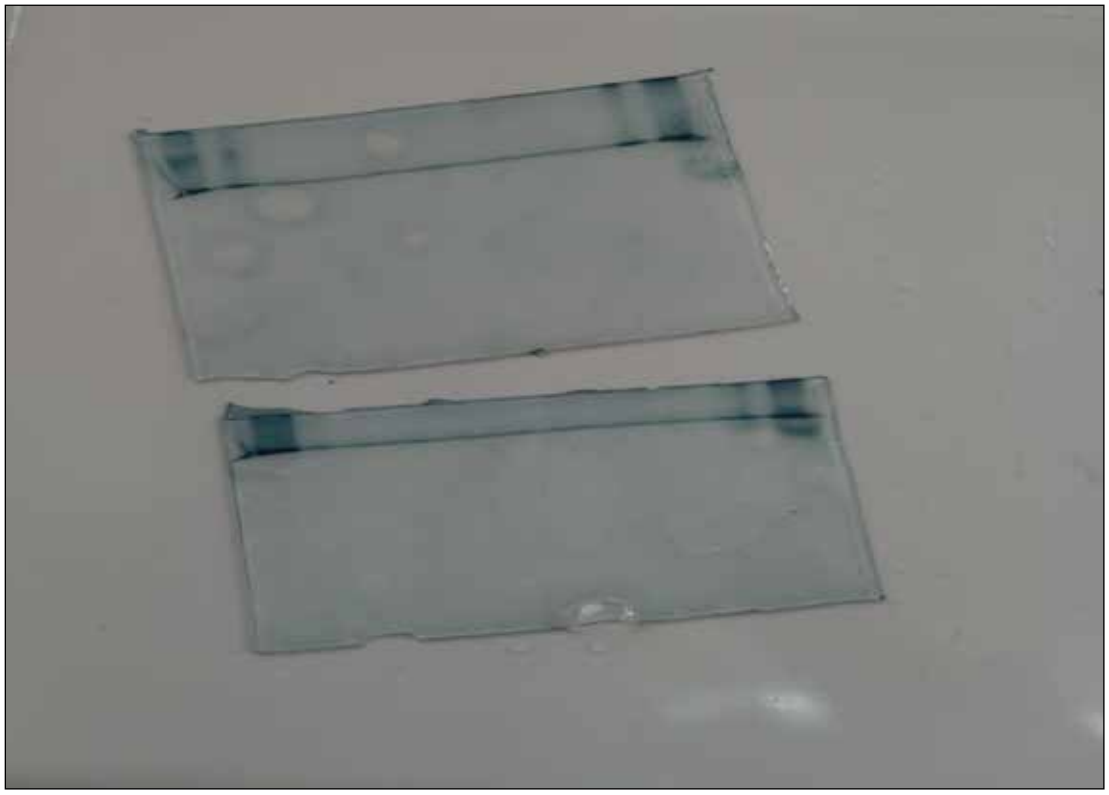


Figure 5.3 Duplicate SDS -PAGE of proteins adsorbed on hydrogels from *in vitro* studies.

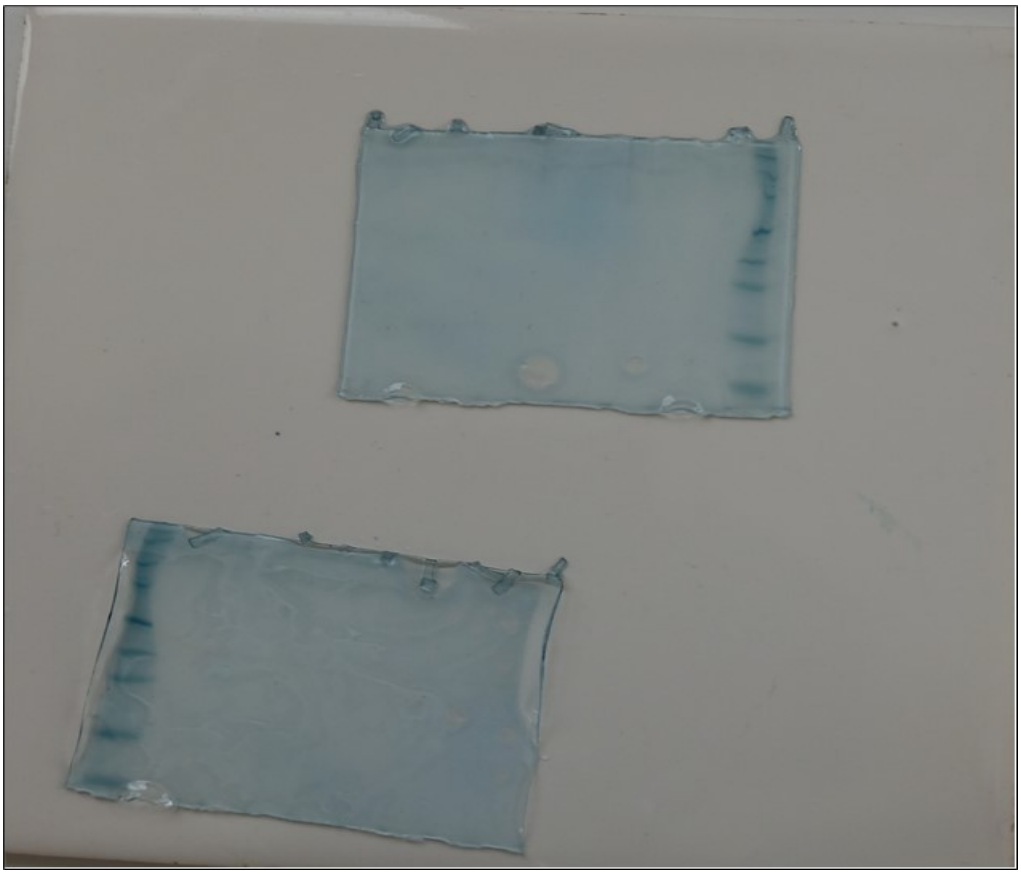


Figure 5.4 Duplicate SDS-PAGE of protein from *ex vivo* studies.

5.3.4 Cell adhesion studies on the hydrogel

A major benefit that can accrue from limited protein adhesion for an ocular implant such as intraocular lens is the potential reduction on the extent of posterior and anterior capsular opacification that frequently results from migration and attachment of lens epithelial cells on the freshly implanted IOL. In addition, as mentioned in the previous section, excessive scarring that mars cataract surgery in children can be reduced using an IOL lens that seriously limits the adhesion of lens epithelial cells. **Figure 5.5** - **Figure 5.7** show the digital micrographs of hydrogel discs with distinct levels of the zwitterionic modifier, SBMA, unto which HREP (representing ocular epithelial cell) were seeded. Each figure shows 3 replicates of each disc, which were seeded and image capture of different zones by the microscope for each replicate. The images of hydrogels stained with DAPI from the confocal laser microscope was not included because no florescence could be detected from any of the gels. The transparency of the hydrogels was so high that the cells that attached on the well plate under the hydrogel were visible through the hydrogel. This was inferred because when the microscope was focused such that the cells attached to the well

plate is in view, the cells seen through the hydrogels becomes hazy whereas if the focus was obtained using the cells on the hydrogels, the cells on the well plate becomes hazy. In the images displayed in **Figure 5.5** -**Figure 5.7**, cells were not visible on the hydrogels. This observation became clearer after the hydrogel discs were transferred to fresh medium as can be seen from all the 3 replicates from the 3 formulations as displayed **Figure 5.5** -**Figure 5.7**. To confirm that the cells seen from the top of the hydrogels were on the well plate, a sample of the hydrogel, PM100-SM0 3 had a cut, with a blade, halfway through the hydrogel. The digital image of the cut hydrogel obtained at a higher magnification shows clearly that the cells were on the well plate not on the hydrogel (**Figure 5.8).** Interestingly, there was no visible difference in the cell adhesion potential across the modified and unmodified hydrogel. This may be chronicling the hydrophilic potential of PVA, the base polymer in PVAGMA to limit cell adhesion as a standalone agent. Various studies involving zwitterionic compound mainly focused on coating the surface of a base material such as polystyrene and gold, (Chou et al., 2016; Sobolčiak et al., 2017), with the zwitterionic agent through grafting from or grafting to polymerization techniques. Unfortunately, the stability of such surface modifications has been called to question particularly when used in dynamic environments. Ultra-low epithelial cell adhesion potential displayed by the developed hydrogels is similar to if not better than that observed for such surface modified substrates (Sobolčiak et al., 2017). The ultra-low cell adhesion capacity of the zwitterionized hydrogels developed may be heralding a role in corneal healing and a potential application in corneal bandages. Huang and colleagues equally explored this potential in a zwitterionic nanocomposite gel containing nanoclay for wound healing even though the ocular space was not their focus. (Huang et al., 2016) As the in vivo studies in rabbits' eyes will subsequently show, cell adhesion unto the hydrogel reflected in the explanted hydrogel with no attachments from the tissues.

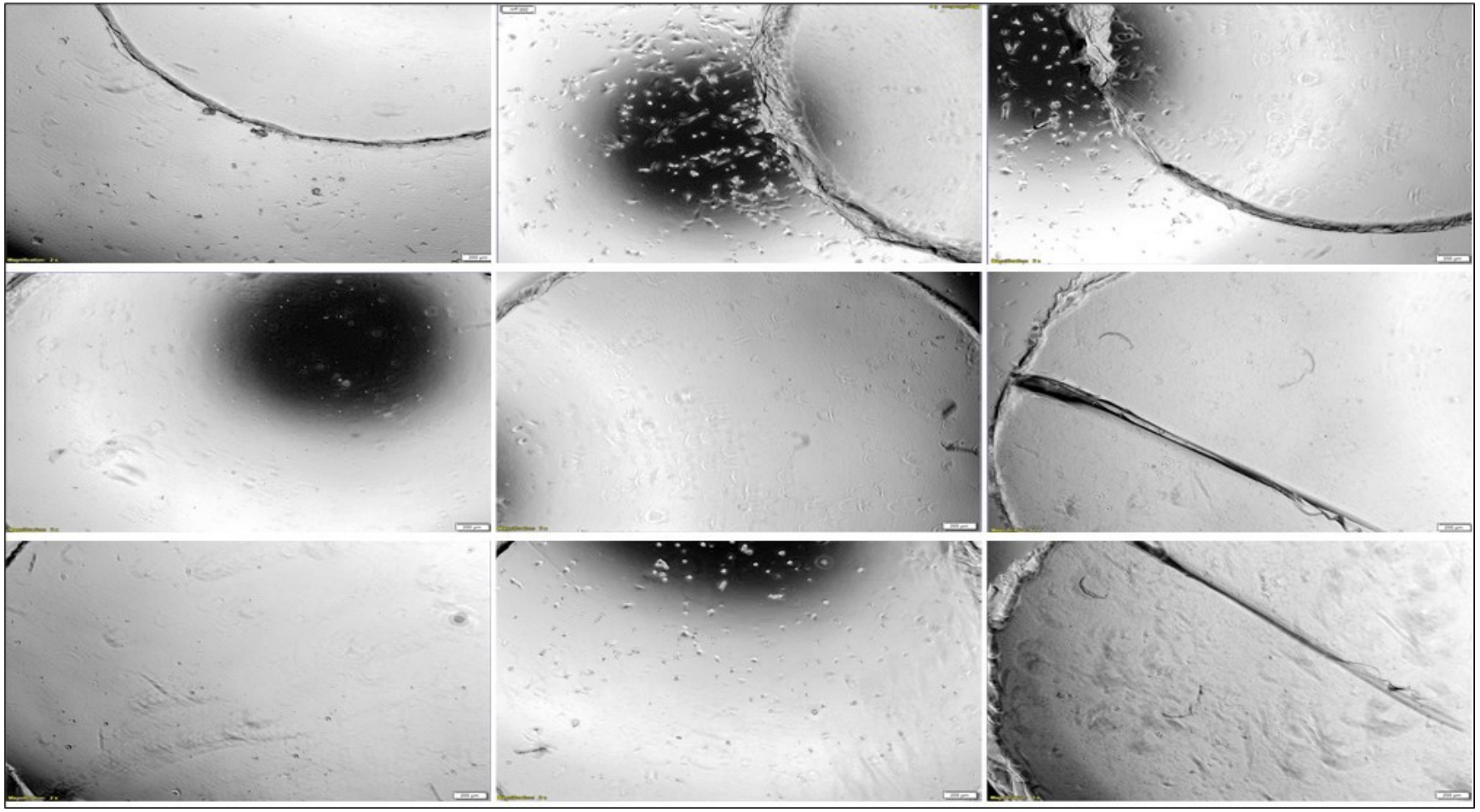


Figure 5.5 Images showing the pattern of cell adhesion on the PM100-SM0 hydrogels (3 replicates). The first row represents the border between the well plate and the hydrogels; the middle row represents focus on the center of the hydrogels; and the last row represents hydrogels after they were transferred to a fresh medium for the 3 hydrogel replicates.

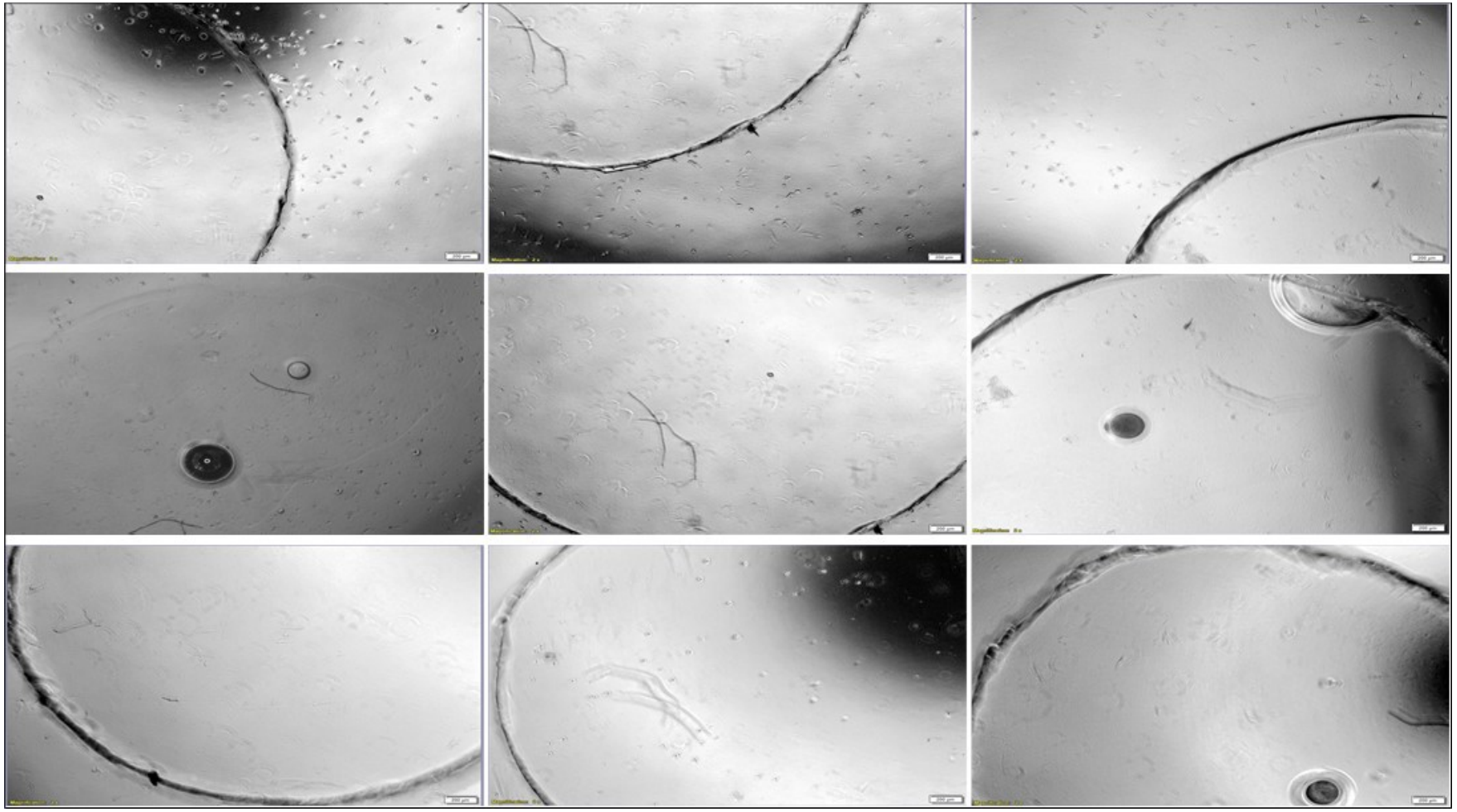


Figure 5.6 Images showing the pattern of cell adhesion on the PM80-SM20 hydrogels (3 replicates). The first row represents the border between the well plate and the hydrogels; the middle row represents focus on the Centre of the hydrogels; and the last row represents hydrogels after they were transferred to a fresh medium for the 3 hydrogel replicates.

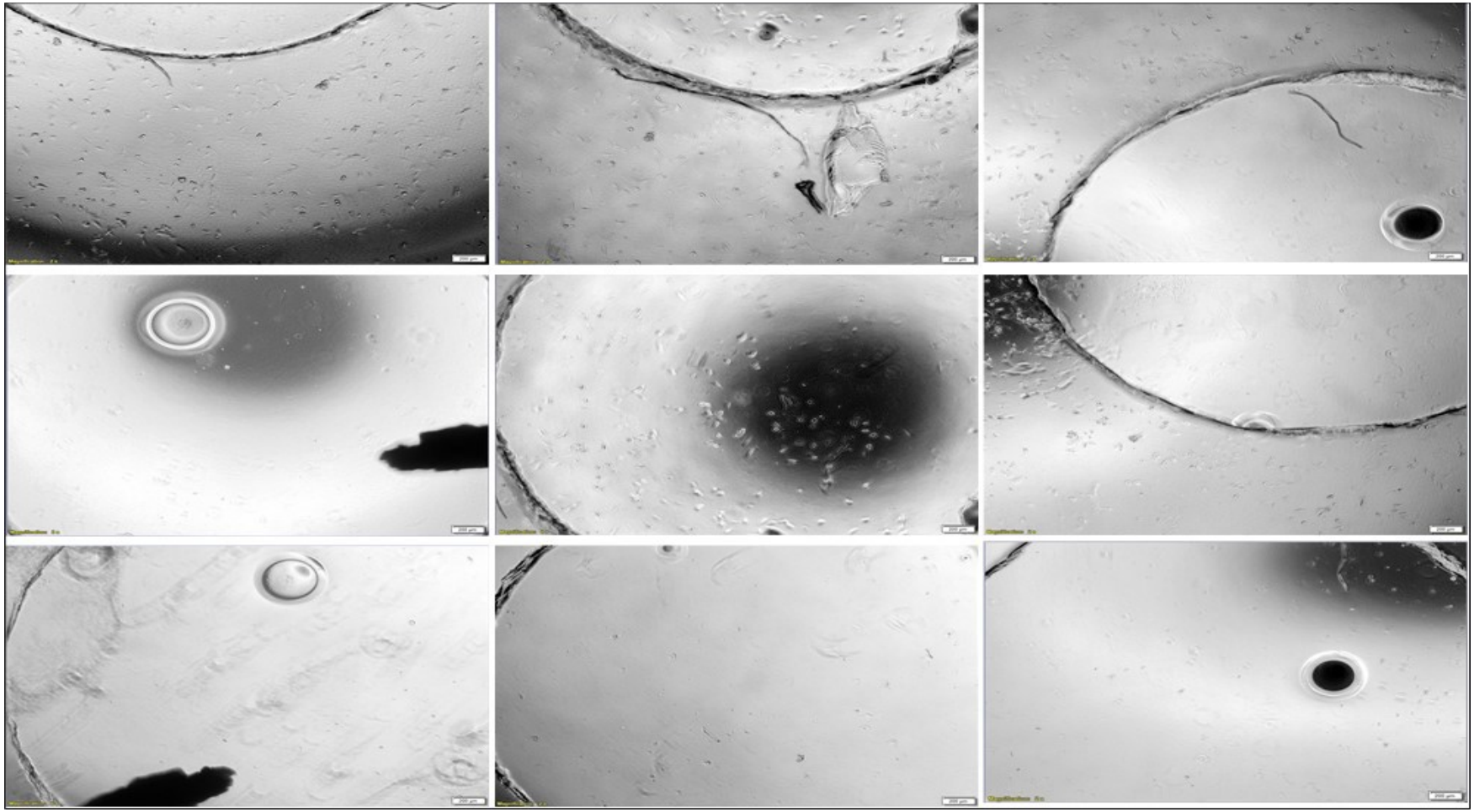


Figure 5.7 Images showing the pattern of cell adhesion on the PM67-SM33 hydrogels (3 replicates). The first row represents the border between the well plate and the hydrogels; the middle row represents focus on the centre of the hydrogels; and the last row represents hydrogels after they were transferred to a fresh medium forthe 3-hydrogel replicates.

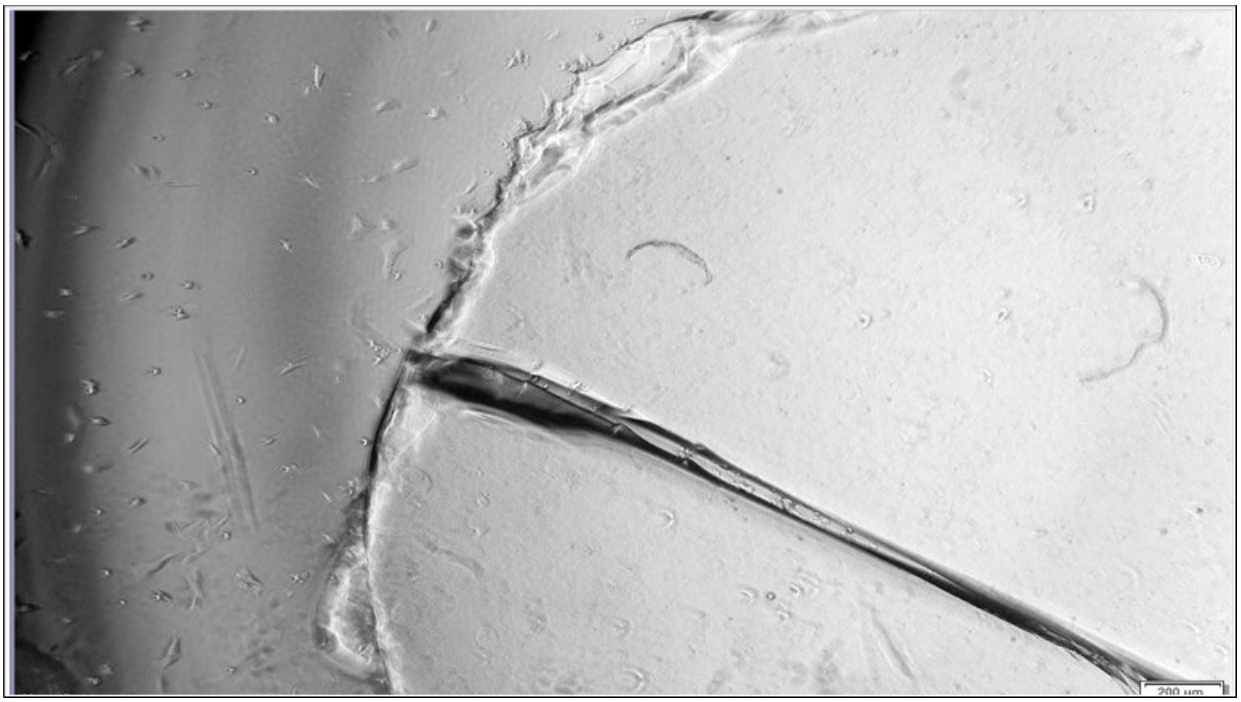


Figure 5.8 Slit hydrogel showing that cells were attached on the well plate and not on the hydrogel.

5.3.5 Biofouling resistance assessment for hydrogels

Biofilm formation associated with implantable devices and consequent sepsis continues to be a challenge motivating the search for biomaterials that will inherently limit it (Jamal et al., 2018) (Fujii et al., 2008). Biofilms usually result when microorganisms adhering to a surface secrete lipopolysaccharides and glycocalyx that ultimately form a shield within which the microbes can grow and multiply, limiting access to external assaults, and causing antibiotic resistance. (Chew & Yang, 2016) Biofouling assessment was undertaken by a third-party blind to the components and formulation process of the disc and the verified report is attached in **Appendix F**. Results obtained from assessment of resistance to biofilm formation showed a graded response that depended on the SBMA content of the hydrogels. Hydrogel PM67-SM33 containing the highest level of zwitterionic SBMA was at least 50 % less susceptible to biofilm adhesion when compared to the pure PVAGMA hydrogel sample, PM100-SM0, at all the time points and across the 2 microbes used for the assessment. In addition, the reduction in bacteria colonies by PM67-SM33 hydrogel between the 1-hour time point and 24-hour time point was over 87 % when compared to the 100% PVAGMA hydrogel. Moreover, the standard deviation for all measurements involving PM67-SM33 hydrogel was very low especially when compared to the-

100 % PVAGMA hydrogel. **Figure 5.9** shows the graph of the number of bacteria adhering to each hydrogel at every time point measured. All the hydrogels showed similar trend in the *S. aureus* medium. The number of colony forming units (CFU) initially increased before going down. A two-way analysis of variance was used to determine the effect of time and the SBMA content of the hydrogels as 2 independent factors on the number of bacteria adhering to the hydrogels. With a p-value of 0.011 and an F-value of 10.31, and at 95 % confidence interval, the SBMA content of the hydrogels significantly affected the number of bacteria adhering to the gels. Studies on biofilm adhesion to materials other than hydrogels abound but very few relates to hydrogels. Ishihara and colleagues (Ishihara et al., 2021) recently studied bacterial adhesion to silicone contact lenses surface-modified with 2-methacryloyloxyethyl phosphorylcholine. The bacterial adhesion observed in their study was of the order of 10^8 cells. Likewise, Wang and colleagues studied the bacterial adhesion unto a carboxybetaine and sulfobetaine modified Poly (ethylene terephthalate) (Wang et al., 2016). The number of CFU cells found on their best modified surface was of the order of 10^6. These are orders of magnitude higher than that observed in this study.

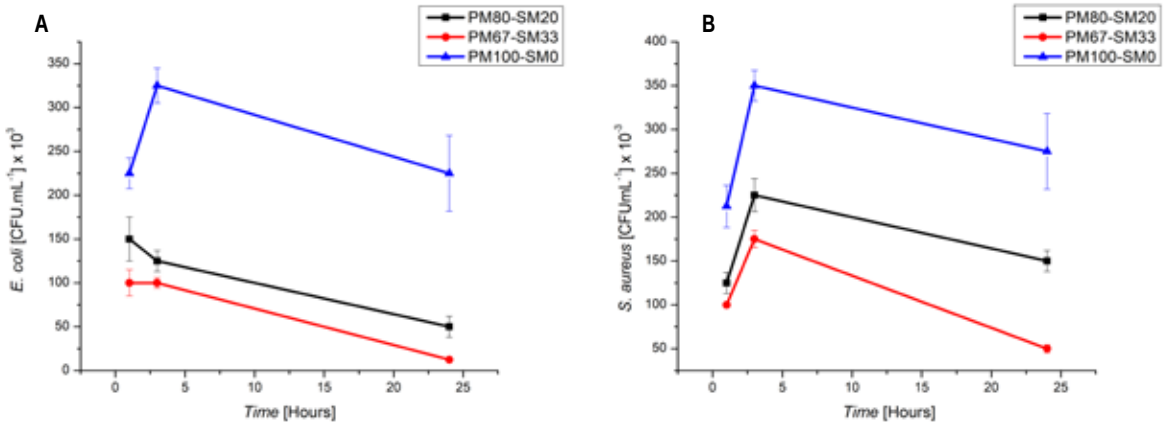


Figure 5.9 Graph showing the number of bacterial cells adhered to each hydrogel at different time points for *E. coli*, (A) and (B) *S. aureus.*

A synergistic relationship arose out of the combination of PVA and the zwitterionic SBMA that resulted in this level of biofilm reduction. The sensitive nature of the ocular environment places an even greater premium on implants designed for ocular application. (Uwaezuoke et al., 2021) Ocular devices such as contact lenses are being constantly removed and replaced on the eye

and hence requires constant soaking in multi-purpose lens cleaning solutions to remove adhering bacteria and lipids that may cause sight threatening infections such as keratitis. The success of such cleaning process depends on the duration of soaking, type of adhering microbe and the type of the cleaning solution (McAnally et al., 2021). Studies have shown that in certain instances, cleaning solutions used for the duration of time stipulated by manufacturer do not remove certain bacteria such as *Pseudomonas aeruginosa* (Dantam et al., 2020) (*Bacteria Survive Longer in Contact Lens Cleaning Solution than Previously Thought, Study Shows*, n.d.). In addition, the possible sudden emergence of superbugs and multi-drug resistance amongst contact lenses adhering microbes could be complicating these issues for contact lens users.

5.3.6 *In vivo* evaluation of hydrogel discs in New Zealand albino rabbits

The eye is unique in having a diverse array of tissues in proximity to each other, an attribute that often leads to an orchestrated scaring in one tissue in response to effects on another tissue. The temporal situation of events following biomaterial implantation is captured aptly in **Figure 5.10** (Maity & Sarkar, 2017). The intensity and timeline of any of the phases depends on the degree of the injury created, and the physicochemical properties of biomaterial. Following surgical implantation of a biomaterial, an interplay between the biomaterial and the macrophage system (as the major markers of inflammatory/immune response) is initiated depending on the nature and types of protein that adheres on the biomaterial surface (Gordon & Plüddemann, 2017).

Table 5.2 Cell types appearing in each subsection of the tissue.

Section	**PM80-SM20**		**PM67-SM33**	
Inner layer	+2 epithelioid macrophages	Heterophils	+2 epithelioid macrophages	Single heterophil
Surrounding stroma	3+ thickness	Lymphoplasmacytic cell 1+	Rich fibrous collagen	
MNGBC*	3.5+		1+	

*MNGBC = Multinucleate giant body cells

Changes in the secondary structure of these adhering protein will cause the macrophage system to either attack and phagocytize the biomaterial or to proceed with tissue repair (the so-called M1 and M2 polarization respectively). If the adhering proteins are identified as membrane or body

proteins, M2 macrophages are activated that recognise these as self and initiate an anti-inflammatory response that tends towards tissue repair. To initiate tissue repair, M2 macrophages must be able to recognise and remove by products of host protein oxidation that are generally termed danger associated molecular patterns (DAMP) and brought about by the action of reactive oxygen species released by the macrophages in the first instance. (Hilhorst et al., 2014). Subsequently, these M2 macrophages serve as antigen presenting cells for the activation of T lymphocytes of the regulatory subset through the transforming growth factor β (TGF-β), platelet derived growth factor (PDGF), and interleukin 10 (IL-10) signalling (Hilhorst et al., 2014). T regulatory lymphocytes residing in non-lymphoid tissues perform a variety of functions in addition to their traditional immune suppressive roles specific to the context and their location. (Traxinger et al., 2022). In many biological procedures such as tissue engineering, surfaces that encourage protein adhesion and subsequent macrophage attachment are most welcome (Xu et al., 2021) whereas in other procedures, (in the eye particularly) such as implantation of IOL or in glaucoma drainage devices, macrophage adhesion following protein adsorption onto the device may lead to extensive fibrotic response that ultimately shuts down the device and necessitates removal.

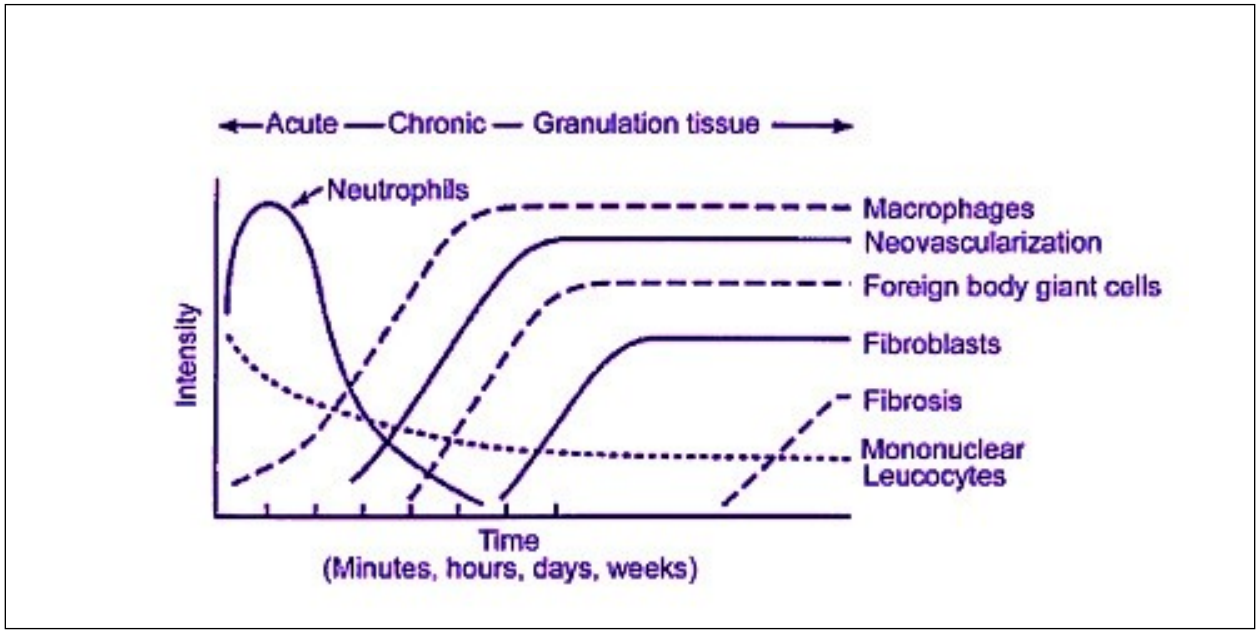


Figure 5.10 Time modulated variation in acute, chronic and granulation tissue inflammation and the effect of cellular immune factors on intensity. Reprinted from Monitoring and Evaluation of Biomaterials and their Performance In Vivo, S. Maity, A. Sarkar, Monitoring fibrous capsule formation: pg 69-80. Copyright (2017) with permission from Elsevier.



Figure 5.11 Representative image of a rabbit eye just after implantation.

(Mahale et al., 2015) Understanding the nature of this interaction, therefore, becomes a prerequisite for designing biomaterials that could limit debilitating microenvironment pathologies (Vishwakarma et al., 2016). The sensitive nature of the eye, which is the primary reason it operates an immune privilege environment, prohibits the inflammatory processes that often may lead to loss of sight. The conjunctiva is histologically differentiated into the epithelium and *substantia propria*. The *substantia propria,* made up of the adenoid and fibrous layer, is interspersed with a variety of tissues that together form the conjunctiva-associated lymphoid tissue (CALT) that modulates the immune and inflammatory responses around the ocular surface (Arnous et al., 2022). **Figure 5.11** show a representative image of an eye just after hydrogel disc implantation while images in **Figure 5.12** were taken after 8 weeks of implantation and show the perfect integration of the hydrogel disc into the superior bulbar conjunctiva. There were no visible signs of desquamations on the explanted hydrogel disc displayed in **Figure 5.13** neither were there adhering tissues stuck to it. In like manner, the hydrogel seen embedded in the tissue in the histological images did not have cells adhering to it. Histological images of tissues obtained from area surrounding the hydrogel discs explanted from rabbit's subconjunctival space after 1 week, 4 weeks, and 8 weeks are shown in **Figure 5. 14** through **Figure 5.16.** Hydrogel discs implanted

for the 1-week study, PM67-SM33 and PM80-SM20, contained various levels of SBMA as earlier stated to determine if the *in vivo* inflammatory response is dependent on the SBMA content. Histological reports (**Appendix G**) graded the presence of different cellular components of inflammation observed in the tissue. These cells are naturally recruited to the injury sight and engage in the tissue repair process that is initiated right after the procedure. **Table 5.2** shows the different sections of the conjunctival tissue from representative hydrogel discs showing the types and number of cells identified in the immediate vicinity of the cavity left by the procedure and these included heterophils, lymphoplasmacytic cells, macrophages, and multinucleated giant body cells. Multinucleated giant body cells (MNGBC), for instance, were graded (+2) in the immediate tissues surrounding of the cavity created by the procedure. MNGBC are usually formed by the fusion of macrophages activated in the acute phase when their attempt at phagocytosis fails particularly because of the size of the presenting stimuli. The response to the implant after a week majorly represented an acute phase of an attempt at tissue repair and encapsulation of the foreign material. In hydrogel PM67-SM33, the stromal response

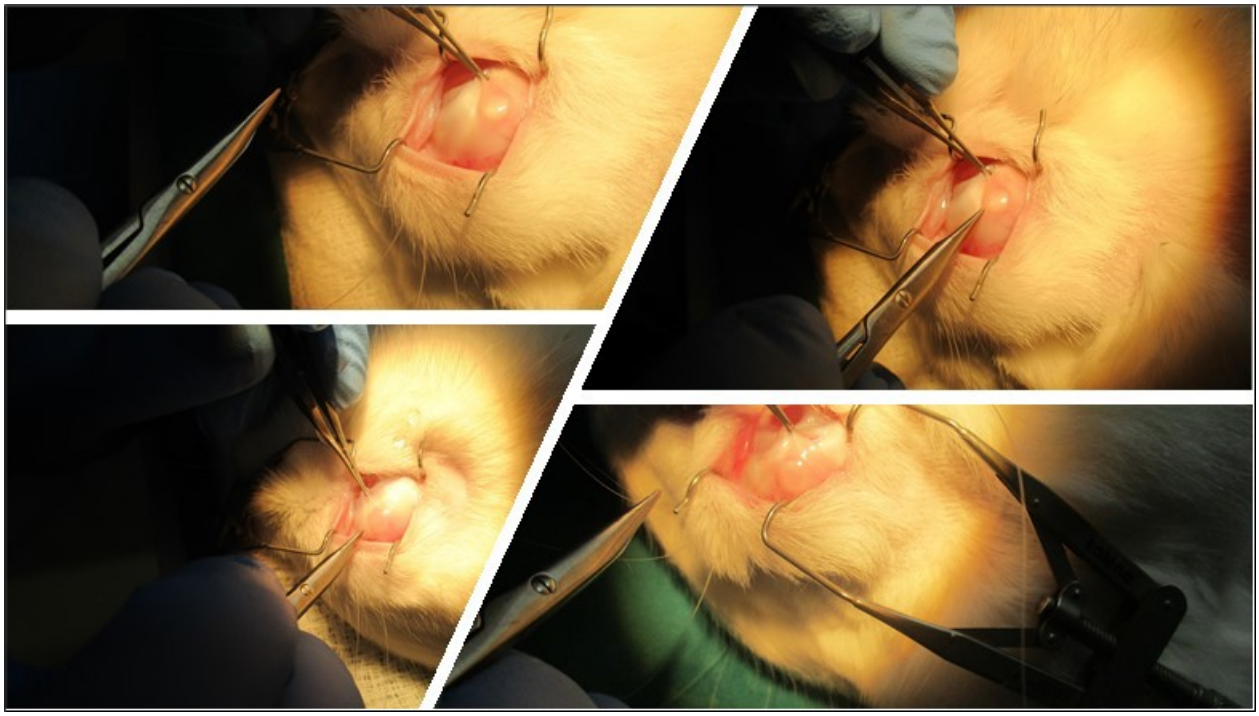


Figure 5.12 Digital image of PM67-SM33 hydrogel disc 8 weeks post implantation.

accompanied by more mature collagen fibres, with horizontally arranged layers represents an advanced level of tissue repair occurring after a week. The number of multinucleated foreign body giant cells (MNGBC) were also lower in PM67-SM33, and this correlates well with the *in vitro* protein adsorption study findings. Histological reports showed that there was minimal presence of inflammatory cells by the 4th week involving heterophils, macrophages, lymphoplasmacytic cells and few MNGBC and all were associated with a sample that had hair shaft as a foreign material in the cystic space. The rest of the samples showed normal mucosa and submucosa with cystic spaces lined or encircled by layers of plump fibroblasts interspersed with connective tissues and making up a granulation tissue in some samples. There was minimal capsule formation as can be seen in the histological images in **Figure 5.15.** One of the hydrogel discs was not found in one of the rabbits by the end of the first and 4th week. This throws up a need to study the extrusion potential should the developed implant be planned for as an implantable drug delivery device. Issues around the extrusion rate of the conjunctiva as has been observed by the ophthalmologist in real life procedures also arises. By the 8th week, histology reports the formation of cystic encapsulation with a fibrosis layer measuring from 4 cells thickness to a thickness of 0.1µm in one sample.

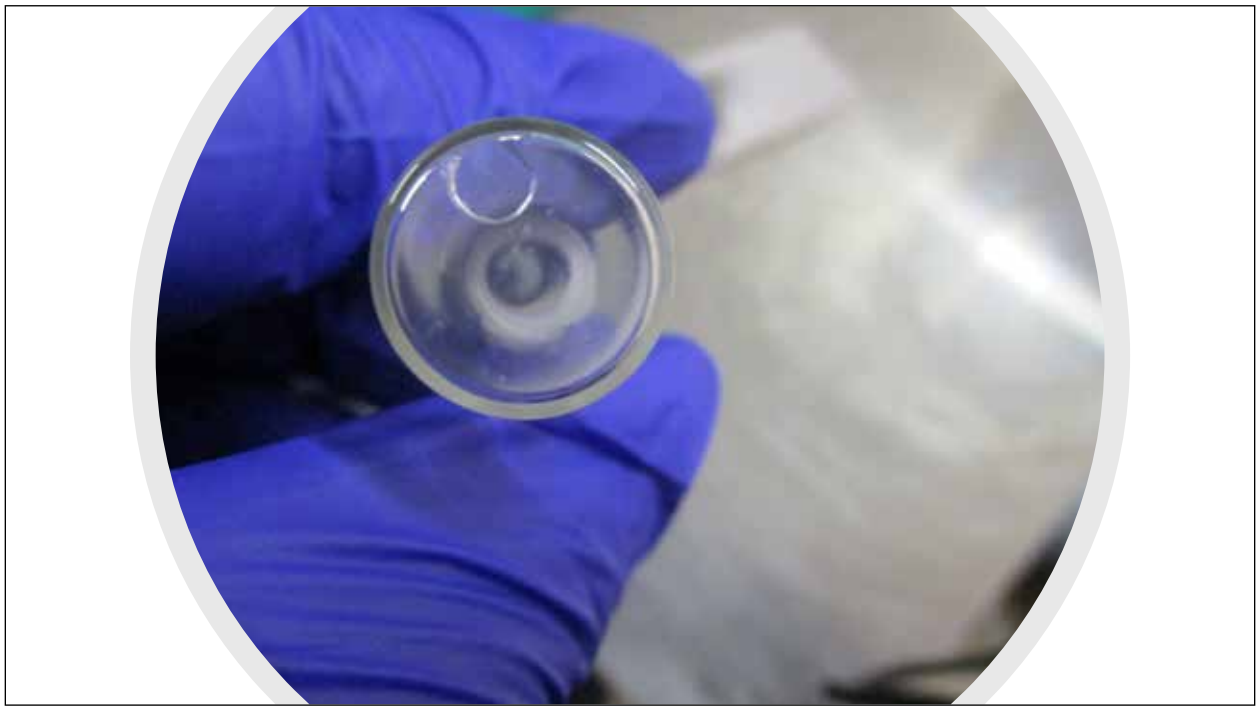


Figure 5. 3 Digital image of a hydrogel disc explanted after 8 week.

Figure 5.17 shows the size of the collagen capsules formed around the implant at various time points after explantation. These measurements were made with ImageJ yellow measuring tool shown in **Figure 5.18**. Inflammatory response to implanted biomaterials usually presents and may be measured by the size and nature of the fibrotic collagen capsule that forms around the implanted device. (Rohner et al., 2021) Bartoli and co-workers reported the formation of a 0.92 ± 0.67 mm thick capsule in cardiac tissue after approximately 208 days. (Bartoli et al., 2010) **Figure 5.17** shows that this capsule was absent at 1 week but present by the 4^{th} and 8^{th} week. There was no significant difference between the sizes of the collagen capsules at both time periods. In addition, in most of the sections captured by histology, this capsule was rather presented as a layer of fibroblasts intermingled with their synthesized collagen and connective tissues. This represents the formation of new tissues that are same as self through which connection with the local tissue environment may be maintained, a very welcome development.

The morphology of cells found on the explanted hydrogel discs was studied using the SEM. **Figure 5. 19** (A3 and A4) shows the SEM image of representative PM67-SM33 hydrogel disc explanted after 4 weeks. **Figure 5. 19** (A1 and A2) are SEM images of a control hydrogel disc that was not implanted. Cells identified on the explanted hydrogel from SEM images were few and occupied less than 50 % of the disc as can be seen from Figure **5. 19**. These represent the lymphocytes, heterophils, and macrophages. **Figure 5.20** show the SEM images of representatives of the same hydrogel explanted after 8 weeks. The morphology of the cells slightly differs from the images in **Figure 5. 19**. On one of the implants, macrophages fusing to form multinucleated giant body cells were identified likewise T lymphocytes. Again, the presence of inflammatory cells was limited to the presence of a few single cell lymphocytes, heterophils and plasma cells. In one of the samples, multinucleate giant body cells were present but was associated with the presence of a foreign material embedded adjacent to the cystic space left by the implant. Often, implanted biomaterials act as a consistent and continuous inflammatory stimuli that eventually results in cytokine storm when inflammatory cells are not able to codon off the biomaterial. The capsule formation effectively cordons off the biomaterial device from the body environment and in applications used as sensors. This effectively leads to device failure. If, however, the fibrotic capsule is perfused with connective tissue, the contact with the body environment is maintained alongside the functions of such devices. Acute inflammatory response to normal wound that is targeted at tissue repair generally begins to resolve by the third week after surgery (Tan et al., 2017) and this is evident in the histological reports obtained at 4 weeks. Inflammation was generally absent in most tissue specimens (confirmed by the general absence of multinucleated foreign body giant cells) and only minimally present in few

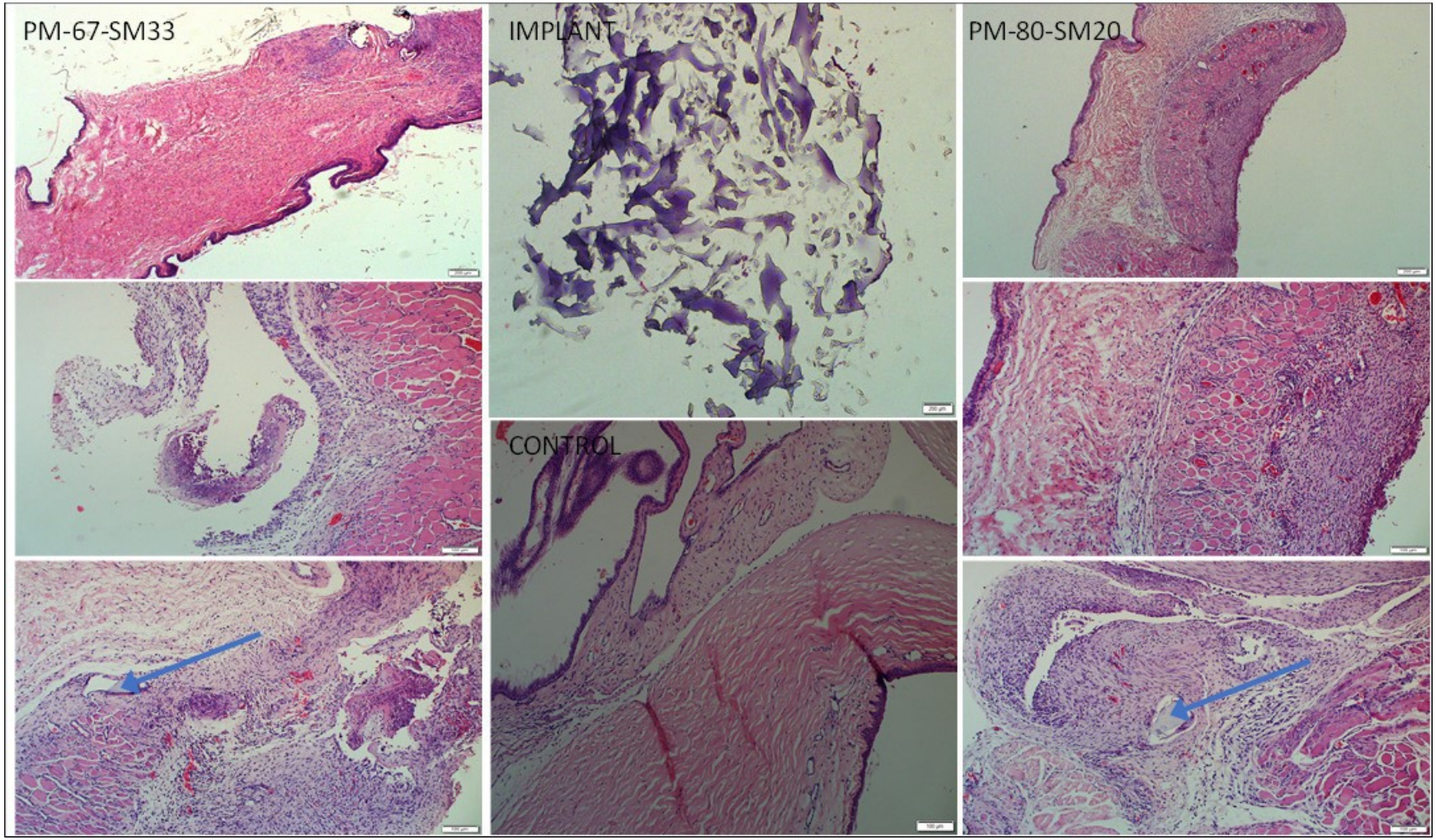


Figure 5.14 The histopathological images reflecting the effect of implanted hydrogels PM67-SM33 and PM80-SM20 on conjunctival tissues after 1 week. The blue arrows show the implant embedded in the tissue.

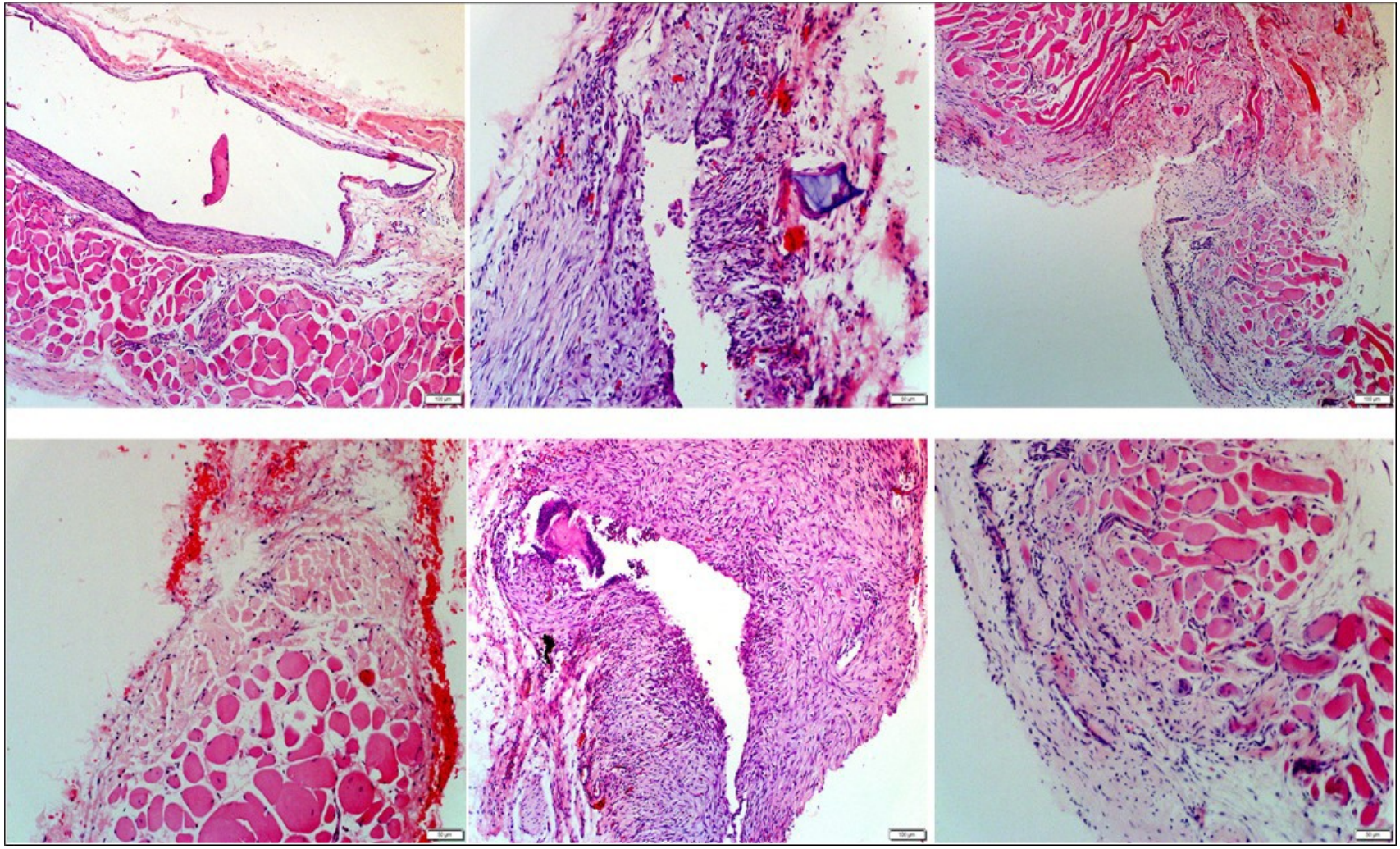


Figure 5.15 The histopathological images reflecting the effect of implanted hydrogel PM67-SM33 discs on conjunctival tissues after 4 weeks.

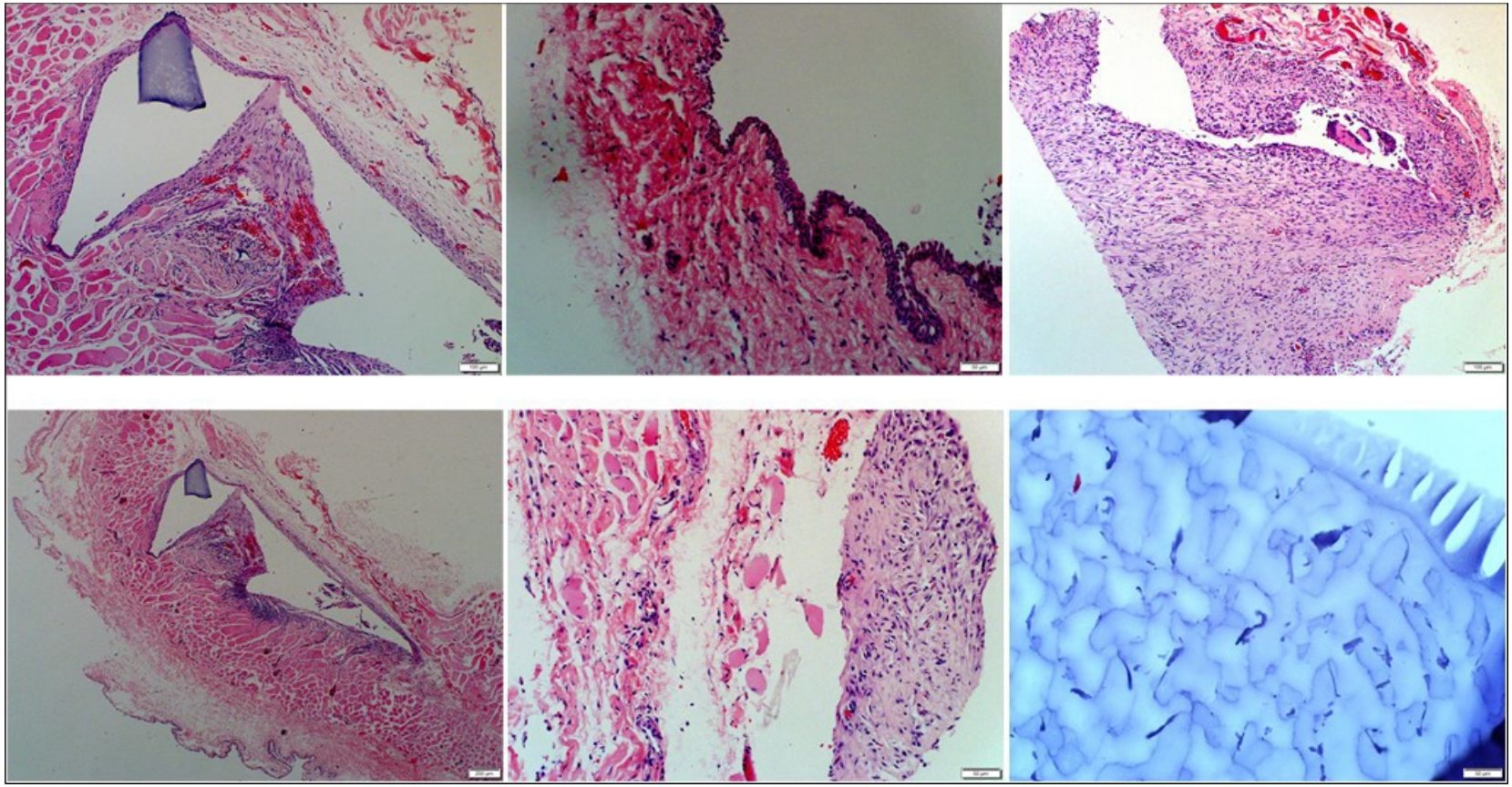


Figure 5.16 The histopathological images reflecting the effect of implanted hydrogel PM67-SM33 discs on conjunctival tissues after 8 weeks. The blue slide is the explanted hydrogel implant.

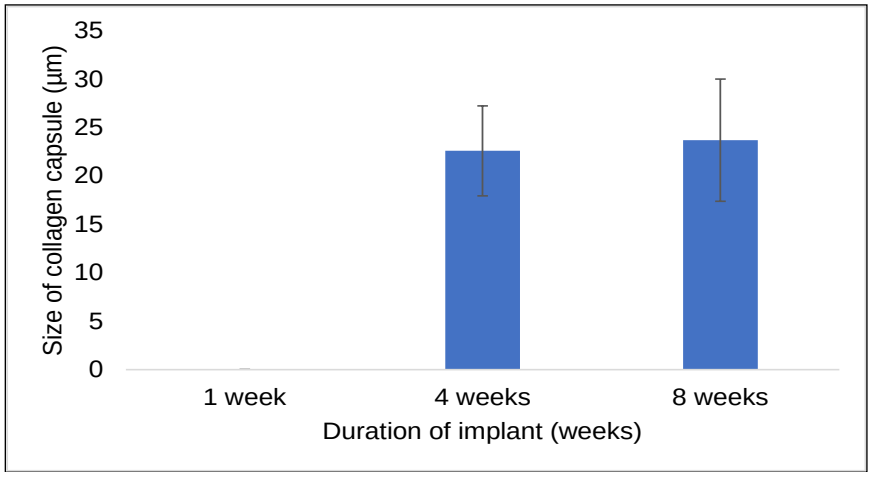


Figure 5.17 Size of collagen capsule formed around the implant after 1-, 4-, and 8-weeks implantation measured with Fiji (Image J).

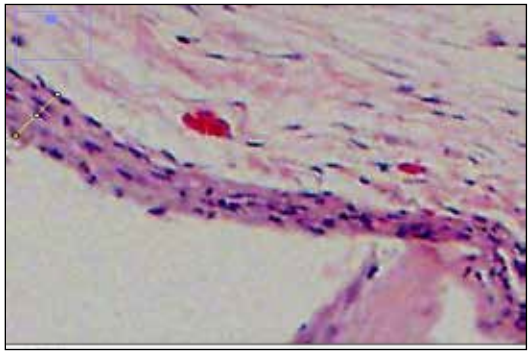


Figure 5.18 Sample of collagen capsule measurement using ImageJ yellow measuring tool.

sections (a multinucleated foreign body giant cell was noted in one section out of three sections in one sample) where it occurred and was related to the presence of hair shafts from the procedure. This observation agrees with the observations of Tan and colleagues that studied the uveal compatibility of MPC modified silicone hydrogel lenses. (Tan et al., 2017) The minimal presence of inflammatory components could derive from the fact that by the 4th and 8th week all acute inflammatory response resulting from tissue injury would have subsided. Huang and co-workers (2016) prepared and used a zwitterionic hydrogel reinforced with nanoclay as a wound dressing. They noted complete connective tissue formation and re- epithelization of the wound by the 12th day in diabetic rats. (Huang et al., 2016) In addition, removal of the dressing was clean without any adhering or intertwined tissues. Surface chemistry of biomaterials has been

explored as a means of modulating inflammatory response to implanted devices. Surface wettability is one property that has frequently been exploited in this regard. Xu and colleagues investigated the adhesion of activated M1 and M2 macrophages onto hydrophobically modified methacrylated gellan gum and the subsequent expression of pro and anti-inflammatory markers in RAW 264.7 cells culture media. (Xu et al., 2021) Their study confirmed that increasing hydrophobicity increased macrophage adhesion and reduced the expression of pro inflammatory tumour necrosis factor-α(TNF-α). Shen and colleagues, on the other hand, studied the influence of the type of adsorbed protein on monocyte adhesion (Shen & Horbett, 2001) and noted that adsorption of albumin reduced monocytes adhesion while fibronectin, plasma, serum, and immunoglobulin G adsorption promoted monocyte adhesion. Rostam and colleagues made a different observation on the effect of hydrophobicity of biomaterial on the expression of

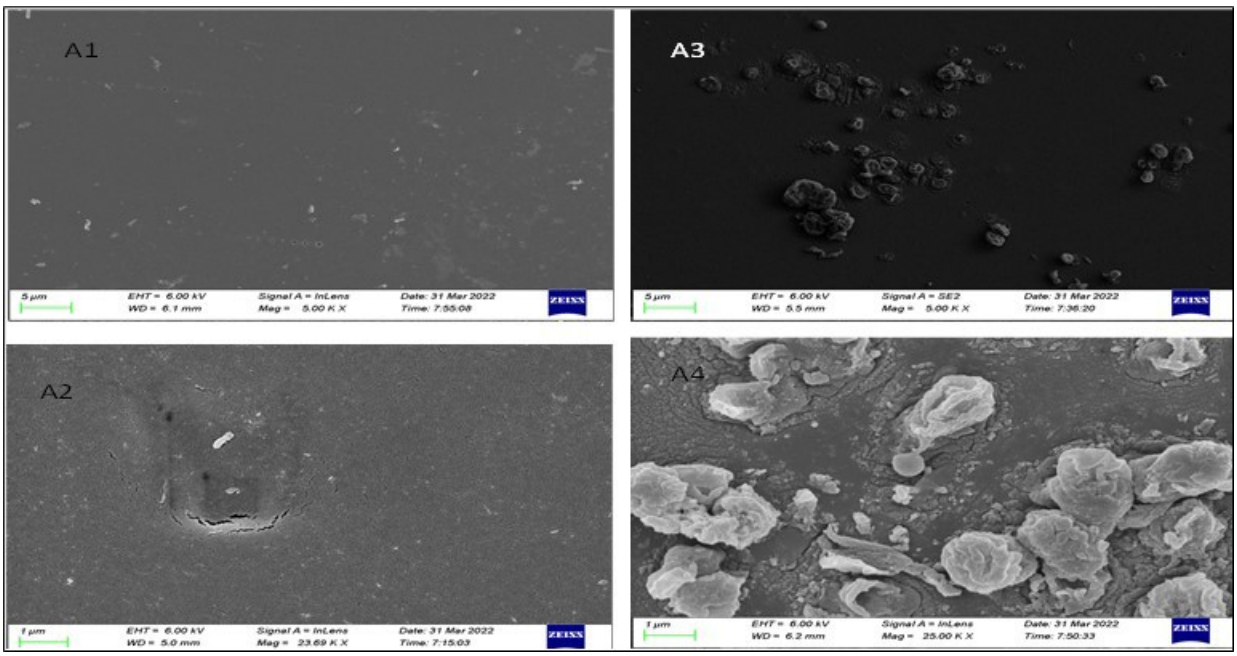


Figure 5. 19 SEM image of hydrogel disc explanted after 4 weeks. (A3 and A4). A1 and A2 are unimplanted control of the same hydrogel at equivalent magnifications.

pro inflammatory markers (Rostam et al., 2016) Their study showed that increasing the hydrophilicity of polystyrene via plasma O_2 etching caused the polarization of macrophages toward the M1 pro inflammatory end. Even though there are conflicting reports on the influence of surface wettability on the macrophage phenotype polarization, it is clear that the type and conformation of adsorbed protein on a surface determines the polarization of macrophages since macrophages will

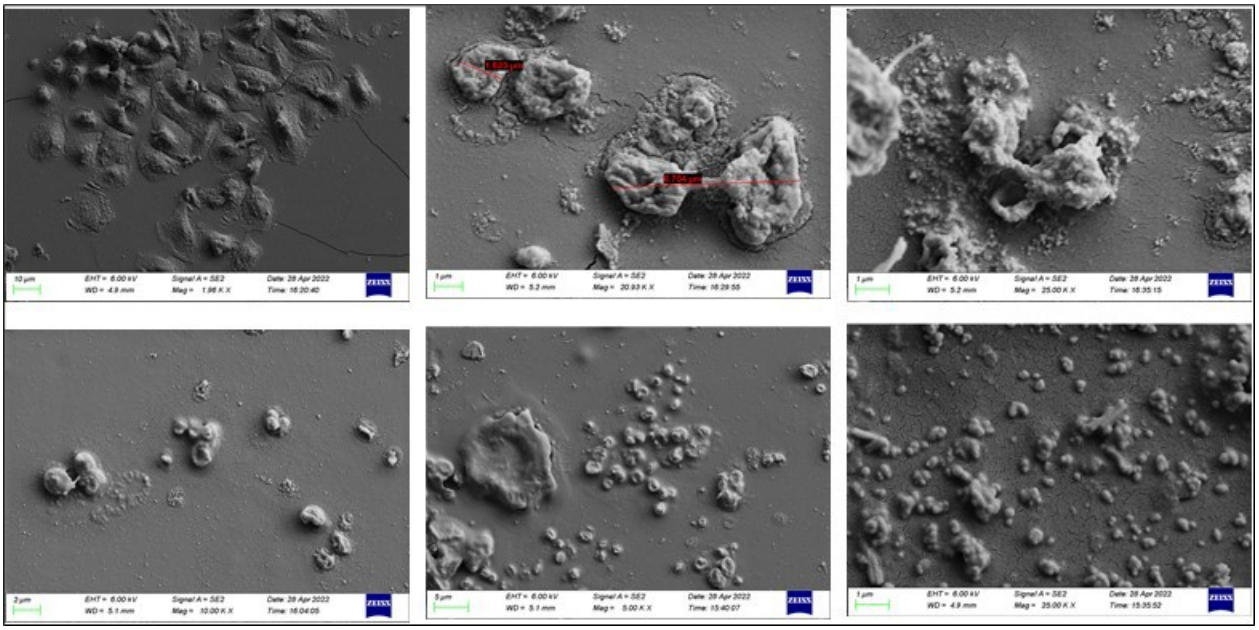


Figure 5.20 SEM images of cells identified on representative hydrogels explanted after 8 weeks.

adhere to any surface in their natural line of duty irrespective of the surface wettability particularly in the presence of tissue injury during implantation. In addition, other biomaterial properties such as topography and stiffness contribute to protein adhesion and invariably to macrophage adhesion and polarization. In all these, the importance of *in vivo* confirmatory studies is further brought to the fore. What is of overriding importance is the need to design biomaterial surfaces that polarize macrophages towards the specific requirements of the particular application intended. This *in vivo* study undertaken here has shown that the observed macrophage adhesion onto the implant caused a macrophage polarization toward anti-inflammatory end given the absence of inflammation after one week.

5.3.7 Characterization of CysA loaded gels

The FTIR spectra of drug loaded and unloaded hydrogels for different hydrogel formulations are displayed in **Figure 5.21** and **Figure 5.22**. The two sides of each hydrogel were examined and the FTIR spectra of both sides differed in terms of the functional groups identified on the surfaces. In addition, The spectra of the drug loaded hydrogel on one side tallied with the spectra of pure cyclosporine for all the hydrogels. Likewise, in the DSC thermogram shown in **Figure 5.23**, the

crystallization exotherm in the thermogram signals the presence of the crystalline SBMA in the hydrogel. There was a general shift in the Tg temperature of the hydrogels upwards from the transferosome-preloaded gels to the pure drug loaded hydrogel to the xerogel loaded by soaking. The shift was in reverse order for the melting endotherms of the three hydrogels. The thermal events that appeared in the pure cyclosporine A were not detected in the thermal event of all the hydrogels irrespective of the CysA loading method.

5.3.8 In vitro cyclosporine A release from hydrogels

Figure 5.24 and **Figure 5.25** depict the *in vitro* release profile from the hydrogels loaded using different approaches. These profiles were fitted to various models that have been used for mechanistic delineation of release from different matrix. Based on model parameters listed in **Table 5.3**, the Korsmeyer-Peppas model was chosen as the best model that describes the release from the hydrogels and has been used previously to describe drug release from polymers. The n factor describes the mechanism of release for such models. An n factor of 0.5 describes release by Fickian diffusion while a value that lies between 0.5 and 0.89 describes non-Fickian diffusion. Results show that the amount of drug released from the hydrogels S2 and L2 obeyed Fickian diffusion in which the amount of drug released is independent of the initial drug loading in the matrix. (Lisik & Musiał, 2019) Many models have described drug release from dry hydrogels in which both swelling, diffusion, and erosion contribute to the release of drug from the hydrogel particularly for tablet dosage forms. (Caccavo et al., 2015). Hydrogels used as implant, contact lenses, intraocular lenses, punctal plugs, etc. are used in an already swollen or hydrated state hence the contributions of swelling to the release of the drug may be considered insignificant. Deswelling may play an important role in such a process for contact lens applications where the hydration of the hydrogel depends partially on the pH of the post lens tear film (POLTF). (Lattimore et al., 2018) Other factor that will impact the release of drug from swollen hydrogels are the pore size viz-a-viz the size of the drug, polarity of the drug, and the form in which the drug exists in the hydrogel.

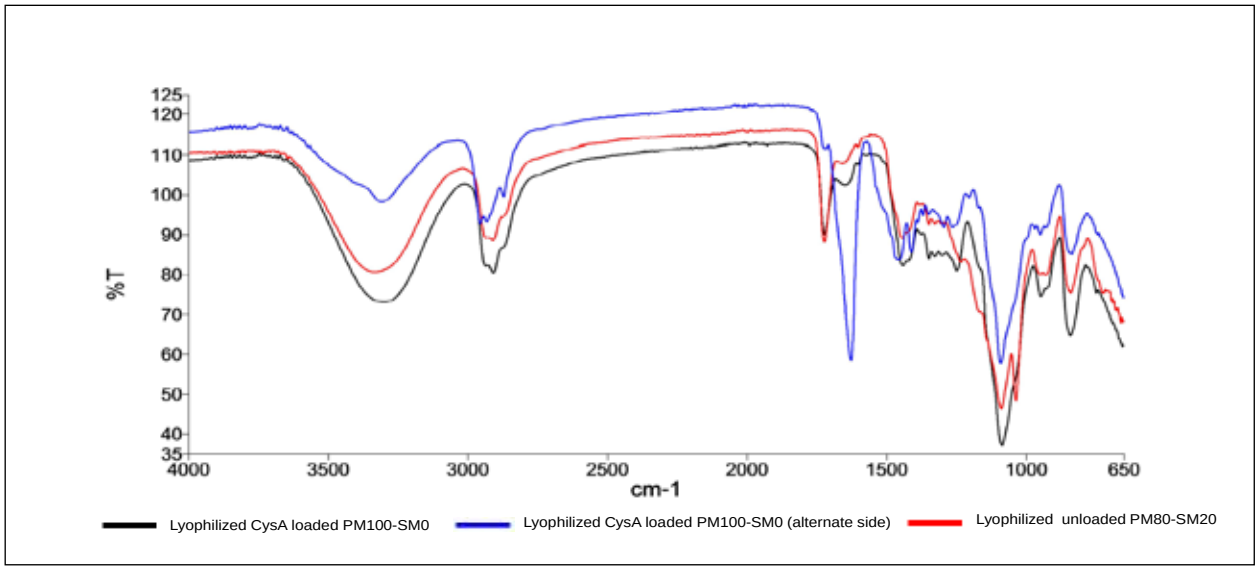


Figure 5.21 Comparative FTIR of CysA-loaded and unloaded PM80-SM20.

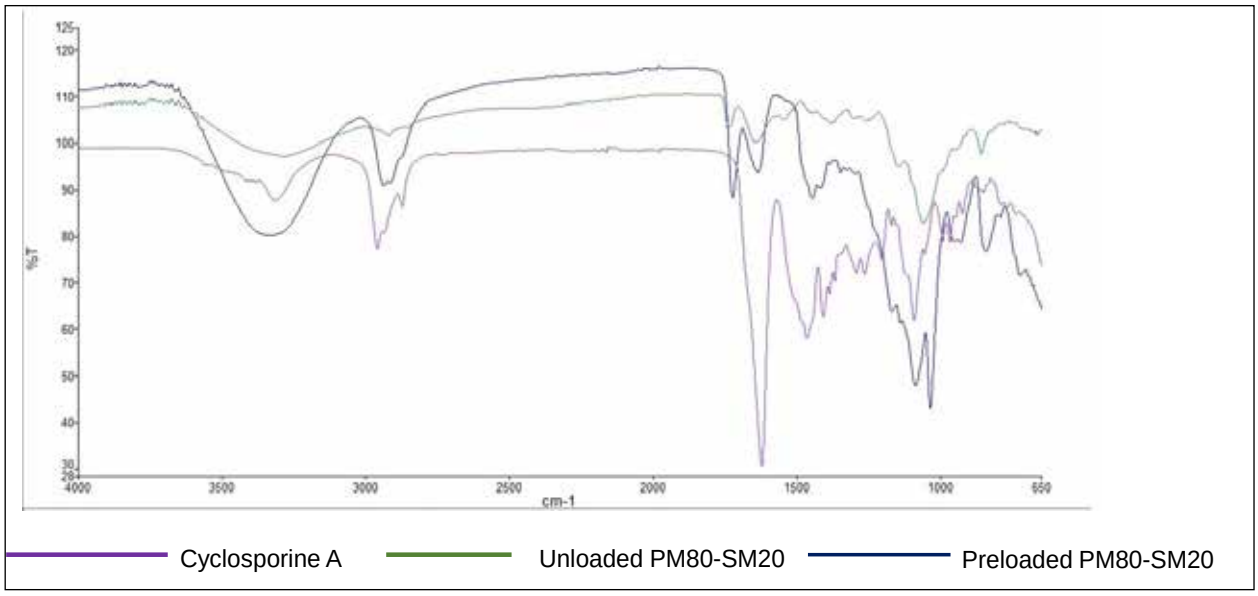


Figure 5.22 FTIR of unloaded and preloaded PM80-SM20.

For instance, Kapoor and colleagues posited that CysA existed as adsorbed particles unto the HEMA hydrogel matrix rather than in a dissolved state in the hydration water and this contributed to their release modelling. (Kapoor et al., 2017) When the release rate is compared based on the zwitterionic content of the hydrogel, the rates increased with increase in the SBMA content across both lyophilized and soaked hydrogel. It is possible that using methanol as a loading solvent for the hydrogels served as an effective carrier to convey the hydrophobic CysA into the hydrogel matrix. Subsequent diffusion from the matrix during the release process was hindered due the poor solubility of CysA in the water swollen hydrogel. This became even more obvious when the release rates between the lyophilised and the soaked hydrogels are compared. The process of lyophilization transforms the hydrogels to xerogels effectively stripping the hydration layer of the bound water molecules. This does not happen when hydrogels are dried in the vacuum oven. During the release process, there could be a potential competition between the super hydrophilic zwitterionic component of the hydrogel and the CysA bound to the xerogel.

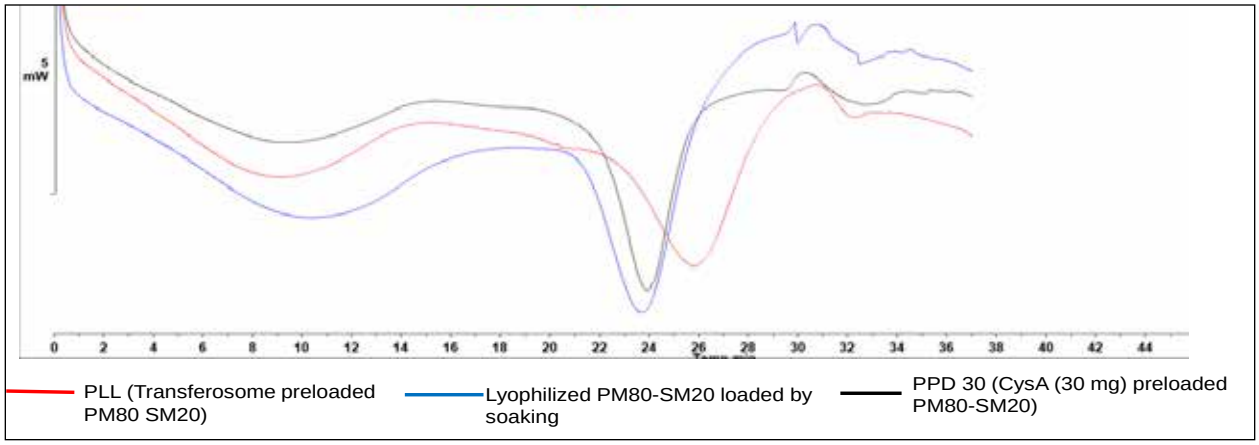


Figure 5.4 DSC of transferosome preloaded, pure drug preloaded, and xerogel loaded by soaking.

As the hydration layer water gets back to the zwitterionic, there is a gradual displacement of the bound drug leading to the release of the drug. The alternate method studied in this report in which both pure drug and drug loaded nanosystems were included in the hydrogel precursor mixture led to a burst release in the first 1 hour. This was followed by a plateau over which the total amount of drug released over the following 13 days was less than 20 % of the amount released in the first 1 hour across both the pure drug and the nanosystems

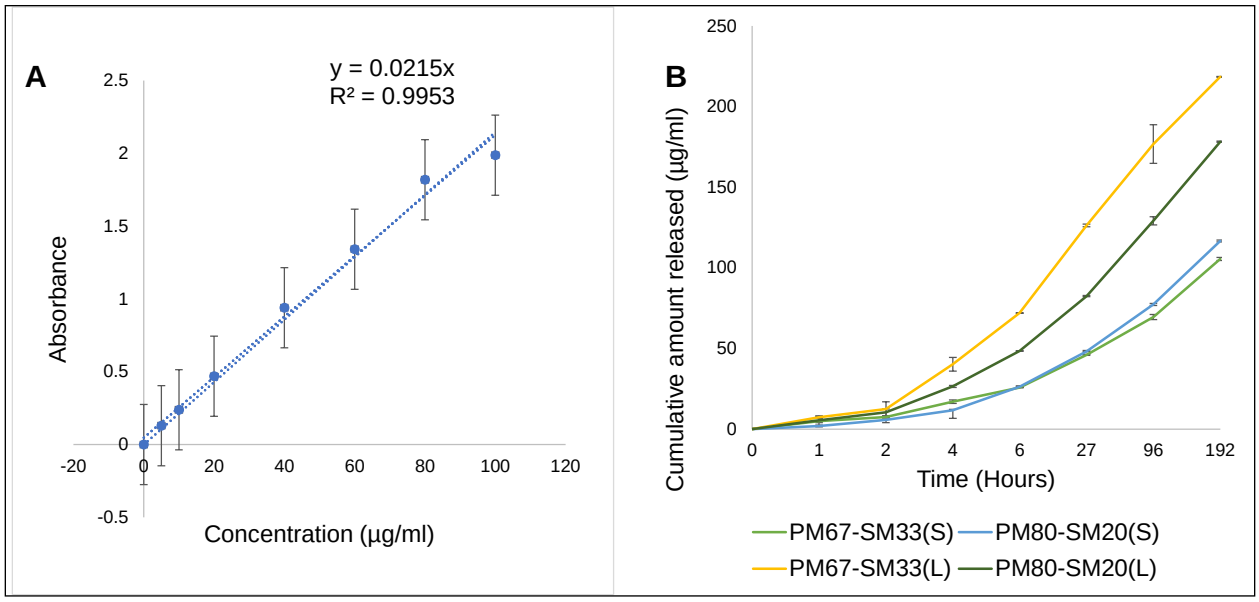


Figure 5.5 Calibration curve of CysA at wavelength of 213 (A) and trend of release over time (B)

loaded hydrogels. The profile shown in **Figure 5.25**B could not be fitted into any of the major drug release models. A comparison was attempted between this observation and that found in previous studies in which both the pure drug and a nano system such as micelles was loaded into a hydrogel. Xu and colleagues (Xu et al., 2019) studied the release of timolol and latanoprost from a micelle loaded hydroxyethyl methacrylate hydrogel contact lens prepared in a similar process. The *in vitro* release profile obtained in their study is similar to that observed in this study. In another study, Xu and colleagues prepared hydrogel contact lens in which bimatoprost microemulsion was loaded using the soaking method. (Xu et al., 2019) In their study, contact lenses was soaked in the microemulsion for 7 days. In all these, the process of preparing the nanosystems increased the complexity of the entire process and may have serious implications for scale up and commercialization. In one of the studies, the effect of protein adsorption was studied leading to ultimate roughening of the hydrogel lens over time. (Xu et al., 2019) This may have serious implications for sight eventually should such a product eventually be commercialized as it is. This issue was addressed in the ocuterial developed in this report.

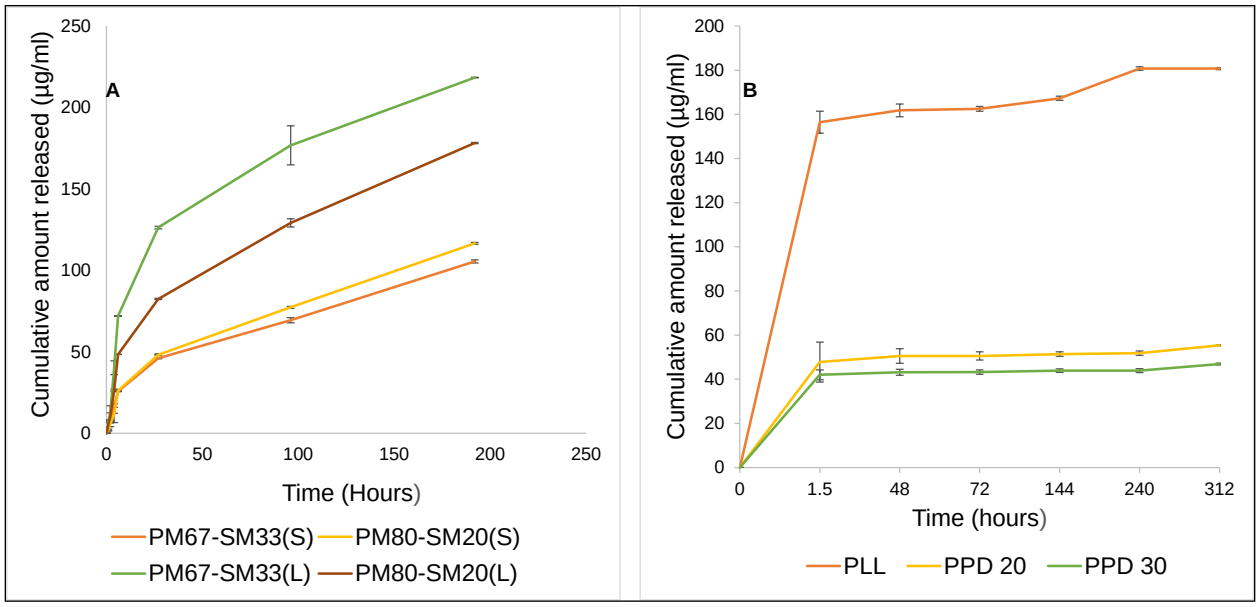


Figure 5.25 *In vitro* release profile from hydrogels in which CysA was loaded after (A) and before (B) crosslinking.

5.4 Conclusions

Herein, the resistance to protein adhesion, cell adhesion and the effect on the anti-biofouling potential of the developed hydrogel discs has been demonstrated. *In vitro* cell studies demonstrated the ability of the ocuterial to limit cell adhesion while being safe to the sensitive retinal cells. Similarly, the ability of the developed ocuterial to limit biofilm formation was equally demonstrated. These findings were corroborated by the *in vivo* implantation in the sub conjunctival space of New Zealand albino rabbits that demonstrated the ability of the hydrogel to limit inflammatory response to an implanted ocuterial. In addition, the contributions of zwitterionization to the drug release process from the new PVA-GMA ocular hydrogel is promising for the delivery of hydrophobic drugs. The zwitterionic monomer, sulfobetaine methacrylate in conjunction with lyophilisation led to effective drug loading of a hydrophobic drug with a potential for sustained drug release from a 6 x 0.75 mm hydrogel disc.

Table 5.3 Parameters from modeling release from hydrogels.

Name	Korsmeyer-Peppas					Higuchi				Hixson-Crowell			
	kKP	N	R^2Adj	MSC	AIC	Kh	R^2Adj	MSC	AIC	kHC	R^2Adj	MSC	AIC
PM80-SM20(S)	4.69	0.59	0.985	3.59	38.76	7.17	0.97	3.37	40.31	0.004	0.96	2.96	43.18
PM67-SM33(S)	5.30	0.54	0.985	3.81	35.10	6.46	0.98	3.90	34.41	0.003	0.94	2.49	44.34
PM80-SM20(L)	12.895	0.488	0.976	3.36	46.73	12.18	0.98	3.63	44.83	0.010	0.95	2.68	51.51
PM67-SM33 (L)	22.989	0.428	0.938	2.40	57.3	16.39	0.94	2.46	56.86	0.011	0.74	1.08	66.53

References

Acosta, A. C., Espana, E. M., Yamamoto, H., Davis, S., Pinchuk, L., Weber, B. A., Orozco, M., Dubovy, S., Fantes, F., & Parel, J.-M. (2006). A Newly Designed Glaucoma Drainage Implant Made of Poly(styrene-b-isobutylene-b-styrene): Biocompatibility and Function in Normal Rabbit Eyes. *Archives of Ophthalmology*, *124*(12), 1742–1749. https://doi.org/10.1001/archopht.124.12.1742

Arnous, R., Arshad, S., Sandgren, K., Cunningham, A. L., Carnt, N., & White, A. (2022). Tissue resident memory T cells inhabit the deep human conjunctiva. *Scientific Reports*, *12*(1), 6077. https://doi.org/10.1038/s41598-022-09886-3

Ashtiani, M. K., Zandi, M., Shokrollahi, P., Ehsani, M., & Baharvand, H. (2018). Surface modification of poly(2-hydroxyethyl methacrylate) hydrogel for contact lens application. *Polymers for Advanced Technologies*, *29*(4), 1227–1233. https://doi.org/10.1002/pat.4233

Bacteria survive longer in contact lens cleaning solution than previously thought, study shows. (n.d.). ScienceDaily. Retrieved 22 April 2022, from https://www.sciencedaily.com/releases/2014/04/140416190926.htm

Bartoli, C. R., Nadar, M. M., & Godleski, J. J. (2010). Capsule Thickness Correlates With Vascular Density and Blood Flow Within Foreign-Body Capsules Surrounding Surgically Implanted Subcutaneous Devices. *Artificial Organs*, *34*(10), 857–861. https://doi.org/10.1111/j.1525-1594.2010.01024.x

Boone, A., Heynen, M., Joyce, E., Varikooty, J., & Jones, L. (2009). Ex Vivo Protein Deposition on Bi-Weekly Silicone Hydrogel Contact Lenses. *Optometry and Vision Science*, *86*(11), 1241–1249. https://doi.org/10.1097/OPX.0b013e3181bbc1b3

Caccavo, D., Cascone, S., Lamberti, G., & Barba, A. A. (2015). Controlled drug release from hydrogel-based matrices: Experiments and modeling. *International Journal of Pharmaceutics*, *486*(1), 144–152. https://doi.org/10.1016/j.ijpharm.2015.03.054

Chew, S. C., & Yang, L. (2016). Biofilms. In B. Caballero, P. M. Finglas, & F. Toldrá (Eds.), *Encyclopedia of Food and Health* (pp. 407–415). Academic Press. https://doi.org/10.1016/B978-0-12-384947-2.00069-6

Chou, Y.-N., Sun, F., Hung, H.-C., Jain, P., Sinclair, A., Zhang, P., Bai, T., Chang, Y., Wen, T.-C., Yu, Q., & Jiang, S. (2016). Ultra-low fouling and high antibody loading zwitterionic hydrogel coatings for sensing and detection in complex media. *Acta Biomaterialia*, *40*, 31–37. https://doi.org/10.1016/j.actbio.2016.04.023

Dantam, J., Subbaraman, L. N., & Jones, L. (2020). Adhesion of Pseudomonas aeruginosa, Achromobacter xylosoxidans, Delftia acidovorans, Stenotrophomonas maltophilia to contact lenses under the influence of an artificial tear solution. *Biofouling*, *36*(1), 32–43. https://doi.org/10.1080/08927014.2019.1710832

Fujii, K., Matsumoto, H. N., Koyama, Y., Iwasaki, Y., Ishihara, K., & Takakuda, K. (2008). Prevention of Biofilm Formation with a Coating of 2-Methacryloyloxyethyl Phosphorylcholine Polymer. *Journal of Veterinary Medical Science*, *70*(2), 167–173. https://doi.org/10.1292/jvms.70.167

Goda, T., Matsuno, R., Konno, T., Takai, M., & Ishihara, K. (2009). Protein adsorption resistance and oxygen permeability of chemically crosslinked phospholipid polymer hydrogel for ophthalmologic biomaterials. *Journal of Biomedical Materials Research. Part B, Applied Biomaterials*, *89*(1), 184–190. https://doi.org/10.1002/jbm.b.31204

Gordon, S., & Plüddemann, A. (2017). Tissue macrophages: Heterogeneity and functions. *BMC Biology*, *15*(1), 53. https://doi.org/10.1186/s12915-017-0392-4

Hilhorst, M., Shirai, T., Berry, G., Goronzy, J. J., & Weyand, C. M. (2014). T Cell–Macrophage Interactions and Granuloma Formation in Vasculitis. *Frontiers in Immunology*, *5*. https://www.frontiersin.org/article/10.3389/fimmu.2014.00432

Huang, K.-T., Fang, Y.-L., Hsieh, P.-S., Li, C.-C., Dai, N.-T., & Huang, C.-J. (2016). Zwitterionic nanocomposite hydrogels as effective wound dressings. *Journal of Materials Chemistry B*, *4*(23), 4206–4215. https://doi.org/10.1039/C6TB00302H

Ishihara, K., Fukazawa, K., Sharma, V., Liang, S., Shows, A., Dunbar, D. C., Zheng, Y., Ge, J., Zhang, S., Hong, Y., Shi, X., & Wu, J. Y. (2021). Antifouling Silicone Hydrogel Contact Lenses with a Bioinspired 2-Methacryloyloxyethyl Phosphorylcholine Polymer Surface. *ACS Omega*, *6*(10), 7058–7067. https://doi.org/10.1021/acsomega.0c06327

Jamal, M., Ahmad, W., Andleeb, S., Jalil, F., Imran, M., Nawaz, M. A., Hussain, T., Ali, M., Rafiq,

M., & Kamil, M. A. (2018). Bacterial biofilm and associated infections. *Journal of the Chinese Medical Association*, *81*(1), 7–11. https://doi.org/10.1016/j.jcma.2017.07.012

Jansen, L. E., Amer, L. D., Chen, E. Y.-T., Nguyen, T. V., Saleh, L. S., Emrick, T., Liu, W. F., Bryant, S. J., & Peyton, S. R. (2018). Zwitterionic PEG-PC Hydrogels Modulate the Foreign Body Response in a Modulus-Dependent Manner. *Biomacromolecules*, *19*(7), 2880–2888. https://doi.org/10.1021/acs.biomac.8b00444

Kapoor, Y., Dixon, P., Sekar, P., & Chauhan, A. (2017). Incorporation of drug particles for extended release of Cyclosporine A from poly-hydroxyethyl methacrylate hydrogels. *European Journal of Pharmaceutics and Biopharmaceutics*, *120*, 73–79. https://doi.org/10.1016/j.ejpb.2017.08.007

Larrañeta, E., Stewart, S., Ervine, M., Al-Kasasbeh, R., & Donnelly, R. F. (2018). Hydrogels for Hydrophobic Drug Delivery. Classification, Synthesis and Applications. *Journal of Functional Biomaterials*, *9*(1), 13. https://doi.org/10.3390/jfb9010013

Lattimore, M. R., Harding, T. H., & Williams, S. T. (2018). Hydrogel Contact Lens Water Content is Dependent on Tearfilm pH. *Military Medicine*, *183*(suppl_1), 224–230. https://doi.org/10.1093/milmed/usx233

Lisik, A., & Musiał, W. (2019). Conductomeric Evaluation of the Release Kinetics of Active Substances from Pharmaceutical Preparations Containing Iron Ions. *Materials*, *12*(5), 730. https://doi.org/10.3390/ma12050730

Lužajić Božinovski, T., Todorović, V., Milošević, I., Prokić, B. B., Gajdov, V., Nešović, K., Mišković-Stanković, V., & Marković, D. (2022). Macrophages, the main marker in biocompatibility evaluation of new hydrogels after subcutaneous implantation in rats. *Journal of Biomaterials Applications*, *36*(6), 1111–1125. https://doi.org/10.1177/08853282211046119

Lynch, C. R., Kondiah, P. P. D., Choonara, Y. E., du Toit, L. C., Ally, N., & Pillay, V. (2020). Hydrogel Biomaterials for Application in Ocular Drug Delivery. *Frontiers in Bioengineering and Biotechnology*, *8*. https://www.frontiersin.org/article/10.3389/fbioe.2020.00228

Mahale, A., Othman, M. W., Shahwan, S. A., Jadaan, I. A., Owaydha, O., Khan, Z., & Edward, D. P. (2015). Altered Expression of Fibrosis Genes in Capsules of Failed Ahmed Glaucoma Valve Implants. *PLOS ONE*, *10*(4), e0122409. https://doi.org/10.1371/journal.pone.0122409

Maity, S., & Sarkar, A. (2017). 4—Monitoring fibrous capsule formation. In R. J. Narayan (Ed.), *Monitoring and Evaluation of Biomaterials and their Performance In Vivo* (pp. 69–80). Woodhead Publishing. https://doi.org/10.1016/B978-0-08-100603-0.00004-3

McAnally, C., Walters, R., Campolo, A., Harris, V., King, J., Thomas, M., Gabriel, M. M., Shannon, P., & Crary, M. (2021). Antimicrobial Efficacy of Contact Lens Solutions Assessed by ISO Standards. *Microorganisms*, *9*(10), 2173. https://doi.org/10.3390/microorganisms9102173

Ramsay, E., del Amo, E. M., Toropainen, E., Tengvall-Unadike, U., Ranta, V.-P., Urtti, A., & Ruponen, M. (2018). Corneal and conjunctival drug permeability: Systematic comparison and pharmacokinetic impact in the eye. *European Journal of Pharmaceutical Sciences*, *119*, 83–89. https://doi.org/10.1016/j.ejps.2018.03.034

Rohner, N. A., Learn, G. D., Wiggins, M. J., Woofter, R. T., & von Recum, H. A. (2021). Characterization of Inflammatory and Fibrotic Encapsulation Responses of Implanted Materials with Bacterial Infection. *ACS Biomaterials Science & Engineering*, *7*(9), 4474–4482. https://doi.org/10.1021/acsbiomaterials.1c00505

Rostam, H. M., Singh, S., Salazar, F., Magennis, P., Hook, A., Singh, T., Vrana, N. E., Alexander, M. R., & Ghaemmaghami, A. M. (2016). The impact of surface chemistry modification on macrophage polarisation. *Immunobiology*, *221*(11), 1237–1246. https://doi.org/10.1016/j.imbio.2016.06.010

Selan, L., Palma, S., Scoarughi, G. L., Papa, R., Veeh, R., Di Clemente, D., & Artini, M. (2009). Phosphorylcholine impairs susceptibility to biofilm formation of hydrogel contact lenses. *American Journal of Ophthalmology*, *147*(1), 134–139. https://doi.org/10.1016/j.ajo.2008.07.032

Shen, M., & Horbett, T. A. (2001). The effects of surface chemistry and adsorbed proteins on monocyte/macrophage adhesion to chemically modified polystyrene surfaces. *Journal of Biomedical Materials Research*, *57*(3), 336–345. https://doi.org/10.1002/1097-4636(20011205)57:3<336::aid-jbm1176>3.0.co;2-e

Skeie, J. M., Roybal, C. N., & Mahajan, V. B. (2015). Proteomic Insight into the Molecular Function of the Vitreous. *PLoS ONE*, *10*(5), e0127567. https://doi.org/10.1371/journal.pone.0127567

Sobolčiak, P., Popelka, A., Mičušík, M., Sláviková, M., Krupa, I., Mosnáček, J., Tkáč, J., Lacík, I., & Kasák, P. (2017). Photoimmobilization of zwitterionic polymers on surfaces to reduce cell

adhesion. *Journal of Colloid and Interface Science*, *500*, 294–303. https://doi.org/10.1016/j.jcis.2017.04.020

Stastna, M., Behrens, A., McDonnell, P. J., & Van Eyk, J. E. (2011). Analysis of protein composition of rabbit aqueous humor following two different cataract surgery incision procedures using 2-DE and LC-MS/MS. *Proteome Science*, *9*, 8. https://doi.org/10.1186/1477-5956-9-8

Tan, X., Zhan, J., Zhu, Y., Cao, J., Wang, L., Liu, S., Wang, Y., Liu, Z., Qin, Y., Wu, M., Liu, Y., & Ren, L. (2017). Improvement of Uveal and Capsular Biocompatibility of Hydrophobic Acrylic Intraocular Lens by Surface Grafting with 2-Methacryloyloxyethyl Phosphorylcholine-Methacrylic Acid Copolymer. *Scientific Reports*, *7*, 40462. https://doi.org/10.1038/srep40462

Traxinger, B. R., Richert-Spuhler, L. E., & Lund, J. M. (2022). Mucosal tissue regulatory T cells are integral in balancing immunity and tolerance at portals of antigen entry. *Mucosal Immunology*, *15*(3), 398–407. https://doi.org/10.1038/s41385-021-00471-x

Uwaezuoke, O. J., Kumar, P., Pillay, V., & Choonara, Y. E. (2021). Fouling in ocular devices: Implications for drug delivery, bioactive surface immobilization, and biomaterial design. *Drug Delivery and Translational Research*. https://doi.org/10.1007/s13346-020-00879-1

Vigata, M., Meinert, C., Hutmacher, D. W., & Bock, N. (2020). Hydrogels as Drug Delivery Systems: A Review of Current Characterization and Evaluation Techniques. *Pharmaceutics*, *12*(12), 1188. https://doi.org/10.3390/pharmaceutics12121188

Vishwakarma, A., Bhise, N. S., Evangelista, M. B., Rouwkema, J., Dokmeci, M. R., Ghaemmaghami, A. M., Vrana, N. E., & Khademhosseini, A. (2016). Engineering Immunomodulatory Biomaterials To Tune the Inflammatory Response. *Trends in Biotechnology*, *34*(6), 470–482. https://doi.org/10.1016/j.tibtech.2016.03.009

Wang, Y., Shen, J., & Yuan, J. (2016). Design of hemocompatible and antifouling PET sheets with synergistic zwitterionic surfaces. *Journal of Colloid and Interface Science*, *480*, 205–217. https://doi.org/10.1016/j.jcis.2016.07.022

Xu, J., Ge, Y., Bu, R., Zhang, A., Feng, S., Wang, J., Gou, J., Yin, T., He, H., Zhang, Y., & Tang, X. (2019). Co-delivery of latanoprost and timolol from micelles-laden contact lenses for the treatment of glaucoma. *Journal of Controlled Release*, *305*, 18–28. https://doi.org/10.1016/j.jconrel.2019.05.025

Xu, W., Jiao, W., Li, S., Tao, X., & Mu, G. (2019). Bimatoprost loaded microemulsion laden contact lens to treat glaucoma. *Journal of Drug Delivery Science and Technology*, *54*, 101330. https://doi.org/10.1016/j.jddst.2019.101330

Xu, Z., Hwang, D.-G., Bartlett, M. D., Jiang, S., & Bratlie, K. M. (2021). Alter macrophage adhesion and modulate their response on hydrophobically modified hydrogels. *Biochemical Engineering Journal*, *165*, 107821. https://doi.org/10.1016/j.bej.2020.107821

Young, J. B., Keppel, T. R., Waas, M., Salmon, A. E., Buchberger, A. R., Skumatz, C. M. B., Gundry, R. L., & Kassem, I. S. (2020). Quantitative proteomic analysis of aqueous humor after rabbit lensectomy reveals differences in coagulation and immunomodulatory proteins. *Molecular Omics*, *16*(2), 126–137. https://doi.org/10.1039/C9MO00169G

Zhang, P., Sun, F., Tsao, C., Liu, S., Jain, P., Sinclair, A., Hung, H.-C., Bai, T., Wu, K., & Jiang, S. (2015). Zwitterionic gel encapsulation promotes protein stability, enhances pharmacokinetics, and reduces immunogenicity. *Proceedings of the National Academy of Sciences*, *112*(39), 12046–12051. https://doi.org/10.1073/pnas.1512465112

Zhang, Z., Chao, T., Liu, L., Cheng, G., Ratner, B. D., & Jiang, S. (2009). Zwitterionic hydrogels: An in vivo implantation study. *Journal of Biomaterials Science. Polymer Edition*, *20*(13), 1845–1859. https://doi.org/10.1163/156856208X386444

CHAPTER SIX

CONCLUSION AND RECOMMENDATIONS

6.1 Concluding remarks

In this study, a new protein resistant hydrogel material was developed by the zwitterionization of PVA methacrylate via a facile photo-initiated crosslinking polymerization process. The physical and chemical properties of the developed hydrogel was determined to evaluate its suitability as an ocuterial and alignment of its properties to that expected of ocuterials. More importantly, the protein resistance potential that underpins many of the challenges confronting implantable ocular devices was studied. The features of the developed hydrogel show it has the potential to be used as an implantable sustained drug delivery system device for hydrophobic bioactives such as CysA. Some of the core properties such as the transmissibility, swelling and by implication, oxygen permeability, mechanical robustness, and protein adhesion resistance, makes it a candidate as an anti-fouling implantable biomaterial. In future, the fabrication process is such that moulding or 3D printing can be explored and used for large scale production od contact lenses for drug delivery. For this application, the properties of the hydrogel precursor mixture with respect viscosity should be tuned towards that required for 3D bioinks by manipulating the polymer content.

Zwitterionics are super-hydrophilic compounds that are heavily deficit in terms of mechanical strength and has rarely been used for mechanical reinforcement. In this study, the strength was improved by combination with another hydrophilic polymer, PVA. Despite having a swelling value of over 300%, hydrogels developed in this study had sufficient mechanical strength requisite for handing. with forceps. The mechanical strength was not compromised by implantation in the sub conjunctiva of the rabbits' eye, and as such, explanted after 8 weeks in an intact form and shape. This property is very important considering the soft nature of the eye and the possible contributions of stiff materials to inflammation in the ocular environment. The contributions of synergy between two highly hydrophilic compounds to limiting the biofilm adhesion potential to a biomaterial became obvious through this study as the bacterial adhesion of the best modified hydrogel was orders of magnitude lower than that that has been obtained in any study till date based on our literature search to date.

The results of *in vitro* drug release have also, for the first time, shown that zwitterionic polymers could be playing a new role in the delivery of poorly water-soluble drugs. Hence an approach towards using zwitterionics as adjuncts to improve drug delivery of hydrophobic drugs from hydrophilic hydrogels, a hitherto very complex and difficult task in terms of drug loading, is hypothesised. *In vitro* release characteristics of the prepared hydrogel may be positioning the hydrogel for potential use in the sustained delivery of hydrophobic drugs.

6.2 Future perspectives

The difference in protein adhesion potential of zwitterionized polyvinyl alcohol methacrylate hydrogel from *in vitro* protein adhesion and that from *ex vivo* ocular fluids calls for further investigation. This work has established the need for the streamlining of *in vitro* experimental standards. Different researchers have previously shown that not every protein adhered unto a biomaterial has negative effect. In this study, it is possible that the close resemblance between the modifying SBMA used in this study to membrane proteins may cause a polarisation of macrophages towards the M2 anti-inflammatory phenotypes as a result of being identified as 'self'. In addition, the need to try out or analyse materials specific to the eye using the ocular environment is brought to the fore. From the *in vivo* implantation study, questions about the extrusion capability of the conjunctiva which has not been previously studied arises as two of the implants were not found in 2 out of the 15 rabbits used in this study particularly if the subconjunctival implantation route which is minimally invasive and fast is under consideration. There is also an additional need to explore the *in vivo* drug delivery from the hydrogel and corelate it with the *in vitro* release properties. Based on the properties of the hydrogel precursor fluid, we propose that, 3D printing could be explored as a preferred method of fabrication particularly if the hydrogel is to be applied as an extended wear contact lens for drug delivery applications. Through this avenue, unloaded hydrogels could be used to print the part of the core of the lens while drug loaded precursor be used to print the outer region so that transparency is not compromised by high drug loading. This may be particularly important for drug delivery applications targeting the many disease of the ocular surface. There is also a need to further evaluate the ocular toxicity and drug delivery potential from the transferosomes developed in this study as a stand-alone formulation either as a topical formulation or as a subconjunctival injection as it holds potential for extended release.

Appendix A. Animal Ethics Certificate

ANIMALS RESEARCH ETHICS COMMITTEE (AREC)

UNIVERSITY OF THE WITWATERSRAND, JOHANNESBURG

STRICTLY CONFIDENTIAL

CLEARANCE CERTIFICATE NUMBER: 2021/03/07/C

APPLICANT: Ms OJ Owaezuoke
School: School of Therapeutic Sciences; Department: N/A; Location: WRAF

PROJECT TITLE: In vivo evaluation of a bioinspired protein resistant ocular biomaterial (BioPROT) in Albino New Zealand rabbits
Category: C; Species and Numbers involved: *70X 2.5 - 3.5 kg male or female, Albino New Zealand rabbits*

Approval is hereby given for the use of animals for the research project named above and described in the application reviewed by a quorate meeting of the AREC held on 30 Mar 2021. This approval remains valid until 20 May 2021 and is conditional to the following (if blank there are no special conditions):

Condition 1	Condition 2	Condition 3	Condition 4
Liaise with the WRAF staff about the feasibility of using an Elizabethan collar if irritation of the eyes			

All material changes to the approved research must be reported to the AREC before they are implemented. Failure to do so will invalidate this clearance certificate.

An annual progress report must be provided to the AREC.

The use of these animals is subject to AREC guidelines on the use and care of laboratory animals, is limited to the procedures described in the application and is subject to additional conditions listed below:

I, the Chair of the AREC (or my designated representative) am satisfied that the proposed research is ethical as judged by local law, international standards and University policy.

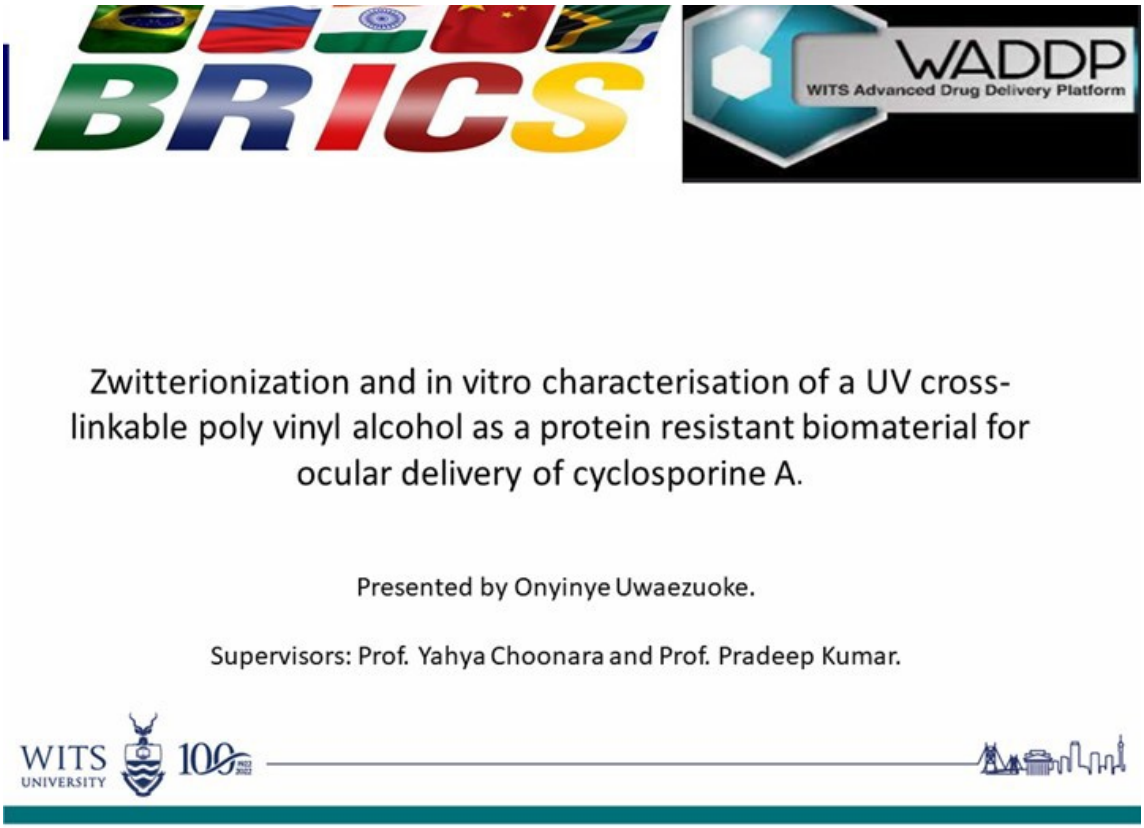
Signed: _____ _____ Date: __21/05/2021_____

(Chairperson of the AREC)

I am satisfied that the persons listed in this application are competent to perform the procedures described in the application, in the context of Section 23 (1) (c) of the veterinary and Para-veterinary Professions Act (19 of 1982).

CC: Student supervisor: «Title1» «Initials1» «Supervisor_surname»
Director Wits Research Animal Facility (WRAF): Dr Kim Jardine

Appendix B. Oral presentation at the BRICS Conference hosted by South Africa November 2021.



Appendix C. Certificate of participation for the PhD seminar competition, 2020



UNIVERSITY OF THE WITWATERSRAND, JOHANNESBURG

Postgraduate Affairs
Research Office

CERTIFICATE OF PARTICIPATION

AWARDED TO

Onyinye Jennifer Uwaezuoke

for presenting a paper at the first edition of **The Wits PhD Seminar** - an exclusive cross-faculty competition held on 29 & 30 September 2020.

The competition was an opportunity for postgraduate students to display their intellectual adaptability, disciplinary flexibility and responsiveness in the face of challenging global topics. The topic chosen for the competition by the Senate Graduate Studies Committee was "PANDEMIC". Sixteen judges selected 23 abstracts from more than a hundred submissions; with a panel of nine judges adjudicating the final competition.

30 September 2020

Professor Joao Rodrigues
Acting DVC: Research & Postgraduate Affairs

Professor Robert Muponde
Director: Postgraduate Affairs (Wits Research Office)

Appendix D. Screenshot of the first page of publication 2

Drug Delivery and Translational Research (2021) 11:1908–1923
https://doi.org/10.1007/s13346-020-00879-1

REVIEW ARTICLE

Fouling in ocular devices: implications for drug delivery, bioactive surface immobilization, and biomaterial design

Onyinye J. Uwaezuoke[1] · Pradeep Kumar[1] · Viness Pillay[1] · Yahya E. Choonara[1]

Accepted: 24 November 2020 / Published online: 16 January 2021
© Controlled Release Society 2021

Abstract
The last 30 years has seen a proliferation of research on protein-resistant biomaterials targeted at designing bio-inert surfaces, which are prerequisite for optimal performance of implantable devices that contact biological fluids and tissues. These efforts have only been able to yield minimal results, and hence, the ideal anti-fouling biomaterial has remained elusive. Some studies have yielded biomaterials with a reduced fouling index among which high molecular weight polyethylene glycols have remained dominant. Interestingly, the field of implantable ocular devices has not experienced an outflow of research in this area, possibly due to the assumption that biomaterials tested in other body fluids can be translated for application in the ocular space. Unfortunately, progression in the molecular understanding of many ocular conditions has brought to the fore the need for treatment options that necessitates the use of anti-fouling biomaterials. From the earliest implanted horsehair and silk seton for glaucoma drainage to the recent mini telescopes for sight recovery, this review provides a concise incursion into the gradual evolution of biomaterials for the design of implantable ocular devices as well as approaches used to overcome the challenges with fouling. The implication of fouling for drug delivery, the design of immune-responsive biomaterials, as well as advanced surface immobilization approaches to support the overall performance of implantable ocular devices are also reviewed.

Keywords Biomaterials · Ocular · Fouling · Protein adsorption · Implantable device · Drug delivery · Immune responsive

Abbreviations

MEMS	Microelectromechanical systems
DME	Diabetic macular edema
AMD	Age-related macular degeneration
FBR	Foreign body response
GDD	Glaucoma drainage device
TF	Tissue factor
PMN	Polymorphonuclear leucocytes
ACAID	Anterior chamber-associated immune deviation
ROS	Reactive oxygen species
TLR	Toll-like receptors
PRR	Pattern recognition receptor
HMGB 1	High mobility group box 1
MCP	Monocyte chemotactic protein
MIP 1β	Macrophage inflammatory protein 1β
DC	Dendritic cells
CLs	Contact lens
IPN or ipn	Interpenetrating polymer networks
MPC	2-Methacryloyloxyethyl phosphorylcholine
PMPC	Poly(2-methacryloyloxyethyl) phosphorylcholine
PSiMA	Poly(bis(trimethylsilyloxy)methylsilylpropyl glycerol methacrylate)
IOL	Intraocular lens
ACO	Anterior capsular opacification
PCO	Posterior capsule opacification
FGF	Fibroblast growth factor
LBL	Layer by layer
ASC	Anterior subcapsular cataract
MIGS	Minimally invasive glaucoma surgery
TBO	Trabeculoctomy
TBE	Trabeculectomy
GFS	Glaucoma filtration surgery
MMPC	2-(Methacryloyloxy)ethyl-[N-(methacryloyloxy)ethyl phosphorylcholine
BSA	Bovine serum albumin
FIH	First in humans

✉ Yahya E. Choonara
yahya.choonara@wits.ac.za

[1] Wits Advanced Drug Delivery Platform Research Unit, Department of Pharmacy and Pharmacology, School of Therapeutic Sciences, Faculty of Health Sciences, University of the Witwatersrand, Johannesburg 2193, South Africa

Appendix E. Screenshot of the first page of publication 1

pharmaceutics

MDPI

Article

Linoleic Acid-Based Transferosomes for Topical Ocular Delivery of Cyclosporine A

Onyinye Uwaezuoke [1], Lisa C. Du Toit [1], Pradeep Kumar [1], Naseer Ally [2] and Yahya E. Choonara [1,*]

[1] Wits Advanced Drug Delivery Platform Research Unit, Department of Pharmacy and Pharmacology, School of Therapeutic Sciences, Faculty of Health Sciences, University of the Witwatersrand, 7 York Road, Parktown, Johannesburg 2193, South Africa
[2] Department of Neurosciences, Division of Ophthalmology, University of the Witwatersrand, 7 York Road, Parktown, Johannesburg 2193, South Africa
* Correspondence: yahya.choonara@wits.ac.za; Tel.: +27-11-717-2274

Abstract: Delivering high-molecular-weight hydrophobic peptides, such as cyclosporine A, across the corneal epithelium remains a challenge that is complicated by other physio-anatomical ocular structures that limit the ocular bioavailability of such peptides. Transferosomes have previously been used to improve transdermal permeability, and have the potential for improving the ocular corneal permeability of applicable drugs. In this study, transferosomes for the potential ocular delivery of cyclosporine A were investigated. Linoleic acid was evaluated for its effect on the stability of the transferosomes and was substituted for a portion of the cholesterol in the vesicles. Additionally, Span® 80 and Tween® 80 were evaluated for their effect on transferosome flexibility and toxicity to ocular cells as edge activators. Attenuated Total Reflectance–Fourier Transform Infrared spectroscopy (ATF-FTIR), differential scanning calorimetry (DSC), and dynamic light scattering (DLS) were used to evaluate the physicochemical parameters of the blank and the cyclosporine A-loaded transferosomes. Cyclosporine A release and corneal permeability were studied in vitro and in a New Zealand albino rabbit corneal model, respectively. The linoleic acid contributed to improved stability and the nano-size of the transferosomes. The Tween®-based formulation was preferred on the basis of a more favorable toxicity profile, as the difference in their corneal permeability was not significant. There was an initial burst release of cyclosporine A in the first 24 h that plateaued over one week. The Tween®-based formulation had a flux of 0.78 µg/cm^2/h. The prepared transferosomes demonstrated biocompatibility in the ocular cell line, adequately encapsulated cyclosporine A, ensured the corneal permeability of the enclosed drug, and were stable over the period of investigation of 4 months at −20 °C.

Keywords: topical ocular drug delivery; transferosomes; linoleic acid; cyclosporine A; nanoparticle drug-delivery systems

check for updates

Citation: Uwaezuoke, O.; Du Toit, L.C.; Kumar, P.; Ally, N.; Choonara, Y.E. Linoleic Acid-Based Transferosomes for Topical Ocular Delivery of Cyclosporine A. *Pharmaceutics* **2022**, *14*, 1695. https://doi.org/10.3390/pharmaceutics14081695

Academic Editors: Hugo Almeida and Ana Catarina Silva

Received: 30 June 2022
Accepted: 5 August 2022
Published: 15 August 2022

Publisher's Note: MDPI stays neutral with regard to jurisdictional claims in published maps and institutional affiliations.

Copyright: © 2022 by the authors. Licensee MDPI, Basel, Switzerland. This article is an open access article distributed under the terms and conditions of the Creative Commons Attribution (CC BY) license (https://creativecommons.org/licenses/by/4.0/).

1. Introduction

Topical ocular delivery is fraught with numerous challenges, arising mainly from the physio-anatomical barriers posed by ocular structures in their normal physiological line of duty [1]. A formidable barrier to topically applied substances is regularly presented by the corneal epithelium, barely permitting the passage of low molecular weight substances by diffusion [2]. The corneal epithelial cells allow the passage of lipophilic drugs that then is barred by the corneal stroma, which is hydrophilic [3]. In addition, the paracellular passage of substances is heavily challenged by the tight junctions presented by the cornea [4]. Consequently, the drive to deliver drugs across the cornea via topical ocular formulations is a continuing venture. There is also the additional challenge of increasing the time that such formulations stay on the ocular surface. This surface residence time is shortened by the blink reflex, as well as the constant flow of the tear film. Various colloidal systems,

Appendix F. Certificate of biofilm analysis

Modderfontein Laboratory Services (Pty) Ltd
Registration Number : 1956/001741/07
P. O. Box 27
Modderfontein
1645
Tel: +27 011 457 1800

Lims ID : 314218-314220

TO: Wits Advanced Drug Discovery Platform
ATT: Onyinye Uwaezuoke
EMAIL: 1911985@students.wits.ac.za

MICROBIOLOGICAL REPORT

Scaffold Biofilm Analysis

1. Sample Description

3 samples of scaffolds were received labelled Pure, Sample A, Sample B.

2. Method

The antibacterial activity of the scaffolds was determined with the use of two typical skin infection inducing bacterial strains Staphylococcus aureus (Gram positive) and Escherichia coli ATCC 25922 (Gram negative) by standard broth- dilutions tests in suspension. The samples were sterilized under a UV-C lamp prior to testing. The sterile scaffold samples were immersed in sterile Dulbeccos Phosphate Buffered Saline (DPBS) solution for one hour to hydrate the samples prior to testing. The scaffolds were then removed and placed in an actively growing microbial culture with approximately 5 x 10^6 microbial cells/ml. The number of bacteria after 1 hour, 3 hours, and 24 hours of incubation at 37ºC. At each time point scaffolds were removed and washed with sterile DPBS solution and then the microbial cells were detached with a rubber policeman and rapid agitation on a vortex. The number of detached viable cells that were resuspended in solution were counted with a hemocytometer and expressed as CFU/ml. Experiments were conducted in triplicate.

3. Results

Table 1: Antibacterial activity of Scaffolds on *E.coli* ATCC 25922 at time periods of 1, 3 and 24 hours.

Sample (1 Hour)	LIMS ID	CFU/ml
Pure	314218	225000 (±17500)
A	314219	150000 (±25000)
B	314220	100000 (±15 000)
Sample (3 Hours)	**LIMS ID**	**CFU/ml**
Pure	314218	325000 (± 20000)
A	314219	125000 (±12000)
B	314220	100000 (±6000)

Appendix G. Certificate for histopathological analysis

IDEXX LABORATORIES

UNIV. OF WITS MEDICAL SCHOOL
7 YORK STREET, 1ST FLOOR - ANIMAL UNIT
JOHANNESBURG
2050

2022/03/08

For attention: DR JARDINE

OUR REF: JB649568, OWAEZUOKE, ONYINYE RABBIT IMPLANTATION STUDY: BIOCOMPATIBILITY OF ZWITTERIONISED HYDROGEL DISCS AND THE EFFECT ON OCULAR TISSUES

SPECIMEN

1 full eye (A), and 4 tissue samples from the conjunctiva (B-E).

CLINICAL HISTORY

Study: Evaluation of the biocompatibility of zwitterionised hydrogel discs and the effect on ocular tissues.

HISTOLOGY

A: control #71:

Globe:
Normal structures of the globe. The retina is loosened which is artifactual.

B: 288:

The conjunctival mucosa and submucosa have a normal histological appearance. An adjacent muscle layer shows mild interstitial fibroplasia and beneath this muscle layer an inflammatory reaction is evident. It shows an inner epitheloid macrophages layer, presumably palisading against the implant, which is however not visible in this location. The macrophages are accompanied by moderate numbers of heterophils and they also extend into the underlying horizontal fibroblastic reaction, which is of moderate thickness. Scattered small congested capillaries are present in the stromal reaction and they are surrounded by single lymphoplasmacytic cells. A small fragment of refractory material is embedded in the connective tissue layer and surrounded by single multinucleate giant cells, macrophages and lymphocytes. It appears light brown and in one area slightly basophilic and the edges polarise.

Inner layer: 2+ epithelioid macrophages and heterophils
Surrounding stroma: 3+ thickness, encircling/horizontal 2+ invaded by heterophils.
Multinucleate giant cells (MNGC): 3 adjacent to foreign material.
Foreign material: small refractory irregular fragment within the stromal reaction.

C: Implant 734:

The mucosal epithelium of the conjunctiva appears slightly flattened and shows mild neutrophilic invasion. In the underlying submucosa a small refractory structure is visible containing several similarly sized round punched out holes, which in another section becomes elongated linear refractory structures, and this appearance is typical for multifilament suture material. It shows single degenerate leukocytes invading the refractory material. The deeper lying muscle layer is multifocally interstitially

1

IDEXX LABORATORIES

UNIV. OF WITS MEDICAL SCHOOL
7 YORK STREET, 1ST FLOOR - ANIMAL UNIT
JOHANNESBURG
2050

2022/04/25

For attention: DR JARDINE

OUR REF: JB656782, UWAEZOUKE, ONYINYE RABBIT BIOCOMPATIBILITY OF ZWITTERIONISED HYDROGEL DISCS

SPECIMEN
5 tissue samples I-V. (at 4 weeks).

CLINICAL HISTORY
Evaluation of the biocompatibility of zwiitterionised hydrogel discs and the effect on ocular tissues.

HISTOLOGY
3 sections from each sample were processed and evaluated.

A (I):
The conjunctival mucosa is normal and the underlying submucosa appears mildly oedematous. The underlying muscle bundle has a normal appearance and beneath the muscle is a collapsed cystic space lined by stratified fibroblasts forming between 5 and 26 layers. Inflammatory cells are not visible and the cyst lumen contains only single loose red blood cells and scant eosinophilic material as well as few small irregular fragments of lightly basophilic material that reveals a peripheral faint refractory appearance with polarising light.

B (II):
The 2 samples consist of skeletal muscle with focal linear interspersed collagen-rich fibrous connective tissue. 1 of the 3 sections shows the presence of few linear mucosal fragments, with a normal histological appearance accompanied by scant basophilic mucus. The skeletal muscle fibres in one sample appear slightly atrophic and angular and are arranged in discrete bundles separated by delicate perimysium. In the other sample the fibres are slightly haphazard arranged. The connective tissue includes plump and active fibroblasts with oval nuclei and very few macrophages, lymphocytes and plasma cells. In a focal area a small amount of fibrillar basophilic material is evident, with scant fibroblastic cells embedded therein. No polarising material is visible.

C (III):
The sample predominantly consists of skeletal muscle bundles and on the one edge of the sample mildly oedematous collagen rich fibrous connective tissue is visible. The fibroblasts and collagen fibres are arranged linearly. In 1 of the sections, it appears to possibly line a collapsed cavity, but this is difficult to confirm as it is evident on the edge of the section as a small fragment. Inflammatory cells are only present in this area and consists of small numbers of macrophages and lymphocytes with scattered few heterophils and plasma cells present, embedded in the stroma. There is no polarising material evident.

D (IV):
the sample contains skeletal muscle bundles that are fairly thin with mild interstitial oedema leading to separation between the fibres. The adjacent connective tissue appears mildly oedematous as well with multifocal haemorrhage. No cystic structure is visible nor are there signs of inflammation or fibrosis/granulation tissue.

IDEXX Laboratories (Pty) Ltd
Co. Reg. No.: 2006/019540/07
Postnet suite 465, Private X29, Gallo Manor, 2052

Laboratory Operations: +27 11 691 8200 (option 2)
Email: lab-sa@idexx.com

IDEXX LABORATORIES

UNIV. OF WITS MEDICAL SCHOOL
7 YORK STREET, 1ST FLOOR - ANIMAL UNIT
JOHANNESBURG
2050

2022/05/06

For attention: DR JARDINE

OUR REF: JB657722, UWAEZUOKE, ONYINYEDR JAR RABBIT RABBITS

SPECIMEN
5x tissues from the eyes (A-E) and one control tissue (F) (At 8 weeks post implantation). 3 sections from each sample were sectioned and evaluated.

CLINICAL HISTORY
STUDY: EVALUATION OF THE BIOCOMPATIBILITY OF ZWITTERIONISED HYDROGEL DISCS AND THE EFFECT ON OCULAR TISSUES.

HISTOLOGY
A: Tissue 1:
The sample is from the conjunctiva. It shows multifocal erosions/ulcers of the mucosal epithelium and the submucosa appears mildly oedematous.

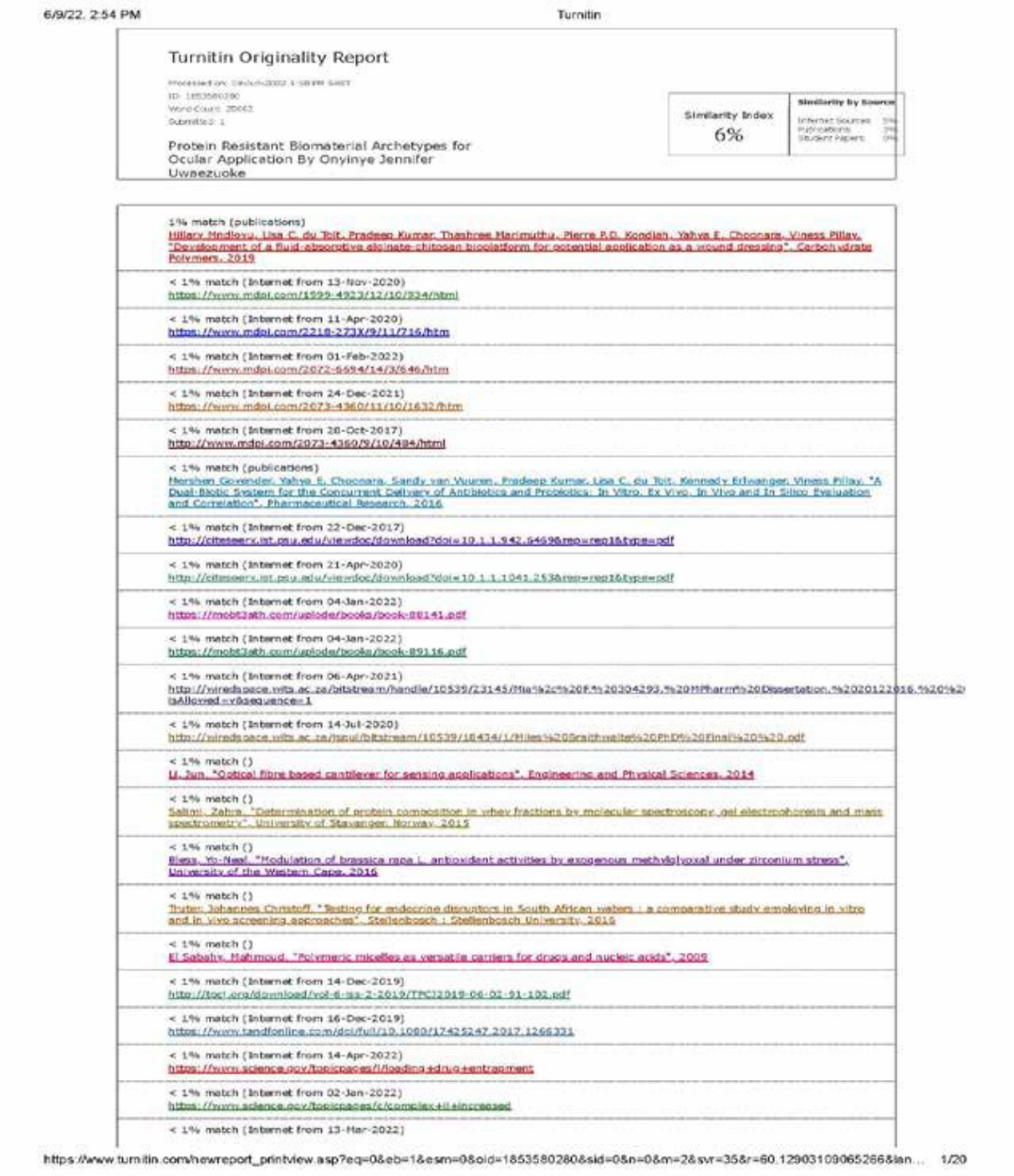
B: Tissue 2:
The sample consists of skeletal muscle and the muscle fibres are arranged in typical bundles that are separated by perimysium as would be normally expected.

C: Tissue 3:
The conjunctival mucosa is multifocally eroded and the underlying submucosa is moderately oedematous. Beneath the submucosa the muscle layer contains an elongated cystic structure. It is lined by encircling fibroblasts that are plump and vary in thickness between 4 and approximately 18 layers of fibroblasts. The cyst is thus lined by a fibrous capsule and is thus a pseudocyst. The cyst lumen contains irregular and angular smudged moderately but variably basophilic and occasionally fragmented material representing foreign material and it is not clearly polarising/refractory. The foreign material is accompanied by several thin linear strands of eosinophilic fibrinous material in which small numbers of heterophils lymphocytes and plasma cells are embedded. Peripheral to the cyst wall are single to small mild perivascular aggregates of lymphocytes. In few areas small fragments of similar basophilic foreign material are present embedded in the muscle adjacent to the cyst and these are surrounded by small to moderate numbers of lymphocytes (2+) and single multinucleate giant cells are also present (6 cells).

D: Tissue 4:
The sample consists of skeletal muscle bundles with a small fragment of adjacent cell poor collagenous connective tissue visible. A small fragment of haphazardly arranged fibroblasts are present in association with the muscle and the fibroblastic nuclei appear plump, hyperplastic and active. The spindle-shaped fibroblasts are associated with interspersed hyalinised lightly eosinophilic collagen. Single odd heterophils and lymphocytes are present within and around the fibroblastic reaction. This small fragment of reactive fibroplasia likely represents a portion of the reactive lesion associated with the test substance, but a clear cystic structure is not visible nor foreign material.

E: Tissue 5:
The sections do not show presence of overlying conjunctival mucosa or submucosa. The muscle tissue contains a fragment of a cystic structure. The cyst lumen is collapsed and contains 2 large multinucleate giant cells and few aggregates of single lymphocytes, heterophils and plasma cells.

Appendix H Turnitin Report



6/9/22, 2:54 PM Turnitin

Turnitin Originality Report

Processed on: [illegible]
ID: 1853580280
Word Count: 28662
Submitted: 1

Protein Resistant Biomaterial Archetypes for Ocular Application By Onyinye Jennifer Uwaezuoke

Similarity Index	Similarity by Source
6%	Internet Sources: 5% Publications: 3% Student Papers: 0%

1% match (publications)
Hillary Mndlovu, Lisa C. du Toit, Pradeep Kumar, Thashree Marimuthu, Pierre P.D. Kondiah, Yahya E. Choonara, Viness Pillay, "Development of a fluid-absorptive alginate-chitosan bioplatform for potential application as a wound dressing", Carbohydrate Polymers, 2019

< 1% match (Internet from 13-Nov-2020)
https://www.mdpi.com/1999-4923/12/10/924/html

< 1% match (Internet from 11-Apr-2020)
https://www.mdpi.com/2218-273X/9/11/716/htm

< 1% match (Internet from 01-Feb-2022)
https://www.mdpi.com/2072-6694/14/3/646/htm

< 1% match (Internet from 24-Dec-2021)
https://www.mdpi.com/2073-4360/11/10/1632/htm

< 1% match (Internet from 10-Oct-2017)
http://www.mdpi.com/2073-4360/9/10/484/html

< 1% match (publications)
Hershen Govender, Yahya E. Choonara, Sandy van Vuuren, Pradeep Kumar, Lisa C. du Toit, Kennedy Erlwanger, Viness Pillay, "A Dual-Biotic System for the Concurrent Delivery of Antibiotics and Probiotics: In Vitro, Ex Vivo, In Vivo and In Silico Evaluation and Correlation", Pharmaceutical Research, 2016

< 1% match (Internet from 22-Dec-2017)
http://citeseerx.ist.psu.edu/viewdoc/download?doi=10.1.1.942.9459&rep=rep1&type=pdf

< 1% match (Internet from 21-Apr-2020)
http://citeseerx.ist.psu.edu/viewdoc/download?doi=10.1.1.1041.253&rep=rep1&type=pdf

< 1% match (Internet from 04-Jan-2022)
https://mobt3ath.com/uplode/books/book-89141.pdf

< 1% match (Internet from 04-Jan-2022)
https://mobt3ath.com/uplode/books/book-89116.pdf

< 1% match (Internet from 06-Apr-2021)
http://wiredspace.wits.ac.za/bitstream/handle/10539/23145/Mia%2c%20F%20304293.%20MPharm%20Dissertation.%2020122016.%20%2(isAllowed=y&sequence=1

< 1% match (Internet from 14-Jul-2020)
http://wiredspace.wits.ac.za/jspui/bitstream/10539/16434/1/Miles%20Braithwaite%20PhD%20final%20%20.pdf

< 1% match ()
Li, Jun, "Optical fibre based cantilever for sensing applications", Engineering and Physical Sciences, 2014

< 1% match ()
Salimi, Zahra, "Determination of protein composition in whey fractions by molecular spectroscopy, gel electrophoresis and mass spectrometry", University of Stavanger, Norway, 2015

< 1% match ()
Bless, Yo-Nael, "Modulation of brassica rapa l. antioxidant activities by exogenous methylglyoxal under zirconium stress", University of the Western Cape, 2016

< 1% match ()
Thater, Johannes Christoff, "Testing for endocrine disruptors in South African waters : a comparative study employing in vitro and in vivo screening approaches", Stellenbosch : Stellenbosch University, 2015

< 1% match ()
El Sabahy, Mahmoud, "Polymeric micelles as versatile carriers for drugs and nucleic acids", 2009

< 1% match (Internet from 14-Dec-2019)
http://toc.org/download/vol-6-iss-2-2019/TPC12019-06-02-91-102.pdf

< 1% match (Internet from 16-Dec-2019)
https://www.tandfonline.com/doi/full/10.1080/17425247.2017.1266331

< 1% match (Internet from 14-Apr-2022)
https://www.science.gov/topicpages/l/loading+drug+entrapment

< 1% match (Internet from 02-Jan-2022)
https://www.science.gov/topicpages/c/complex+ii+increased

< 1% match (Internet from 13-Mar-2022)

https://www.turnitin.com/newreport_printview.asp?eq=0&eb=1&esm=0&oid=1853580280&sid=0&n=0&m=2&svr=35&r=60.12903109065266&lan... 1/20

Appendix I. Oral presentation at the 13th Cross Faculty Postgraduate Symposium

